NTNU
Norwegian University of
Science and Technology

Dynamic Response Analysis of a Spar Floating Wind Turbine in Level Ice with Varying Thickness

Efstathios Tsigkris

European Wind Energy Master

Dynamic response analysis of a spar floating wind turbine in level ice with varying thickness

Department of Marine Technology, NTNU
Department of Offshore & Dredging Engineering, TU Delft

Efstathios Tsigkris
08/07/2016

Dynamic Response Analysis of a Spar Floating Wind Turbine in Level Ice with Varying Thickness

Master of Science Thesis

For obtaining the degree of Master of Science in "Technology-Wind Energy" at Norwegian University of Science and Technology, and in "Offshore Engineering and Dredging" at Delft University of Technology.

Efstathios Tsigkris

NTNU: 763389
TU Delft: 4412346

8th July, 2016

European Wind Energy Master – EWEM

Delft University of Technology
Faculty of Mechanical, Maritime and Materials Engineering
Department of Maritime and Transport Technology
Section of Offshore and Dredging Engineering

Norwegian University of Science and Technology
Faculty of Engineering Science and Technology
Department of Marine Technology

Trondheim
_____
Place

08/07/2016
_____
Date

_____
Signature

MSC IN MARINE TECHNOLOGY

SPRING 2016

FOR

STUD. TECH. Efstathios Tsigkris

Dynamic Response Analysis of a Spar Floating Wind Turbine in Level Ice with Varying Thickness

Background:

Offshore wind is an attractive source of renewable energy. In regions with cold climates, such as Canada, the Baltic Sea, and the Bohai Bay, a good understanding of ice loads and induced responses is essential for design of reliable and cost effective support structures for offshore wind turbines. For example in level ice, depending on the ice thickness and the drift speed, the mean ice load on the cylindrical spar of a floating wind turbine might be even larger than the mean aerodynamic load on the rotor. To mitigate the ice load, an ice-breaking cone is deployed at the mean water level, which changes the ice crushing failure to the bending failure. During the breaking process, the ice sheet will fail periodically. This will induce dynamic loads on the spar wind turbine at the ice loading frequency. For floating wind turbines, the ice loads will also induce rigid-body motions of the floater (in addition to the vibrations normally experienced by a bottom-fixed structure) and therefore increase the tension in mooring lines. The dynamic response of the spar wind turbine considering constant ice thickness and drift speed has been studied in a master thesis last year. This thesis will be a continuation of the previous work.

The thickness of ice sheet might vary along the path that is in contact with the offshore wind turbine and this will increase the dynamic effect of the ice loads. Therefore, a probabilistic approach should be used to assess the ice conditions and the ice induced loads and responses. The purpose of this thesis is to formulate a theoretical distribution of the ice thickness based on the existing measurements reported in various literatures, and to investigate the response characteristics of the spar wind turbine in such ice conditions. The effect of the coupling between the ice-induced and aerodynamic loads and responses for both operational and parked conditions of the rotor should also be studied.

The MSc candidate will be provided with the design of a 5MW spar wind turbine and the corresponding numerical model in HAWC2, as well as a Fortran DLL for ice failure model, which should be further developed considering varying ice thickness and coupled to HAWC2 for dynamic response analysis of spar wind turbines in level ice.

Assignment:

The following tasks should be addressed in the thesis work:

1. Literature review on ice properties, formulation of level ice and variation of ice thickness. Literatures with real sea measurements and probabilistic approaches for assessing level ice conditions should be focused on. Literature review on ice loads on conical structures and ice failure mechanism. This involves a study of different semi-empirical ice failure models that were developed and applied in analysis of ice loads on offshore oil & gas platforms. Validations of such theoretical or numerical models against lab and field measurements should also be reviewed. Literature review on numerical modelling and dynamic response analysis of spar floating wind turbines. In particular, the numerical code HAWC2 for global response analysis of wind turbines from DTU-Wind Energy should be studied.

2. As an extension of the project work carried out last semester, investigate the existing measurements of thickness in level ice, and formulate a probabilistic distribution for ice thickness along the path of the contact with the spar wind turbine. A stochastic process approach should be used in order to represent not only the variance of the ice thickness, but also the (1D) spatial variation. If time allows, simulations of a random field (2D) of ice thickness might also be considered.

3. Study the ice failure module already developed in Fortran and understand the key parameters used in the formulation of the failure mechanism. Extend this module to cover the case with varying ice thickness. An iterative procedure to obtain the actual breaking length due to bending might be introduced. This module can be tested on a bottom-fixed rigid coned structure.

4. Study and use the code HAWC2 for dynamic analysis of offshore wind turbines. Study the coupling between the ice load DLL and HAWC2 and understand the exchange of internal parameters and the inner and outer loops of iteration. A convergence study should be performed with respect to transient phase, time step and duration of the simulations.

5. Perform dynamic analysis of the spar wind turbine only in level ice and compare the dynamic response results with varying thickness and those with constant ice thickness. The response parameters considered should be spar rigid-body motions, bending moments at tower top and bottom as well as mooring line tension. The comparison should be made only for steady-state results and on spectra and statistics. Different mean values of ice thickness and drifting speed should be considered.

6. Then also consider the cases with aerodynamic loads included. Compare the responses due to pure wind loads, pure ice loads and combined loads and investigate the relative importance for design.

7. Conclude on the investigation and write the thesis report.

Supervisors:

NTNU: Zhen Gao
                                        Wei Shi

TU Delft: Andrei Metrikine
                                        Chris Keijdener

Deadline: 08.07.2016

Acknowledgements

First of all I would like to thank, Zhen Gao, Andrei Metrikine, Wei Shi and Chris Keijdener for giving me the opportunity to realize my MSc thesis under their supervision and having always found time to advise me. I want to also thank the whole European Wind Energy Master committee for the opportunity that has given me to realize this double degree in both TU Delft and NTNU.

To Prof. Zhen Gao for his constant guidance and the precious time he has found to answer my questions even out of meeting hours.

To Prof. Andrei Metrikine who even if we haven't discussed a lot, has been very helpful with his right at the point comments during every Skype session.

To Ph.D canditate Chris Keijdener who took the time to answer all my e-mails very quickly and his very targeted discussions

Special and many thanks must be given to Dr. Wei Shi for his immeasurable help regarding software issues and software teaching of HAWC2. For all the advice he gave me during this last year of my presence in Trondheim and for the patience he showed to answer all my outnumbered question.

Another special thank you to all the people mentioned above, for understanding my weird situation and were kind enough to help me by giving me two extra deadline extensions.

I would also like to thank my Offshore EWEM friends for these two wonderful years we have spent together learning new and interesting knowledge. Also, I would like to thank all of my friends from Volos and their psychological support, because I am in this place with their help.

Also, I would like to thank my girlfriend Katerina, who has always been supportive in every difficult situation I have confronted. Without her, my life would not be that great and joyful.

Finally and most of all, I would like to thank my beloved parents, for everything! For supporting me, for believing in me, for helping me, for being close to me, for loving me. This work is dedicated to them.

Trondheim, July 8, 2016

Summary

This master thesis is the final step before graduation from the Offshore Engineering track of the European Wind Energy Master. Both the Diploma award universities contributed significantly in the completion if this work by excellent supervision.

The graduation project consists of the dynamic response analysis of a spar floating wind turbine in level ice with varying thickness. This topic is important in the field of renewable energies given the fact that wind energy is known as the fastest growing renewable energy. In the case of regions with cold climates, ice loads become significant and have to be taken into account when designing and offshore structure like an offshore wind turbine.

Relevant literature study was examined in order to establish a theoretical background regarding ice properties, formulation of level ice, variation of ice thickness, ice loads on conical structures, ice failure mechanisms, numerical modelling and dynamic response analysis of a spar floating wind turbine.

As soon as this basic knowledge is founded, a set of existing measurements of level ice was used in order to formulate a random varying thickness ice field. This field was implemented considering the 2D case meaning that the ice thickness varied along the path of the contact with the spar wind turbine.

The greatest challenge came up when the existing model needed to be modified in order to account for the variation in thickness. This was accomplished by modelling the ice floe as an Euler - Bernoulli beam of varying cross - section assuming linear variation of ice between each space interval. The stress distribution along the beam's length was obtained and as a result the behaviour of the ice floe at each cross - section is investigated and analysed.

This new model was implemented in FORTRAN as a DLL file and coupled to HAWC2 in order to simulate the behaviour of the spar floating wind turbine in the varying thickness level ice environment.

The results obtained generally revealed a decrease in the ice loads when a varying ice field is considered. Moreover, it is observed that the varying ice thickness field introduces a more dynamic effect on the structure, especially for the low drifting speeds. As soon as aerodynamic loads are also included, then it is also noticed that the combined wind and ice loads, give rise to frequencies different from the ones only the ice loads excite.

Contents

Index of figures

Index of tables

Abbreviations

BEM	*Blade Element Momentum*
cnst	*constant*
DLL	*Dynamic Link Library*
DNV-GL	*Det Norske Veritas - Germanischer Lloyd*
DOF	*Degrees of Freedom*
FEM	*Finite Element Method*
FORTRAN	*Formula Translating System*
HAWC2	*Horizontal Axis Wind turbine simulation Code 2nd generation*
Mathematica	*Wolfram Mathematica software*
NREL	*National Renewable Energy Laboratory*
WAFO	*Wave Analysis for Fatigue and Oceanography*
OC3	*Offshore Code Comparison Collaboration*
IEC	*International Electrotechnical Commission*
ISO	*International Organization for Standardization*
SPD	*Spectral Density Function*
SWL	*Sea water level*
cm	*centimetres*
CM	*Center of mass*
GPa	*Gigapascal*
GW	*Gigawatts*
km	*Kilometres*
kN	*Kilo Newton*
kNm	*Kilo Newton meter*
m/s	*Meters per second*
MPa	*Megapascals*
MWh	*Megawatt hours*
vs	*versus*

List of symbols

Roman Characters

$\overline{U}_{ref}$	*Wind speed at reference height z_{ref}*
$\dot{u}$	*Fluid acceleration*
A	*Nominal contact area*

A	*The added mass*
a	*Vertical shear exponent*
A_{cr}	*Contact area*
b	*Heat conduction exponent, Width of the beam face contact with the foundation*
B	*The damping coefficient*
c	*Cohesion of the ice rubble, Chord length*
C	*The restoring force*
$C_d(\alpha)$	*Drag coefficient*
$C_{D,t}$	*Drag (viscous) coefficient on the specific direction that has projected area $D_t(z)dz$*
c_f	*Experimental coefficient*
C_{FDD}	*Accumulated of freezing degree days*
$C_l(\alpha)$	*Lift coefficient*
C_M	*Inertia coefficient for the spar*
C_n	*Normal load coefficient*
C_t	*Tangential coefficient*
D	*Diameter of the support structure at the waterline*
D_s	*Diameter of the spar*
D_t	*Diameter of the tower*
E	*Elastic modulus of ice*
e	*Porosity of the ice rubble*
F(X)	*Cumulative distribution function*
F_G	*Global ice action*
f_N	*Wind turbine structural eigenfrequency.*
G, g	*Gravity acceleration*
h	*Thickness of the ice sheet*
h_1	*Reference thickness (1 m)*
H_B	*Breaking load*
H_D	*Static force due to crushing*
H_{dyn}	*Force due to dynamic loading*
hi	*Ice thickness at the left hand side of each blocl*
H_L	*Load required to lift the ice rubble over the advancing ice sheet prior to breaking*
h_{mean}	*Mean ice thickness to be achieved*
H_P	*Load component required to push the sheet ice through the ice rubble*
H_R	*Load to push the ice blocks up the slope through the ice rubble*
h_r	*Rubble height*
H_T	*Load to turn the ice block at the top of the slope (=0 for downward cone)*
I(x)	*Second moment of area of each cross section $I(x) = \frac{bh(x)^3}{12}$*
K	*Foundation modulus*

k1	*Shape factor for the shape of the support structure on the ice impact side*
k2	*Contact factor for the ice contact against the support structure*
k3	*Form factor*
L	*Length of beam element*
l_C	*Total length of the circumferential crack*
m	*Empirical coefficient*
M	*The mass of the structure*
n	*Empirical coefficient*
N	*Normal force in the edge of the beam per unit width*
P	*Pressure of seawater, Applied load (Figure 2.24)*
p_{av}	*Average contact pressure*
p_G	*Ice pressure averaged over the nominal contact area*
p_w	*Sea water density*
r	*Radius*
R_N	*Normal reaction force on the wall per unit width*
R_T	*Tangential reaction force on the wall per unit width*
S	*Transversal force in the edge of the beam per unit width*
$S(\omega i)$	*Spectrum value at each angular frequency (ω)*
S_h	*Salinity*
t	*Time*
T_{fr}	*Freezing point of seawater*
U	*Ice floe speed*
u	*Undisturbed fluid velocity*
U	*Node displacements*
U(z,t)	*Wind velocity along the tower/Nacelle height z and in time t*
U_r	*Randomly generated number between 0 and 1*
v	*Poisson ratio*
V_0	*Wind speed*
v_2	*The normal relative speed of the ice floe*
V_{brine}	*Porosity of sea ice*
w	*Projected width of the structure*
w(x)	*Deflection of the beam*
X	*Random variable*
xi	*Length of the ice floe with the selected length interval*

Greek Characters

$\dot{\eta}_1$	*Velocity of the body*
α	*Slope of the connection line, Site specific constant, Axial induction factor*

xvi

α'	*Tangential induction factor*
$\Delta\omega$	*Angular frequency step as obtained from the spectrum*
θ	*Angle the rubble makes with the horizontal*
θ_w	*Angle of the arc (wegde)*
μ	*Mean value of the random variable*
μ_i	*Ice to ice friction coefficient*
μ_S	*Kinematic friction coefficient between beam and wall*
σ	*Standard deviation*
σ_C	*Crushing strength of ice, determined from statistical data*
σ_f	*Flexural strength of ice*
φ	*Friction angle of the ice rubble, Flow angle*
φ_i	*Random phase generated between 0 and 2π*
φ_w	*Wall angle*
ω_i	*Angular frequency at each time*

1 Introduction

In the past years, a great concern regarding global warming and greenhouse effects has raised among people and societies. This is the reason why the European Union's Renewable Energy Directive has set a binding target of 27% of the final energy consumption should come from renewable sources by 2030 (European Commission 2014). As a result, renewable energy sources are growing and evolving, gaining more and more share of the pie in the energy consumption not only within the European Union but also worldwide.

Wind energy is believed to be the most cost effective of all currently exploited renewable energies (Islam, et al. 2013). Therefore, the growth that is observed the last years is not a surprise. So far, approximately 130 GW of installed capacity within the European Union account for the 36% of the total renewable energy sources installed, which is the lion's share of the pie (Global Wind Energy Council 2014). Even if predictions show that this percentage will gradually decrease to at least 21%, wind energy will keep holding the first place by all of the sustainable energies by 2030 (European Wind Energy Association 2015).

Out of this installed capacity, only 8 GW --or equivalently 6%-- belong to offshore wind (Global Wind Energy Council 2014). This is fairly reasonable due to the increased cost of offshore wind per MWh compared to onshore wind. It is worth mentioning that onshore wind costs vary approximately between 52 and 100 €/MWh while offshore wind costs fluctuate from 110 to 150 €/MWh (Ecofys 2014). On the other hand, offshore wind has advantages like reliable wind resources, significantly less visual impact compared to onshore wind farms and also significantly less noise pollution. These are some of the reasons why offshore wind is a concept that not only is not abandoned but also it gets funded for more research and development.

Offshore wind can be divided into two main categories with respect to the type of foundation used for the support of wind turbines, namely bottom founded wind turbines and floating wind turbines. The bottom founded ones are the most common in the offshore wind industry. In particular, bottom founded wind turbines are the only ones which are operating at the moment in offshore wind farms. However, the need of higher capacity ratios and higher efficiency is becoming more and more intense. In order to cover these needs, the wind energy industry has to go further offshore, to move into deeper waters where bottom founded wind turbines cannot be deployed anymore. This is the main reason why floating wind turbines have been studied extensively in the past years.

Many concepts have been introduced as potential offshore wind turbine support structures for floating wind turbines, namely: the Tension Leg Platform (TLP) concept, the Semi - Submersible concept and the Spar concept. In June 2009, the world's first operating large capacity floating wind turbine was introduced as a prototype by Statoil with the Hywind project. This prototype is using a spar buoy as a floater/support structure. This prototype after years of testing presented outstanding performance. As a result, in 2015 Statoil received permission to install 30 Hywinds, 29 km outside Peterhead in Scotland which together they will consist the Hywind Scotland Pilot Park; the first floating wind farm ever existed, fully operational by the end of 2017 (Statoil 2014).

In this project assignment, the spar floating wind turbine concept is a matter of concern not only because of the above mentioned achievement but also because of other advantages that make it interesting for research. A spar floating wind turbine shows --among other things-- satisfying heave motion performance and small wave forces. Moreover, spar buoys are cheaper to build and easier to install and maintain than other floating concepts (Biswajt and Dinh 2013).

After this realization has been made, a new market is opening further away in regions with deep waters, cold and harsh environments where the wind resources are plentiful and forceful. In regions like Canada, Barents Sea, the Arctic and Antarctic there is room for development for the wind energy industry.

The purpose of this report is to study the ice actions on a spar floating wind turbine and to perform a dynamic response analysis under both ice loads and aerodynamic loads. Specific attention has been paid to the comparison of the response results under the loading from a varying thickness ice filed and those from the constant thickness ice field. Also, the responses due to pure ice loads, pure wind loads and combine loads have been compared in order to investigate their relative importance for design and development.

This study is divided in the following general sections. First of all, an extensive literature and theory review is realised. Then, the model implementation is been analytically described. Finally, the results are presented and discussed hopping to bring theory and practice one step closer.

2 Theoretical background

Since the marine activity is increasing in ice regions and polar areas, the need of studying the ice covered waters became a necessity. In particular, the presence of sea ice increases the difficulty of various operations; therefore this complex material needed to be investigated and analyzed (Timco and Weeks 2010).

2.1 Ice regimes

Beginning with an encyclopaedic introduction; frozen water is the consequence of very low temperatures and severe winters and usually can be found in the most remote regions of planet earth. Sea ice can be found in Arctic and Antarctic Ocean, Kara Sea, the Great Lakes of Canada, Beaufort Sea, Bohai bay, Baltic Sea etc.

Ice can be categorized with respect its age and its origin. With respect to the age criterion there is First Year (FY) ice and Multi Year (MY) ice. Regarding the origin criterion both the aforementioned ice types are formed by sea water and there is also Glacial ice which has been formed from compacted snow and fresh water.

Additionally, there are many different ice regimes that have been generally observed. The next table can be used as an indicator of the different regimes.

Table 2.1 Common Ice features

First Year Ice	Multi Year Ice	Glacial Ice
Level ice floes	Ice floes	Ice islands
Rafted ice	Ice ridges	Icebergs
Ice ridges	Rubble fields	
Rubble piles		
Rubble fields		

Ice structure interaction is not a new subject of research. However, ice interaction with wind turbines is a newcomer. Even though offshore wind farms are becoming more and more popular, there are no thoughts for placing them in the arctic yet. Wind turbines interacting with ice has been a subject of study the last 10-15 years. As a result, the most common ice regimes should be examined first.

Level ice is the most common feature that is met in environments where wind turbines are feasible to be placed. For this reason, this current assignment does not account for any other

ice regimes than level ice. In the next chapters, several details regarding ice will be covered that are essential for understanding the complexity and difficulty ice holds.

2.2 Formulation of level ice

Level ice is an ice regime of first year ice and it is formulated when the sea water temperature is low enough to begin forming ice crystals. The freezing point of sea water is lower than the freezing point of pure water due to the presence of various compounds such as salt and various microorganisms. This phenomenon is commonly known as freezing point depression. In sea water, the compound that is found in majority other than H_2O is sodium chloride (NaCl), together with other salts. As the air above an ocean starts cooling down the sea surface below its freezing point, the upper layer of the sea becomes slightly supercooled and the first molecules in the sea water start forming crystals of ice. A supercooled liquid is a liquid at a temperature below its freezing point without it becoming a solid. As soon as sea water starts freezing the first flat ice platelets are formed. At the same time salt ions, because of their size, cannot be incorporated into the crystal lattice of the ice and neither they fit into the ice crystal as interstitial molecules. Therefore, the salt crystals are rejected from the ice while the ice crystals are forming. Consequently, the first formed platelets consist of approximately pure ice and also the forming of ice on the water surface is accompanied by an increase of salinity in the surrounding water (Timco and Weeks 2010).

Usually at sea, wind and waves will agitate the surface layer, mixing the initial ice crystals near the air-water interface with the water beneath, causing supercooling to extend to deeper levels. Therefore, instead of the initial ice crystals staying near the air-water interface, they are suspended in the supercooled water column. This suspension of ice crystals may occur up to several meters. As time passes these crystals naturally stick together forming frazil particles of ice in the form of small discoids or fine spicules. While the concentration of these formations increases, the roughness of the sea state is reduced and as a result, ice floe pieces start to coagulate and consolidate forming level ice. As ice growth continues, the dominant ice crystals have their c-axes completely horizontal (Figure 2.1). Those ice crystals that have their c-axes vertical as they unite together with the initial scheme, due to their "strange" geometry cause a rapid increase in the grain size. The vertical domain below this initial pattern that has been formed, where the crystal orientation has a rapid change is known as the transition zone. However, still the dominant crystals are oriented in such way the ice to growth is taking place vertically down into the water beneath the ice floe. This part of the ice is known as the

columnar zone and its vertical domain is known as the growth zone or skeleton layer. The transition, columnar and growth zone together are known as secondary or congelation ice (Cole 2010), (Hoving 2015).
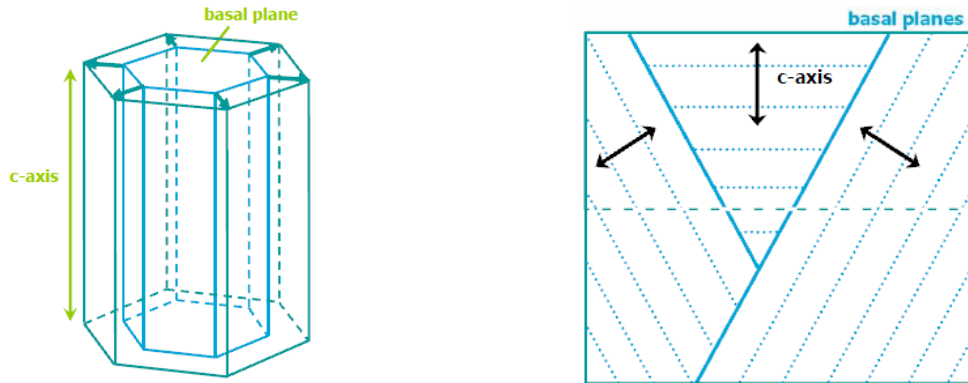
Figure 2.1 Formation of level ice (Hoving 2015)

The heat flux in water is the main contributor to the growth of ice thickness. When there is equality between the heat flux through the sea and the heat flux through the ice, then the ice thickness growth stops and the final formulation of the ice is achieved.
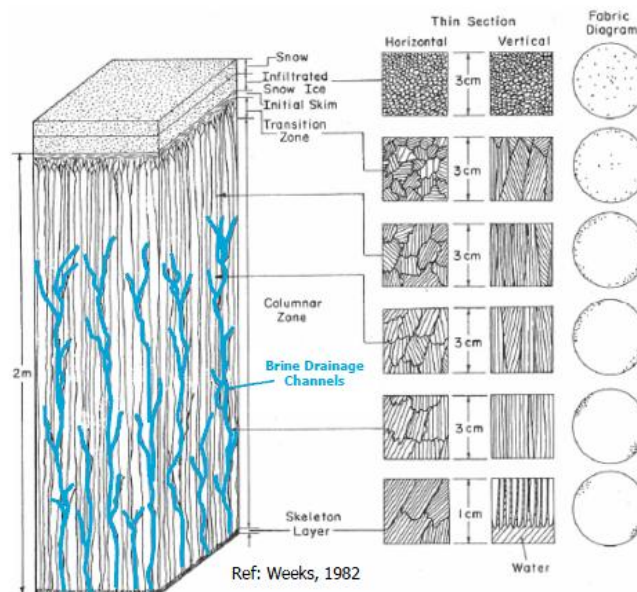
Figure 2.2 Structure of first year level ice

In Figure 2.2, the main layers of the structure of first year level ice are observed. First of all is the initial scheme where it all started from namely: the transition zone, the columnar zone and the skeleton layer. It can also be observed that the total growth, in thickness, of the level ice depends directly on the growth of the columnar zone.

2.3 Ice physical properties

According to the ISO19906, the design standard for offshore arctic structures, the physical properties ice holds are the following:

- Crystallography
- Salinity
- Temperature
- Porosity
- Strength

2.3.1 Crystallography

The unit cell is the fundamental building block of a crystalline material. Since ice is a crystalline material, the complete three-dimensional crystallographic structure is formed by stacking unit cells in perfect alignment.
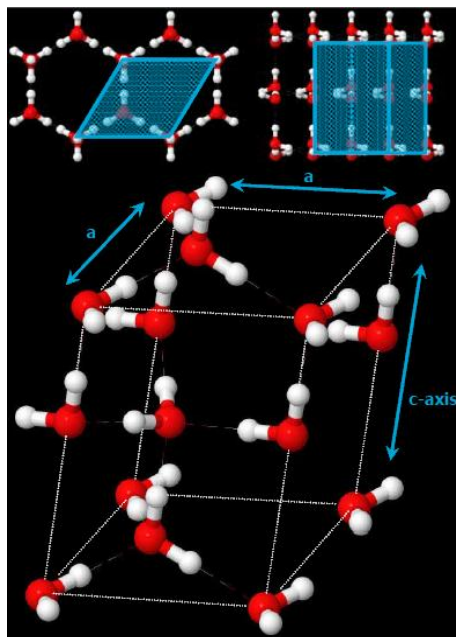
Figure 2.3 Unit cell of ice (Hoving 2015)

Ice shows an anisotropic behaviour because of the properties of the unit cell and the bonds that are holding the atoms together. As a result, ice fails by gliding and cleaving perpendicular to the c-axis (see Figure 2.3), rather than by fracturing along the c-axis.

2.3.2 Salinity

Ice salinity is usually expressed as the fraction by weight of salts contained in a unit mass (Timco and Weeks 2010). The salinity varies over the depth of an ice sheet. This depth dependence of the salinity reduces throughout the life of the ice sheet as the salt within the ice is gradually expelled out of it. According to the ISO19906 the average salinity of a growing FY ice sheet with respect to its ice thickness is found empirically.

$$S_h = \begin{cases} 13.4 - 17.4h \text{ for } h \leq 0.34m \\ 8.0 - 1.62h \text{ for } h \geq 0.34m \end{cases} \tag{2.1}$$

Where:
  h: Thickness of the ice sheet

2.3.3 Temperature

The freezing point of seawater depends on salinity and pressure and is found as (UNESCO 1983):

$$T_{fr} = -(57.5S + 1.71S\sqrt{S} - 0.2155S^2 - 7.53P) \cdot 10^{-3} \tag{2.2}$$

Where:
  S: Salinity of seawater
  P: Pressure of seawater

This is the critical temperature for the seawater to start forming into ice according to the procedure described in Chapter 2.2

2.3.4 Porosity

The porosity of sea ice has been analyzed in terms of the brine volume V_{brine} present in the ice. The brine volume is the amount of liquid within the ice matrix that has not solidified yet. Brine volume and consequently porosity is influenced by both the temperature and salinity. According to the ISO19906 it can be found as:

$$V_{brine} = S\left(\frac{49.18}{|T|} + 0.53\right) \tag{2.3}$$

Where:
  T: Temperature is $-22.9^o C < T < -0.5^o C$
  S: Salinity

2.3.5 Strength

All of the aforementioned physical properties have a great influence on the strength of the ice sheet. It has been observed that at the surface of the ice, the grain size is very small and its orientation is random. The grain size increases rapidly though when moving towards the bottom of the ice. Therefore, due to *crystallography*, the ice is strong at the top (small grain size) and much weaker at the bottom (larger grain size). Moreover, an ice floe is coldest at its surface and its temperature increases (up to the freezing point) while moving to its bottom. As a result, the ice is strong at the top and weaker at the bottom because of its *temperature* profile. *Salinity* and *porosity* affect the strength of the ice sheet as their profiles change over time along the depth of the ice sheet. In FY ice, the salinity profile is almost constant, while the salinity profile for older ice increases with depth. On the other hand, the porosity profile is relatively constant, but is smallest at the top and largest near the bottom (Hoving 2015). This leads to the conclusion that first year level ice is stronger at the top and it gets weakened as moving towards the bottom.
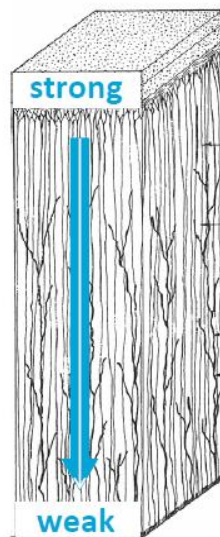
Figure 2.4 Strength profile of level ice (Hoving 2015)

2.4 Ice mechanical properties

Since an ice breaking cone is going to be installed at the waterline of the spar floating wind turbine that is going to be examined, the mechanical properties that are the most interesting for this study are:

- Friction
- Flexural strength

2.4.1 Friction

On sloped and conical structures, the resistance of the ice against sliding may be significant. This effect plays an important role for the clearance of the broken ice pieces that may pile up on an upward breaking cone or accumulate under a downward breaking cone. There are two types of friction:

- Static friction: resistance against sliding at rest (stick)
- Kinetic friction: resistance against sliding during movement (slip)

Laboratory tests have shown that the static friction may be up to five times greater than the kinetic friction. Also it is shown that the kinetic friction is largely dependent on the relative velocity between the contacting surfaces. The following table indicates various kinetic friction coefficients for ice against steel and concrete based on laboratory measurements (ISO19906 2010).

Table 2.2 Measured values of kinetic friction coefficient

Construction material	Influence of sliding velocity					
	$v_s \leqslant 0,01$ m/s		$v_s = 0,1$ m/s		$v_s = 0,5$ m/s	
	mean	st. dev.	mean	st. dev.	mean	st. dev.
Smooth steel	0,10	0,02	0,05	0,01	0,05	0,01
Smooth concrete	0,12	0,02	0,05	0,015	0,05	0,01
Corroded steel	0,15	0,03	0,10	0,03	0,10	0,03
Rough concrete	0,22	0,05	0,10	0,03	0,10	0,03

2.4.2 Flexural strength

To begin with, it needs to be mentioned that the flexural strength of ice is not a basic material property because it is usually determined from the measured failure force by applying linear bending theory with homogenous and isotropic material properties throughout the ice thickness (Su, Riska and Moan, 2010) something that is not entirely correct because, as it was mentioned in section 2.3.1 , ice shows anisotropic behaviour. Because of its importance, though, several scientists have taken measurements of the flexural strength of ice. Flexural strength is important because a lot sea ice failure occurs due to flexure. The most characteristic example that fits this project is the one of the bending of ice on conical shaped structures. The ISO19906 states that *"flexural strength is defined as the extreme fibre stress in tension"*. The flexural strength of ice sheets, rafted ice and the consolidated layer of ridges is used for estimating ice actions on sloping structures.

Based on a large number of small-scale tests (Timco and O'Brien 1994), (ISO19906 2010), the flexural strength, σ_f, of sea ice decreases with increasing brine volume.

$$\sigma_f = 1.76e^{-5.88\sqrt{V_b}}$$ (2.4)

Where:
$\quad$ V_b: $\quad$ Brine volume

For downward breaking, the in situ flexural strength usually fluctuates between 0.3 and 0.5 MPa (ISO19906 2010).

2.5 Variation of ice thickness

Ice thickness of level ice is an important subject of this study since the level ice floe considered does not have a uniform thickness, but a varying one.

According to the ISO19906, the maximum thickness of undisturbed level ice grown in one winter can be found as:

$$h = a \cdot C_{FDD}^b$$ (2.5)

Where:
$\quad$ α: $\quad$ Site specific constant
$\quad$ b: $\quad$ Heat conduction exponent, 0.5 for linear heat conduction
$\quad$ C_{FDD}: $\quad$ $|T_{air,average}-T_{water,freezing\ point}| \cdot N_{winterdays}$ Accumulated freezing degree days

The maximum sea ice thickness is in the range of 2 meter for the Arctic region at the end of the winter (Melling, et al. 2005).

Likewise ISO, the IEC standard suggests an equation to estimate the ice thickness at the end of a frost period. It is also stated that for wind turbines in the open sea, the thickness may be taken as a category corresponding to the 50-year recurrence period. Furthermore, for wind turbines in archipelagos and land-locked waters, the thickness of moving ice may be chosen to correspond to "normal winters" and the land fast ice cover thickness corresponding to the 50-year recurrence period. The equation proposed by IEC is the following:

$$h = 0.0032\sqrt{0.9K_{max} - 50}$$ (2.6)

Where:

$$K_{max} = \sum_{days} |\tau_{mean}(day)| \ , \tau_{mean} < 0^oC$$

K_{max} means that the absolute value of the total of those mean day temperatures that are less

than 0°C in a frost period are accounted for. This is something that is quite similar to the freezing degree days that ISO suggests.

However, in principle ice thickness along a certain cross section is not constant due to the randomness of the formation procedure. The first year ice is directly associated with the ambient air temperature, freezing time, snow type and thickness, wind speed ocean heat flux and surface radiation balance. The first two factors play the most significant role and this is why Arctic sea is always thicker than milder climates (Timco and Weeks 2010). Moreover, all of these parameters can vary significantly within the same ice sheet (Kujala 1996).

Usually when scientists are aiming to form a model that is able to predict or generate the stochastic nature of ice processes, data ice charts from various institutes and expeditions are used. Another way is the usage of numerical models in combination with datasets.

Ice charts may include ice thickness variations, ice concentration, degree of ridging etc. The next figures come from the Finnish Meteorological Institute and comprise a characteristic example of ice charts used for modelling. Figure 2.5 presents the maximum ice thicknesses (in cm) in the Bothnian Bay in the Baltic Sea by calculating the average of the maximum ice thicknesses that occurred in the period between 1996 and 2011. Figure 2.6 shows the values of maximum ice thickness corresponding to the 10, 20, 50 year of return period in the same area.
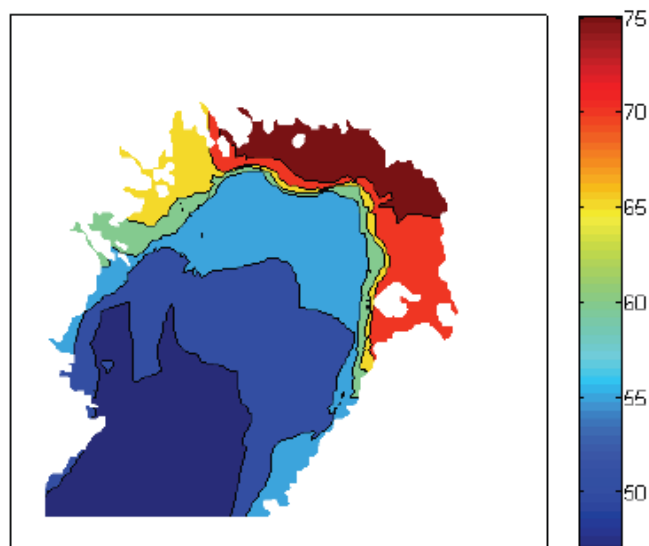
Figure 2.5 Averaged maximum ice thickness (cm)

a)

b)

c)
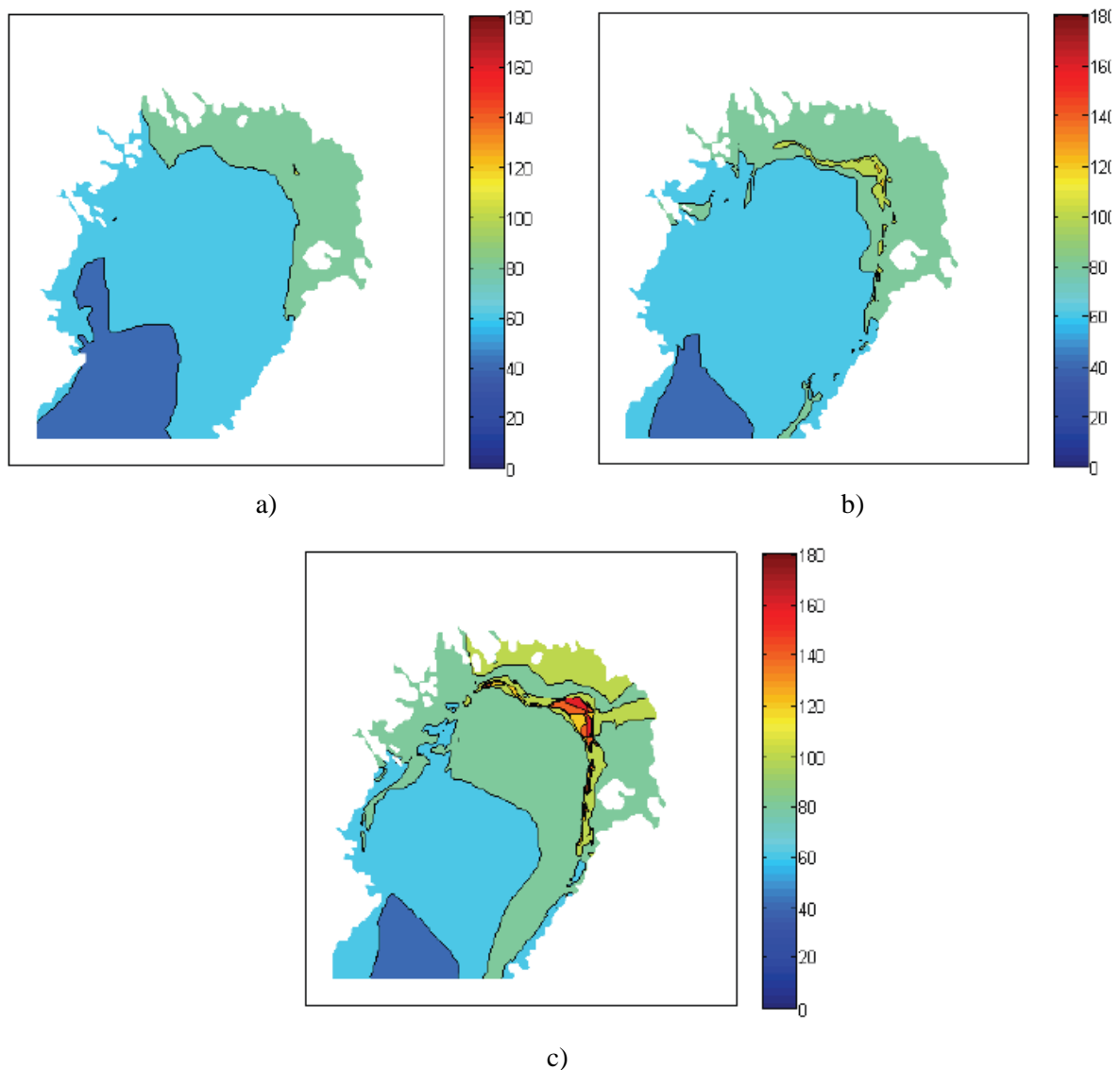
Figure 2.6 Maximum ice thickness (cm) corresponding to 10 (a), 20 (b) , 50 (c) year return period

The findings from these charts were fitted into a graph distribution (Figure 2.7) that aims to represent the variations of the ice thickness that were illustrated in Figure 2.5 and Figure 2.6.
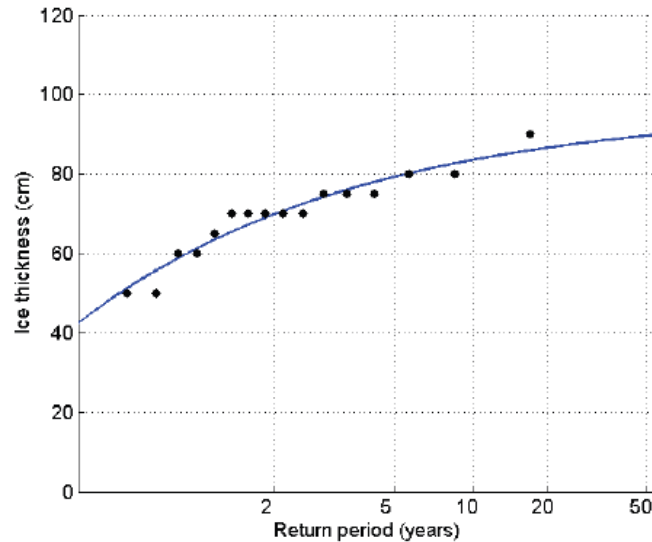
Figure 2.7 Fitted distribution of the maximum ice thickness (Tikanmaki, Heinonen and Makkonen 2012)

In Figure 2.7 the dots represent the observed ice thicknesses. Based on these, a distribution function was fitted and it is represented by the solid curve. This was an example of combining a numerical model together with datasets. This work by (Tikanmaki, Heinonen and Makkonen 2012) has shown that the determination of the local ice conditions when using historical chart data is encouraging. These predictions can be used not only for offshore wind turbines but also for other structures related to the Oil & Gas industry.

In order to formulate a varying thickness ice field, the same principle procedure was followed. Initially a dataset of thickness measurements was obtained and throughout a constructed procedure, a new dataset was generated. This new dataset comprised the input basis for the necessary simulations.

The initial dataset was obtained from (Pfaffling, Haas and Reid 2007). They used the measurements from the "ARISE" expedition that took place in East Antarctica in 2003. The expedition involved drilling measurements of a level ice sheet as illustrated below.
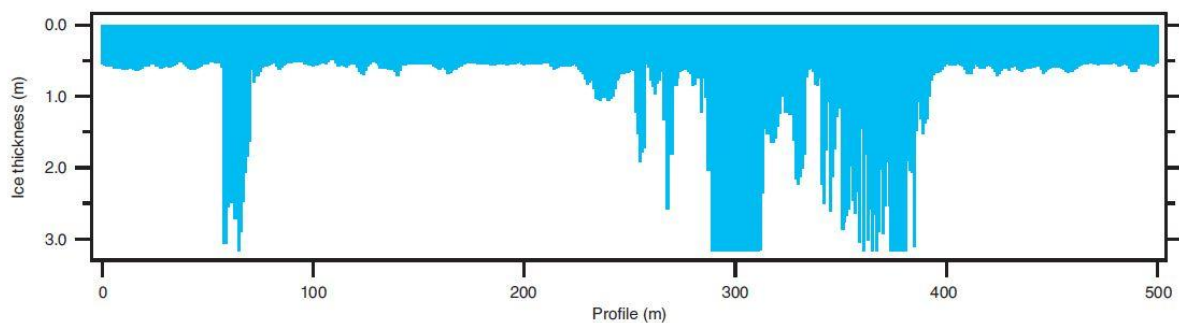
Figure 2.8 ARISE 2003 field data measurements

From Figure 2.8, it is observed that the profile of the measured level ice field also includes some pressure ridges. Obviously, during the extraction of the measurements these ridges were ignored and skipped, resulting the level ice field forming to the following shape.
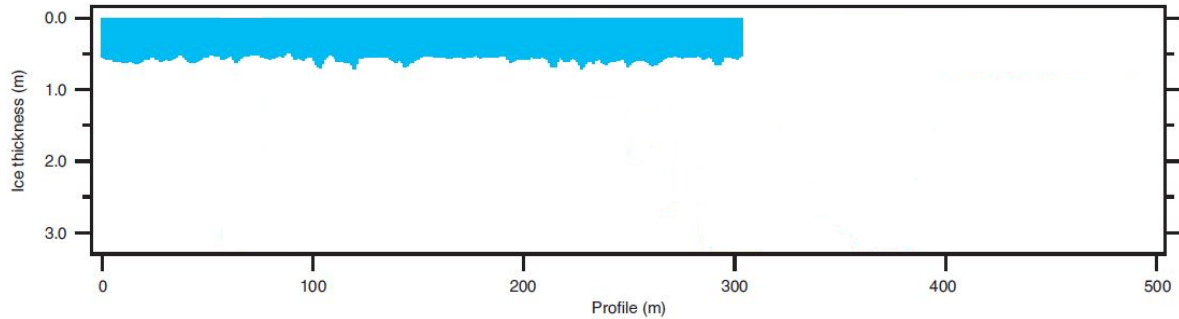
Figure 2.9 Level ice field measurements used

The resulting ice field is approximately 200 metres shorter than the initial one, but still it is long enough to be used in order to extract safe results regarding the new randomly generated ice field. Another important observation that needs to be mentioned is that, as expected, the level ice does not have a uniform thickness but a varying one. Moreover, this variation cannot be characterised as totally random since it seems to follow a mild pattern which does not allow severe or high fluctuations like in the pressure ridges case. This effect will be attempted to be captured by the proposed data manipulation method.

Initially, Figure 2.9 is digitized and the spectrum of the length series is obtained. Based on the spectrum created, a new length series is generated by making use of the direct summation equation.

$$h(x) = h_{mean} + \sum \sqrt{2S(\omega_i)\Delta\omega} \cdot \cos{(\omega_i\, x_i + \varphi_i)} \tag{2.7}$$

Where:

h_{mean}: Mean ice thickness to be achieved
$S(\omega i)$: Spectrum value at each angular frequency (ω)
ω_i: Angular frequency at each time
$\Delta\omega$: Angular frequency step as obtained from the spectrum
x_i: Length of the ice floe with the selected length interval
φ_i: Random phase generated between 0 and 2π

At this point is has to be mentioned that usually a spectrum is obtained from a timeseries and not from a length series. However, in the case considered there is no dependency of the thickness with time. Therefore, a trick is introduced and the length is translated as time and vice versa.

In order to verify whether the new generated length series is a realistic one and can be used as input for the upcoming simulations, it was compared with the initial length series. Firstly, the form of the length series should be similar and secondly the shape of the spectrum should be similar as well. Several tests were carried out in order to find the proper length interval for the generated length series. The conclusion is presented analytically in Chapter 4.4

At this point it is worth to mention that during the project assignment, last semester, a totally different approach was implemented. In particular, a Monte Carlo method was utilized in order to generate a random varying ice thickness field based on a specific mean value and a standard deviation. This simulation was successfully implemented by (Su, Riska and Moan 2010) in order to generate an ice field where the ice thickness was randomly generated by using a certain specified probability distribution along an ice sheet. If a normal distribution is assumed then the cumulative distribution function (CDF) F(X) and its inverse $F^{-1}(U)$ can be expressed (Su, Riska and Moan 2010):

$$F(X) = \frac{1}{\sqrt{2\pi}\sigma} \int_{-\infty}^{X} e^{\left[\frac{-(s-\mu)^2}{2\sigma^2}\right]} ds$$

$$U \sim U(0,1)$$

$$X = F^{-1}(U_r)$$

(2.8)

Where:
- X: Random variable
- μ: Mean value of the random variable
- σ: Standard deviation
- U_r: Randomly generated number between 0 and 1

If a particular mean value and standard deviation are given, then a random value of X can be generated. These values can be obtained from statistical analysis of datasets like the ice charts in Figure 2.6.

However, the random varying ice thickness field that was generated, did not correspond to a realistic level ice field such as the measured one at all. This can easily be observed by comparing the figure below and Figure 2.9. As a result the data manipulation approach is finally utilized as explained above.
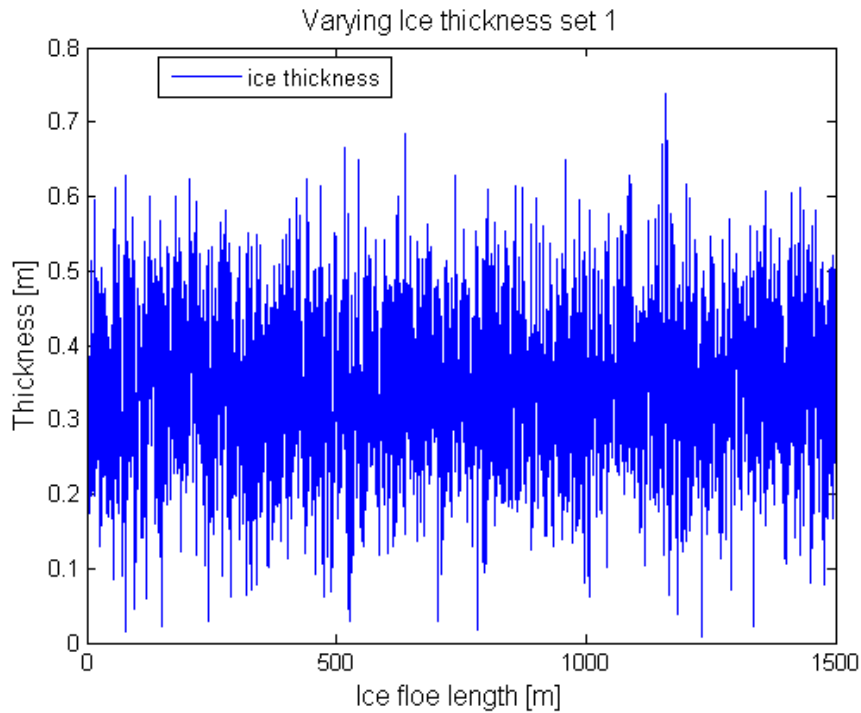
Figure 2.10 Ice varying thickness (pre - thesis project)

2.6 Dynamic analysis of spar floating wind turbines

In the case of a spar floating wind turbine, the buoyancy force comes from a hollow cylindrical substructure which supports the whole wind turbine while the tension of mooring lines keeps the station position of the structure. The dynamics of a spar-type offshore wind turbine due to wind, wave and ice excitations is usually evaluated in terms of rigid body degrees of freedom as a floating structure. The station keeping regarding the horizontal degrees of freedom surge and sway are mainly influenced by the mooring system, while the other degrees of freedom are largely affected by the floating platform characteristics (Jeon, et al. 2013).

The equation of motion of the structure can be written in the frequency domain as (Gao and Bachinsky 2014):

$$-w^2\big(\mathbf{M} + \mathbf{A}(w)\big)\eta + iw\mathbf{B}(w)\eta + \mathbf{C}(w) = F(w) \qquad \textbf{(2.9)}$$

Where:
- **M:** The mass of the structure
- **A:** The added mass
- **B:** Linear damping
- **C:** The restoring force

Equation (2.9) can be rewritten by defining the following terms (Gao and Bachinsky 2014):

$$
\begin{aligned}
\mathbf{A}(w) &= a(w) + A_\infty \\
\mathbf{B}(w) &= b(w) + B_\infty = b(w) \\
\mathbf{K}(w) &= iwa(w) + b(w)
\end{aligned}
\tag{2.10}
$$

Combining Equation (2.9) and (2.10) and using an inverse Fourier transform, then Equation (2.9) is expressed in the time domain:

$$
(\mathbf{M} + A_\infty)\ddot{\eta}(t) + \int_{-\infty}^{+\infty} k(t-\tau)\dot{\eta}(\tau)d\tau + C\eta(t) = F(t)
\tag{2.11}
$$

The second term in the above equation is a convolution integral and k is the retardation function that shows the memory effects caused by the free surface. It can be noted though, *"linear hydrodynamic damping is not included because in ice covered water the ice load is considered to be the most major source of energy consumption"* (i.e. B=0) (Tan, Riska and Moan 2013). The convolution integral is also zero and the **A** matrix is not considered frequency dependent.

Generally, the motion of the structure around its mean oscilatory position can be also written as (Faltinsen 1990), (Bredmose 2014):

$$
(\mathbf{M} + \mathbf{A})\ddot{\eta}(t) + \mathbf{B}\dot{\eta}(t) + \mathbf{C}\eta(t) = F(t)
\tag{2.12}
$$

Where:
  M: The mass of the structure
  A: The added mass
  B: The damping coefficient
  C: The restoring force

It should also be noted that displacement η is a vector containing the six degrees of freedom, three translations and three rotations, meaning: $\eta = [\eta_1\,\eta_2\eta_3\,\eta_4\,\eta_5\,\eta_6\,]^T$. The index 1 to 6 indicate the degrees of freedom surge, sway, heave, roll, pitch and yaw respectively and according to Figure 2.11.
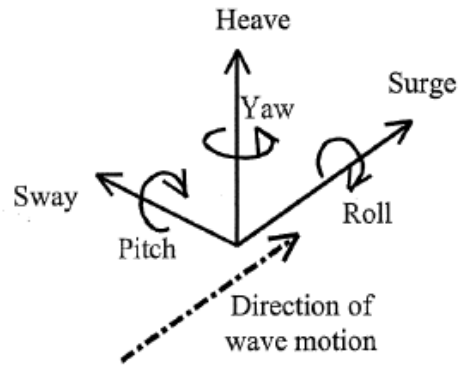
Figure 2.11 Degrees of freedom coordinate system

The force F(t) it should include the following loads:

- Ice loads

- Aerodynamic loads

- Hydrodynamic loads on mooring lines

- Hydrodynamic loads

Moreover, the M, A and C matrixes can be expressed according to (Faltinsen 1990) and (Bredmose 2014):

$$
M = \begin{bmatrix}
M & 0 & 0 & 0 & M_{ZG} & 0 \\
0 & M & 0 & -M_{ZG} & 0 & 0 \\
0 & 0 & M & 0 & 0 & 0 \\
0 & -M_{ZG} & 0 & I_4 & 0 & -I_{46} \\
M_{ZG} & 0 & 0 & 0 & I_5 & 0 \\
0 & 0 & 0 & -I_{46} & 0 & I_6
\end{bmatrix}
\tag{2.13}
$$

$$
A = \begin{bmatrix}
A_{11} & 0 & A_{13} & 0 & A_{15} & 0 \\
0 & A_{22} & 0 & A_{24} & 0 & A_{26} \\
A_{31} & 0 & A_{33} & 0 & A_{35} & 0 \\
0 & A_{42} & 0 & A_{44} & 0 & A_{46} \\
A_{51} & 0 & A_{53} & 0 & A_{55} & 0 \\
0 & A_{62} & 0 & A_{64} & 0 & A_{66}
\end{bmatrix}
\tag{2.14}
$$

$$
C = \begin{bmatrix}
0 & 0 & 0 & 0 & 0 & 0 \\
0 & 0 & 0 & 0 & 0 & 0 \\
0 & 0 & C_{33} & 0 & C_{35} & 0 \\
0 & 0 & 0 & C_{44} & 0 & 0 \\
0 & 0 & C_{53} & 0 & C_{55} & 0 \\
0 & 0 & 0 & 0 & 0 & 0
\end{bmatrix}
\tag{2.15}
$$

However, it needs to be mentioned that the HAWC2 programme uses a different coordinate system than the one depicted in Figure 2.11. Therefore, attention must be paid when

implementing the load model into the software. In the upcoming sections a load implementation review will be presented case by case.

In HAWC2, Equation (2.12) is solved by the Newmark method. It is a step by step integration in time method and the main assumption is that the acceleration between times t_i and t_{i+1} varies linearly between each time step:

$$\ddot{\eta}_{k+1} = \ddot{\eta}_k + (\ddot{\eta}_{k+1} - \ddot{\eta}_k)\gamma \tag{2.16}$$

The parameters β and γ are fixed as the default ones and ensure the unconditional stability of the method. The method is unconditionally stable if (Langen and Sigbjornsson 1977):

$$\gamma \geq \frac{1}{2} \; (\gamma = 0.51 \; in \; this \; case)$$
$$\beta \geq \frac{1}{4}\left(\gamma + \frac{1}{2}\right) = 0.255025 \; (\beta = 0.27 \; in \; this \; case) \tag{2.17}$$

The method is based on the following integral equation for the velocity and the displacement at the $(k+1)^{th}$ timestep (Langen and Sigbjornsson 1977), (Tan, Riska and Moan 2013):

$$\dot{\eta}_{k+1} = \dot{\eta}_k + h[\gamma\ddot{\eta}_{k+1} + (1 - \gamma)\ddot{\eta}_k)]$$
$$\eta_{k+1} = \eta_k + \dot{\eta}_k h + \frac{1}{2}h^2[2\beta\ddot{\eta}_{k+1} + (1 - 2\beta)\ddot{\eta}_k)] \tag{2.18}$$

Where:
    h: The timestep length

At each timestep Equation (2.12) should be satisfied:

$$(\mathbf{M} + \mathbf{A})\ddot{\eta}_{k+1} + \mathbf{B}\dot{\eta}_{k+1} + \mathbf{C}\eta_{k+1} = \mathrm{F}_{k+1} \tag{2.19}$$

Together with Equation (2.18) the incremental displacement is derived:

$$\Delta\eta_{k+1} = \dot{\eta}_k h + \frac{1}{2}h^2(1 - 2\beta)\ddot{\eta}_k) + (\mathbf{M} + \mathbf{A})^{-1}(F_{k+1} - C\eta_{K+1})2h^2\beta \tag{2.20}$$

The variables are updated and can be used as initial values for the next iteration:

$$\ddot{\eta}_{k+1} = \frac{1}{h^2\beta}[\Delta\eta_{k+1} - \dot{\eta}_k h - \frac{1}{2}h^2(1 - 2\beta)\ddot{\eta}_k)]$$
$$\dot{\eta}_{k+1} = \dot{\eta}_k + \Delta\dot{\eta}_{k+1}$$
$$\eta_{k+1} = \eta_k + \eta_{k+1} \tag{2.21}$$

2.7 Ice loads

The ice actions that occur during the most interesting failure mechanisms are going to be presented. Firstly, the ice actions due to crushing and afterwards the ice actions due to bending will be introduced according to both the ISO and IEC standards. These methods form a solid basis and according to (Bjerkås, Albrektsen and Gürtner 2010) more work is needed to figure out the most realistic load amplitudes for predefined loading functions.

2.7.1 Ice loads on vertical structures

When ice crushing occurs against a structure, the global ice action normal to the surface can be expressed according to the following equation (ISO19906 2010).

$$F_G = p_G A$$
$$p_G = C_R \left(\frac{h}{h_1}\right)^n \left(\frac{w}{h}\right)^m \tag{2.22}$$

Where:

p_G: Ice pressure averaged over the nominal contact area

A: Nominal contact area

w: Projected width of the structure

h: Thickness of the ice sheet

h_1:   Reference thickness (1 m)

m: Empirical coefficient (=0.16)

n: Empirical coefficient (=-0.5+h/5 for h<1 m and -0.3 for h≥1m)

C_R: Ice strength coefficient (obtained from data)

Apart from the ice thickness that plays a significant role in the ice action when ice crushes, it should be mentioned that the drifting velocity of ice is very important as well. According to (ISO19906 2010) and (DNV-GL 2014), the ice velocity arises ice-structure dynamic processes. However, it should be noted that the ISO equations do not include any velocity components.

Key

t   time

F   ice action

u   structure displacement
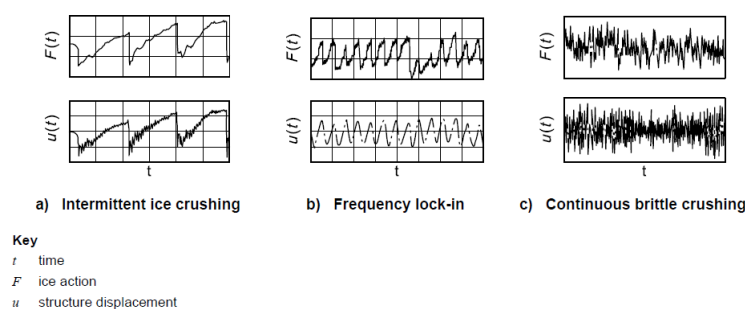
Figure 2.12 Modes on time varying action and the corresponding dynamic response component (DNV-GL 2014)

The figure above illustrates the three main modes that occur when ice crushes onto a structure. These modes mainly depend on the ice drifting velocity.

Intermittent ice crushing: Low and intermediate velocities, resulting loads that are dynamic, which may or may not have a regular pattern either in peak ice load or in period of interaction. The peak load is governed by brittle crushing although the load rise is covered by creep behaviour.

Frequency lock in: This is a special case of intermittent crushing at intermediate velocities where the ice load frequency matches that of the structure. This behaviour can result in highly amplified response of the structure.

Continuous brittle crushing: Highest velocities resulting a sustained crushing load but with low amplitude random vibrations. Here the pressures are lower than at intermediate velocities, though very high local pressures may occur as well.

It is also suggested by DNV-GL one extra mode, that is omitted from the ISO. The mode suggested by DNV-GL is called Creep or Plastic Deformation. This occurs in low relative velocities, resulting in sustained forces without any significant dynamic component, thus can be considered as a static load.

On the other hand, IEC uses a different approach in calculating the ice actions on vertical cylindrical shapes. The maximum static force due to crushing may be estimated from:

$$H_D = k_1 k_2 k_3 h D \sigma_C \qquad \textbf{(2.23)}$$

Where:

k_1: Shape factor for the shape of the support structure on the ice impact side

=1 for rectangular shape

=0.9 for circular shape

k_2: Contact factor for the ice contact against the support structure
=0.5 when ice is continuously moving
=1 when ice is frozen to the support structure surface at the time the ice starts moving
=1.5 when frozen ice is locally increased in thickness around the support structure

k_3 $= \sqrt{1 + 5h/D}$

D: Diameter of the support structure at the waterline

σ_C: Crushing strength of ice, determined from statistical data

Also, IEC suggests other equations when dynamic loading occurs on the structure due to movement of the ice sheet.

$$H_{dyn} = H_D(\frac{3}{4} + \frac{1}{4}\sin(2\pi f_N t)) \qquad \textbf{(2.24)}$$

Where:

t: time

f_N: Wind turbine structural eigenfrequency.

The criterion for tuning, which can be parallelized as the frequency lock in, according to (Singh, et al. 1990) is:

$$\frac{U}{hf_N} > 0.3 \qquad \textbf{(2.25)}$$

Where:

U: Ice floe speed

It is observed that in the IEC is not emphasising in the different ice velocities and the corresponding crushing that may occur (ductile, brittle) contrary to the ISO.

2.7.2 Ice loads on conical structures

When an ice sheet acts on a wide slope or cone, the flexural failure component can be evaluated considering the ice sheet as an elastic beam on elastic foundation. This method can also be used for downward breaking slopes by replacing ice weight in air by ice buoyancy in water. Utilizing the physics between an upward against downward bending it is found that the flexural strength of the ice is different for upward and downward bending.

It should be noted that in the ISO19906 the flexural strength is calculated as an average flexural strength over the ice thickness and therefore cannot distinguish between upward or downward bending (Hoving 2015).

However, (Frederking and Schwarz 1982) have shown that a downward breaking cone experiences lower ice forces than an upward breaking cone reducing both the horizontal and vertical ice actions. In addition to that, a downward breaking cone would have a more immediate application in a floating structure.

The general pattern that is followed by an ice sheet when approaching a sloped cone can be presented as following:

1.   Loading
2.   Unloading
3.   No loading
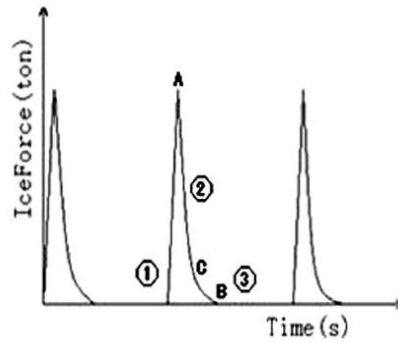
Figure 2.13 Ice force variation during interaction with cone (Xu and Yue 2014)

A simplified approach of "loading" can be applied when a level ice sheet interacts with a sloping cone.
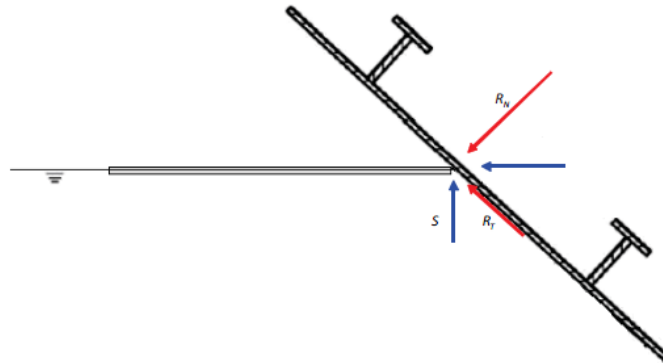
Figure 2.14 2D modelling of interaction of level Ice with a sloped cone (Metrikine 2015)

This interaction can be modelled according to the following equations:

$$S = R_T \sin\varphi_w - R_N \cos\varphi_w$$
$$N = R_T \cos\varphi_w + R_N \sin\varphi_w \qquad \text{(2.26)}$$
$$R_T = \mu_S R_N$$

Where:

μ_S: Kinematic friction coefficient between beam and wall

φ_w: Wall angle

S: Transversal force in the edge of the beam per unit width

N: Normal force in the edge of the beam per unit width

R_T: Tangential reaction force on the wall per unit width

R_N: Normal reaction force on the wall per unit width

Also, the relation between the vertical and horizontal components is:

$$S = \frac{N}{\xi}$$

(2.27)

Where:

$$\xi = \frac{\sin a + \mu_s \cos a}{\cos a - \mu_s \sin a}$$

These equations correspond to one dimension modelling of an ice sheet when it approaches a downward sloping cone.

In the beginning it was mentioned that the ice sheet can be considered as an elastic beam on elastic foundation. According to this model the horizontal action component S, can be determined (ISO19906 2010):

$$S = \frac{H_B + H_P + H_R + H_L + H_T}{1 - \frac{H_B}{\sigma_f l_C h}}$$

(2.28)

Where:

H_B: Breaking load
H_P: Load component required to push the sheet ice through the ice rubble
H_R: Load to push the ice blocks up the slope through the ice rubble
H_L: Load required to lift the ice rubble over the advancing ice sheet prior to breaking

H_T: Load to turn the ice block at the top of the slope (=0 for downward cone)

R_N: Normal reaction force on the wall per unit width

l_C: Total length of the circumferential crack $l_C = w + \frac{\pi^2}{4} L_C$

The load component H_B is given by:

$$H_B = 0.68 \xi \sigma_f \left(\frac{p_w g h^5}{E}\right)^{0.25} \left(w + \frac{\pi^2 L_c}{4}\right)$$

(2.29)

Where:

p_w: Sea water density
g: Gravity acceleration
E: Elastic modulus of ice

$$L_C = \left[\frac{E h^3}{12 p_w g (1 - v^2)}\right]^{1/4}$$

(2.30)

Where:

v: Poisson ratio

The load component H_P is given by:

$$H_P = w h_r^2 \mu_i p_i g (1-e) \left(1 - \frac{\tan\theta}{\tan a}\right)^2 \frac{1}{2\tan\theta}$$

(2.31)

Where:

- h_r: Rubble height
- μ_i: Ice to ice friction coefficient
- e: Porosity of the ice rubble
- θ: Angle the rubble makes with the horizontal

The load component H_R is given by:

$$H_R = wP \frac{1}{\cos a - \mu \sin a}$$

(2.32)

Where:

$$P = 0.5\mu_i(\mu_i + \mu)p_i g(1-e)h_r^2 \sin a \left(\frac{1}{\tan\theta} - \frac{1}{\tan a}\right)\left(1 - \frac{\tan\theta}{\tan a}\right)$$
$$+ 0.5(\mu_i + \mu)p_i g(1-e)h_r^2 \frac{\cos a}{\tan a}\left(1 - \frac{\tan\theta}{\tan a}\right) + h_r h p_i g \frac{\sin a + \mu\cos a}{\sin a}$$

The load component H_L is given by:

$$H_L = 0.5 w h_r^2 p_i g(1-e)\xi\left(\frac{1}{\tan\theta} - \frac{1}{\tan a}\right)\left(1 - \frac{\tan\theta}{\tan a}\right) + 0.5 w h_r^2 p_i g(1-e)\xi\left(1 - \frac{\tan\theta}{\tan a}\right)^2$$
$$+ \xi c w h_r \left(1 - \frac{\tan\theta}{\tan a}\right)$$

(2.33)

Where:

- c: Cohesion of the ice rubble
- φ: Friction angle of the ice rubble

The load component H_T is given by:

$$H_T = 1.5 w h^2 p_i g \frac{\cos a}{\sin a - \mu\cos a}$$

(2.34)

Of course, dynamic behaviour can also be observed in ice interaction with conical structures. The vibrations are enhanced when stable ice rubble does not form in front of the front face of the cone. The time history of this kind of ice action is illustrated in Figure 2.15.
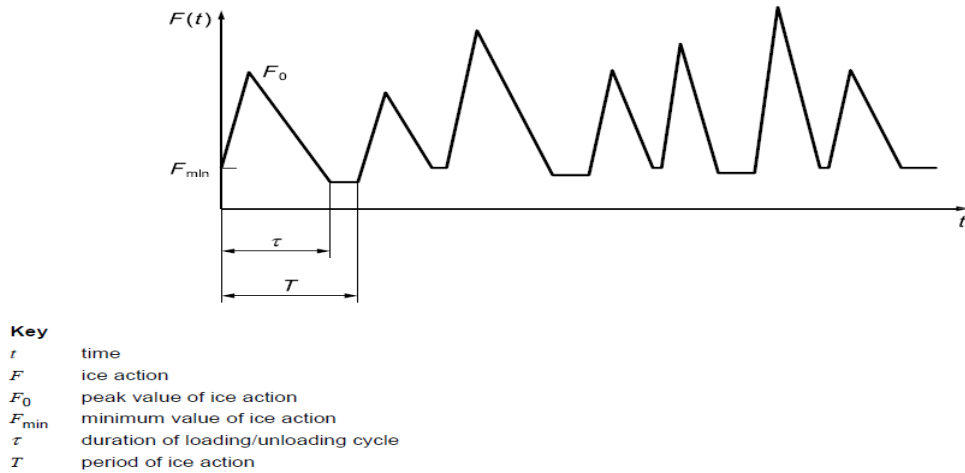
Figure 2.15 Dynamic horizontal action on a conical structure (ISO19906 2010)

The dynamic response of the structure due to this kind of random forcing function is less than due to frequency lock-in on a similar vertical structure.

Again, similarly to the ice loads on a vertical structure, IEC suggests the equation by Ralston (1977), in order to compute the horizontal and vertical loads on a sloped structure. In correspondence with Figure 2.14 the horizontal load can be written as N and the vertical as S:

$$S = B_1 H + B_2 p_w gh(D^2 - D_T^2)$$
$$N = A_4 \left[A_1 \sigma_b h^2 + A_2 p_w ghD^2 + A_3 p_w gh(D^2 - D_T^2) \right]$$

(2.35)

Where:

A_{1-4}, B_{1-2}: Dimensionless coefficients functions of the ice to cone friction coefficient μ_s and the cone angle α. Values can be taken from graphs.

σ_b: Bending strength of ice

D: Waterline cone diameter

D_T: Cone top diameter

It should be mentioned that for a downward bending cone the only change is that the p_w should be replaced by $\frac{p_w}{9}$.

The dynamic variation of loading IEC suggests may be approximated by the following formula:

$$H_{dyn} = H_D \left(\frac{3}{4} + \frac{1}{4} \sin(2\pi f_B t) \right)$$

(2.36)

Where:

f_B= U/Kh, the value of K which gives the highest load should be chosen 4≤K≤7

It is observed that this equation is very similar to Equation (2.24). The only difference is that here, the effect of the ice sheet velocity is taken into account in a more direct way.

Ice interaction with a surface (vertical or sloped) will cause dynamic effects. The most interesting effect is the vibrations that are induced when the ice floe interacts with a sloped structure. Nonetheless, according to a study by (Xu et al. 2011) based on full scale measurements; the most dominant vibration that occurs is a random vibration. Moreover, the most dangerous vibration --the quasi resonant vibration-- seldom happens. Therefore, when a cone is deployed at the waterline of a vertical structure not only causes the ice actions being reduced but also it almost eliminates dangerous vibrations that could occur.

2.8 Ice failure mechanism

To assess the design ice actions due to an ice - structure interaction scenario, the type of ice-structure interaction has to be determined first. Three different types of ice - structure interactions are defined, where each type of interaction is described by a limiting mechanism. A limiting mechanism can be defined as: The interaction mechanism that limits the ice action on a structure. According to the ISO19906 and DNV-GL the three limiting mechanisms and the corresponding types of ice - structure interaction that are identified are:

- Limit Energy - Ice Impact
- Limit Force - Driving Forces
- Limit Stress - Ice Failure

The most relevant limiting mechanism for the current project is the Limit Stress one. Limit stress will only occur when the driving forces are large enough to cause the interacting ice feature to fail. Ice actions for limit stress largely depend on: The geometry of the ice - structure interaction and the occurring failure mode, such as crushing, bending, splitting, spalling or buckling.

Crushing is the failure mode that occurs extensively in vertical shaped structures. The term crushing refers to a complex compressive failure process, involving the development of a damaged layer as well as sequential development of horizontal splits or cleavage cracks as well as flakes or spalls (ISO19906 2010) , (DNV-GL 2014).

a) Ice sheet interaction with the flat surface of a narrow vertical structure

b) Profile of ice sheet interaction with vertical structure
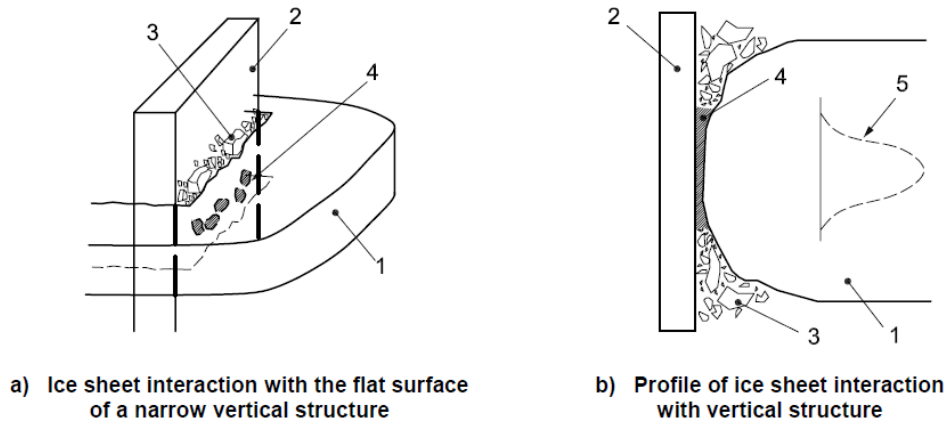
Key

1   ice sheet
2   structure
3   spalls and extrusion
4   high pressure zones in a), layer of crushed ice of high pressure zone in b)
5   pressure distribution over the contact surface

Figure 2.16 Crushing failure, schematic interaction

As it is observed from Figure 2.16, in the beginning the high pressure zones are the ones which are crushed first. As these pieces are moved away, another surface takes their place as the ice is moved towards the structure and new high pressure zones are formed. This procedure repeats its self until the whole ice sheet passes through the structure.

On the other hand, the failure mode of bending is the more appropriate to be examined due to the fact that the wind turbine used in the models has a downward conical structure deployed at the mean sea level. Ice actions in such failure mode can be significantly lower than in a crushing failure mode (Mroz, Holnicki-Szulc and Karna 2008), (Barker, et al. 2005), which is typical for vertical sided structures.
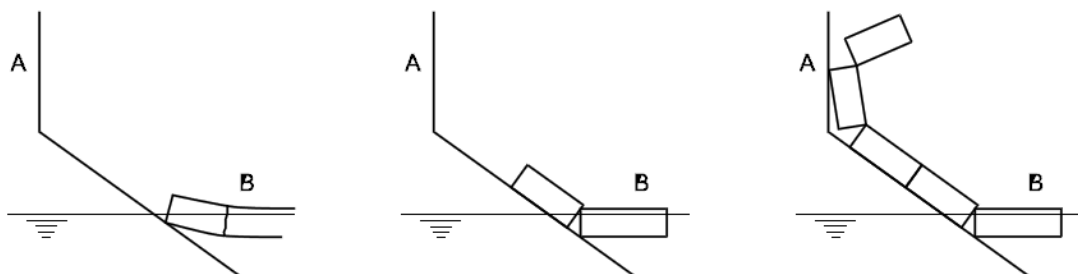
Figure 2.17 Ice interaction with an upward sloping surface (ISO19906 2010)

Key
A   open water in wake of structure
B   encroaching ice sheet
C   top of sloping face of structure
D   waterline of structure
E   cracks forming in encroaching ice sheet
F   clearing of ice rubble blocks around structure
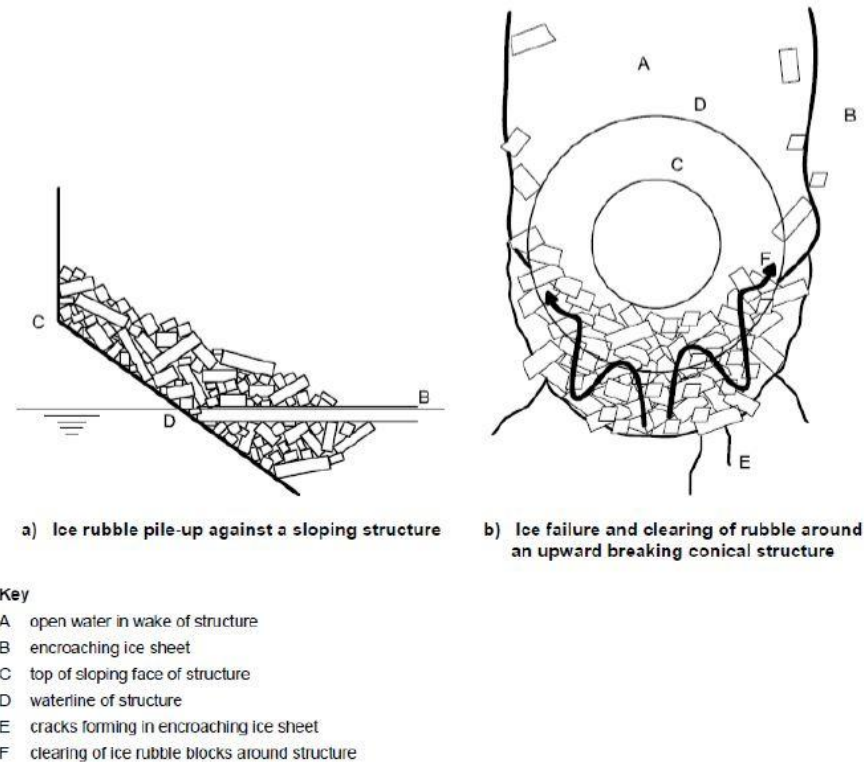
Figure 2.18 Ice rubble pile-up and clearing around a sloping structure (upward cone) (ISO19906 2010)

Throughout Figure 2.17 and Figure 2.18 the understanding of the ice interaction with a bending cone can become easier.

- The ice floe approaches the structure until contact occurs
- The floe is compressed and gets lifted up along the interacting surface
- Radial and circumferential crack appear (Kerr 1975). They propagate and an increase of the ice force occurs until the ice floe fails in bending.
- The ice rides up the face of the structure
- Ice rubble accumulates and gets cleared by the sides of the cone

These findings come to an agreement with (Wang, et al. 2014). According to their study, when the ice sheet meets a sloped cone spalling of flaking occurs first and as soon as the sheet is loaded at the junction of the cone bending failure follows.

2.9 Modelling of the ice - structure interaction

The ice load model is implemented into HAWC2 using an external DLL (Dynamic Link Library) file. The global ice load is calculated by integration of the local forces over the contact zones. The numerical procedure is briefly described in the next points:

i.   Definition of geometry

Regarding the ice edge, initially the geometry is set arbitrarily. As the procedure continues the boundary conditions for the ice edge are obtained by the ice - structure interaction. When the waterline surface of the wind turbine is defined, the motions due to the six DOF of the structure are taken into account. The waterline surface is determined by the instantaneous waterline and an assistant waterline as depicted in the next figure. This geometry, aims towards the detection of the contact area.
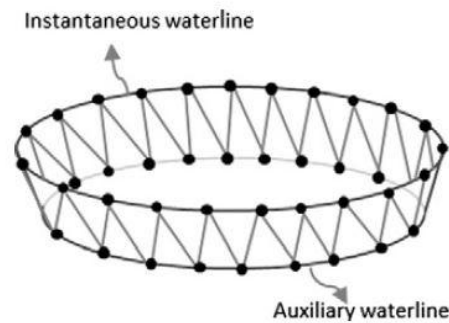
Figure 2.19 Geometry at the MSL (Shi, et al. 2016)

ii.   Contact detection

The main idea in order to determine whether there is contact of the ice edge with the wind turbine, is to look for overlaps between the ice floe and the wind turbine as shown in the figure below.
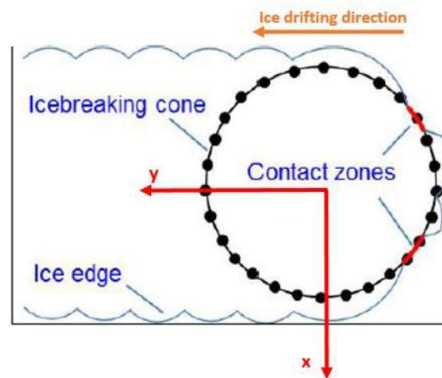
Figure 2.20 Contact detection procedure

The contact area A_{cr} can be calculated based on the indentation depth L_d, the contact length L_h, the cone angle φ and the ice thickness h_i. There are two types of contact interfaces as depicted in Figure 2.21 that may occur.

$$A_{cr} = \begin{cases} \dfrac{1}{2} L_h \dfrac{L_d}{\cos\varphi}, L_d \tan\varphi \leq h_i \ (\text{Case 1}) \\ \dfrac{1}{2} \left(L_h + L_h \dfrac{L_d - \dfrac{h_i}{\tan\varphi}}{L_d} \right) \dfrac{h_i}{sin\varphi}, L_d \tan\varphi > h_i \ (\text{Case 2}) \end{cases}$$ (2.37)
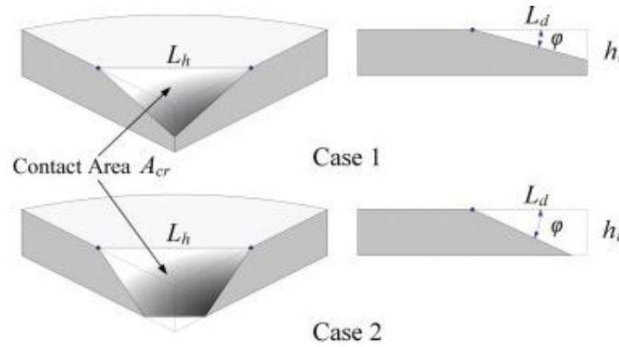
Figure 2.21 Ice contact geometry, 2 cases (Su, Riska and Moan 2010)

i. Determination of local crushing force

As soon as the contact area is determined, the local crushing force due to the ice - structure interaction can be calculated. In order to calculate this force, the model proposed by (Riska 1995) is used.

$$F_{cr} = p_{av} A_{cr}$$ (2.38)

Where:

p_{av}: Average contact pressure

A_{cr}: Contact area

The average contact pressure most importantly depends on the magnitude of the contact area.

$$p_{av} = k A_{cr}^n$$ (2.39)

Where:

k, n: Empirical parameters

ii. Determination of contact forces

The next step is to calculate the contact forces. This is done by integrating the local forces over all the contact zones.
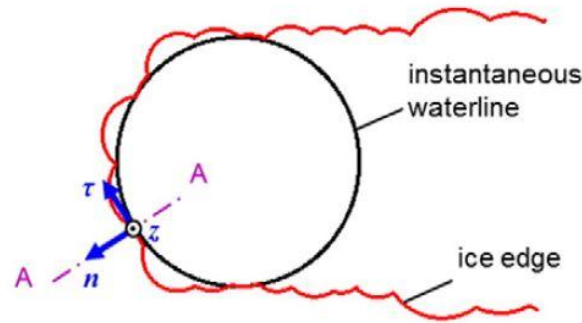
Figure 2.22 Local contact zone (Shi, et al. 2016)
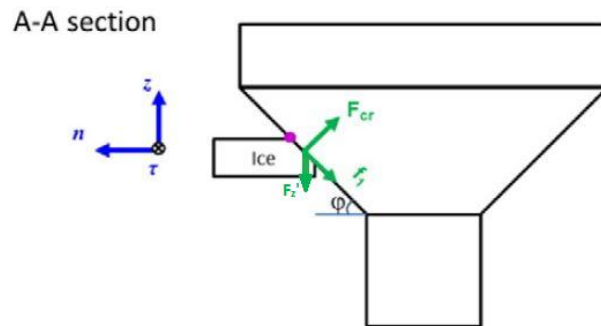
Figure 2.23 Contact force on the structure (Shi, et al. 2016)

The structure is loaded as in Figure 2.23 with crushing and friction forces, F_{cr} and f_1 respectively. Their reactions are seen by the ice sheet and as a result the vertical reaction force F'_z reads $F'_z = -F_z = -(F_{cr}\cos\varphi - f_1\sin\varphi)$. Finally, after substituting the analytical expressions for F_{cr} and f_1 it is obtained:

$$F'_z = \left(\cos\varphi - \mu \frac{v_n\sin\varphi\cos\varphi + v_z\sin^2\varphi}{\sqrt{v_\tau^2 + (v_n\cos\varphi + v_z\sin\varphi)^2}} \right) p_{av}A_{cr} \qquad (2.40)$$

Where:
- v_n: Normal velocity component
- v_z: Tangential velocity component
- v_τ: Tangential velocity component to the contact surface
  (See Figure 2.22, Figure 2.23)

This load is the one responsible for the downward bending of the ice floe and analytical information regarding the derivation of the above formulas can be found in (Tan, Riska and Moan 2013) work. Finally, when the minimum load required for the ice flow to break is reached, failure occurs.

2.9.1 Semi - empirical constant thickness model

An offshore wind turbine is subjected to excessive dynamic effects and the aforementioned standards and guidelines are not always suitable for the design of such structures. (Shi, et al 2016). As a result, a more appropriate model is adopted in order to capture these dynamic effects due to the ice - structure interaction. The semi - empirical model for constant ice thickness which forms the basis of this study and is going to be upgraded, is briefly explained below and detailed information can be found in (Tan, Riska and Moan 2013) work.

This model, was initially implemented for icebreakers. An icebreaker moves forward and has the ability to clear the ice rubble that accumulates underneath the hull. The same principle stands for the wind turbine. The difference is that the turbine does not move forward but the ice floe drifts towards the structure. Therefore, the assumption that the ice rubble is well cleared from underneath the downward cone is necessary to be done.

   i.   Bending failure criterion

It has been shown that a vertical force is acting on the ice edge due to crushing and friction action. When the vertical force (Equation (2.40)) exceeds the bearing capacity P_f of the ice edge, bending failure occurs.

$$P_f = (1.65 + 2.47v_2^{0.4})\sigma_f h_i^2 \left(\frac{\theta_w}{\pi}\right)^2 \tag{2.41}$$

Where:
v_2:	The normal relative speed of the ice floe
σ_f:	Flexural strength of ice
h_i:	Ice floe thickness
$\left(\frac{\theta_w}{\pi}\right)^2$:	Geometry factor specifying the wedge size in circumferential dimension

Equation (2.41) has been determined semi-empirically by (Tan, Riska and Moan 2014) based on Kashtelyan's work (Kerr 1975) and (Varsta 1983) studies. The initial equation obtained by Kastelyan, is experimentally determined and considers the static loading case of an actual sea ice wedge floating on the sea:

$$P_f = c_f \sigma_f h_i^2 \left(\frac{\theta_w}{\pi}\right)^2 \tag{2.42}$$

Where:
c_f:	Experimental coefficient

So, for Equation (2.41) one can observe that the coefficient c_f is modified accordingly in order

to account for the relative speed between the ice floe and the structure and thus consider dynamic effects.

ii.   Ice breaking pattern

As explained in the ice failure mechanism (section 2.8) when ice breaks, radial and circumferential cracks appear. Based on the studies of (Enkvist 1972) and (Varsta 1983); (Wang 2001) suggested that the shape of the circumferential crack can be modelled as a circular arc and the size of the broken ice floe can be determined by a quantity called "ice floe radius".

$$R = C_l l(1 + C_v v_2)$$ (2.43)

Where:

C_l, C_v: Empirical coefficients (equal to 0.1 and -0.1 respectively)

$$l = \left[\frac{E h_i^3}{12 \rho_w g (1 - v^2)} \right]^{1/4}$$ (2.44)

Where:

    v: Poisson ratio
    g: Gravity acceleration
    E: Elastic modulus of ice
    ρ_w: Density of sea water
    h_i: Ice thickness

The characteristic length l (Equation (2.44)) is coming from static theory of a plate on elastic foundation. In this particular case though, the effect is rather dynamic but is has been proved by (Fox 2001) that the characteristic length derived for static cases gives a proper length magnitude for dynamic responses as well. Moreover, in (Tan, Riska and Moan, 2014) an supplementary condition is added to describe the geometry that ice fails. Based on (Milano 1973) the ratio between the length ($c_2 l$) and the depth ($c_1 l$) of the formed cusp should be between 3.0 and 6.0.
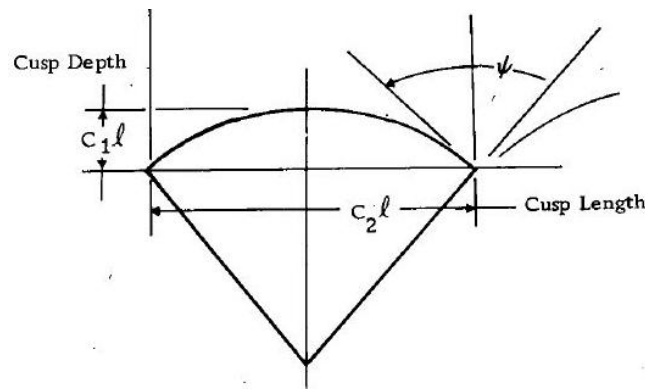

Figure 2.24 Cusp criterion (Milano 1973)

So, the coefficient $C_r = \frac{c_2 l}{c_1 l} = 3.0$ is introduced in the numerical procedure and the broken piece size is adjusted if needed. Based on the size of the broken ice floe, the new geometry of the ice edge can be updated for every time breaking occurs.

This model takes into consideration the whole effect of the ice - spar interaction. Also, it is worth to mention that since the spar has a larger diameter compared to the size of the broken ice piece, the ice floe will have multiple contact points along the circumference of the spar (2.9 ii. Contact detection) and fail at multiple locations. This effect introduces a dynamic effect on the ice loading that is not captured by ISO and IEC standards.

Equations (2.41) and (2.43) account for uniform ice thickness of the ice field while in reality thickness varies along the length of the ice floe. As a result, this model should be updated in order to account for ice floes with varying thickness.

2.9.2 FEM varying thickness model

The new model accounting for the variations in ice thickness is based on the stress distribution along the level ice floe. This, contributes to a more realistic approach of the physical problem.

Initially, the ice floe is modelled as an Euler - Bernoulli beam with varying cross - section. In order to account for the hydrodynamics from the sea, the beam is placed on elastic (Winkler) foundation (Metrikine 2015). The sketch below shows a schematic representation of a simple case of the problem.
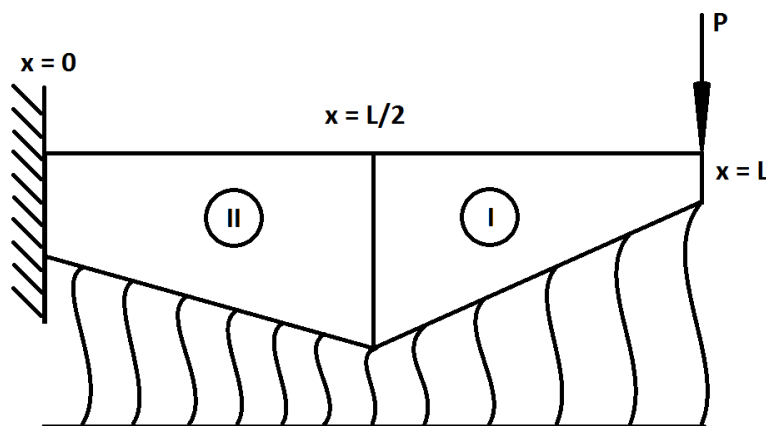

Figure 2.25 Schematic representation of beam with varying cross-section on elastic foundation

The beam has a length L and the thickness is varying along the x axis. The load P is applied at x = L by the downward bending cone when the ice floe is in contact with the spar. At the left

hand side, it is assumed that the beam is clamped at such distance from the ice - structure interaction that the deflection and rotation of the beam are negligible. This simple case can be solved analytically.

First of all, the beam is separated into two domains namely I (L/2<x<L) and II (0<x<L/2). The equation of motion for domain I and II is the same:

$$\frac{d^2}{dx^2}\left[EI(x)\frac{d^2w(x)}{dx^2}\right] + \rho_w g w(x) = 0 \tag{2.45}$$

Where:

E: Elastic Modulus of ice

w(x): Deflection of the beam

I(x): Second moment of area of each cross section $I(x) = \frac{bh(x)^3}{12}$

ρ_w: Density of the water

g: Acceleration of gravity

The boundary conditions at x = L

$$\left.\frac{d^2w(x)}{dx^2}\right|_{x=L} = 0 \tag{2.46}$$

$$\left.EI_I\frac{d^3w(x)}{dx^3}\right|_{x=L} = P \tag{2.47}$$

The boundary conditions at x = 0

$$w(x)|_{x=0} = 0 \tag{2.48}$$

$$\left.\frac{dw(x)}{dx}\right|_{x=0} = 0 \tag{2.49}$$

Of course at x = L/2 there are interface conditions that couple the motion between the two ice blocks.

$$w(L/2)^- = w(L/2)^+ \tag{2.50}$$

$$\frac{dw(L/2)^-}{dx} = \frac{dw(L/2)^+}{dx} \tag{2.51}$$

$$EI_{II}\frac{d^2w(L/2)^-}{dx^2} = EI_I\frac{d^2w(L/2)^+}{dx^2} \tag{2.52}$$

$$EI_{II}\frac{d^3w(L/2)^-}{dx^3} = EI_I\frac{d^3w(L/2)^+}{dx^3} \tag{2.53}$$

Equation (2.45) is solved:

$$E[I''(x)w''(x) + 2w'''(x)I'(x) + I(x)w''''(x)] + \rho_w g = 0 \tag{2.54}$$

In between the generated thickness points (at x = 0, x = L/2 and x = L) linear variation is assumed. Even if the nature of ice formulation is quite random and probably the variation is not actually linear, this gives a neat approximation with the less computational cost than using another variation e.g. quadratic or cubic.

The equation that connects the two adjustment points reads:

$$h(x) = h_i + ax \tag{2.55}$$

Where:
    h_i: Ice thickness at the left hand side of each block
    α: Slope of the connection line

Inserting Equation (2.55) into Equation (2.54):

$$\frac{E}{12}[(h_i + ax)^3 w''''(x) + 6a(h_i + ax)^2 w'''(x) + 6a^2(h_i + ax)w''(x)] + \rho_w g = 0 \tag{2.56}$$

Utilising the substitution of z = h_i+αx, the equation above transforms

$$z^4 w''''(z) + 6z^3 w'''(z) + 6z^2 w''(z) + \frac{12\rho_w g}{a^4 E} zw(z) = 0 \tag{2.57}$$

This is an Euler - Cauchy equation and it can be transformed into a linear equation with constant coefficients by means of the substitution z=e^t. Therefore, the deflection equation w(x) can be found for domain I and II and the corresponding constants can be found by the boundary and interface conditions.

Afterwards, as soon as the deflection equation is determined, by making use of the moment definition $M(x) = -EI(x)\frac{d^2 w(x)}{dx^2}$ and the stress distribution equation for a beam $\sigma(x) = \frac{M(x)y}{I(x)}$, it is possible to identify the spots in the ice floe where the stress exceeds the flexural strength of ice. At this point it should be noted that y is taken as the half average thickness of each ice block ($y = h_{avg}/2$).

Even if this seems like an easy problem to solve analytically; in reality the ice blocks that should be used are significantly more than two. As a result, a numerical procedure should be established in order for this problem to be solved.

The Finite Element Method was selected to proceed with the solution. Initially the beam is discretized per 0.1 m and the corresponding properties (elastic modulus and second moment of area) are assigned to each beam element. An important part in this FEM problem was the

construction of the stiffness matrix including the elastic foundation. The stiffness matrix of a beam element considering bending moment and transversal load at the nodes reads:

$$K_b = \frac{EI}{L^3} \begin{bmatrix} 12 & 6L & -12 & 6L \\ 6L & 4L^2 & -6L & 2L^2 \\ -12 & -6L & 12 & -6L \\ 6L & 2L^2 & -6L & 4L^2 \end{bmatrix} \tag{2.58}$$

Where:

L: Length of each beam element

Moreover, the Winkler's foundation stiffness matrix for each element reads (Janco 2010):

$$K_f = \begin{bmatrix} \dfrac{13bLK}{35} & \dfrac{11bL^2K}{210} & \dfrac{9bLK}{70} & -\dfrac{13bL^2K}{420} \\ \dfrac{11bL^2K}{210} & \dfrac{bL^3K}{105} & \dfrac{13bL^2K}{420} & \dfrac{bL^3K}{140} \\ \dfrac{9bLK}{70} & \dfrac{13bL^2K}{420} & \dfrac{13bLK}{35} & -\dfrac{11bL^2K}{210} \\ -\dfrac{13bL^2K}{420} & -\dfrac{bL^3K}{140} & -\dfrac{11bL^2K}{210} & \dfrac{bL^3K}{105} \end{bmatrix} \tag{2.59}$$

Where:

b: Width of the beam face contact with the foundation

K: Foundation modulus

This stiffness matrix is formulated by utilising energy concepts and detailed information can be found in (Janco 2010) work. The total stiffness matrix of a beam element that accounts for elastic foundation is the sum of Equation (2.58) and (2.59), $K_b + K_f$.

Similarly to the analytical approach once the deflection of the beam is calculated (Mathisen 2015).

$$U = (K_b + K_f)^{-1}P \tag{2.60}$$

Where:

U: Node displacements

P: Applied load

The moment distribution is calculated as well (Mathisen 2015).

$$M(x) = -\frac{EI(x)}{L^2}[B][q] \tag{2.61}$$

Where:

B: Strain displacement vector $[-6L + 12 \quad -4L + 6 \quad 6L - 12 \quad -2L + 6]$

q: Vector of nodal degrees of freedom

Finally the stress distribution is computed revealing the point at which the ice floe will fail. As it was mentioned before, according to (Fox 2001), the characteristic length derived for static cases gives a proper length magnitude for dynamic responses as well. Therefore the characteristic length obtained can be inserted to Equation (2.43) in order to determine the ice floe radius. The coefficients C_l and C_v are empirically determined for constant ice thickness. Nevertheless, for this study, it assumed that the values 0.1 and -0.1 for C_l and C_v respectively can be used for varying ice thickness as well.

Moreover, since circumferential cracks occur during the ice - structure interaction, a way to account for the arc shape ice wedge has to be introduced. The idea is simple and it is based on the angle that the arc forms. According to the angle, each beam element has a specific width b that faces in contact with the foundation.

$$b_i = 2 \cdot L_i \cdot \tan(\theta/2) \tag{2.62}$$

Where:
   i: Number of element
   θ: Angle of the arc (wedge)

As a result, varying widths for each element build up an approximation of an arc and the corresponding failure load is computed. A better overview of this approximation follows in Figure 2.33.

At this point it can be mentioned that serious attempt was made to find the correlation between the ice thickness and the characteristic length, and the correlation between the ice thickness and the failure load when there is a varying thickness ice field. The initiative is underlying in Equations (2.41),(2.43) and (2.44). Since in these equations the dependence from the ice thickness is quite clear, the question on how to account for varying thickness was risen. However, the establishment of analytical expressions is quite complex and enters into deep plate theory analysis on elastic foundation. Moreover, both the failure load and the characteristic length depend on the stress distribution which depends not only on the thickness of each cross section but also on the neighbouring cross sections, increasing the complexity.

Moreover, an alternative solution was tested. A curve was attempted to fit the characteristic length and the failure load with respect to ice thickness. The failure load seems to increase as the ice thickness increases, but for the characteristic length was rather impossible to identify a pattern. However, fitting a curve does not correspond to any physical meaning, therefore this attempt was aborted. The plots though can be seen in Appendix A (page 124).

2.9.3 Numerical procedure explained

The procedure that is used to determine the breaking radius and failure load of a varying thickness ice floe consists of the FEM varying thickness model and some parts from the constant thickness model as explained below.

2.9.3.1 Determination of l, F_{cr}

In the constant thickness model, the thickness of the ice floe is known from the beginning. Based on this thickness, the characteristic length of the ice floe is determined ($l = \left[\frac{Eh_i^3}{12\rho_w g(1-v^2)}\right]^{1/4}$). Afterwards, the initial conditions of the ice floe, meaning the ice edge border, that has been set beforehand becomes known as well (Figure 2.26).
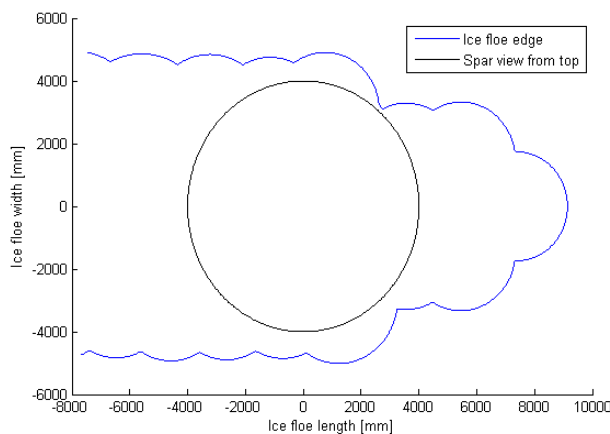
Figure 2.26 Ice floe initial edge and spar   **Figure 2.27 Ice floe initial edge and spar overlap**
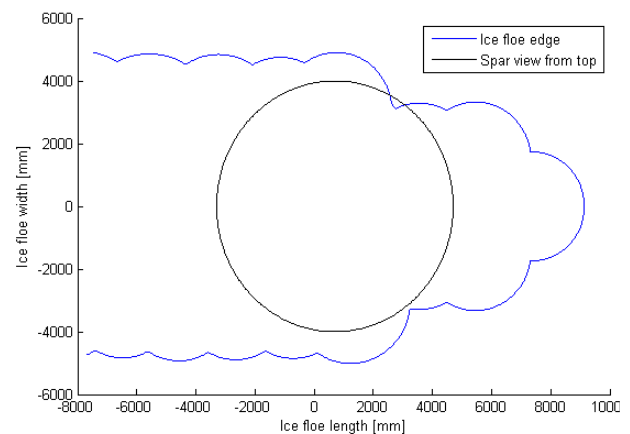
Due to the drifting speed of ice the edge and the whole floe moves towards the structure until contact occurs. Contact occurs whenever an overlap between the structure and ice edge happens (Figure 2.27- note that for simplicity of the figure, the spar was moved forward and the result is the same). As explained in section 2.9 - ii and depicted in Figure 2.21 there are two possible cases of contact. In any case the contact area is determined by use of Equation (2.37) and some geometric tools that can be found in (Su, Riska and Moan 2010). Moreover, the local crushing force is determined by $F_{cr} = kA_{cr}^n \cdot A_{cr}$. Below, Figure 2.22 and Figure 2.23 are repeated for a better overview.
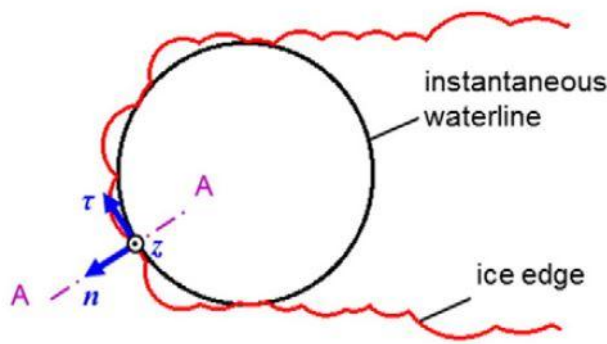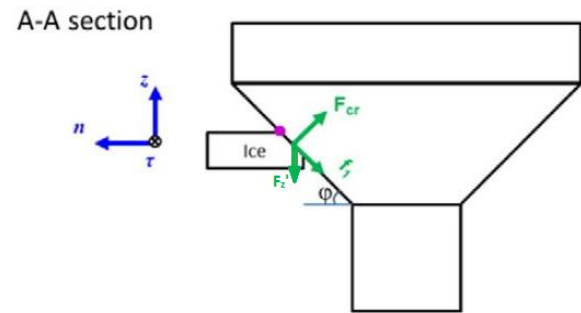
Figure 2.28 Local contact zone (Shi, et al. 2016)

Figure 2.29 Contact force on the structure (Shi, et al. 2016)

The resulting forces from crushing are the crushing force F_{cr} normal to the cone surface and the friction force f_1. By analysis of their reactions, the sum of the vertical components F_z' occurs (Equation (2.40)). It has to be mentioned that in both the constant thickness model and the FEM model the horizontal components of the force analysis are ignored.

2.9.3.2 Determination of R, θ, P_f

The next step in the numerical procedure is the determination of the ice floe radius $R = C_l l(1 + C_v v_2)$ and the angle of the ice wedge.
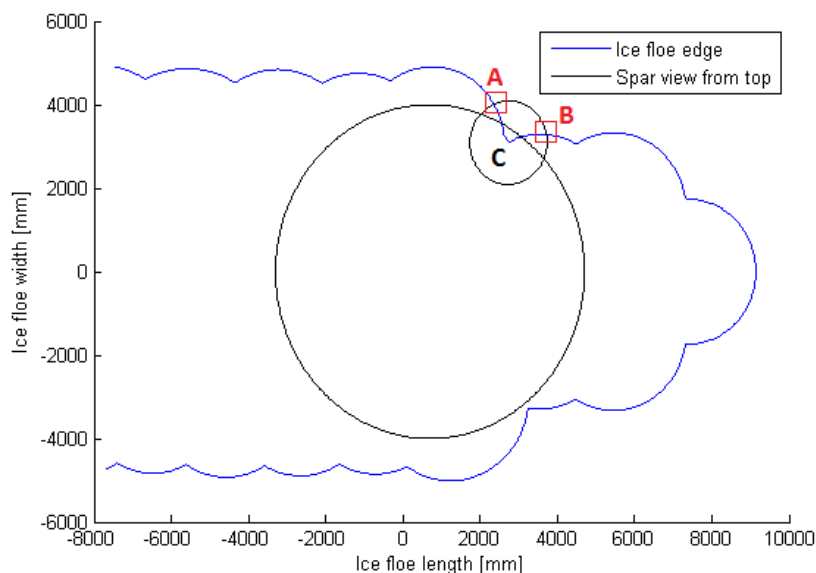
Figure 2.30 Ice floe radius and wedge angle determination

As soon as the ice flow radius is determined, a circle is "drawn" with centre the point of the ice edge (C). This circle has two common points with the ice edge namely A and B. A check is performed whether the cusp size is in accordance with (Milano 1973) criterion and it is adjusted accordingly if needed. With application of geometric tools found in (S. Wang 2001)

and (Su, Riska and Moan 2010) the wegde angle θ is determined. Therefore, the failure load P_f can be determined as well ($P_f = (1.65 + 2.47v_2^{0.4})\sigma_f h_i^2 \left(\frac{\theta_w}{\pi}\right)^2$). This failure load is compared to the vertical load F_z' which is responsible for the bending of the ice floe as explained in 2.9 - ii. The volume of ice that overlaps the downward bending cone is assumed to be crushed. Furthermore, as soon as the failure load P_f is reached, then the ice wedge that corresponds to the CAB area fails in bending and the ice edge geometry is updated. As can be seen in the figure below, the new ice edge is formed and it is going to be used as input for the next timestep. Lastly, the procedure explained may consist of multiple contant points at a time. In this case, everything is looped over the number of contacts.
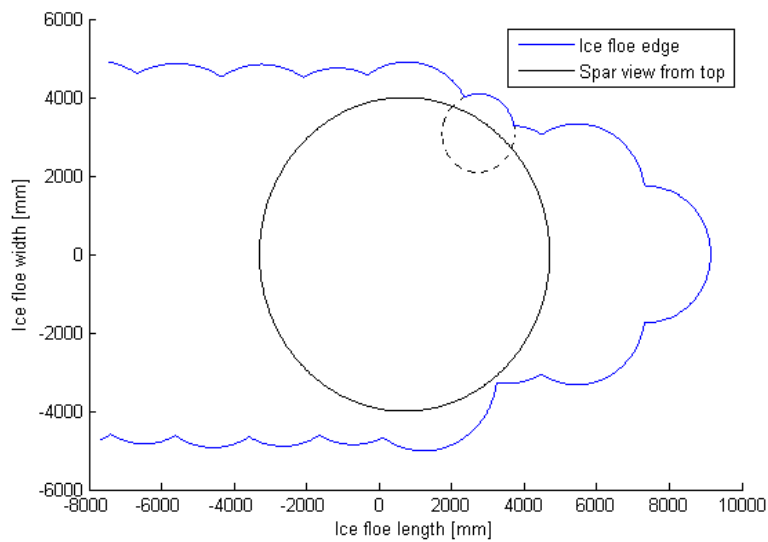
Figure 2.31 Ice edge geometry updated after failure

As mentioned before, the varying thickness model is an update of the constant thickness model. Therefore it is deliberate to list the main assumptions made, before proceeding to the description of the varying thickness model.

a) The wedge angle θ obtained by the constant thickness model is used in the varying thickness model.

b) The contact procedure (overlap method) used in both models has not changed.

c) The computation of the crushing force has not changed between the two models.

d) The same empirical factors for the ice floe radius (C_l and C_v) and for the failure load (c_f) of the constant thickness model are used by the varying thickness model.

These main assumptions considered while updating to the varying thickness model, are discussed regarding their validity and influence on the results, together with some other assumptions of more general interest in section 2.9.4 .

Moving on to the varying thickness model; initially it should be mentioned that the logic behind the model is rather opposite from the semi - empirical constant thickness model. Meaning that, based on a given wedge angle, the failure load for the wedge is determined and whenever the stress due to the applied load exceeds the flexural strength of ice, failure occurs at a known point (section 2.9.2). Moreover, like in the constant thickness model, the characteristic length is determined by the FEM model and used for the computation of the ice floe radius and consequently the corresponding breaking geometry as explained similarly to the constant thickness model. Moreover, the overlapping mechanism for the detection of the contact zones is the same and the crushing force determination still holds.

How the FEM model is actually working though? Regarding the variations in thickness, the beam is discretized per 0.1 m and each beam element constructed by the finite element model, has different thickness and second moment of area assigned to it. The figure below illustrates how each beam element (red rectangular) is constructed based on the example of Figure 2.25 using as thickness the average thickness of each block.
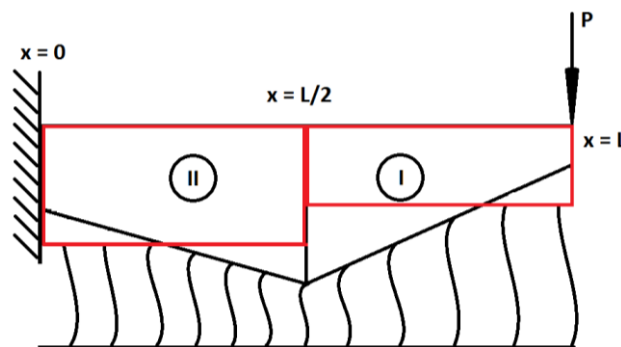

Figure 2.32 FEM beam elements with varying thickness

The greater challenge comes when the beam has to account for the variations in width, meaning that to make the beam account for the ice wedge that is formed. As soon as the wedge angle is known, the geometrical tool constructed assigns to the individual beam elements different widths that are in contact with the elastic foundation as in the following figure.
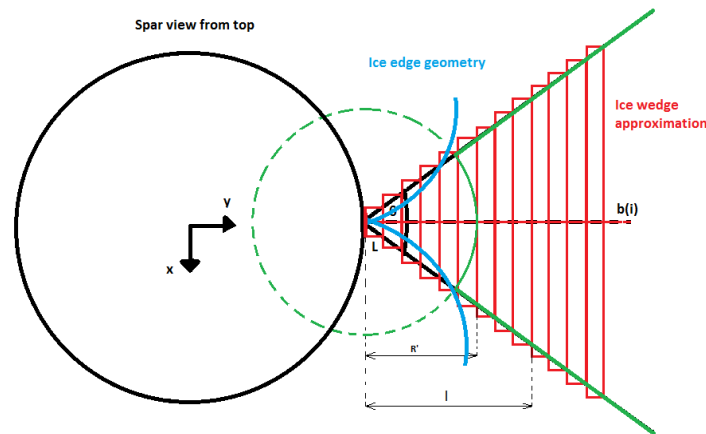
Figure 2.33 FEM different width per element

It can be observed that each beam element has the same length (L) equal to the discretization, 0.1 m. Each width is determined by $b_i = 2 \cdot L_i \tan(\theta/2)$ and the result is the approximation of the ice wedge. A unit load is applied at the contact between the ice and the structure and based on the stress distribution obtained, the minimum load required for the wedge to fail, is calculated. Moreover, the characteristic length l_c is obtained as in the constant thickness model by making use of the varying ice thickness floe that has been generated. The l_c is inserted into $R = C_l l_c (1 + C_v v_2)$ and the floe radius is computed. Finally, following the same procedure as in the constant ice thickness model, the new ice edge border (continuous green line) is determined.

In the flowchart below the whole procedure is overviewed. Initially, the thickness when contact occurs, the relative velocity and ice edge geometry are passed to the DLL file and the procedure runs as described. As can be observed, after the determination of the wedge angle, the contribution to the update of the constant thickness model in order to account for varying thickness ice fields is shown in the green contoured boxes.
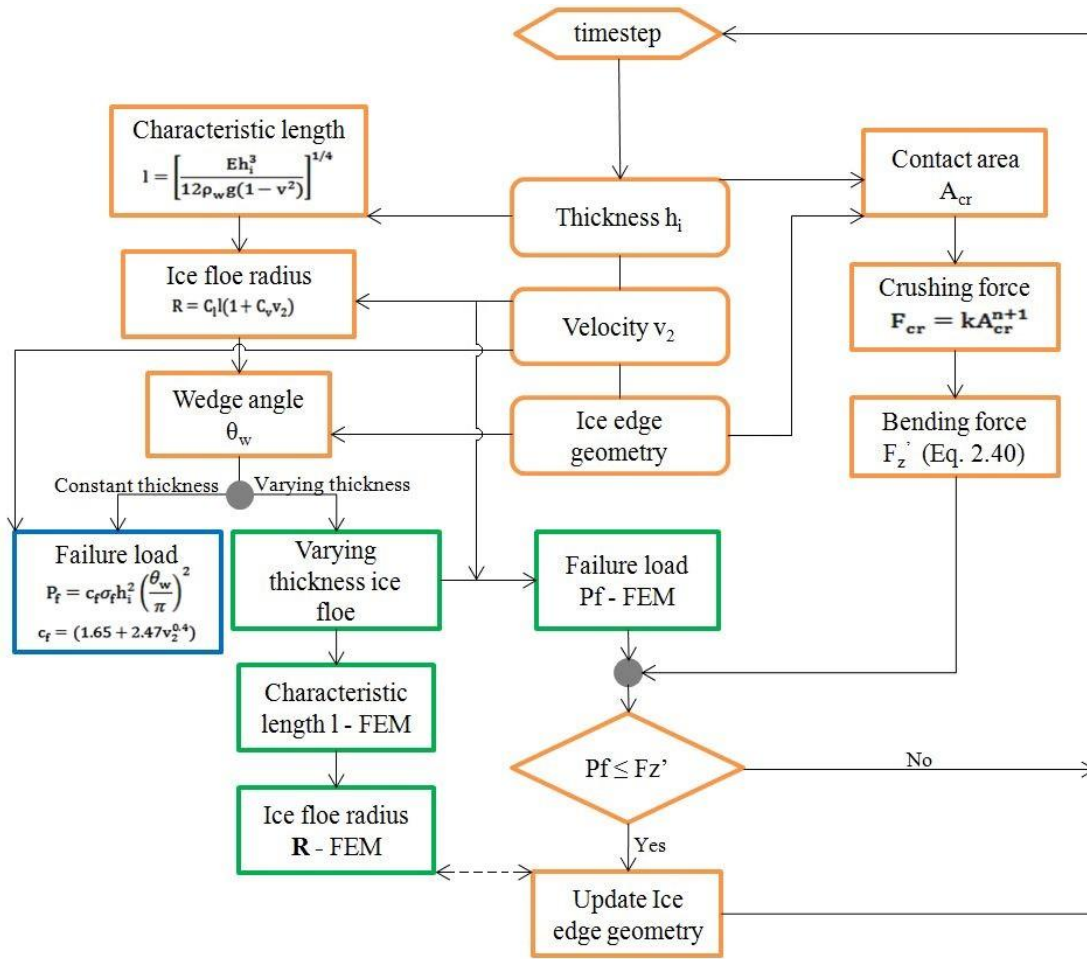
Figure 2.34 Flowchart of numerical procedure

2.9.4 Assumptions discussion

In this section a thorough discussion that concerns the assumptions made in order to update the constant ice thickness load model to the varying thickness load model is conducted.

i. Discussion on wedge angle θ

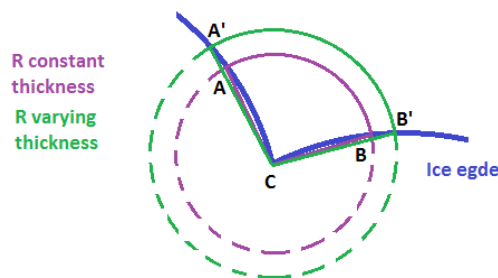To begin with the wedge angle. The method of calculation of the wedge angle is depicted in the following figure.

Figure 2.35 Wedge angle calculation

One can observe that the ice edge consists of two parts from two circles that are intersected (blue line). When the common points of the ice edge and circle created by the ice floe radius are defined, then straight lines from the centre of the circle are "drawn" to these points. So, the wedge angle is approximated by the angle $A\hat{C}B$. Therefore, an error is already introduced in the calculation. However, this approximation as explained in (S. Wang 2001) is deemed accurate enough. Moreover, geometrically the wedge angle calculated in this way will always be larger than the actual angle, therefore an overestimation for the failure load occurs which allows the calculations to be "on the safe side" with an extra load margin. The circle with a radius coming from the varying thickness model can be larger or smaller than the initial one. If it is larger, like in the figure, that means the wedge angle for the varying thickness model should be $A'\hat{C}B'$ which is larger than angle $A\hat{C}B$. So, if the angle $A'\hat{C}B'$ was used in the varying thickness model, an extra overestimation for the failure load would occur on top of the existing one. In case the circle is smaller, the wedge angle calculated would be smaller than the initial one, but still larger than reality. In order to capture both effects, an extra loop after the "Ice floe radius R - FEM" computation for varying thickness (see flowchart) in order to determine a new wedge angle θ_w, could be added. Due to heavy computations and non-efficiency of the programme though, this loop was not included. Ideally, in any case, a new method for the wedge angle calculation by making use of tangent lines running from the intersection point of the two circles that form the ice edge border, would work the best.

ii. Discussion on contact detection and F_{cr}

The second point is regarding the contact mechanism and the crushing force. Exactly the same procedure is followed by the varying thickness model as in the contact thickness model. This assumption is valid because the overlap between the ice edge and the spar cone that occurs depends only on the ice geometry. Moreover, the computation of the crushing force and the vertical reaction force F'_z has also remained the same. According to Equation (2.37) and Case 2, the contact area depends on the local thickness. In both models, the thickness used for this calculation is the thickness at point of contact between the ice and the structure.

iii. Discussion on coefficients from the semi - empirical model

The biggest discussion is risen at the point where the empirical factors C_l and C_v for the ice floe radius (Equation (2.43)) and for the failure load c_f (Equation (2.41)) are used by the varying thickness model from the constant thickness model. To begin with the ice floe radius and the factors C_l and C_v. Both of them are empirically determined by test data and experiments (S. Wang 2001) on level ice floe of constant thickness. If the experiments were conducted on a level ice floe of varying thickness these coefficients might be completely

different. Unfortunately, due to lack of experience, no clear conclusion can be drawn regarding the value of these coefficients when a varying ice thickness floe is considered. Regarding the failure load, the factor c_f has been determined by extrapolation of the results from (Varsta 1983) studies on specific ice conditions. Again, before the extrapolation, the initial results have been determined semi - empirically by field measurements on an icebreaker and an FEM model constructed by professor Petri Varstra where the ice thickness was assumed constant. So, in both cases, the dynamic coefficients of the ice floe radius and of the failure load should ideally be determined by experiments in ice basins and field test measurements.

iv. Discussion on ice floe breaking

Moving on to more general assumptions. By observing Figure 2.33, the FEM model indicates that the ice floe should break at a straight line. By introducing the ice floe radius, the ice floe is forced to break in a curved line, meaning that the FEM model is not followed accurately. On the other hand, in this way the geometrical effect which is a very important part that needs to be introduced, is captured and passed along the next timestep. This does not give a difference in the failure load results but in order to comply with both the ice edge geometry and the FEM model, curved beam elements could be introduced.

v. Discussion on ice wedge orientation

Another issue that rises within the varying thickness model is regarding the ice floe orientation and in particular the wedge orientation. Every time contact occurs and the bisector of the wedge angle is not parallel to the y axis of the spar coordinate system (Figure 2.36), the discretization that takes place assigns to each beam element the properties that it should have if the contact was parallel to the y axis (Figure 2.33).
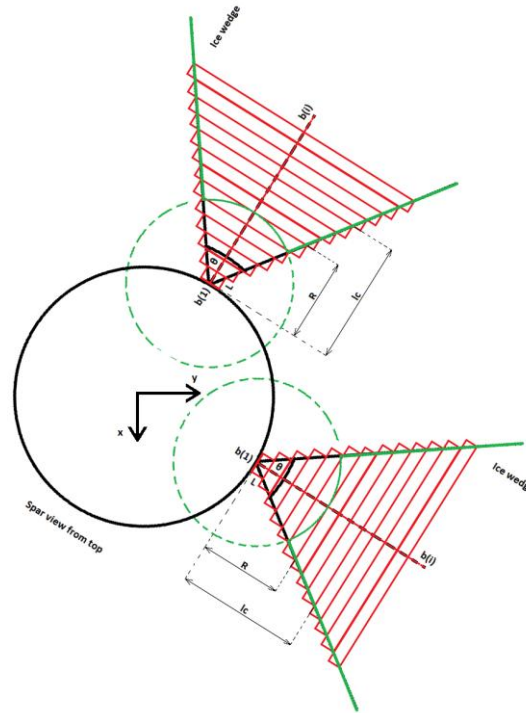
Figure 2.36 Ice - spar contact under inclination

This is a drawback of the FEM model used because when the ice floe field is generated, the thickness variation takes place perpendicular to the y axis. This weakness of the model could be improved by projecting each element's width on the y axis and assigning the properties that correspond to the projection. In this study where this effect is not accounted, practically means that the ice floe is allowed to rotate around the spar and each contact is treated the same way. On the other hand, this approach always accounts for the maximum of the thickness variations; resulting more fluctuant failure loads.

vi. Discussion on meshing the beam

Regarding the mesh used to discretize the beam, each element was selected to have a length of 0.1 m. The order of magnitude for the ice floe radius is in the order of meters, therefore by adding one decimal, significant breaking effects are captured. Moreover, the use of 0.1 m as beam element, reduces the memory needed by the computer to run the programme, increasing the efficiency. It is possible that a finer mesh, such as 0.001 m, could give more accurate results but the computational cost would be enormous. As a result, the selection of 0.1 m was based on the trade of between breaking detail and computational load.

vii. Discussion on ice rubble accumulation

Another very important assumption made is regarding the ice accumulation under the breaking cone. As mentioned before, the constant thickness model has been modified by a model initially intended to simulate the icebreaking procedure of ice - going ships. In this

case, the ice rubble is well cleared under the keel as the ship moves forward. In order to apply this model for wind turbines, it is assumed that the ice rubble under the breaking cone is well cleared. This is not entirely true because even if the ice floe passes through the wind turbine, the breaking cone does not have the optimal design for clearing the ice rubble like ice - going ships have. Therefore, in reality the wind turbine experiences accumulated ice under its cone.
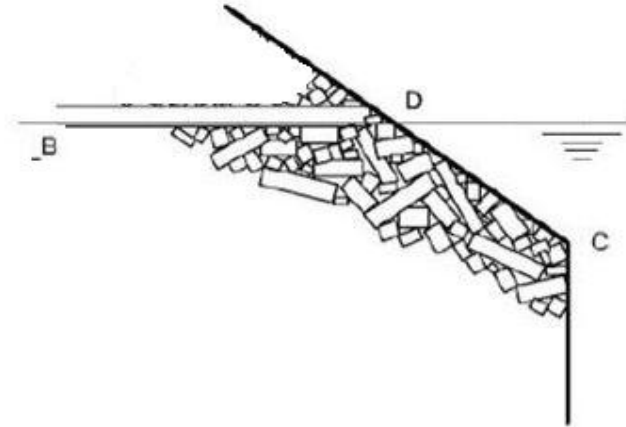
Figure 2.37 Ice rubble accumulation at a sloping structure (downward cone)

The effect of the ice accumulation under a downward breaking cone is depicted in the figure above. As can be observed, this accumulation in some way sabotages the work done by the breaking cone which is to change the ice failure mechanism from crushing to bending. Therefore, if the accumulation is not well cleared, the crushing failure mechanism becomes more and more important. During ice crushing, the global loads that develop are significantly higher than bending. The varying thickness model accounts for a small crushing event when overlapping occurs. However, this cannot describe crushing due to ice accumulation since it concerns the ice - structure interaction while according to the figure, it would be more appropriate to consider ice - ice interaction. Moreover, this ice - ice interaction could introduce extra dynamic effects on the spar. The bottom line of this discussion is that accumulated ice rubble can give rise to ice forces that are not captured by the model. This effect is currently under study by Dr. Wei Shi who also is one of the supervisors of this thesis.

viii. Discussion on beam & plate theory

Finally, a fundamental assumption regarding the varying thickness model has to be discussed. The ice floe is modelled as an Euler - Bernoulli beam of varying cross section and in principle, this assumption is quite accurate. However, in the constant thickness model and therefore in the varying thickness model as well, a three dimensional effect is attempted to be captured. This is the reason why in the constant thickness model, solutions from plate theory

on elastic foundation are used (Equation (2.41) and Equation (2.44)). In the varying thickness model, the three dimensional effects of a plate are approximated by using the Euler - Bernoulli beam model. Any results obtained from the varying thickness model and beam theory are following the same logic as the constant ice thickness model results and plate theory, since plate theory is actually an extension of beam theory. The drawback of this approximation has to do with accuracy, meaning that if plate theory was used in the varying thickness model, a better representation of reality would occur and therefore more appropriate results would be obtained. Euler - Bernoulli beam theory was used though, due to the simplicity of implementation and as presented in the upcoming section 5.1 , where an indicative validation takes place, this approximation is appropriate enough.

2.10 Aerodynamic loads

Normally, wind velocity varies over time and shows fluctuations. In this current study, in order o keep the model simple, constant wind is applied as input.

When a slender structure like a wind turbine is subjected to aerodynamic loads, an important phenomenon is observed. This phenomenon is called wind shear, or vertical wind profile variations. It is the phenomenon where the wind speed increases as the distance from the ground increases. The most common model found in literature that accounts for wind shear is the power law model (Gao and Bachinsky 2014).

$$\overline{U}(z) = \overline{U}_{ref} \left(\frac{z}{z_{ref}} \right)^a \tag{2.63}$$

Where:
   a: Vertical shear exponent
   $\overline{U}_{ref}$:   Wind speed at reference height z_{ref}

In HAWC2 different models are included namely: constant, logarithmic, power law, linear. However, in the spar floating simulations, wind shear is not taken into account and the constant model is applied (Jonkman 2010). The reason for this is that the spar floating wind turbine concept is meant to be placed far offshore where the wind shear phenomenon is less significant than in rough areas.

Aerodynamic loads can be observed at the rotor, at the tower and the nacelle. On the two later ones the loads are calculated through the pressure integration method combined with the Morison's equation which is valid for slender structures (Faltinsen 1990).

$$dF_{aero} = \frac{1}{2} p_a C_{D,t} D_t(z) dz [U(z,t)|U(z,t)|]$$

(2.64)

Where:

D_t: Diameter of the tower

$C_{D,t}$:   Drag (viscous) coefficient on the specific direction that has projected area $D_t(z)dz$

$U(z,t)$:   Wind velocity along the tower/Nacelle height z and in time t

$\dot{U}(z,t)$:   Wind acceleration along the tower/Nacelle height z and in time t

Regarding the rotor, HAWC2 uses the Blade Element Momentum (BEM) theory for calculating the aerodynamic loads. Another popular model is the Generalised Dynamic Wake one. However, this model was developed for helicopters and its use is not appropriate for wind speeds below 8 m/s (Gao and Bachinsky 2014).

The BEM theory is quite old and was introduced by Glauert in 1935. The goal of the theory is to quantify not only the steady aerodynamic loads but also the thrust and power for different wind and rotational speeds and pitch angles (Hansen 2008). To reach the goal, the BEM theory is coupled with the local events occurring on the actual blades (Hansen 2008). The wind turbine is discretized in N annular elements of height dr. Each single element is studied using the 1D Momentum theory and by combining the individual results and the integral momentum equation, the trust is possible to be computed. As a result, all local loads are obtained. For detailed information see (Hansen 2008).
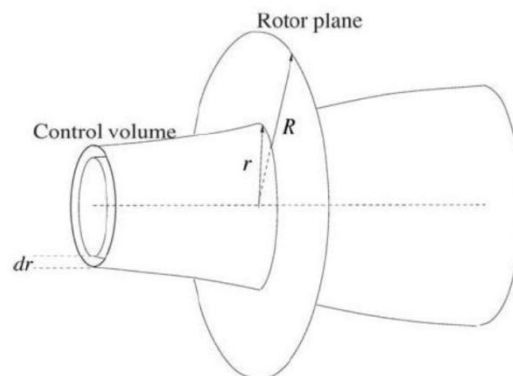
Figure 2.38 Annular element control volume, exploited in BEM (Hansen 2008)

In order to understand the BEM theory, main focus should be paid in the 1D model for an ideal rotor.
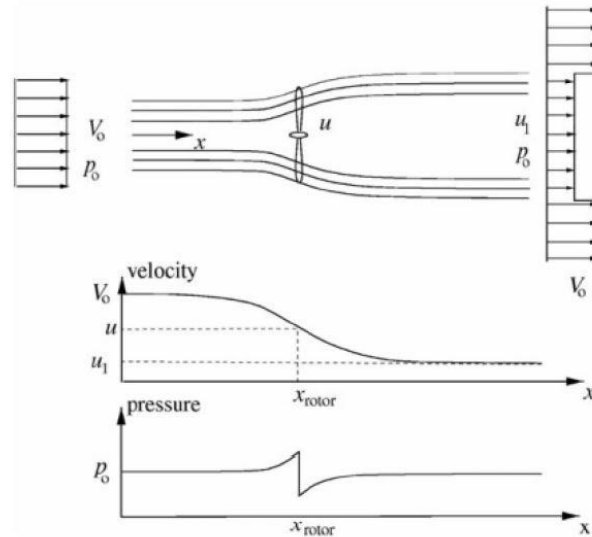
Figure 2.39 Streamlines passing the rotor, axial velocity, pressure up and downstream of the rotor (Hansen 2008)

The wind turbine extracts mechanical energy from the kinetic energy of the wind by creating thrust. This force is created due to pressure drop (Δp) over the rotor and results the reduction of the wind speed from V_0 to u_1 in the wake as shown in Figure 2.39 and in the following equations (Hansen 2008), (Gao and Bachinsky 2014).

$$\text{Thrust} = \Delta p A \tag{2.65}$$

Where:
  A: Area of the rotor

$$\Delta p = \frac{1}{2} p_\alpha (V_0^2 - u_1^2) \tag{2.66}$$

$$u = (1 - \alpha) V_0 \tag{2.67}$$

$$\text{Thrust} = 2 p_\alpha V_0^2 \alpha (1 - \alpha) A \tag{2.68}$$

The 1D results are extended to account for the number of blades B and finally obtain the thrust equation which applies for the 3D control volume.

$$dT = \frac{1}{2} p_\alpha B \frac{V_0^2 \alpha (1 - \alpha)^2}{\sin^2 \varphi} c C_n dr \tag{2.69}$$

Where:
  φ: Flow angle
  C_n: Normal load coefficient
  c: Chord length
  α: Axial induction factor

More information regarding the algorithm used in order to compute the thrust force can be found in (Hansen 2008) work.

However, in order to implement the BEM theory in HAWC2, some corrections need to be applied. First of all, the Prandtl tip loss correction is applied in order to fix the assumption of

infinite number of blades from the BEM theory. Also, the MHH Beddoes method (a dynamic stall model) is applied in order to fix the drag and moment coefficients. Finally, a correction is applied in order to fix the fact that the simple momentum theory is no longer valid when the axial induction factor is larger than 0.4. (Hansen 2008).

2.11 Mooring line tension

The spar floating wind turbine is moored by a system of three catenary lines (Jonkman 2010). According to (Faltinsen 1990), the theory of inelastic cables can be applied to model the catenary lines. As explained by (Bredmose 2014) the basic assumptions applied are:

- The cable is in a vertical x-z plane
- The sea bed is horizontal
- Bending stiffness, hydrodynamic forces and dynamic effects are neglected
- Buoyancy is included

The mathematical derivation for the catenary mooring line equation follows briefly.
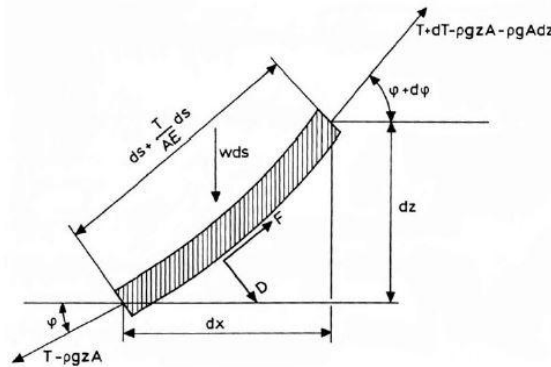
Figure 2.40 Differential analysis of catenary mooring line (Bredmose 2014)

The force equilibrium along the cable reads:

$$dT - pgAdz = \left[w\sin\varphi - F\left(\frac{1+T}{AE}\right) \right] ds \qquad (2.70)$$

Where:
  A: Cross section area of the cable
  E: Young modulus of the cable

The force equilibrium normal to the cable:

$$Td\varphi - pgzAd\varphi = \left[w\cos\varphi + D\left(\frac{1+T}{AE}\right) \right] ds \qquad (2.71)$$

In Equations (2.70) and (2.71) by changing the variable to $T' = T - pgzA$, the equilibrium equations become:

$$dT' = w\sin\varphi ds \tag{2.72}$$
$$T'd\varphi = w\cos\varphi ds \tag{2.73}$$
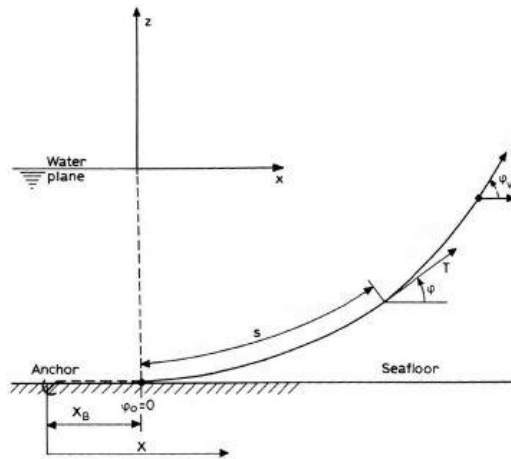
Figure 2.41 Catenary line in x-z plane (Bredmose 2014)

By rearranging the terms to $T'\sin\varphi = ws$ and $T'\cos\varphi = T_0'$ it is obtained that $s = \alpha\sinh\frac{x}{\alpha}$ and $z + h = \alpha(\cosh\frac{x}{\alpha} - 1)$, where $\alpha = \frac{T_0'}{w}$.
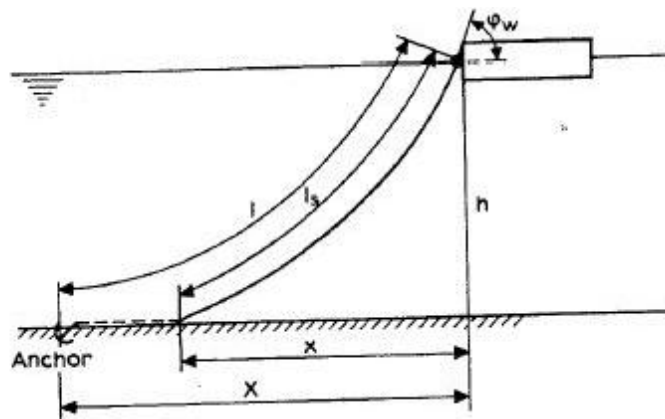
Figure 2.42 Catenary line geometry (Bredmose 2014)

From the geometry of the above figure it is found that $X = l - l_s + x$. As result, this leads to the catenary mooring line equation.

$$X = l - h\left(1 + 2\frac{\alpha}{h}\right)^{0.5} + \alpha\cosh^{-1}\left(\frac{h}{\alpha} + 1\right) \tag{2.74}$$

Therefore, given the X, l and h, Equation (2.74) can be solved for α. But, $\alpha = \frac{T_0'}{w}$, hence not only the horizontal tension component in the cable can be obtained but also the vertical one

through the vertical equilibrium $T'_{vertical} = T'\sin\varphi = ws.$ For more details regarding the inelastic cable theory, see (Faltinsen 1990). In HAWC2, the mooring line tension is computed using and external DLL file where the calculations of the mooring forces are taking place and are transferred to the programme at each timestep.

2.12 Hydrodynamic loads

A brief reference to the hydrodynamic loads implemented in HAWC2 is discussed. The hydrodynamic loads are calculated by the pressure integration method combined with the Morison equation (Faltinsen 1990).

$$dF_{hydro} = p_w C_M V\dot{u} + \frac{1}{2} p_w C_D D_s dz(u - \dot{\eta}_1)|u - \dot{\eta}_1| \qquad (2.75)$$

Where:
- p_w: Density of sea water
- D_s: Diameter of the spar
- C_D: Viscous coefficient on the specific direction that has projected area Ddz
- C_M: Inertia coefficient for the spar
- u: Undisturbed fluid velocity
- $\dot{u}$: Fluid acceleration
- $\dot{\eta}_1$: Velocity of the body

This formula applies to slender structures such as the spar buoy where the dimensions of the spar are small compared to the wavelength.

HAWC2 takes into account the wave loads as external DLL files and it can simulate different types of waves such as Linear airy waves, Irregular airy waves (with directional spreading using Jonswap spectrum), Deterministic irregular waves, Wheeler stretching for load application points.

The hydrodynamic loads are significantly reduced because of the ice and according to the ISO they still should be considered with the use of models that account for wave attenuation in ice covered waters. Also, ideally speaking hydrodynamic effects due to current loads should be included in the model. However, in this current study neither current nor waves are considered due to the sea ice presence on the sea surface. This is because this study's goal is to contribute to a model which compares ice loads and aerodynamic loads and initially the idea is to keep the model simple. Moreover, in this case the hydrodynamic loads are expected to have a minor contribution to the total loading of the structure and as a result they can easily be ignored with no severe error.

3 Spar floating model and 5MW wind turbine model

3.1 Spar floating model

The spar floating model that was used in this current project is the OC3 Hywind concept. The draft of the platform is 120 m. At the waterline of the floater has been positioned a linearly tapered conical region, a downward bending cone. The linearly tapered conical region extends from a depth of 4 m to a depth of 12 m below the SWL, therefore the cone angle is 45°. Moreover the floater is kept in position with the help of three mooring lines (Jonkman 2010). In the table below the properties of the floating platform are presented.

Table 3.1 OC3 Spar properties (Jonkman 2010)

Depth to Platform Base Below SWL (Total Draft)	120 m
Elevation to Platform Top (Tower Base) Above SWL	10 m
Depth to Top of Taper Below SWL	4 m
Depth to Bottom of Taper Below SWL	12 m
Platform Diameter Above Taper	6.5 m
Platform Diameter Below Taper	9.4 m
Platform Mass, Including Ballast	7,466,330 kg
CM Location Below SWL Along Platform Centerline	89.9155 m
Platform Roll Inertia about CM	4,229,230,000 kg m^2
Platform Pitch Inertia about CM	4,229,230,000 kg m^2
Platform Yaw Inertia about Platform Centerline	164,230,000 kg m^2
Number of Mooring Lines	3
Angle Between Adjacent Lines	120°
Depth to Anchors Below SWL (Water Depth)	320 m
Depth to Fairleads Below SWL	70.0 m
Radius to Anchors from Platform Centerline	853.87 m
Radius to Fairleads from Platform Centerline	5.2 m
Unstretched Mooring Line Length	902.2 m
Mooring Line Diameter	0.09 m
Equivalent Mooring Line Mass Density	77.7066 kg/m
Equivalent Mooring Line Extensional Stiffness	384,243,000 N
Additional Yaw Spring Stiffness	98,340,000 Nm/rad

3.2 NREL 5 MW wind turbine model

The wind turbine model that was placed on top of the OC3 Hywind floater is the so called "NREL offshore 5-MW baseline wind turbine" and it is also known as the reference wind

turbine. When it was established, the objective was to create detailed specifications of a large wind turbine that is representative of typical utility - scale, land- and sea based multimegawatt turbines that is suitable also for deployment in deep waters. The NREL 5 MW is a variable speed, pitch controlled wind turbine with a rotor diameter of 126 m. The hub height is 90 m and the cut-in, rated and cut-out wind speed of 3 m/s, 11.4 m/s and 25 m/s respectively (Jonkman et al. 2009). More information about the NREL are presented in the next table.

Table 3.2 NREL offshore 5-MW baseline wind turbine properties (Jonkman, 2009)

Rating	5 MW
Rotor Orientation, Configuration	Upwind, 3 Blades
Control	Variable Speed, Collective Pitch
Drivetrain	High Speed, Multiple-Stage Gearbox
Rotor, Hub Diameter	126 m, 3 m
Hub Height	90 m
Cut-In, Rated, Cut-Out Wind Speed	3 m/s, 11.4 m/s, 25 m/s
Cut-In, Rated Rotor Speed	6.9 rpm, 12.1 rpm
Rated Tip Speed	80 m/s
Overhang, Shaft Tilt, Precone	5 m, 5°, 2.5 $^{\circ}$
Rotor Mass	110,000 kg
Nacelle Mass	240,000 kg
Tower Mass	347,460 kg
Coordinate Location of Overall CM	(-0.2 m, 0.0 m, 64.0 m)

The next figure illustrates the NREL 5 MW on top of the OC3 Hywind floater.
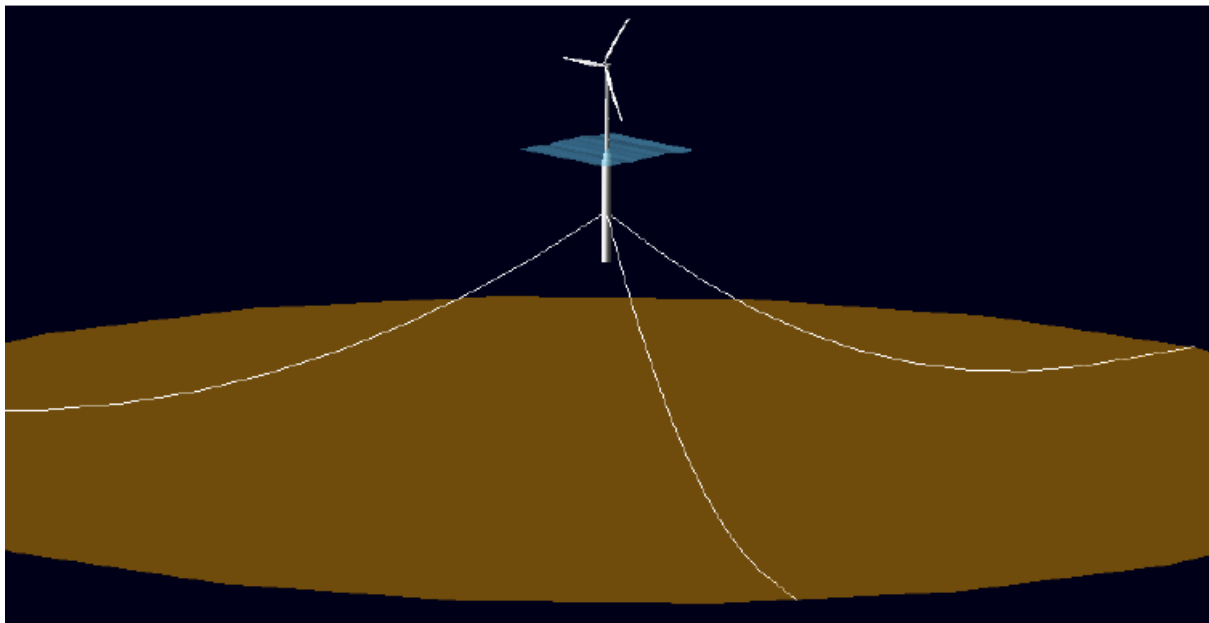
Figure 3.1 Illustrations of the NREL 5 MW wind turbine on the OC3-Hywind spar (Jonkman 2010)

4 Simulation set up

HAWC2 is an aeroelastic code intended for calculating wind turbine response in time domain. The code consists of models describing the external effect, applied loads, structural dynamics and connection to the control system. The external effects model how the wind, waves and soil is expected to behave. The applied loads model how the external effects interact with the structure through aerodynamic, hydrodynamic and soil models. The structural formulation of HAWC2 is based on a multibody system. This enables a wide range of model capabilities and the possibility to include non - linear geometric effects. Wind turbine control is preformed through external DLL´s that operates the system under different conditions (DTU Wind Energy 2015). Moreover, with the use of external DLL files there is control of the external forcing of the wind turbine such as ice loads. Therefore, they are very important for the scope of this project.

4.1 Simulation initial set up

First of all it is necessary to define the coordinates that HAWC2 works with. In the next figure the coordinate system is depicted.
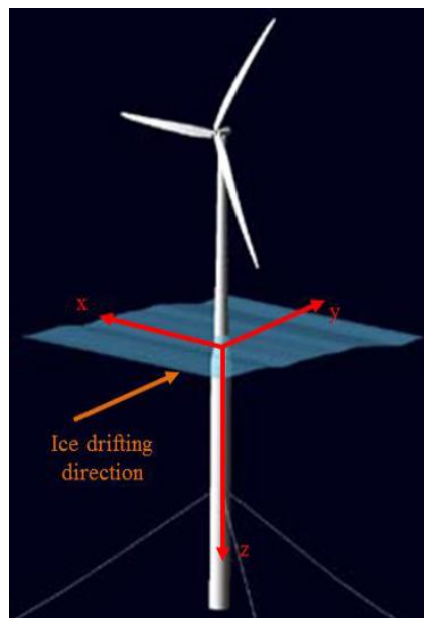
Figure 4.1 HAWC2 coordinate system (Saccoman 2015)

All the positive x, y and z directions are defined as it is shown in the figure above. It is observed the ice floe drifts to the y direction. The y direction is also referred as Fore - Aft direction and the x as Side - Side.

Three different **drifting speeds** of the ice floe were selected **0.1 m/s**, **0.3 m/s** and **0.5 m/s**. Even if these ice drifting speeds can be characterised rather large for level ice, according to (McPhee 2008) and (Lewis, et al. 2008) the ice drifting speed can be approximated by the 2% of the wind speed. Therefore in remote areas such as the ones presented below where sea ice often occurs, the selected ice drifting speeds are not unreasonable but rather extreme. Moreover, it should be mentioned that the approximation mentioned does not account for sea current which is another very important parameter that defines the ice drifting speed.

Table 4.1 Examples of wind speeds in remote areas and corresponding ice drifting speeds (Hoving 2015)

	Wind speed (max)	Ice drifting speed
Sea of Okhotsk	25-35 m/s	0.5-0.7 m/s
Beaufort Sea	18-32 m/s	0.36-0.72 m/s
Barents Sea	20-25 m/s	0.4-0.5m/s

A comparison should be made between the different loadings. Therefore, in order to produce aerodynamic loading a constant **wind speed** of **12 m/s** was selected. This wind speed is slightly above the rated wind speed of the wind turbine and it was selected because it will cause a very large thrust force on the rotor. In order to perform any simulation though, the DLL files need to be set up according to their theoretical background and the ice conditions encountered.

Table 4.2 Ice characteristics

Parameter	Value
Density	880 kgm^{-3}
Bending failure (σ_f)	0.58 MPa
Crushing Strength	2.3 MPa
Young modulus (E)	5.4 GPa
Poisson's ratio (v)	0.33
Friction coefficient	0.05

To summarize sententiously the steps of the analysis:

- Implementation of a DLL file accounting for the generated varying thickness
- Convergence study with respect to timestep and duration of the simulations
- Generation of a level ice floe with varying thickness
- Validation of the DLL file
- Simulations using HAWC2

4.2 FEM numerical implementation

The model for ice - structure interaction described in section 2.9.2 , was initially implemented into Matlab software and the beam of 300 m depicted in Figure 4.3 was tested under static loading. When the varying ice thickness beam was inserted to the FEM model, the characteristic length l revealed the behaviour presented in the next figure.
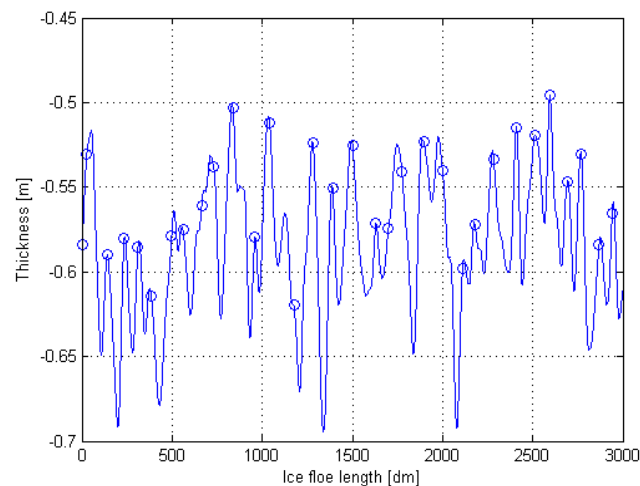
Figure 4.2 Breaking points of the varying ice thickness field

From the figure above each blue circle shows where the ice will fail under continuous loading. Initially the loading is applied at x = 3000 dm and as soon as the ice fails the loading is applied at the spot it failed. It can be observed that in most cases the ice floe with varying thickness fails at the local weakest points where the thickness is the smallest. This is an interesting finding that could be useful in understanding the breaking pattern of the varying thickness floe. In the next table are indicatively presented the first 10 characteristic lengths of the above floe and the thickness at which they failed. As soon as the Matlab code proved to be working, it is rewritten in FORTRAN as part of the existing FORTRAN DLL file.

Table 4.3 Characteristic lengths of static loading on a varying thickness beam

Characteristic length [m]	Failure thickness [m]
12.5	0.5795
11	0.5287
17	0.4956
9	0.5220
9.6	0.5142
13	0.5285
10.5	0.5707
17	0.5461
11.4	0.5214
13.4	0.5270
Mean values based on all points	
12.275 m	0.5431

4.3 Convergence study

Convergence tests were carried out with respect to the timestep and the total duration of the simulation in order to verify that the proposed procedure gives accurate solutions.

Initially focus was given to the timestep and afterwards to the total simulation time. Four different timesteps were examined namely: 0.0005, 0.001, 0.05 and 0.01 s. The simulation time for the timestep study was 3000 s and the ice drifting speed was 0.5 m/s. In order to conclude which timestep is the optimal one, any response parameter could be chosen. In this project the velocity of the spar in side - side and fore - aft direction is obtained and illustrated in the next table.

Table 4.4 Statistic results of the velocity and computational time as a function of timestep

Timestep [s]	Computational Time [h]	Mean [m/s]		Std [m/s]	
		F-A	S-S	F-A	S-S
0.0005	120	0.0025	$1.46 \cdot 10^{-4}$	0.0984	0.0421
0.001	100	0.0023	$1.53 \cdot 10^{-4}$	0.0914	0.0464
0.005	70	0.0024	$6.03 \cdot 10^{-4}$	0.1642	0.0368
0.01	35	0.0036	$4.86 \cdot 10^{-4}$	0.1131	0.028
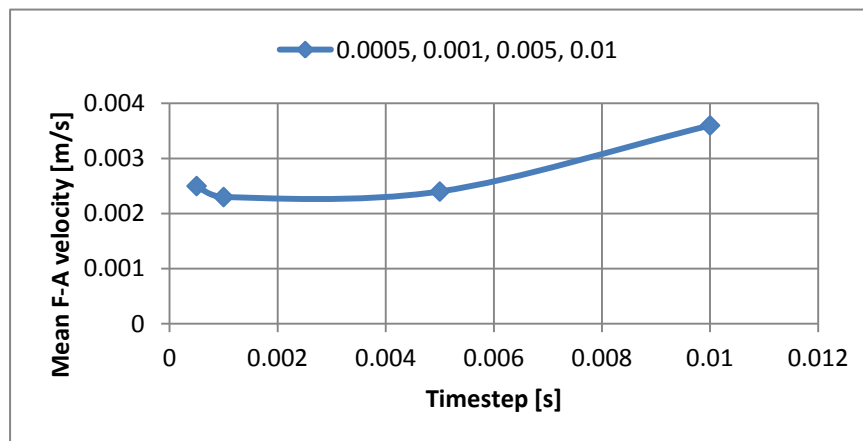
It is observed that the results start to converge from the timestep of 0.005 s and onwards. Taking also into the computational effort needed for a simulation to be performed, the selected **timestep** was **0.001 s**.

In order to select the proper simulation time length four different simulations were tested, namely: 1500, 2000, 2500 and 3000 s. The selected timestep was indeed 0.001 s and the selected drifting speed 0.5 m/s. Again the velocity of the spar at the waterline was selected to compare the convergence between the selected running times.

Table 4.5 Statistic results of the velocity and computational time as a function of simulation length

Simulation length [s]	Computational Time [h]	Mean [m/s]		Std [m/s]	
		F-A	S-S	F-A	S-S
1500	65	0.0068	$8.88 \cdot 10^{-4}$	0.113	0.0447
2000	82	0.0042	$1.1 \cdot 10^{-4}$	0.0973	0.0424
2500	90	0.002	$3.4 \cdot 10^{-4}$	0.0923	0.047
3000	100	0.0023	$1.53 \cdot 10^{-4}$	0.0914	0.0464
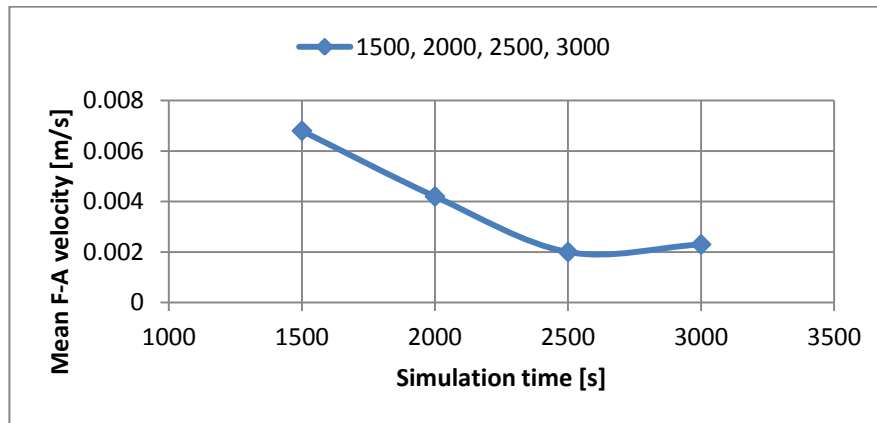
It is observed that as the simulation length increases, the computational time increases as well. Also as the simulation time increases the results become more precise due to the fact that there is more data computed by the programme and as a result the statistical analysis becomes more accurate. Convergence seems to start from 2500 s simulation time, but the selected **simulation time** was **3000s** in order to capture as much loading cycles as possible. The convergence simulations were run using the semi - empirical model. Studies and similar findings from other reports (Saccoman 2015), show that the combination of timestep 0.001 s and simulation length 3000 s in HAWC2, generates accurate results in tolerable amount of time.

Moreover, when coupling the ice load DLL module with HAWC2, numerical issues have been observed especially for when a spar floating wind turbine is considered (Saccoman 2015). In order to avoid unexpected numerical issues, initial conditions and transient phases (i.e. ice load ramp duration and final value) are also investigated.

Following experience from other studies, the **ramp duration** has been selected **1000 s**. At this point it should be noted that the 3000 s simulation time correspond to 1000 s ramp phase and 2000 s ice - structure interaction. Moreover, the final value of the ramp force and moment should not deviate a lot from the initial ice load produced when the ice floe collides with the structure. Therefore, after performing a few test cases, the final value of the Fore - Aft ramp force, was found that it should be approximately 110 kN. Similarly, the final value of the Fore

- Aft ramp moment was found that it should be approximately 400kNm. As observed the ramp function is applied not only on the Fore - Aft force but also on the Fore - Aft moment. The reason for this is due to the fact that a large input of moment could also cause an abrupt change in motion and therefore numerical issues.

It must be mentioned for fellow researchers that this step is very important to be performed accurately, otherwise precious time and resources could be lost. However, it must also be mentioned that the ramp function technique is does not assure convergence at all situations.

4.4 Implementing the varying thickness of the ice floe

It was mentioned in section 2.5 that a data manipulation procedure would be implemented in order to generate a randomly varying ice thickness. Indeed, as soon as the dataset was digitized, the generation of the varying ice field was utilized.

The digitized dataset is presented in the figure below and it is compared with the actual measurements. The digitization took place with a 0.35 m interval.
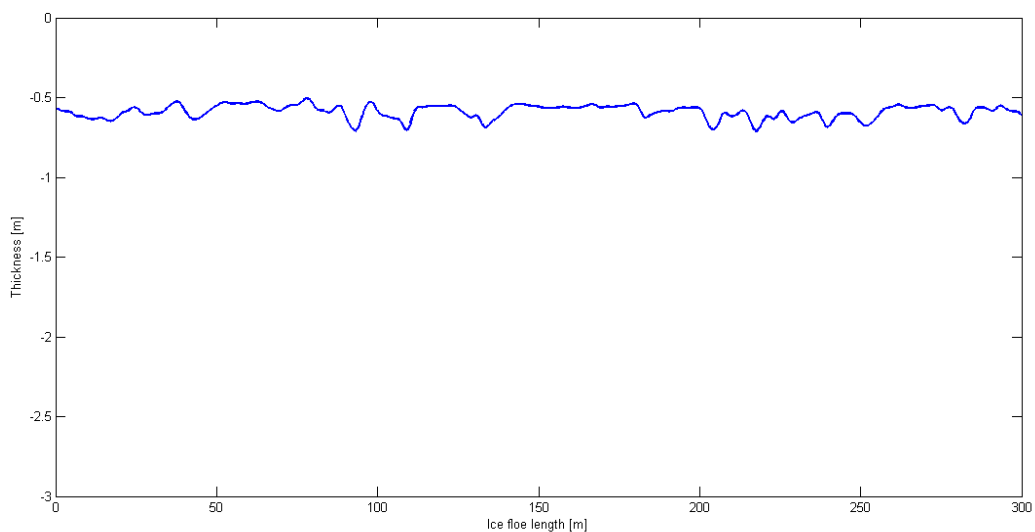
Figure 4.3 Digitized level ice field measurements
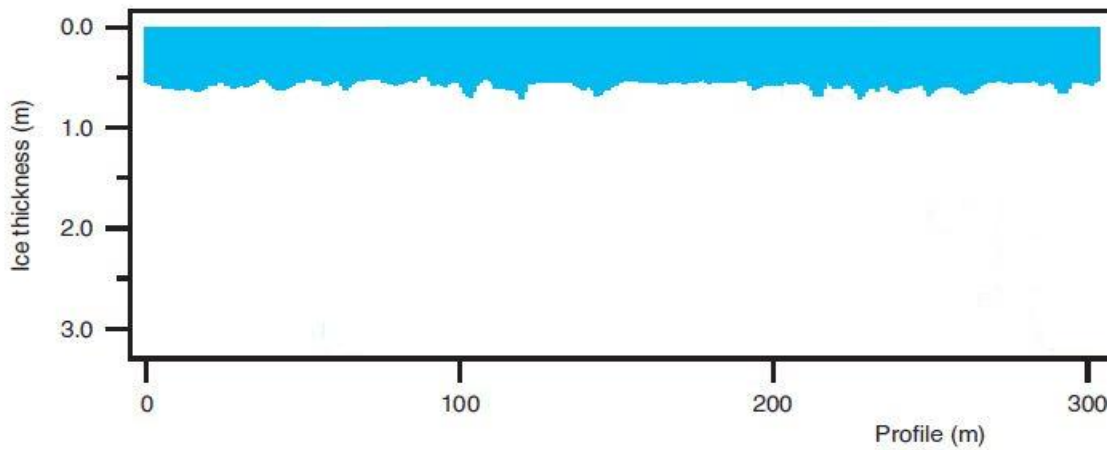
Figure 4.4 Level ice field measurements

The corresponding spectrum of the digitized field measurements was obtained by using Matlab software and the WAFO package for data analysis; in particular the dat2spec2.m function. This function is using the fast Fourier transformation and the outcome is spectral density and angular frequency in m^2/rad·s and rad/s respectively. Therefore when plotting the result, a division by 2π gives m^2/Hz and Hz. However, since the trick of translating the seconds into meters is applied, the Hz created correspond to 1/m than 1/s. The corresponding spectrum is presented.
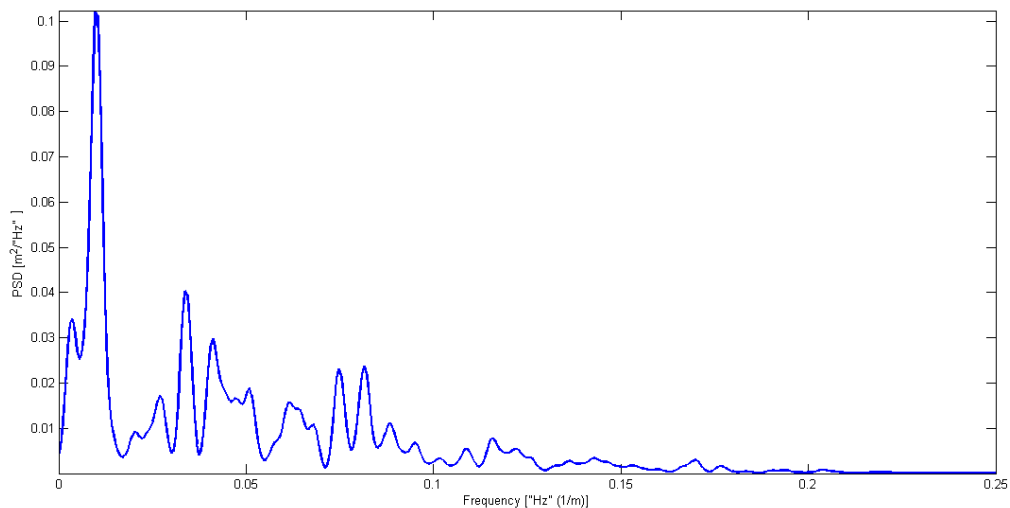
Figure 4.5 Spectrum from real measurements (Figure 4.3)

By utilizing the direct sum equation $(h(x) = h_{mean} + \sum \sqrt{2S(\omega_i)\varDelta\omega} \cdot \cos(\omega_i x_i + \varphi_i))$, a random ice field with varying thickness is generated based on the above spectrum. The mean value used as input is the mean value obtained from the measurements **h_{mean}=0.59 m** and the random phase φ_i was generated by Mathematica software and passed on to Matlab. The biggest issue that was confronted in last semester's project assignment was the selection of

length interval between the randomly generated points. Since there is no theoretical model that could predict this value, its initial selection was rather vague. Still there is no theoretical model to describe the formulation of the ice thickness but the field that is attempted to be generated is going to be based on the original measurements and their spectrum. In this way, the correlation of each point with the neighbouring ones, is captured. Therefore, the closer the form looks to the original, the more representative it is.

Many attempts were made (see Appendix B, page 124) in order to find the best match. The one that appeared the closest corresponds to **0.5 m length interval**. The points in between the intervals where defined through linear interpolation. The figure below shows the comparison of the length series.
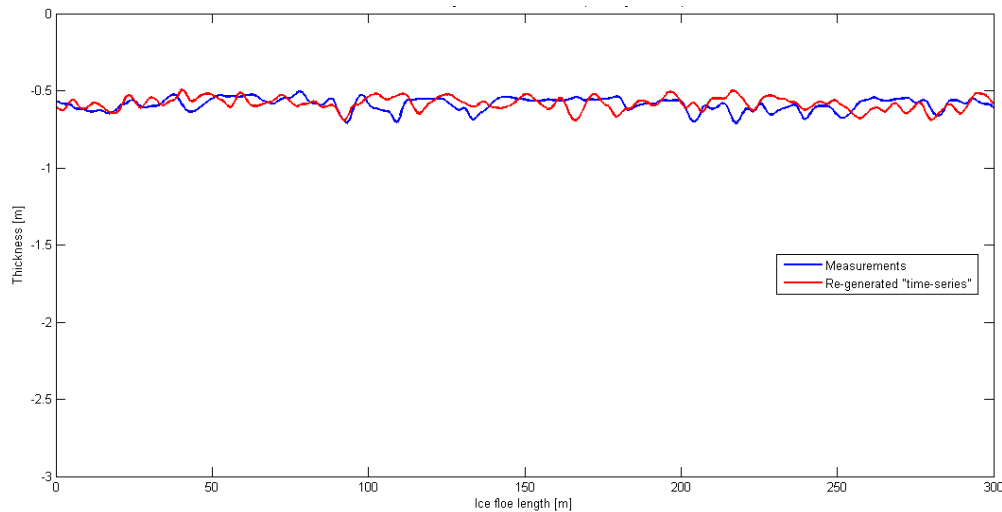
Figure 4.6 Comparison of the generated ice floe and the original measurements

It is observed that the generated length series are very close with the field measurements. However there is another issue that needs to be discussed. The length series that will be used in the simulations should be larger than 300 m. From the convergence study, the simulation time selected is 3000 s. Having in mind that the 0.5 m/s is the highest speed used, the maximum ice floe length that needs to be generated is 1500 m, even if the actual ice - structure interaction takes place for 2000 s. In order to obtain such long series, the measurement dataset was repeated until it becomes 1500 m long. Afterwards, a random timeseries is generated using the length interval of 0.5 m. The comparison of the length series and the corresponding spectra are presented in the figures below.
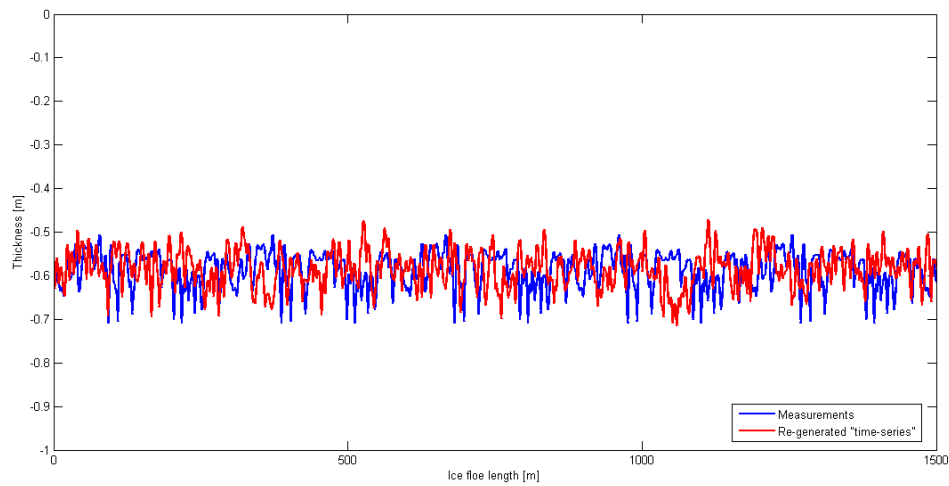
Figure 4.7 Comparison of the generated ice floe and the original measurements (1500 m)
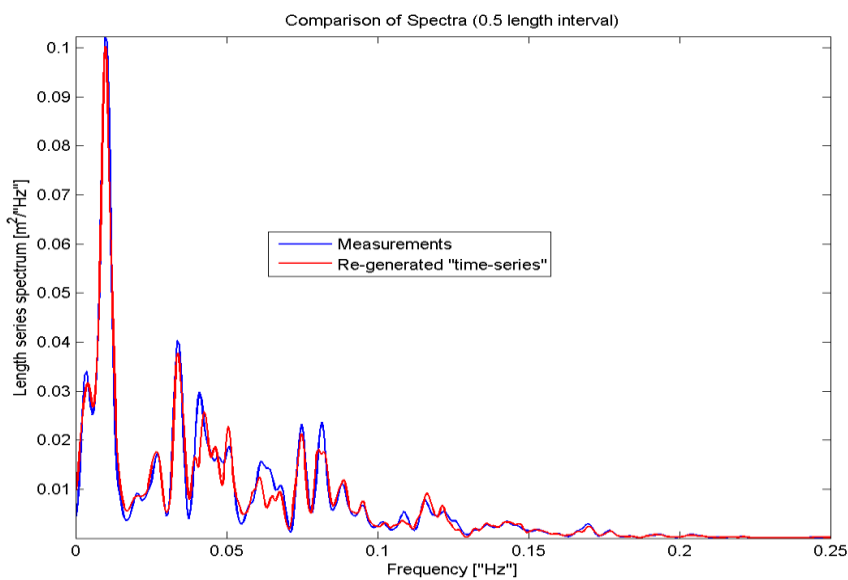
Figure 4.8 Comparison of the generated ice floe spectrum and the original spectrum

Again, it is observed that both the generated length series and the corresponding spectrum are close to the field measurements. Therefore, the generated ice field can be used as an input to the simulation.

5 Results and Discussion

5.1 Validation of the FEM model

The FEM model for ice - structure interaction described in section 2.9.2 , was initially implemented into Matlab software. After it was tested for static load cases the programme is re - written in FORTRAN as part of the existing FORTRAN DLL file that considers an ice floe of uniform thickness. In order to confirm that the proposed model for the thesis work is accurate enough, benchmark tests were carried out and compared to the initial constant thickness model.

5.1.1 Validation considering static loading

Initially, the characteristic length $l = \left[\frac{Eh_i^3}{12\rho_w g(1-v^2)} \right]^{1/4}$ is compared. For a thickness of 0.59 m, the equation yields a characteristic length of 10.1 m. It should not be forgotten that this equation is derived from static plate theory on elastic foundation. In this case, the characteristic length coincides with the breaking length of the plate.

The FEM model is based on the stress distribution of the ice floe beam and whenever the stress is above the flexural strength, the characteristic length is obtained. The figures below present the deflection diagram and the stress distribution of a 300 m constant ice thickness (0.59 m) beam under the minimum load required for failure (7.5 kN/m).
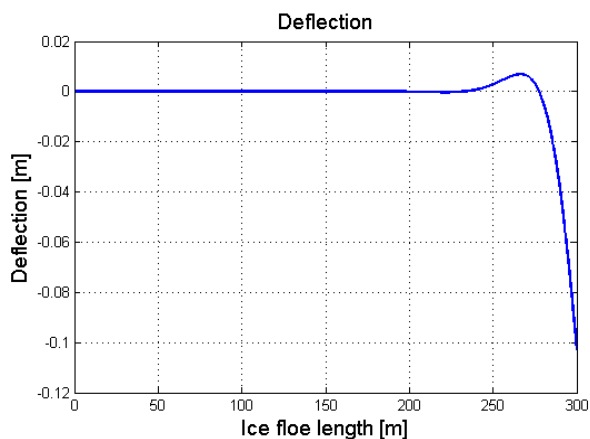
Figure 5.1 Deflection diagram of a uniform thickness beam (FEM model)
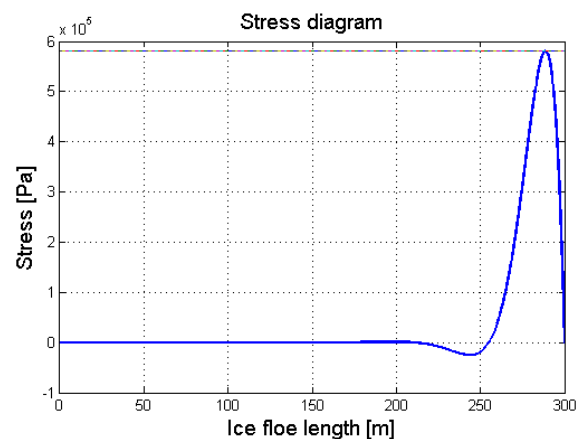
Figure 5.2 Stress distribution of a uniform thickness beam (FEM model)

It is observed that the maximum deflection is obtained at the point where the force is applied. Furthermore, in a distance far away from the load, at approximately 60 m (240 m on the

figure) the effect of the load is not seen by the beam. The small upward curve that occurs between 250 and 275 m is a result of the hydrostatic force (elastic foundation) that acts opposite to the force direction.

The stress distribution diagram reveals at which point the stress exceeds the flexural strength which is indicated by the straight line just below 0.6 MPa. The characteristic length obtained by the FEM model is 11.0 m. It is observed that there is a difference of 9% with the analytical solution. The difference it is believed that occurs due to the discretization of 0.1 m that is used for the beam. Indeed, as soon as the discretization was set 0.01 m the characteristic length calculated from the FEM model yields 10.59 m, therefore the difference with the analytical formula dropped to 5%. Unfortunately, due to "RUN OUT OF MEMORY" issues, a finer mesh could not be tested, but it is believed that a mesh such as 0.001 m would result even closer results.

Furthermore, a validation test was implemented by using a constant ice thickness wedge (h_i = 0.59 m) with an opening angle θ_w of 140°. This angle is selected to be tested because it has been observed during testing of the DLL files that the wedge angle is approximately larger than 90° and lower than 170°. Kastelyan's experimentally determined formula reads $P_f = \frac{1}{0.996} \sigma_f h_i^2 \left(\frac{2.44}{\pi}\right)^2$ (Kerr 1975) and the resulting failure load is equal to 121.79 kN. The FEM model for the same conditions results a failure load equal to 114.87 kN. The difference between the constant thickness model and the FEM model is approximately 6% and can be characterised rather small.

In conclusion, the load from the FEM model and the experimental formula agree with each other with a small difference. Therefore, taking also into account the fact that the difference in the characteristic length is small as well; this is a good sign that the FEM model constructed can lead to proper results.

5.1.2 Validation considering dynamic loading

Additional validation tests were carried out considering dynamic analysis in HAWC2. Initially, the original DLL file that accounts for uniform ice thickness is used in the validation simulation. Afterwards, the updated DLL file that includes the FEM model is coupled in HAWC2, considering a constant ice thickness floe. At this point it has to be mentioned that since a validation of the FEM DLL file, which is the one producing the ice loads, is performed, no responses from the structure were considered.

5.1.2.1 Validation against a monopile

Initially, the validation took place against a monopile structure, the simulation time was 1000 s and the timestep 0.001 s. Moreover, three different speeds were tested, namely 0.1 m/s, 0.3 m/s, 0.5 m/s. In the next pages, the statistical values, considering the steady state case, of all the forces and moments for all directions are presented. Also, indicative ice loads are shown. All the ice loads and moments compared for all the cases in all directions and all drifting speeds can be found in Appendix C1 (page 126).

To begin with the drifting speed of 0.1 m/s, the force in the Fore - Aft direction is presented.
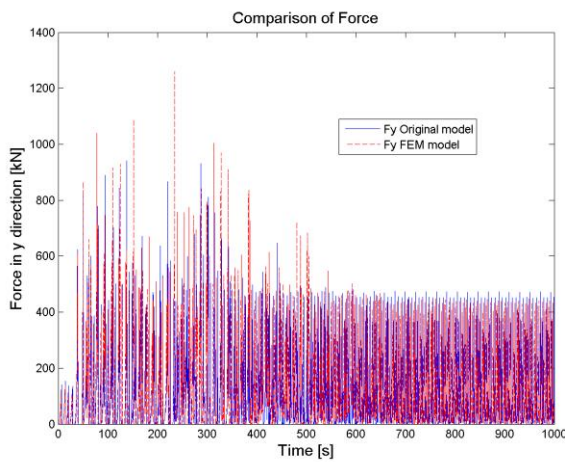
Figure 5.3 Comparison of Force in y direction (validation monopile)
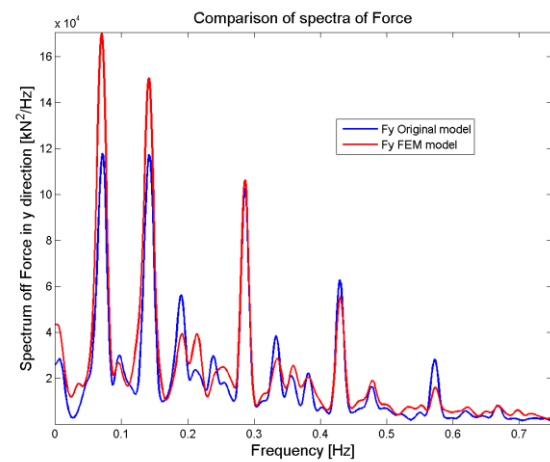
Figure 5.4 Comparison of spectra of the Force in y direction (validation monopile)
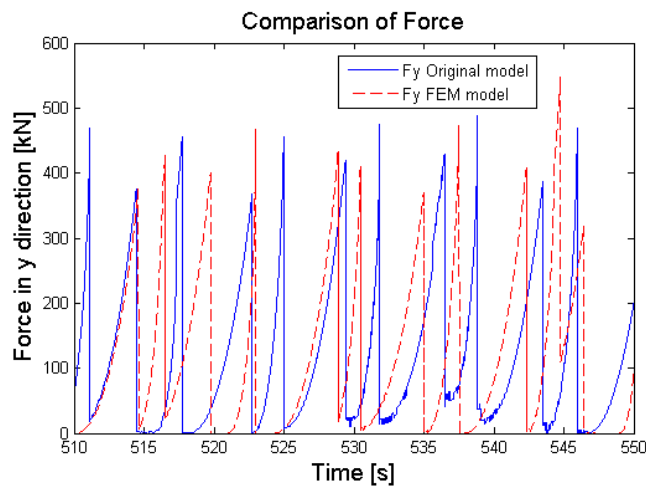
Figure 5.5 Comparison of Force in y direction (validation monopile - ZOOM)

It is observed that the ice loads generated from the FEM DLL file agree closely with the ones generated from the initial constant ice thickness DLL file. Moreover, in the zoomed area, the ice breaking pattern of loading, failure and unloading is clearly observed.

Table 5.1 Statistics for the case of 0.1 m/s (validation monopile)

	Constant thickness model 0.1 m/s	FEM model 0.1 m/s (cnst thickness)
Force in x direction [kN]		
Mean value	1.98	2.10
Standard deviation	107.98	120.31
Force in y direction [kN]		
Mean value	113.53	120.33
Standard deviation	132.22	144.26
Force in z direction [kN]		
Mean value	-121.55	-135.54
Standard deviation	131.62	-151.66
Moment in y direction [kNm]		
Mean value	-7.91	-8.42
Standard deviation	432.43	481.97
Moment in x direction [kNm]		
Mean value	320.86	335.46
Standard deviation	383.67	414.96
Moment in z direction [kNm]		
Mean value	-2.11	-2.06
Standard deviation	111.66	122.05

At this point it has to be mentioned that the statistical values obtained concern the steady state of the ice breaking. From Figure 5.3, this occurs at approximately 400 s, meaning that the effective simulation time is 600 s. So, from the statistical table it is observed that all the values do not deviate much from each other. An interesting ice load to observe is the one in the y direction since it is the one that is aligned with the ice floe's direction towards the structure. The difference between the ice load in the y direction coming from the FEM model and the corresponding load from the constant thickness model is approximately 6% and can be deemed rather small. Accordingly small are the differences in the force and moment for the y direction.

The 0.3 m/s drifting speed of ice follows, considering the ice load in the z direction. The ice load in the z direction is also interesting to observe since it is the one that is compared with the responsible load for downward bending of the ice floe.
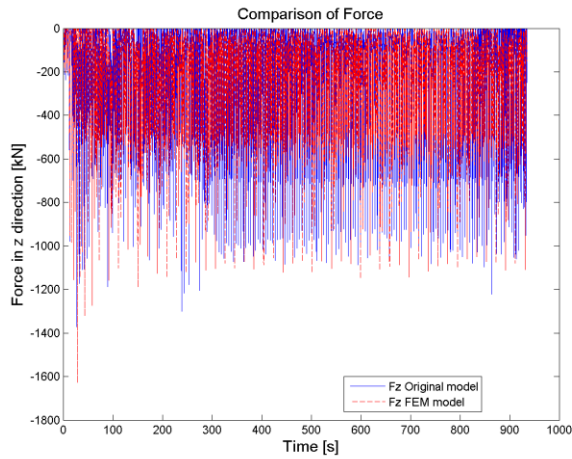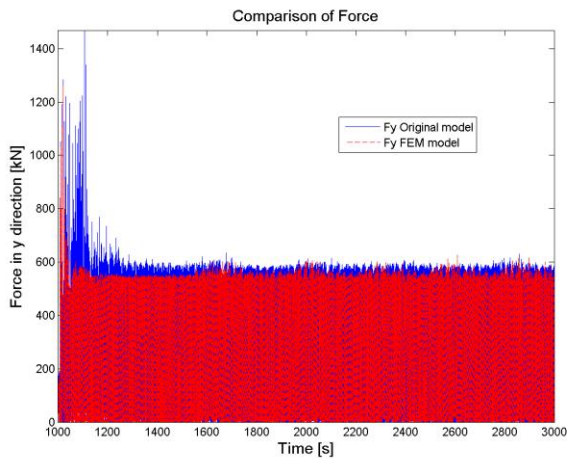
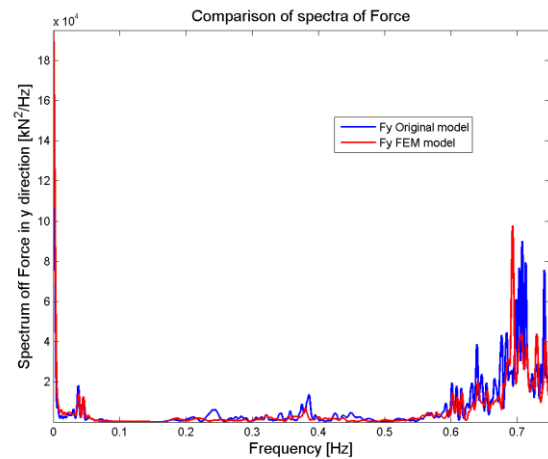**Figure 5.6 Comparison of Force in z direction (validation monopile)**
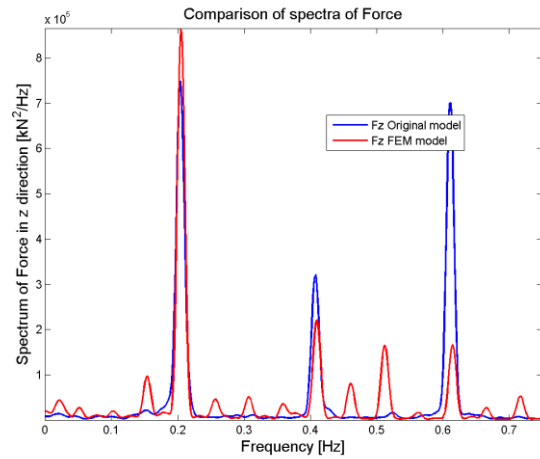
Figure 5.7 Comparison of spectra of the Force in z direction (validation monopile)
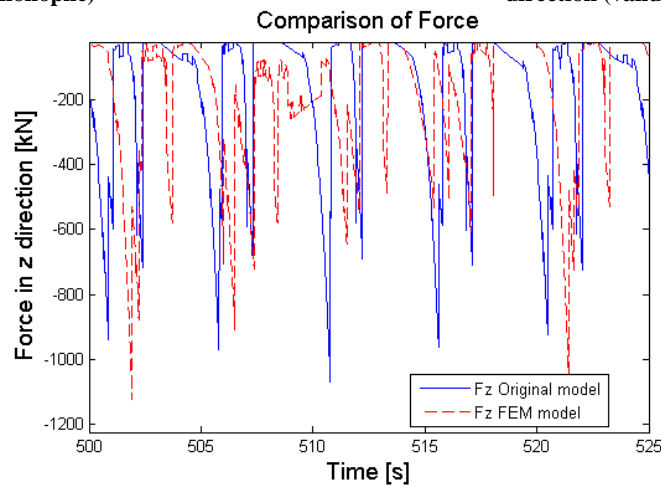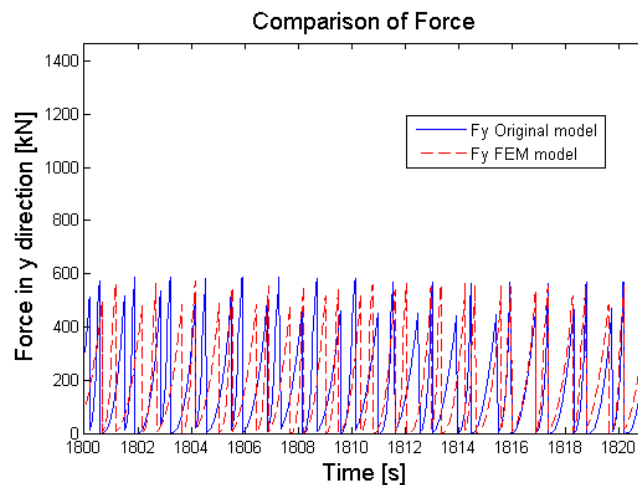

Figure 5.8 Comparison of Force in z direction (validation monopile - ZOOM)

Table 5.2 Statistics for the case of 0.3 m/s (validation monopile)

	Constant thickness model 0.3 m/s	FEM model 0.3 m/s (cnst thickness)
Force in x direction [kN]		
Mean value	0.77	0.99
Standard deviation	92.98	125.02
Force in y direction [kN]		
Mean value	144.21	150.24
Standard deviation	223.80	202.91
Force in z direction [kN]		
Mean value	-161.45	-178.28
Standard deviation	217.39	203.12
Moment in y direction [kNm]		
Mean value	-2.76	-4.09
Standard deviation	364.46	400.78
Moment in x direction [kNm]		
Mean value	402.85	410.96
Standard deviation	652.60	586.71
Moment in z direction [kNm]		
Mean value	-0.66	-0.79
Standard deviation	91.68	129.47

It can be observed from the timeseries that the general pattern of the ice load from the initial constant thickness DLL is closely followed by the FEM DLL with some minor differences in some peak loads. The zoomed area reveals though that these differences are not chaotic. This can also be seen from the statistical values of the FEM and the constant thickness model. For example when comparing the forces in y and z direction, the difference does not exceed 10%, which is a proper difference margin. Again, these values are obtained from the steady state case which starts at about 300 s (Figure 5.6). Therefore, the effective simulation time is approximately 650 s.

The case of 0.5 m/s drifting speed of ice is presented next, considering the ice load in the z direction.
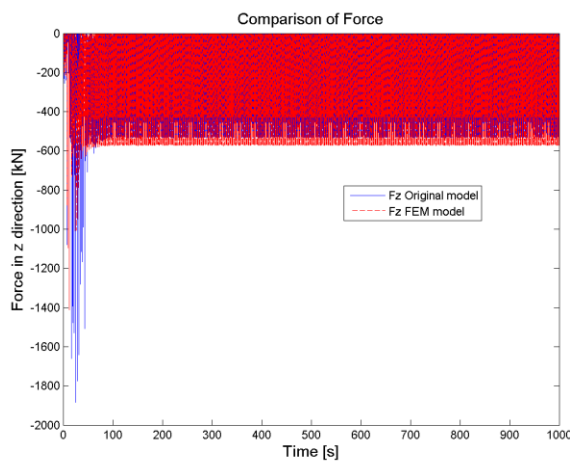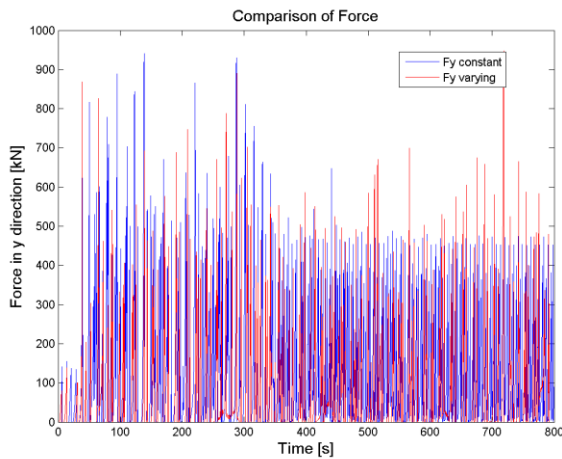

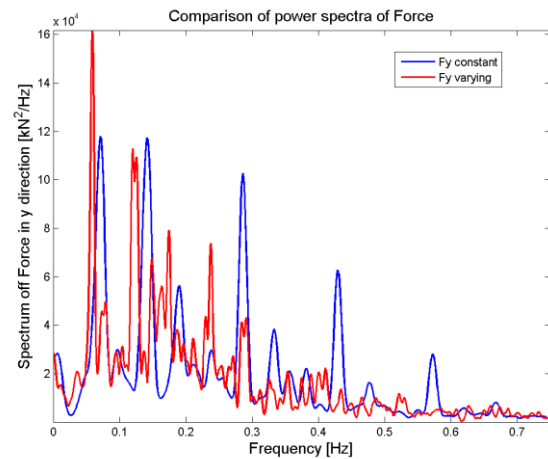**Figure 5.9 Comparison of Force in z direction (validation monopile)**
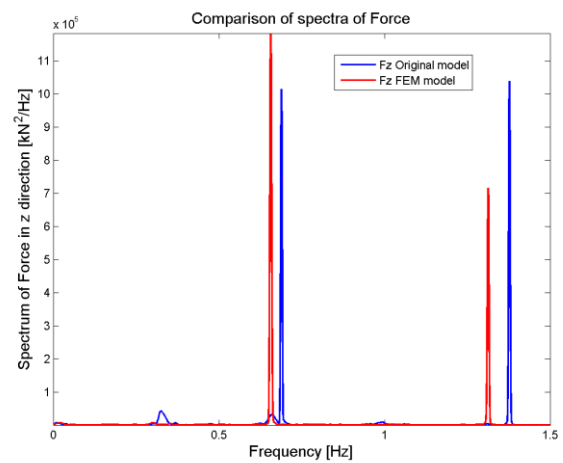
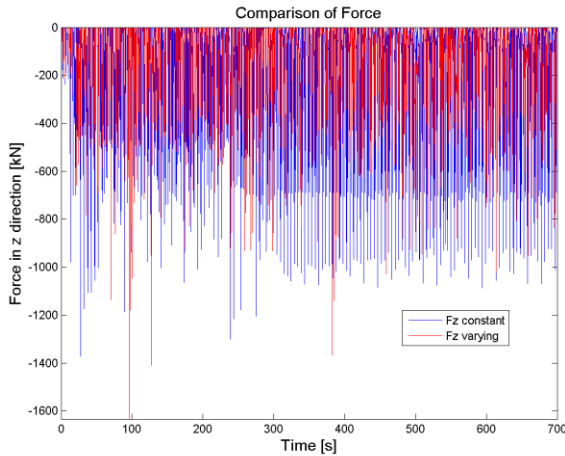**Figure 5.10 Comparison of spectra of the Force in z direction (validation monopile)**
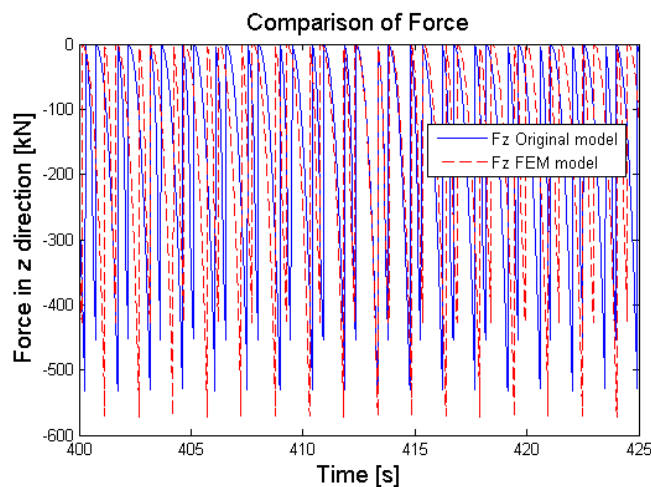
Figure 5.11 Comparison of Force in z direction (validation monopile - ZOOM)

Table 5.3 Statistics for the case of 0.5 m/s (validation monopile)

	Constant thickness model 0.5 m/s	FEM model 0.5 m/s (cnst thickness)
Force in x direction [kN]		
Mean value	-0.83	-0.56
Standard deviation	139.65	147.49
Force in y direction [kN]		
Mean value	200.45	180.49
Standard deviation	174.3	168.09
Force in z direction [kN]		
Mean value	-201.09	-185.96
Standard deviation	155.23	160.35
Moment in y direction [kNm]		
Mean value	3.14	2.74
Standard deviation	559.29	592.59
Moment in x direction [kNm]		
Mean value	576.01	525.11
Standard deviation	508.62	491.05
Moment in z direction [kNm]		
Mean value	0.83	0.46
Standard deviation	150.56	159.49

For the case of 0.5 m/s it is observed from the timeseries and the zoomed part that the breaking procedure is of the initial constant thickness DLL is followed quite accurately by the FEM DLL. In this case the transient state has its minimum value compared to the other drifting speeds and as a result the effective length is approximately 950 s. Moreover, when observing the mean values of the loading the differences that occur do not exceed 10%. In the spectra figure, however, it is observed a small shift of the frequencies excited within the ice floe. As a general comment though, the validation against a monopile for the case of 0.5 m/s drifting speed of ice can be characterised successful.

5.1.2.2 Validation against a spar

Since the comparison of the effect of the varying ice thickness floe will be performed against a spar structure, it was decided to carry out another set of validation tests considering a spar structure and a uniform ice thickness (0.59 m) floe, as well.

Initially, the original DLL file was used in the simulation and afterwards the FEM DLL file was coupled with HAWC2. The simulation time was set to 3000 s and the timestep 0.001 s. The drifting speeds of 0.3 m/s and 0.5 m/s and also the case of 0.3 m/s including constant wind speed of 12 m/s were tested. Similarly to the monopile validation tests, all the statistical values for forces and moments for all directions are presented in tables, for the steady state

case, and indicative ice load timeseries are presented as well. All the forces and moments compared for all the cases in all directions can be found in Appendix C2 (page 131).

To begin with the 0.3 m/s drifting speed with no wind. The force in the y direction is presented.
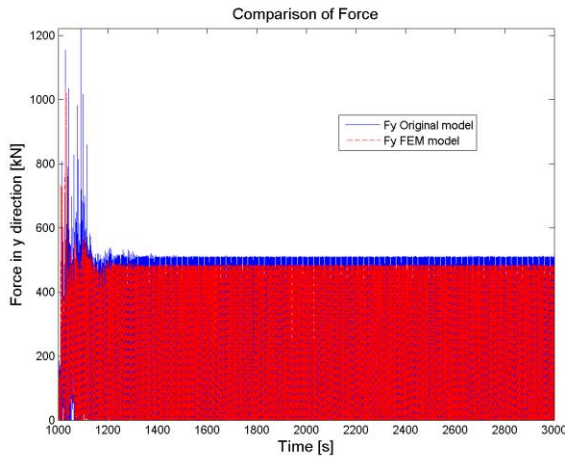
Figure 5.12 Comparison of Force in y direction (validation spar)
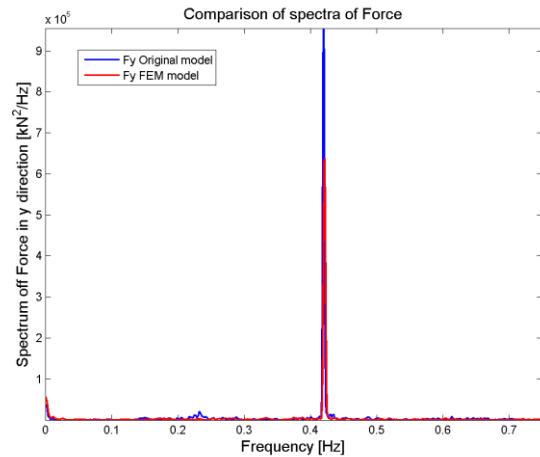
Figure 5.13 Comparison of spectra of the Force in y direction (validation spar)
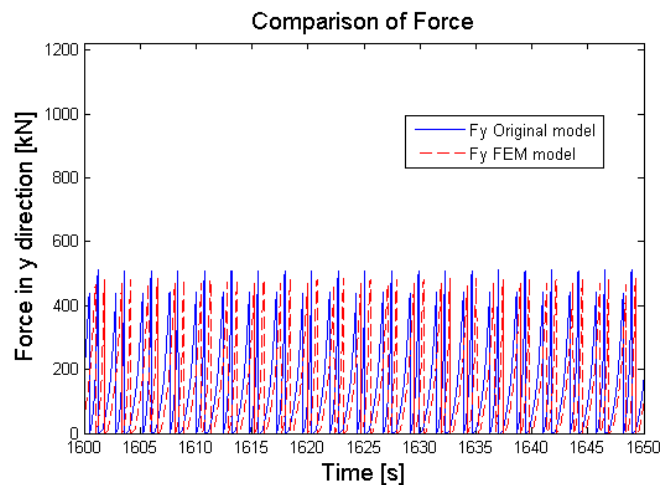
Figure 5.14 Comparison of Force in y direction (validation spar - ZOOM)

It is observed that the ice loads coming from the FEM model comply with the ones produced by the initial constant thickness model. Again, in the zoomed area the ice breaking pattern is clearly defined.

Table 5.4 Statistics for the case of 0.3 m/s with no wind speed (validation spar)

	Constant thickness model 0.3 m/s	FEM model 0.3 m/s (cnst thickness)
Force in x direction [kN]		
Mean value	-0.58	0.04
Standard deviation	113.13	120.18
Force in y direction [kN]		
Mean value	131.46	142.34
Standard deviation	131.89	137.90
Force in z direction [kN]		
Mean value	-119.02	-129.93
Standard deviation	-134.33	140.70
Moment in y direction [kNm]		
Mean value	2.08	-0.12
Standard deviation	455.72	483.95
Moment in x direction [kNm]		
Mean value	764.49	795.68
Standard deviation	1245.3	1241.4
Moment in z direction [kNm]		
Mean value	0.25	-0.14
Standard deviation	123.13	131.65

The statistical values, consider the effective simulation time where the initial transient part is excluded. The transient part lasts approximately 300 s, therefore the effective simulation time is about 1700 s (Figure 5.12). It is observed from the table, that all the values do not differ from each other. Their difference in the load in the z direction and in the y direction is approximately 8% and can be considered rather small. Moreover, similarly small are the differences in the force and moment both for the mean values and standard deviations.

The 0.3 m/s drifting speed of ice including constant wind 12 m/s follows.
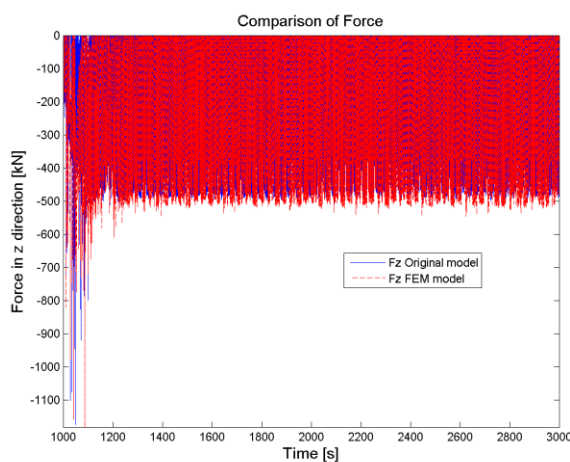
Figure 5.15 Comparison of Force in z direction (validation spar)
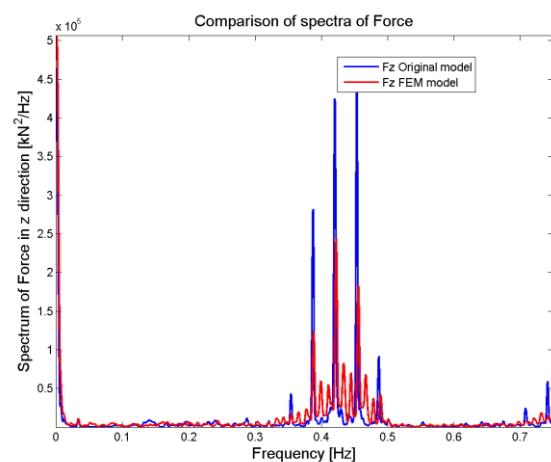
Figure 5.16 Comparison of spectra of the Force in z direction (validation spar)
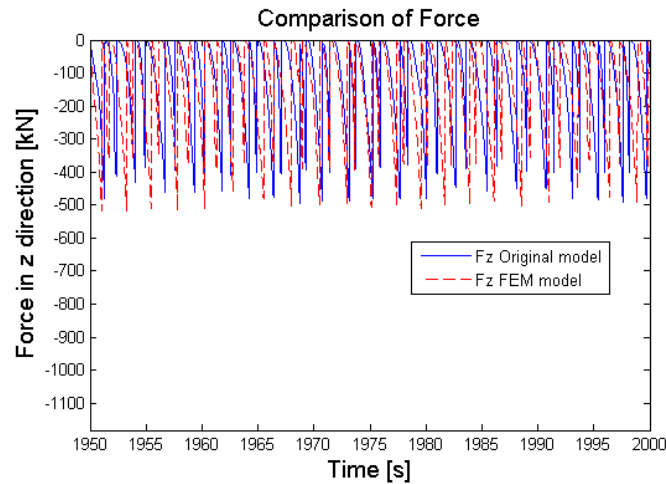
Figure 5.17 Comparison of Force in z direction (validation spar - ZOOM)

Similarly to the case of 0.3 m/s without wind, the ice loads coming from the FEM and the constant ice thickness model agree with each other.

Table 5.5 Statistics for the case of 0.3 m/s with constant wind speed (validation spar)

	Constant thickness model 0.3 m/s	FEM model 0.3 m/s (cnst thickness)
Force in x direction [kN]		
Mean value	-0.38	-0.31
Standard deviation	114.93	124.59
Force in y direction [kN]		
Mean value	131.34	143.12
Standard deviation	132.07	139.47
Force in z direction [kN]		
Mean value	-119.20	-134.12
Standard deviation	134.68	144.06
Moment in y direction [kNm]		
Mean value	1.60	1.28
Standard deviation	463.92	502.90
Moment in x direction [kNm]		
Mean value	764.55	796.48
Standard deviation	1245.6	1242.8
Moment in z direction [kNm]		
Mean value	0.43	0.26
Standard deviation	125.80	136.60

As in the case of the 0.3 m/s without wind, the effective simulation time is 1700 s and the statistical values are close with each other. The difference for the mean value of the load in z direction is approximately 11%, while for the load in y direction the difference is approximately 9%. Both are larger than in the case without wind but the difference is still not enormous.

Lastly the ice load for the y direction for the drifting speed of 0.5 m/s is considered.

Figure 5.18 Comparison of Force in y direction (validation spar)

Figure 5.19 Comparison of spectra of the Force in y direction (validation spar)

Figure 5.20 Comparison of Force in y direction (validation spar - ZOOM)

It is observed form the timeseries that the ice loads pattern coming from the FEM and the constant ice thickness model agree well with each other.

Table 5.6 Statistics for the case of 0.5 m/s (validation spar)

	Constant thickness model 0.5 m/s	FEM model 0.5 m/s (cnst thickness)
Force in x direction [kN]		
Mean value	-0.26	-0.14
Standard deviation	130.74	138.54
Force in y direction [kN]		
Mean value	162.45	173.62
Standard deviation	155.03	159.57
Force in z direction [kN]		
Mean value	-149.89	-162.85
Standard deviation	153.96	160.70
Moment in y direction [kNm]		
Mean value	0.97	0.56
Standard deviation	530.98	562.71
Moment in x direction [kNm]		
Mean value	855.94	886.70
Standard deviation	1240.7	1236.1
Moment in z direction [kNm]		
Mean value	0.13	0.12
Standard deviation	144.13	153.15

In this case the transient phase lasted slightly longer than in the 0.3 m/s case, namely 200 s. Therefore, the effective simulation time was 1800 s. It can be observed that he ice loads produced by the FEM model are matching well with the ones from the constant thickness model. The moments and forces are close to zero for the x direction and the difference in the force in the z and y direction does not exceed 8%.

In all tests both for the monopile and the spar, the icebreaking pattern of loading, breaking and unloading can be observed. Moreover, according to the statistical values the ice load timeseries obtained by the FEM model are very similar to the ones obtained by the constant thickness model. Furthermore, in all cases the trend the spectra follow is similar for both model, revealing the same effect on ice floe.

Taking into consideration the validation study performed with a monopile and especially with a spar floater, it is concluded that the FEM model implemented as a DLL file can give appropriate results. Therefore, the comparison between the effect of the varying thickness floe against the constant thickness floe can be deemed proper and reliable.

5.2 Ice actions, constant vs varying thickness

Before proceeding with the comparison between the constant ice thickness floe and the varying one, a test of the functionality of the FEM DLL file including a varying thickness ice floe is performed considering a monopile, 0.1 m/s and 0.3 m/s drifting speed of ice. The simulations run for 800 s and 700 s respectively and the corresponding timestep was 0.001 s. As in the validation tests, the ice loads are concerned for comparison. Also the statistical data, considering the steady state case, for all ice actions in all directions are presented while indicative loads are presented as well. The results of the comparison as a whole can be found in Appendix D1 (page 137) and D2 (page 138).

To begin with the case of 0.1 m/s and the force in the y direction.

Figure 5.21 Comparison of Force in y direction (comparison monopile)

Figure 5.22 Comparison of spectra of the Force in y direction (comparison monopile)
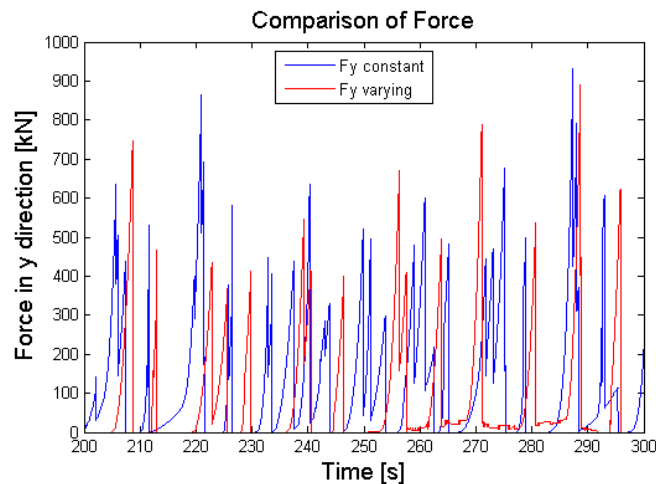
Figure 5.23 Comparison of Force in y direction (comparison monopile - ZOOM)

From the timeseries it can be observed that the ice loads for the varying thickness floe are fluctuating and do not follow the smooth breaking procedure of the constant thickness floe

that can be observed from approximately 400 s and onwards. These fluctuations are the result of the varying thickness field. Moreover, from the zoomed area, can be observed that there is more time that the ice floe is not in contact with the structure, meaning that the ice broken pieces are larger, which corresponds to a larger characteristic length. Also, some small differences can be observed in the spectra between the constant ice thickness flow and the varying one due to the differences in the load fluctuations. The effective simulation time of this case is 400 s. Also, due to the different breaking pattern of the varying thickness floe, there is also a shift in the spectrum, where it can be observed that is more condensed closer to high frequencies.

Table 5.7 Statistics for the case of 0.1 m/s (comparison monopile)

	Constant thickness model 0.1 m/s	sFEM model 0.1 m/s (var. thickness)
Force in x direction [kN]		
Mean value	1.98	4.38
Standard deviation	107.98	77.36
Force in y direction [kN]		
Mean value	113.53	68.47
Standard deviation	132.22	123
Force in z direction [kN]		
Mean value	-121.55	-72.42
Standard deviation	131.62	120.67
Moment in y direction [kNm]		
Mean value	-7.91	-17.53
Standard deviation	432.43	309.92
Moment in x direction [kNm]		
Mean value	320.86	193.45
Standard deviation	383.67	357.68
Moment in z direction [kNm]		
Mean value	-2.11	-3.35
Standard deviation	111.66	77.72

From the statistical table, mostly focus can be given to the mean values of the force and in z and y direction and of the moment in y and x direction. A noticeable drop in the mean values of the ice load is observed, namely 40% for the force both in z direction and y direction. Also, a drop in the order of 40% is observed in the moment in y direction as well. On the other hand the moment in x direction is approximately 2.5 times higher than the initial one (the same increase is observed also in the force in x direction). However their value is close to zero as it should be. As explained above, due to the fact that the ice broken pieces are larger in the varying thickness floe, there is more time where there is no ice - structure interaction. As a result, when there is no contact, the ice load is zero and the mean values generally drop.

In the case of 0.3 m/s, the force in the z direction is presented.

Figure 5.24 Comparison of Force in z direction (comparison monopile)
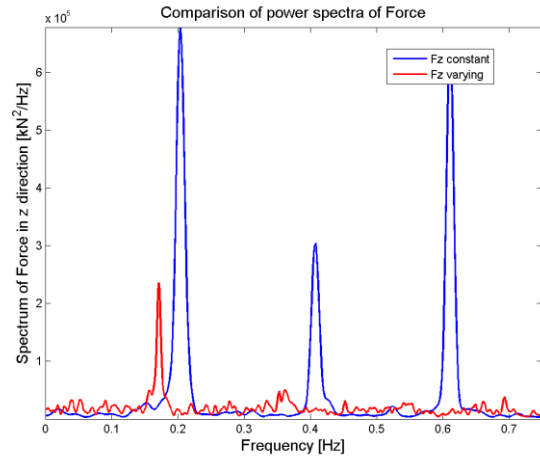
Figure 5.25 Comparison of spectra of the Force in z direction (comparison monopile)
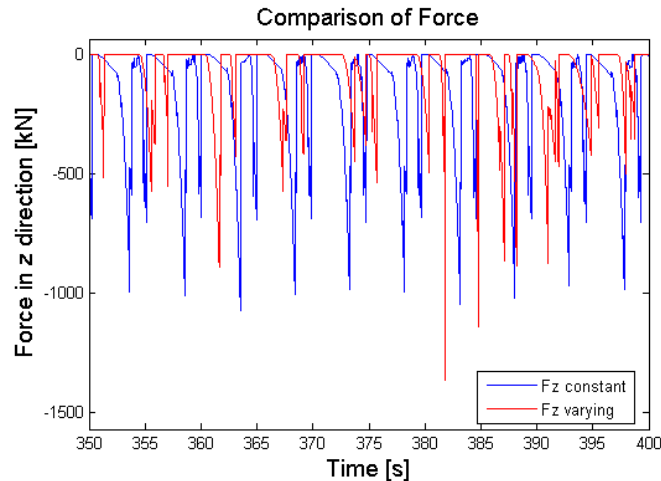
Figure 5.26 Comparison of Force in z direction (comparison monopile - ZOOM)

Similarly to the 0.1 m/s case, it can be observed that the ice loads coming from the varying thickness floe fluctuate more that the ones coming from the constant thickness floe. The effective length of the simulation is 400 s. From the zoomed area, it is clearly observed that there is quite some time where no ice - structure interaction is taking place. Due to the different breaking pattern, a difference in the spectrum of the varying thickness load is also observed.

Table 5.8 Statistics for the case of 0.3 m/s (comparison monopile)

	Constant thickness model 0.3 m/s	FEM model 0.3 m/s (var. thickness)
Force in x direction [kN]		
Mean value	0.77	1.94
Standard deviation	92.98	97.60
Force in y direction [kN]		
Mean value	144.21	86.64
Standard deviation	223.80	149.73
Force in z direction [kN]		
Mean value	-161.45	-90.75
Standard deviation	217.39	148.54
Moment in y direction [kNm]		
Mean value	-2.76	-7.84
Standard deviation	364.46	390.83
Moment in x direction [kNm]		
Mean value	402.85	245.65
Standard deviation	652.60	433.88
Moment in z direction [kNm]		
Mean value	-0.66	-1.81
Standard deviation	91.68	98.95

From a statistical point of view, again it is noticed that the mean values of forces in the y and z direction and the mean value of moment in y direction show a significant drop in the order of 40%. Moreover, the mean values for the force in x direction and the mean values of moment in x and z direction are close to zero as expected.

The case of 0.5 m/s and the force in the y direction is upcoming. All the loadings for all directions can be found in Appendix E3 (page 145).
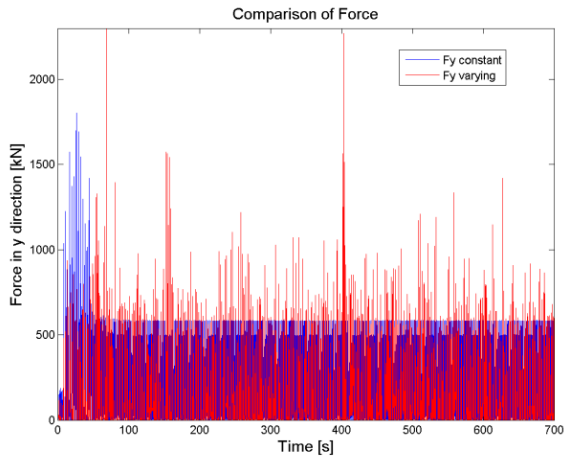
Figure 5.27 Comparison of Force in y direction (comparison monopile)
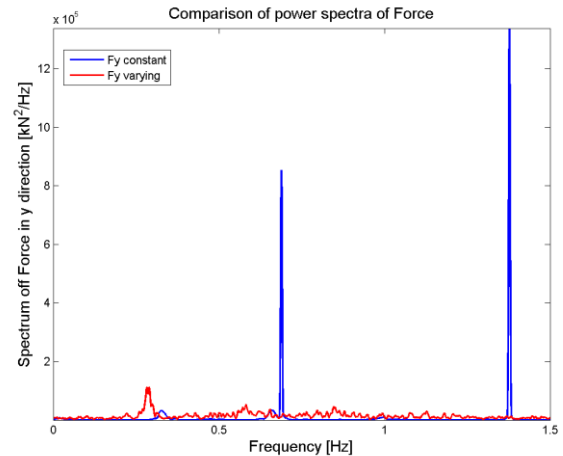
Figure 5.28 Comparison of spectra of the Force in y direction (comparison monopile)
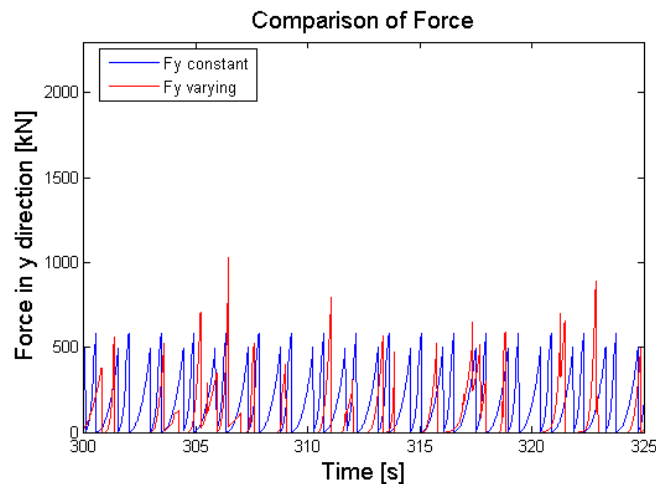
Figure 5.29 Comparison of Force in y direction (comparison monopile - ZOOM)

From the timeseries it can be observed that the ice loads for the varying thickness floe are fluctuating in a more severe way than when the constant thickness ice floe is considered. These fluctuations are the result of the varying thickness field. Furthermore, when the zoomed area is observed, then it can be seen that less time of ice structure interaction occurs. As explained this can be linked to the fact that in the varying thickness floe the characteristic length can reach some high values and as result the broken ice pieces are larger. Regarding the spectra, no significant dynamic effect are introduced in this case except a very small peak at approximately 0.28 Hz. In general the energy density seems to be spread out in the whole range of frequencies. The effective simulation time is 650 s.

Table 5.9 Statistics for the case of 0.5 m/s (comparison monopile)

	Constant thickness model 0.5 m/s	FEM model 0.5 m/s (var. thickness)
Force in x direction [kN]		
Mean value	-0.83	-1.50
Standard deviation	139.65	115.68
Force in y direction [kN]		
Mean value	200.45	104.84
Standard deviation	174.3	177.91
Force in z direction [kN]		
Mean value	-201.09	-109.27
Standard deviation	155.23	175.55
Moment in y direction [kNm]		
Mean value	3.14	5.88
Standard deviation	559.29	463.38
Moment in x direction [kNm]		
Mean value	576.01	297.22
Standard deviation	508.62	515.41
Moment in z direction [kNm]		
Mean value	0.83	1.02
Standard deviation	150.56	117.53

From a statistical point of view the most interesting loads to consider are the forces on y and z direction. Both of them, when the varying thickness floe is considered, a significant decrease of approximately 50% in the mean values is observed. The same decrease is also observed in the moment in y direction. The force though in the x direction, as well as the moment in x and z direction are close to zero. Since there is less time of ice - structure interaction, there are more zero values of loading that are considered, therefore the mean generally drops.

Generally, it should be mentioned that the effect of the drifting speed is obvious for the loads. Higher drifting speed of ice results higher loads as expected from the dynamic factor $c_f = (1.65 + 2.47v_2^{0.4})$. Furthermore, when a varying ice thickness floe is considered, the loads show an important drop in the mean value. However, as explained, this low mean value is also an outcome of the fact that there is less time of ice - structure interaction. Moreover, the spectra of the forces show a different behaviour due to the difference in the breaking pattern.

Moving on to the comparison of the varying thickness floe with the constant one against a spar structure. In every simulation, the ice force is applied on the structure during the last 2000 seconds of the total simulation time as explained in section 4.3 . In most cases, convergence was successful. However, during the simulations of 0.1 m/s drifting speed of ice, both for the constant and the varying thickness model numerical convergence issues were encountered.

5.2.1 Semi - empirical constant thickness model results

To begin with a indicative discussion of the results obtained during last semester's project assignment that come from the model explained in section 2.9.1 . A dynamic analysis of the spar wind turbine in level ice with varying thickness was performed and compared with the results from a constant ice thickness floe regarding the ice loads. The ice floe used is the one presented in Figure 2.10, with a mean thickness of 0.34 m. The figures presented below refer to a drifting ice speed of 0.5 m/s and show the force in the Fore - Aft direction and the corresponding spectrum. Moreover, the statistical properties of all ice drifting speeds are presented regarding the force in the y direction.
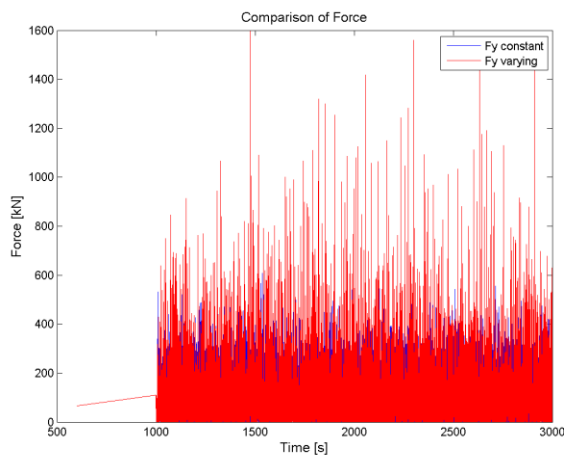
Figure 5.30 Comparison of Force in y direction (project assignment)
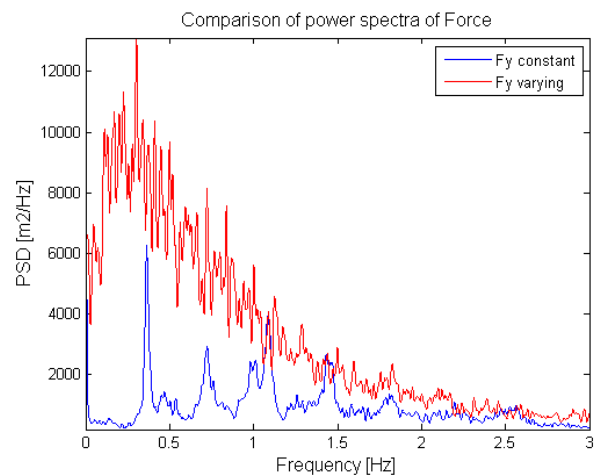
Figure 5.31 Comparison of spectra of the Force in y direction (project assignment)

Table 5.10 Statistics for Force in y direction for all simulations (pre-thesis)

Simulation	Force in y direction [kN]	
	Mean value	Standard deviation
Constant 0.1 m/s	40.4	50.82
Varying 0.1 m/s	41.8	66.19
Constant 0.3 m/s	67.3	56.9
Varying 0.3 m/s	81.7	96.9
Constant 0.5 m/s	75.55	61.9
Varying 0.5 m/s	89.5	107.7

A general comment that could be extracted is that the varying thickness behaviour in terms of spectra is different than the constant thickness one where some peaks can be clearly defined. Also, as the speed increases the observed ice actions increase as well both for the varying and the constant ice thickness. However, it should be mentioned again that these results include the assumption that when the ice collides with the structure, then the thickness of the ice floe

is considered constant and equal to the one the floe has at the contact point with the structure. Meaning that, these are the ice loads if the structure is hit by multiple constant ice thickness floes of different thickness at each time. This is a very rough approximation of a varying thickness field that is be considered quite unreliable. More figures showing the ice force and moment in different directions and speeds can be found in Appendix D3 (page 140).

5.2.2 Drifting speed 0.1 m/s and spar

In the case of 0.1 m/s drifting speed an important issue regarding convergence of HAWC2 was faced. The combination of such low drifting speed and quite thick ice, results the solution of the equations of motion for the whole system (section 2.6) not to converge. This practically means that the ice floe is keep pushing the spar without bending failure to occur. Meaning that there is continuous crushing the failure load in bending is never reached. The corresponding error message displayed by the compiler was:

forrtl: severe <159>: Program Exception – breakpoint
Image	*PC*	*Routine*	*Line*	*Source*
MSVCRTD.DLL	*10212AD0*	*Unknown*	*Unknown*	*Unknown*

Different ramp loads and ramp duration lengths were tested; however the error message kept appearing. Therefore, simulations with 0.1 m/s drifting speed were not successful. It should be mentioned that such problem was also encountered during the project assignment (for the thickness of 0.34 m) and it was encountered by other studies as well (Saccoman 2015).

5.2.3 Drifting speed 0.3 m/s and spar

In the case of 0.3 m/s drifting speed, as soon as the ramp function was clearly set from the convergence study, no issues regarding convergence of HAWC2 occurred. Similarly to the monopile case, the comparison of direct ice loads regarding statistical values if performed and indicative timeseries of interesting loads are presented. The ice load simulations of all ice loads in all directions are appearing in Appendix E2 (page 143).

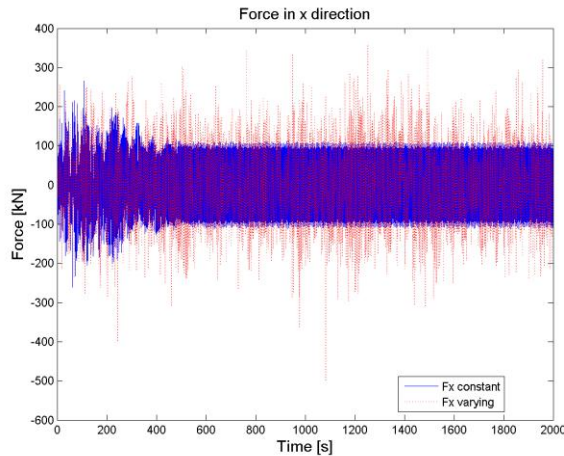The force in the y direction is presented.
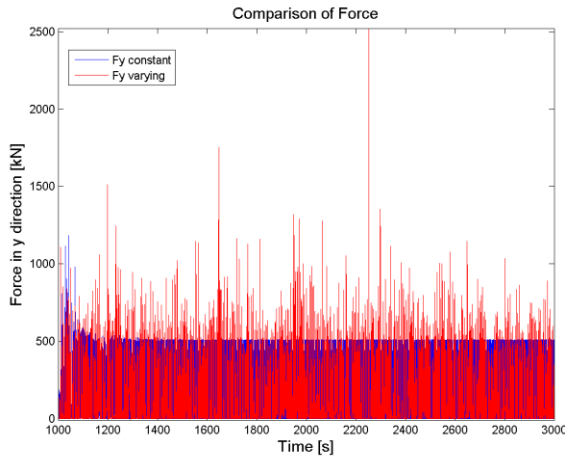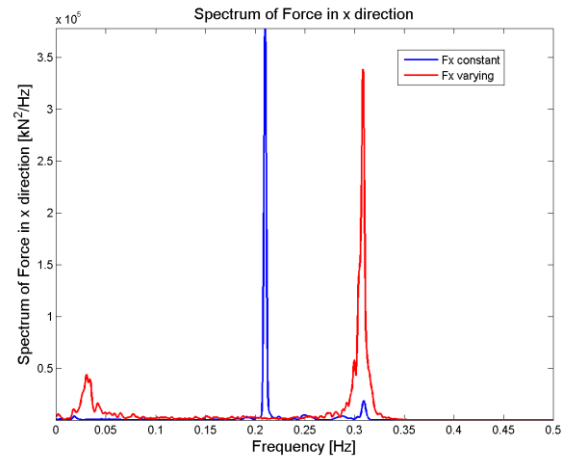
Figure 5.32 Comparison of Force in y direction
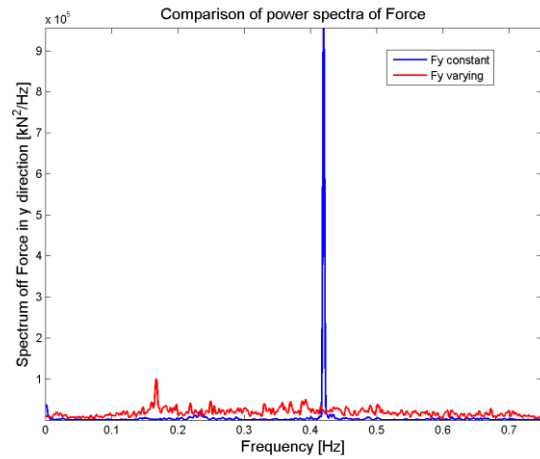
Figure 5.33 Comparison of spectra of the Force in y direction
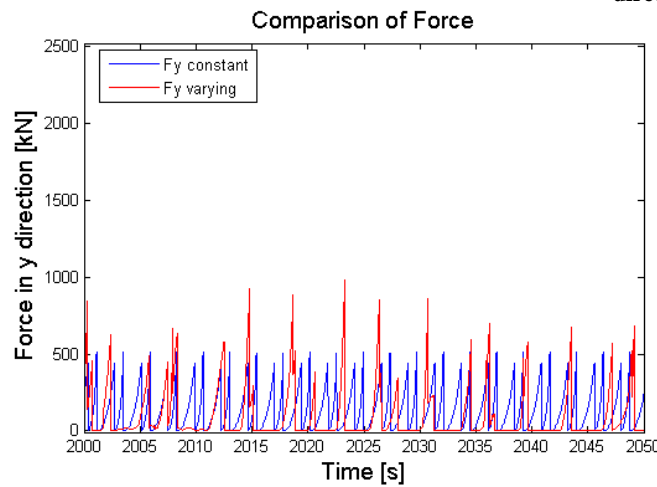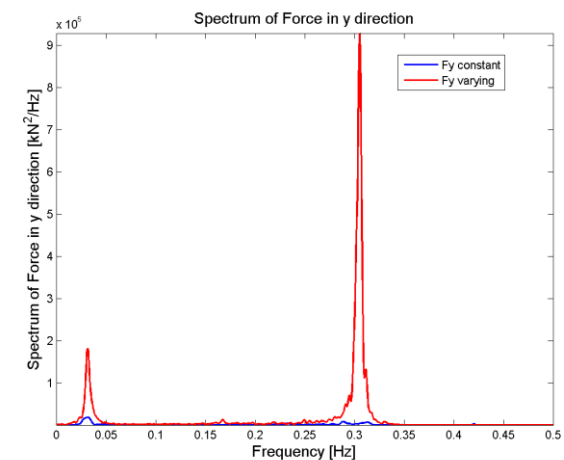

Figure 5.34 Comparison of Force in y direction (comparison spar - ZOOM)

Table 5.11 Statistics of ice loads for the case of 0.3 m/s (comparison spar)

	Constant thickness model 0.3 m/s	FEM model 0.3 m/s (var. thickness)
Force in x direction [kN]		
Mean value	-0.58	-2.49
Standard deviation	113.13	91.40
Force in y direction [kN]		
Mean value	131.46	92.68
Standard deviation	131.89	150.18
Force in z direction [kN]		
Mean value	-119.02	-88.97
Standard deviation	134.33	151.81
Moment in y direction [kNm]		
Mean value	2.08	11.28
Standard deviation	455.72	371.14
Moment in x direction [kNm]		
Mean value	764.49	271.88
Standard deviation	1245.3	441.56
Moment in z direction [kNm]		
Mean value	0.25	3.29
Standard deviation	123.13	99.42

The effective length of the timeseries concerns the steady state case and lasts from 1200 s until 3000 s. It can be observed that the ice loads show significant fluctuations and many load peaks are quite higher than the maximum value of the peaks coming from the constant thickness model. Due to this fluctuations there is no significant peak standing out from the spectrum representation but a small one at approximately 0.17 Hz. The ice breaking frequency is equal to $f_{br} = \frac{V_{ice}}{L_b}$, where v_{ice} is the relative speed of ice and L_b is the ice breaking length (Naess and Moan 2013). In the case of the varying thickness floe though, the breaking length cannot be clearly identified due to the changes in the characteristic length. Even if this large uncertainty holds, it is believed that this frequency corresponds to the main ice breaking frequency of the varying thickness floe. Moreover, the zoomed area clearly shows the ice breaking pattern of loading, breaking and unloading and also that again, there more time without ice - structure interaction. The statistical data, when a varying ice floe is considered show the same behaviour as for the monopile case. Meaning that the forces in y and z direction significantly drop about 30%. What is also remarkable to mention, is the fact that that the moment in y direction drops approximately 3 times from the value of the constant thickness model. It is believed that this is a result mainly due to the less ice - structure interaction time and the fluctuations in the load.

5.2.4 Drifting speed 0.5 m/s and spar

For the case of 0.5 m/s drifting speed of ice, the ice load presented is the force in z direction. The other loads considering all directions can be found in Appendix E3 (page 145).
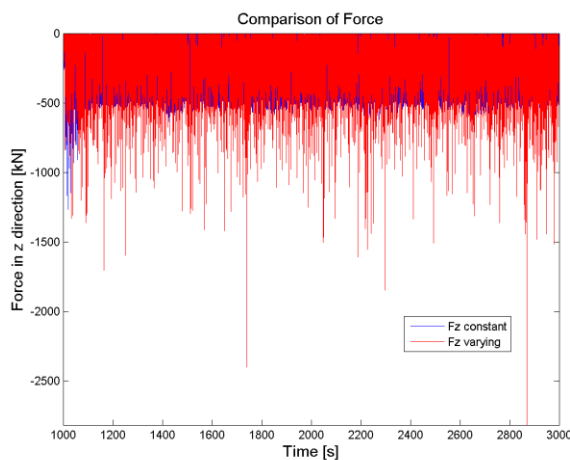
Figure 5.35 Comparison of Force in z direction
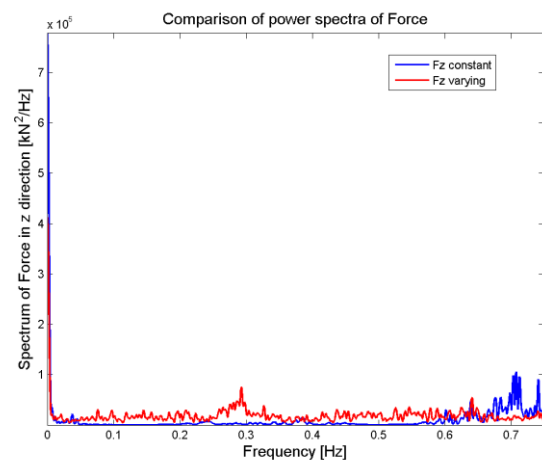
Figure 5.36 Comparison of spectra of the Force in z direction
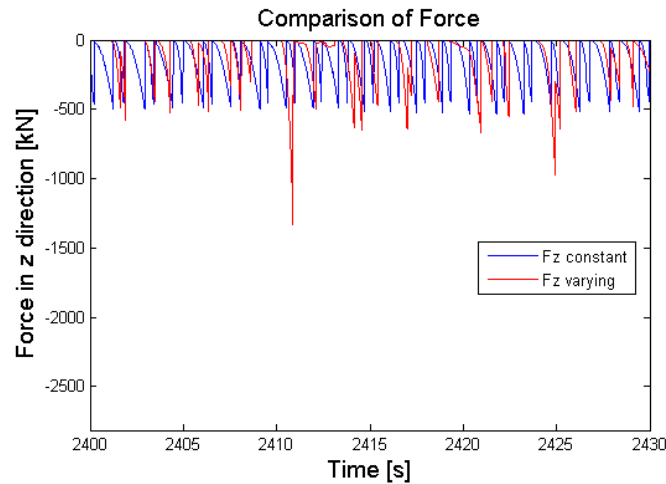
Figure 5.37 Comparison of Force in z direction (comparison spar - ZOOM)

Table 5.12 Statistics of iceloads for the case of 0.5 m/s (comparison spar)

	Constant thickness model 0.5 m/s	FEM model 0.5 m/s (var. thickness)
Force in x direction [kN]		
Mean value	-0.26	-0.89
Standard deviation	130.74	106.57
Force in y direction [kN]		
Mean value	162.45	106.79
Standard deviation	155.03	171.01
Force in z direction [kN]		
Mean value	-149.89	-102.58
Standard deviation	153.96	170.25
Moment in y direction [kNm]		
Mean value	0.97	3.30
Standard deviation	530.98	431.65
Moment in x direction [kNm]		
Mean value	855.94	301.54
Standard deviation	1240.7	499.18
Moment in z direction [kNm]		
Mean value	0.13	0.62
Standard deviation	144.13	112.92

As in the validation case the effective simulation time was 1750 s. Again, from the timeseries the high fluctuations of the loads can be observed. Moreover, no significant peaks can be defined in the spectrum (but a small one about 0.3 Hz). In the constant thickness case though there is a distinguishing peak at around 0.7 Hz. It is seems like the energy is spread out in the whole range o frequencies for the varying thickness floe. This is believed to occur because of the many fluctuations of the load timeseries. From the zoomed area, the ice breaking patterns of the constant thickness floe and the varying thickness floe are clearly defined. Furthermore, still there is a significant drop in the mean values of the forces that reaches 35% and 30% for the force in y and z direction respectively. Also, the same large drop is observed in the

moment in the x direction as in the 0.3 m/s case. The force in x direction and moments in x and z direction are close to zero as they should be.

As a general outcome, it can be clearly observed the effect of the drifting speed of ice as in the monopile case. Moreover, as discussed in section 4.2 , the varying thickness ice floe is more likely to fail at the local weakest points. Therefore, the characteristic length can differ a lot compared to the characteristic length of the initial constant thickness model. Sometimes the characteristic length is larger and as a result the ice broken piece (though the ice floe radius) is larger. This explains why there is more time with no ice - structure interaction when the varying thickness field is considered.

However, the true and most important effect of the varying thickness ice field on a structure is when considering the corresponding responses. In the upcoming section, this comparison is realised.

5.3 Response analysis, constant vs varying thickness

During the post process analysis of the results obtained from HAWC2, many channels where selected as outcomes, namely displacements, velocities, forces, bending moments at mean sea level and tower top (all both for fore - aft and side to side direction) and all three mooring line tensions. However, in order to keep the main content of this study at a normal level, only the displacements, forces, moments at mean sea level for both x and y direction, and one mooring line tension are going to be presented. All the rest of the responses can be found in Appendix F2 (page 149) and F3 (page 151).

The following figure and table present the natural frequencies and mode shapes of the lowest 20 modes of the structure as obtained by HAWC2 (Saccoman 2015). This table is used as a reference anytime a frequency needs to be identified from the corresponding spectra.
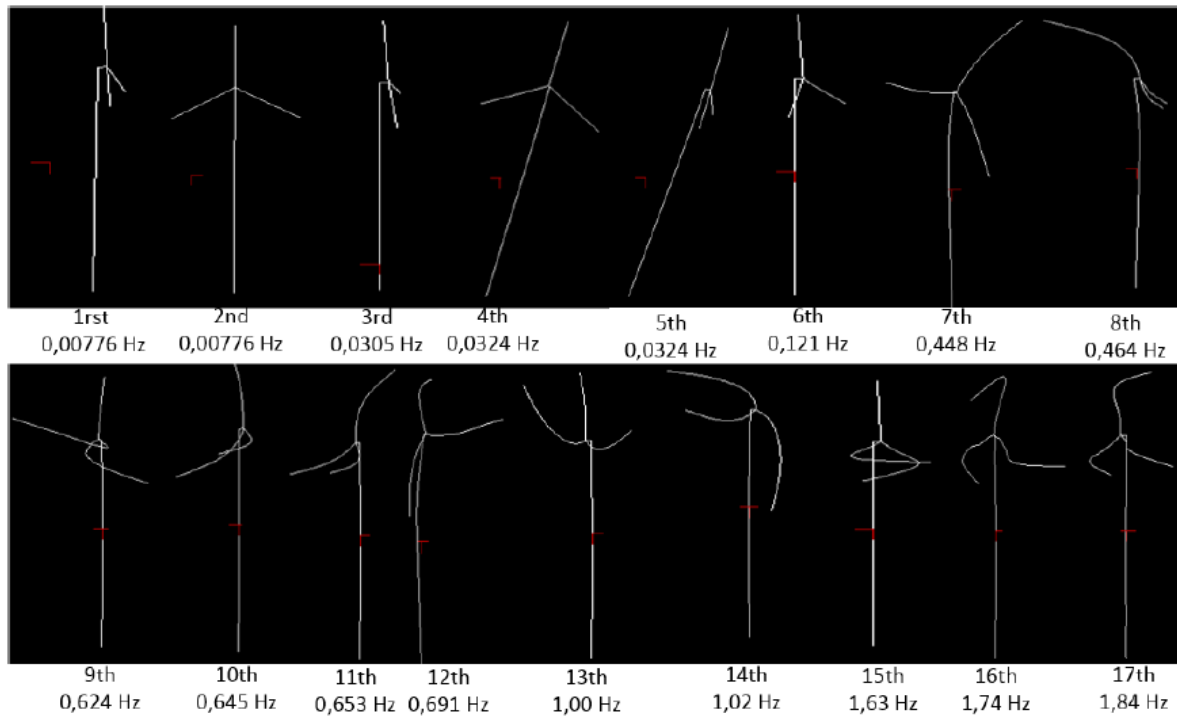
Figure 5.38 Natural frequencies and mode shapes of 20 lowest modes (Saccoman 2015)

Table 5.13 Full system eigenmodes (Saccoman 2015)

Mode number	Natural Frequency [Hz]	Period [s]
1 - Platform Surge	0.00776	128.84
2 - Platform Sway	0.00776	128.84
3 - Platform Heave	0.0305	32.76
4 - Platform Roll	0.0324	30.84
5 - Platform Pitch	0.0324	30.84
6 - Platform Yaw	0.121	8.26
7 - 1st Tower Side to Side	0.448	2.22
8 - 1st Tower Fore - Aft	0.464	2.15
9 - 1st Blade Assymetric Flapwise Yaw	0.624	1.60
10 - 1st Blade Assymetric Flapwise Pitch	0.645	1.54
11 - 1st Blade Collective Flap	0.653	1.53
12 - 1st Drivetrain Torsion	0.691	1.44
13 - 1st Blade Assymetric Edgewise Pitch	1	0.99
14 - 1st Blade Assymetric Edgewise Yaw	1.02	0.98
15 - 2nd Blade Assymetric Flapwise Yaw	1.63	0.61
16 - 2nd Blade Assymetric Flapwise Pitch	1.74	0.57
17 - 2nd Blade Collective Flap	1.84	0.54

5.3.1 Semi - empirical constant thickness model results

An indicative discussion regarding the results obtained during the last semester's project assignment where the assumption that when the ice collides with the structure, then the thickness of the ice floe is considered constant and equal to the one the floe has at the contact point with the structure, is considered. The figures below show the Force in y direction and the corresponding spectrum when the ice drifting speed is 0.5 m/s. Moreover, the statistics for all ice drifting speeds are also presented.
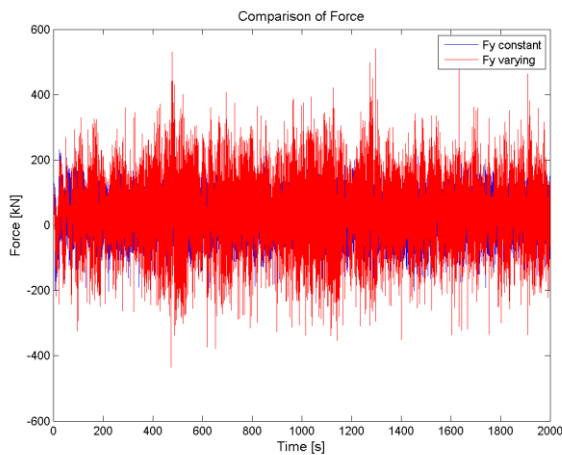
Figure 5.39 Comparison of Response in y direction, 0.5 m/s (pre-thesis)
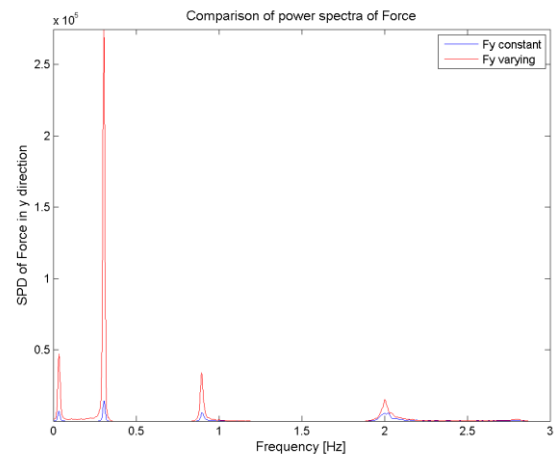
Figure 5.40 Comparison of spectra of the Response in y direction, 0.5m/s (pre-thesis)

Table 5.14 Statistics for Force in y direction for all speeds

Simulation	Force in y direction [kN]	
	Mean value	Standard deviation
Constant 0.1 m/s	13.41	43.88
Varying 0.1 m/s	16.09	51.55
Constant 0.3 m/s	16.71	40.80
Varying 0.3 m/s	23.35	77.07
Constant 0.5 m/s	20.56	14.20
Varying 0.5 m/s	27.05	93.76

The force increases as the drifting speed increases. Moreover, the spectra of the responses show the same peaks both for the varying thickness and the constant thickness simulations. However, the order of magnitude is different. This can be connected to the variation of the ice field, meaning that as the thickness varies, the oscillations become more severe and so the order of magnitude of the spectra peaks gets higher. More figures regarding the project assignment's results are indicative presented in Appendix F1 (page 147). However, it should be mentioned that the above discussion is based on rough assumption regarding the varying ice thickness floe, therefore it should not be taken into consideration

5.3.2 Drifting speed 0.1 m/s and spar

As explained in section 5.2.2 , the simulations of 0.1 m/s drifting speed were not successful due to numerical convergence issues. Therefore, no responses were obtained.

5.3.3 Drifting speed 0.3 m/s and spar

To begin with the case of 0.3 m/s drifting speed and the displacements in x and y direction.
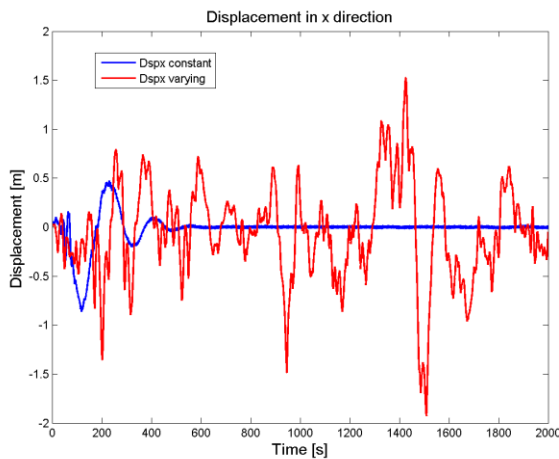
Figure 5.41 Comparison of Displacement in x direction
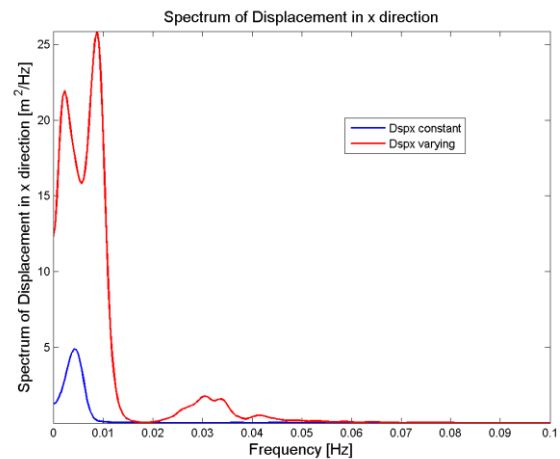
Figure 5.42 Comparison of spectra of the Displacement in x direction
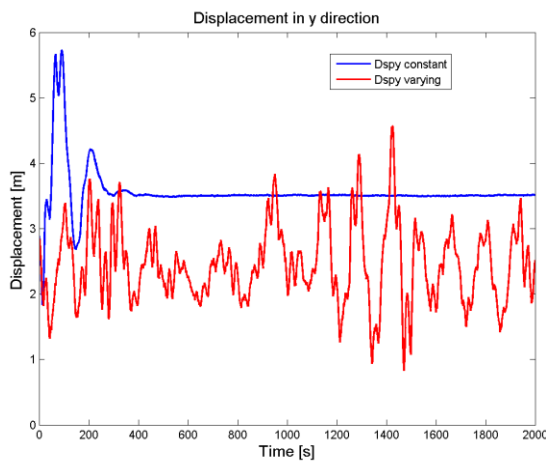
Figure 5.43 Comparison of Displacement in y direction
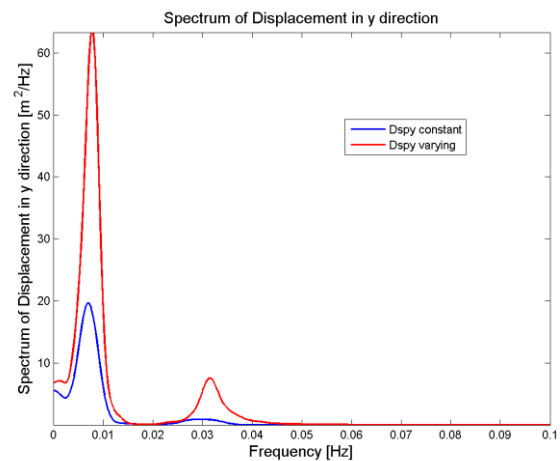
Figure 5.44 Comparison of spectra of the Displacement in y direction

Table 5.15 Statistics for Displacement in the x and y direction for 0.3 m/s

	Constant thickness model 0.3 m/s	FEM model 0.3 m/s (var. thickness)
Displacement in x direction [m]		
Mean value	-0.01	-0.07
Standard deviation	0.15	0.49
Displacement in y direction [m]		
Mean value	3.54	2.43
Standard deviation	0.35	0.58

The steady state response of the spar is observed after 400 s. Therefore, the effective simulation time is approximately 1600 s. Regarding the timeseries in x direction it can be observed that there is much more movement of the structure side to side. In the constant thickness model there is one clear peak identified from the spectrum at approximately 0.005 Hz, which is close to the natural frequency of sway/surge motion. On the other hand, in the varying thickness ice floe spectrum two large peaks can be seen in 0.003 Hz and 0.008 Hz. The later one together with a smaller peak that occurs around 0.03 Hz are very close to the platform sway/surge and mostly heave respectively. From a statistical point of view, the mean value of the motion is nearly zero as it should be due to the symmetry of the structure. In the y direction, the same observation stands for the timeseries. More fluctuations are observed in the varying thickness floe than in the constant thickness floe. The same high peak at approximately 0.007 Hz is observed in both spectra and corresponds to the platform's surge/sway motion. It should be noticed though that the energy density of this peak is quite higher for the varying thickness floe (as in the x direction as well). Moreover, another peak at approximately 0.03 Hz is also observed for both cases (in the varying case is distinguishing more) and corresponds closely to the structure's pitch/roll/heave. Regarding the mean values of platform's motion in the fore - aft direction, a slight decrease is observed for the varying thickness case.

Generally, it is noticed that for the x direction, the varying ice thickness field inserts a more dynamic behaviour on the structure due to the greater amount of frequencies that seem to be excited. For the y direction, the same frequencies are identified from the varying thickness floe as in the constant thickness floe, but with higher density. The differences in both directions could be explained due to the different breaking pattern that occurs in the x and y direction.
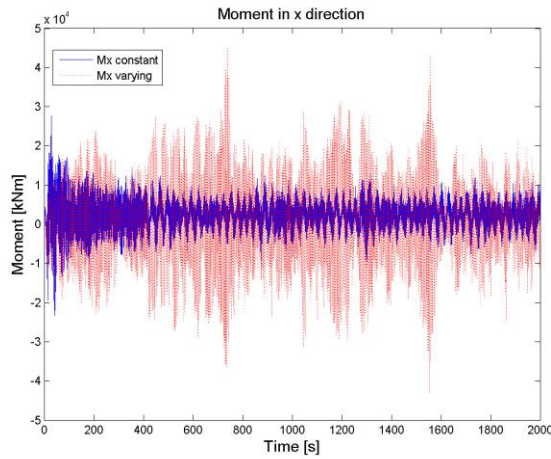
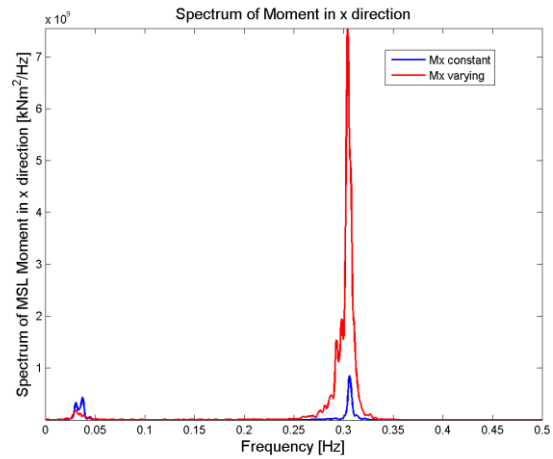**Figure 5.45 Comparison of Force in x direction**

Figure 5.46 Comparison of spectra of the Force in x direction
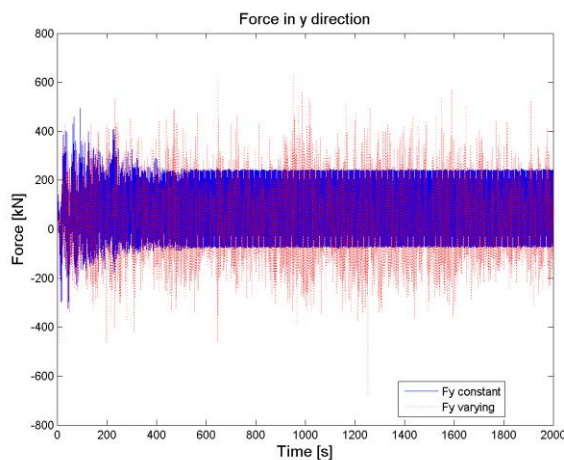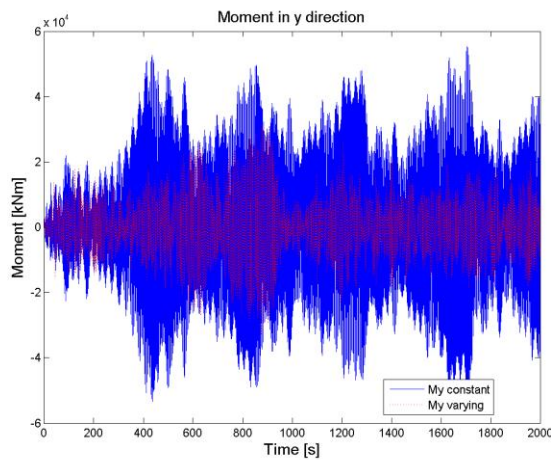

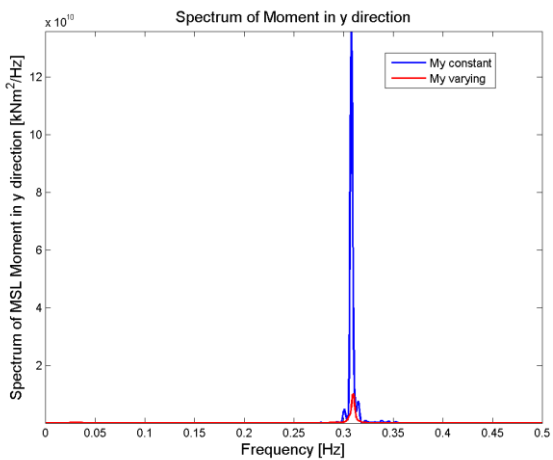**Figure 5.47 Comparison of Force in y direction**

Figure 5.48 Comparison of spectra of the Force in y direction

Table 5.16 Statistics for Force in the x and y direction for 0.3 m/s

	Constant thickness model 0.3 m/s	FEM model 0.3 m/s (var. thickness)
Force in x direction [kN]		
Mean value	-0.23	-1.27
Standard deviation	50.93	72.15
Force in y direction [kN]		
Mean value	44.88	28.01
Standard deviation	53.54	112.60

According to the timeseries, the effective simulation time is 1600 s, as before. The force in the x direction for the varying thickness ice floe fluctuates much more than the constant ice thickness floe response. In the constant ice thickness case one clear peak is defined at 0.21 Hz. The same peak is also observed in the ice induced moment in the y direction (see Appendix E2, page 143). For the varying thickness floe, there is a peak observed in 0.03 Hz, for both directions that corresponds closely to the roll/pitch/heave motion of the platform. However, most of the energy is concentrated at around 0.3 Hz. The mean value of the force in

the x direction is increased while the mean value of the force in y direction is decreased for the varying thickness floe. In both directions the standard deviations are higher due to the more severe fluctuations that can be observed from the timeseries.

In the case of x and y direction and the varying thickness floe, a platform's motion is exited with a higher energy density. On the other hand, for the constant ice thickness this mainly occurs only in the y direction but not so significantly. As a result, one can say that the varying thickness floe introduces more dynamic effects on the structure.
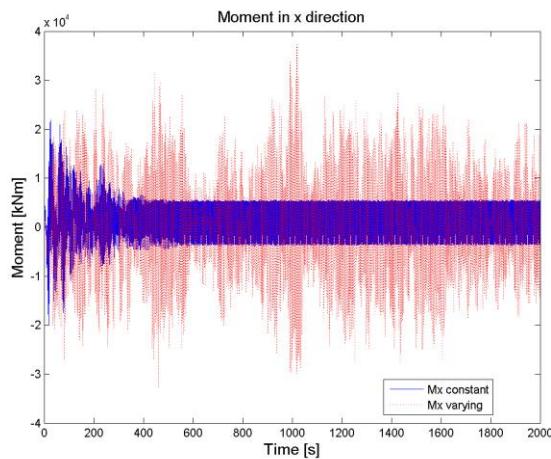
Figure 5.49 Comparison of Moment in x direction
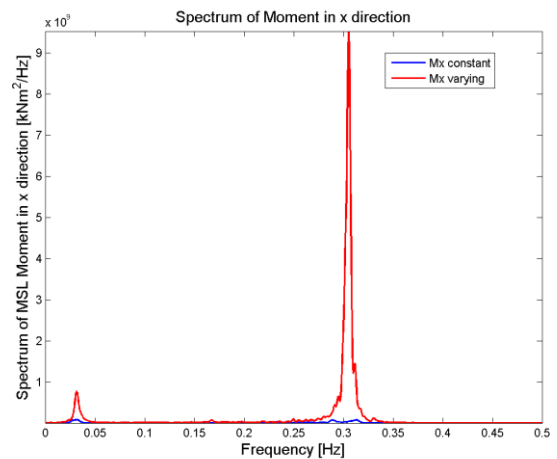
Figure 5.50 Comparison of spectra of the Moment in x direction
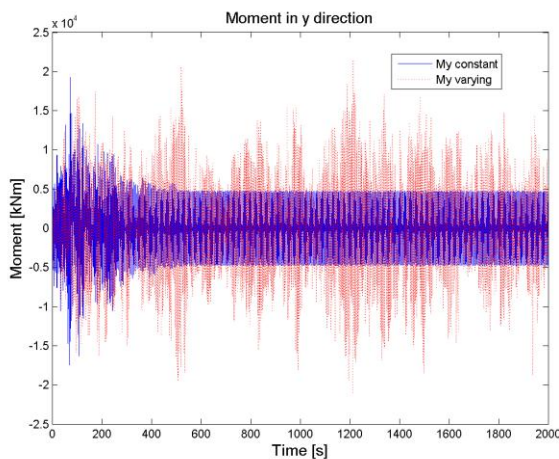
Figure 5.51 Comparison of Moment in y direction
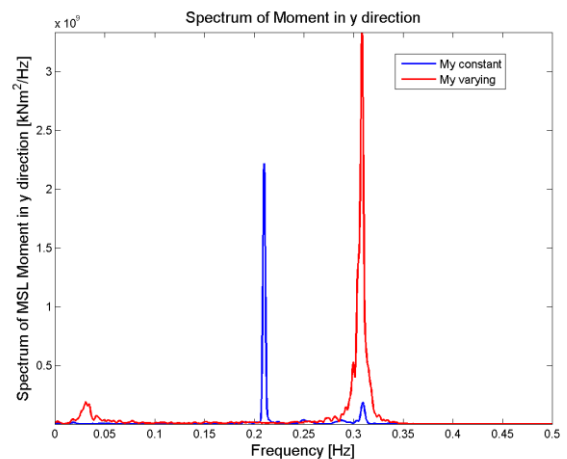
Figure 5.52 Comparison of spectra of the Moment in y direction

Table 5.17 Statistics for Moment in the x and y direction for 0.3 m/s

	Constant thickness model 0.3 m/s	FEM model 0.3 m/s (var. thickness)
Moment in x direction [kNm]		
Mean value	1331.6	268.58
Standard deviation	2967.6	9510.1
Moment in y direction [kNm]		
Mean value	14.26	79.70
Standard deviation	3139.5	5764.9

When looking at the timeseries of moments in both directions it is clearly observed that the effective simulation time is 1600 s. Forces and moments are linked with each other. This relation can be seen when comparing the spectra of the force in x direction with the spectra of the moment in y direction. Meaning that the force at the side to side direction (x axis) produces a moment about the fore - aft direction (y axis). The same holds for the fore and moment in y and x direction respectively. The identified peaks are similar, therefore the effect on the structure is similar. What is remarkable to notice, is the significant decrease of the mean value of the moment in x direction when the varying thickness floe is considered. The decrease is approximately five times less of the initial value while the standard deviation is increased about three times the initial value. On the other hand in the y direction both the mean value and standard deviation of moment are increased by approximately 5.7 and 1.86 times the initial value. The increase in the standard deviation is rather logical due to the high fluctuations that occur from the timeseries. Also, from the timeseries in the x direction, in combination with the mean value, can be concluded that a more symmetric effect occurs when the varying ice thickness floe is considered. Furthermore, the increase of the moment in the y direction can be seen in combination with the increase of the force in the x direction.

Before proceeding with the analysis of a mooring line tension and the corresponding spectrum, it is worth to realise how the mooring system is installed. The next figure depicts the situation.
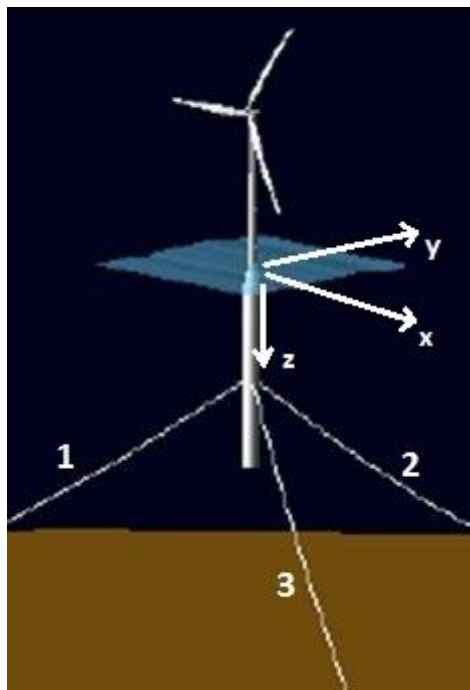
Figure 5.53 Mooring lines position

The y direction is the main direction when the wind turbine is operating, sees the largest forces and motions for the state case. Moreover, the y direction is the ice drifting direction as well. From the statistic table below it is observed that mooring line tension 2 is the one more affected by the varying thickness field. Therefore, it was decided to analyse in the main text mooring line 2.
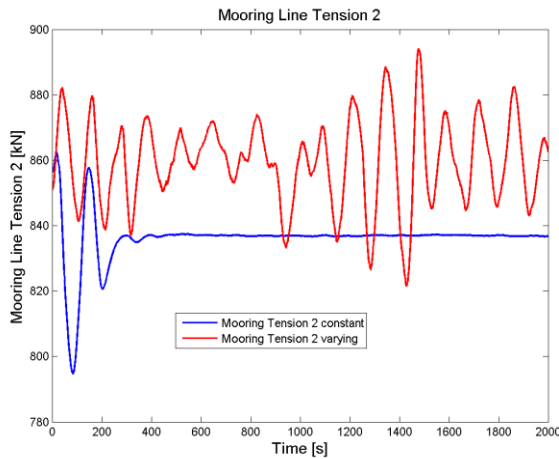
Figure 5.54 Comparison of Mooring line tension 2
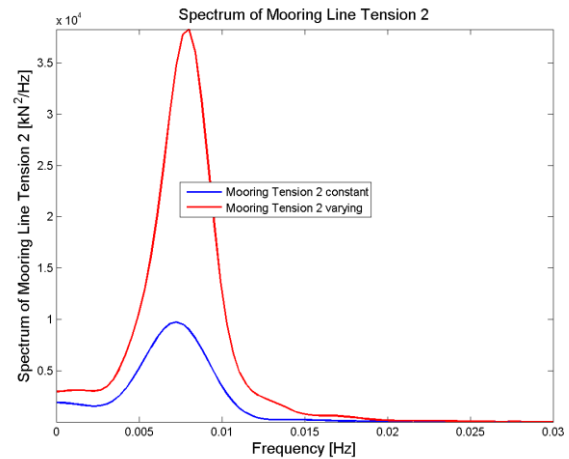
Figure 5.55 Comparison of spectra of the Mooring line tension 2

Table 5.18 Statistics for Mooring lines tension for 0.3 m/s

	Constant thickness model 0.3 m/s	FEM model 0.3 m/s (var. thickness)
Mooring line tension 1 [kN]		
Mean value	955.55	940.32
Standard deviation	5.68	12.45
Mooring line tension 2 [kN]		
Mean value	836.18	859.39
Standard deviation	7.35	13.11
Mooring line tension 3 [kN]		
Mean value	956.17	943.31
Standard deviation	6.28	14.92

The mooring line tension for the constant thickness ice floe shows a constant behaviour after it reaches the steady state position. On the other hand the mooring line tension of the varying thickness floe is fluctuating severely. This is an outcome due to the fluctuations that have been observed in the displacements of the spar. In the constant thickness floe spectrum, a single wide peak is identified at approximately 0.007 Hz and corresponds closely to the platform's surge/sway motion. In the varying thickness floe spectrum the same peak can be observed but the consecrated energy is less. From a statistical point of view, the tension of the mooring lines is in the same level for both the constant thickness and the varying thickness floe. Also, as expected, mooring lines 1 and 3 are the ones that carry out the heavy duty and due to symmetry their mean values show only a very small difference in the order of 1%.

However, it must be mentioned that when the spar floating wind turbine is placed offshore, initially the 3 mooring lines should have the same tension due to symmetry. The varying thickness floe displacement mean value for the y direction is lower than the constant thickness floe. As a result the new equilibrium position is closer to the initial position, meaning that the differences between the mooring line tension should be smaller. This effect is observed in Table 5.17.

5.3.4 Drifting speed 0.5 m/s and spar

For the 0.5 m/s, similarly to the 0.3 m/s case, the displacements, forces, moments and a mooring line tension and the corresponding spectra are examined.
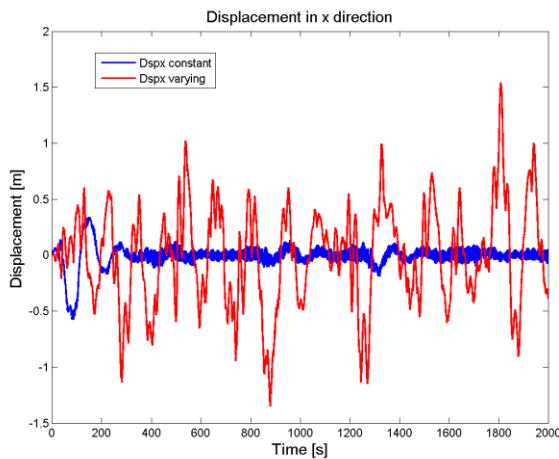
Figure 5.56 Comparison of Displacement in x direction
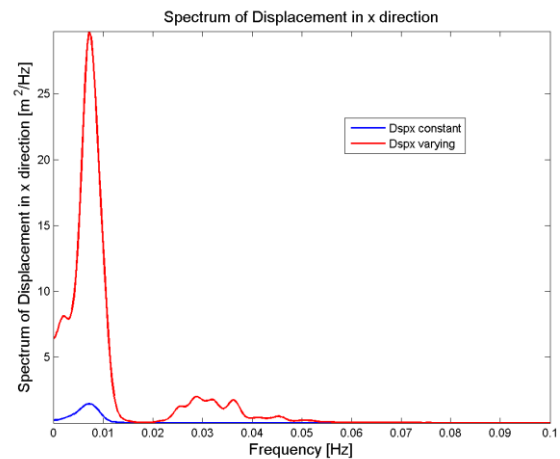
Figure 5.57 Comparison of spectra of the Displacement in x direction
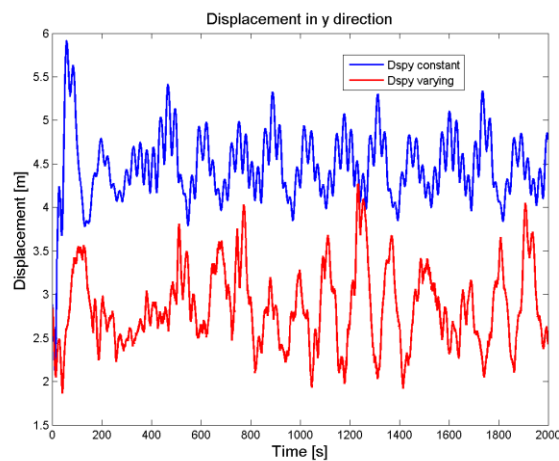
Figure 5.58 Comparison of Displacement in y direction
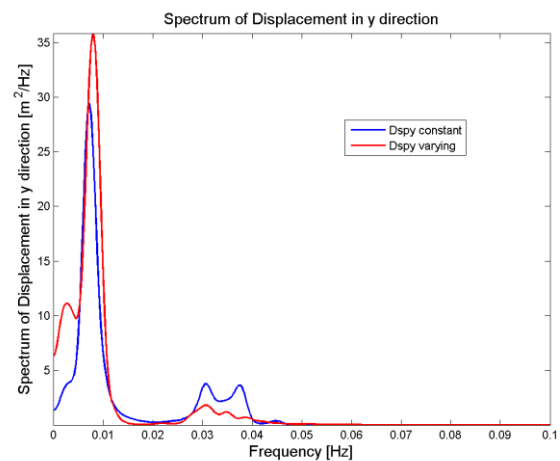
Figure 5.59 Comparison of spectra of the Displacement in y direction

Table 5.19 Statistics for Displacement in the x and y direction for 0.5 m/s

	Constant thickness model 0.5 m/s	FEM model 0.5 m/s (var. thickness)
Displacement in x direction [m]		
Mean value	-0.0077	-0.0215
Standard deviation	0.10	0.44
Displacement in y direction [m]		
Mean value	4.45	2.83
Standard deviation	0.40	0.45

In the case of 0.5 m/s the transient state seems to end at approximately 200 s and as a result the effective simulation time is approximately 1800 s. Contrary to the 0.3 m/s case, the constant thickness ice floe causes to the spar larger oscillations in the x but mainly in the y direction. Similarly though to the 0.3 m/s case, the displacements in both directions show a large fluctuation when the varying thickness field is considered. For the x direction, both the constant and the varying ice floe show a peak at approximately 0.007 Hz that corresponds to the sway/surge motion of the platform. Moreover, the varying thickness field shows a wide peak that cover the frequencies from about 0.025 Hz to 0.036 Hz. In these frequencies all heave, roll and pitch motion are covered. In the spectra of the y direction, for the constant thickness floe the most significant peak occurs at 0.007 Hz where the platforms surge/sway natural frequency is. Moreover, two smaller peaks are identified at approximately 0.031 Hz and 0.037 Hz. Both of these frequencies can be connected to the platforms pitch/roll and heave motion. Moreover, the most significant peak of the varying thickness floe is observed at about 0.007 Hz and corresponds to the platforms surge/sway motion. Another small peak is seen at about 0.031 Hz where the frequencies of pitch, roll and heave are identified. The mean values of the displacements in x direction are close to zero as expected. In the y direction, the mean value of the displacement shows a drop, just like the 0.3 m/s case.

What should be noticed is the fact that for the constant ice thickness floe the effect of the drifting speed is quite distinguishing through the mean values of the displacements mainly in the fore - aft direction where there is an increase of 25%. On the other hand, the mean value of the displacement in the y direction for the varying thickness field increased by 15%. Generally, the dynamic effects that are introduced with the varying thickness field are more severe in the x direction than in the y direction where the frequencies of pitch, roll and heave motion peak higher for the constant thickness floe.
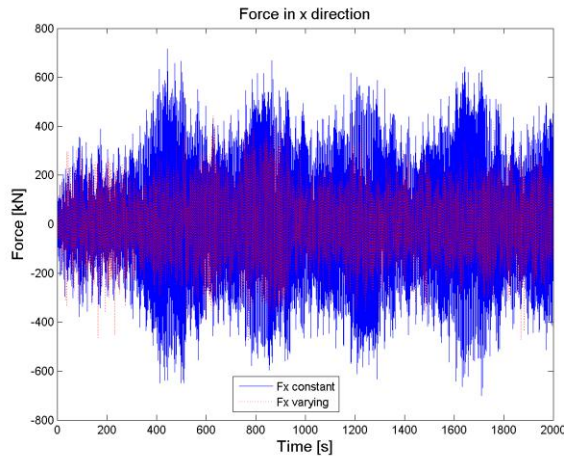
Figure 5.60 Comparison of Force in x direction
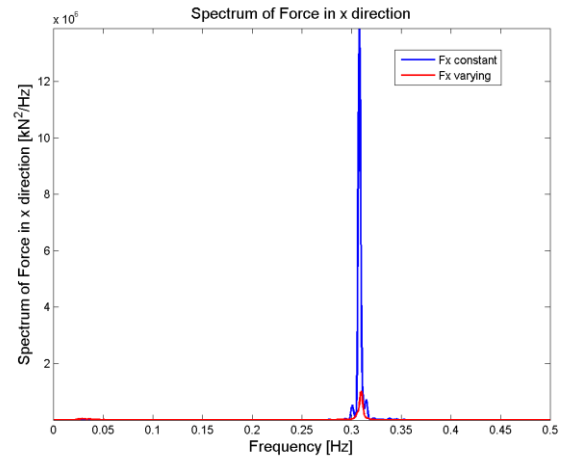
Figure 5.61 Comparison of spectra of the Force in x direction
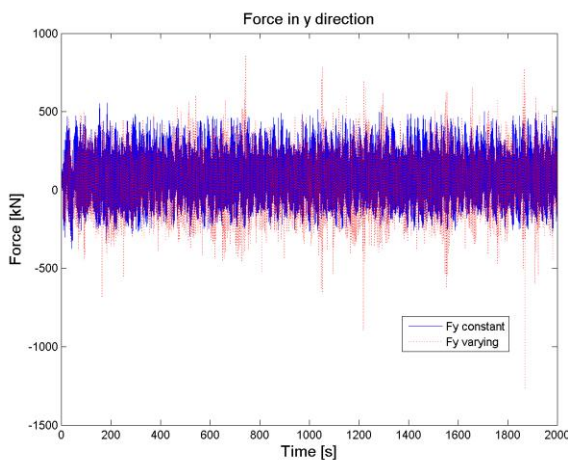
Figure 5.62 Comparison of Force in y direction
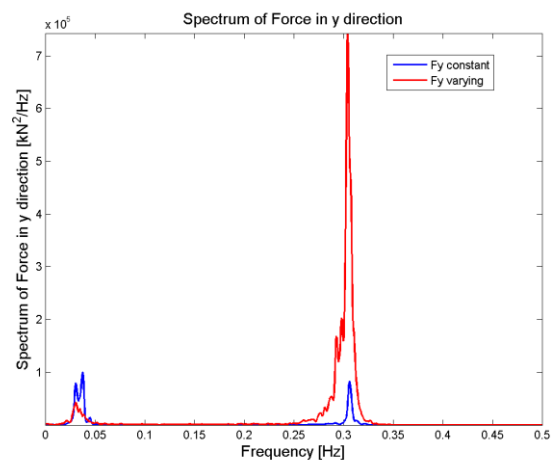
Figure 5.63 Comparison of spectra of the Force in y direction

Table 5.20 Statistics for Force in the x and y direction for 0.5 m/s

	Constant thickness model 0.5 m/s	FEM model 0.5 m/s (var. thickness)
Force in x direction [kN]		
Mean value	-0.04	-0.37
Standard deviation	224.41	101.84
Force in y direction [kN]		
Mean value	58.43	34.12
Standard deviation	111.01	125.37

As previously the effective simulation time is taken 1800 s. The force in the x direction shows more fluctuations when the constant ice thickness floe is considered. This can be also observed from the increases standard deviation compared to the varying thickness floe. Both mean values however are close to zero as expected. In the spectrum diagram only one peak is observed for both the constant and the varying thickness floe at approximately 0.3 Hz. It is observed that for the x direction, the peak has a much larger density for the constant thickness field. This peak is also identified in the ice loading force (see Appendix E3, page 145). In the

case of y direction and the varying thickness floe, the peak at 0.3 Hz is observed, with the difference that here the peak is higher. This peak is also observed in the corresponding ice loading force for the y direction (see Appendix E3, page 145). Moreover, it is also observed another small series of peaks at starting from approximately 0.03 Hz until 0.037 Hz. These can be identified that correspond closely to pitch/roll/heave motion of the platform. For the constant thickness floe, especially the 0.03 Hz one can be also identified with a higher density than the varying thickness floe. Regarding the statistics of the force in the y direction the mean value shows a drop of about 40% while the standard deviation shows an increase of 12% due to the more severe fluctuations.

Generally, it can be stated that for the x direction, the constant thickness floe dominates the dynamics of the structure. On the y direction, it seems that the varying thickness floe inserts the ice identified frequency of 0.3 Hz quite strongly in the excitation but still the constant thickness floe peaks higher in the important low frequencies of heave/roll/pith motions. Finally, due to the increased speed, the mean values of the force in y direction are increased while the mean values of the force in x direction are closer to zero. This reveals that the loading is more targeted at the fore - aft direction with less influence on the side to side one.

Figure 5.64 Comparison of Moment in x direction

Figure 5.65 Comparison of spectra of the Moment in x direction

Figure 5.66 Comparison of Moment in y direction

Figure 5.67 Comparison of spectra of the Moment in y direction

Table 5.21 Statistics for Moment in the x and y direction for 0.5 m/s

	Constant thickness model 0.5 m/s	FEM model 0.5 m/s (var. thickness)
Moment in x direction [kNm]		
Mean value	2177.4	654.72
Standard deviation	3505.9	9773.3
Moment in y direction [kNm]		
Mean value	-0.71	23.79
Standard deviation	2156.2	8266.4

Similarly to the 0.3 m/s case, the effect of the force in the x direction is observed in the moment in the y direction. Also, the effect of the force in the y direction is observed in the moment in the x direction. The corresponding spectra follow the same behaviour and statistical values show a similarly large decrease for the moment in x direction, while an increase in the moment in the y direction is observed.

Similarly to the 0.3 m/s case, mooring line 2 is examined.
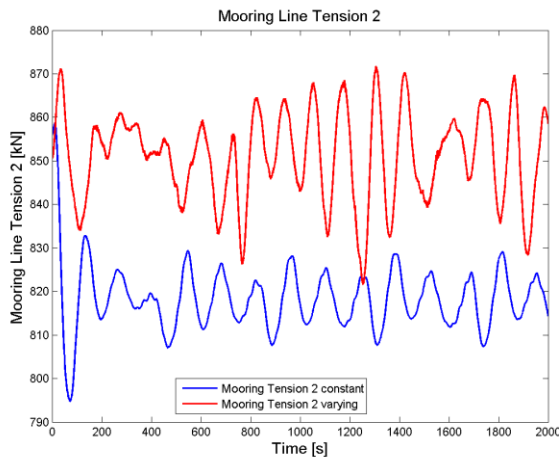
Figure 5.68 Comparison of Mooring line tension 2
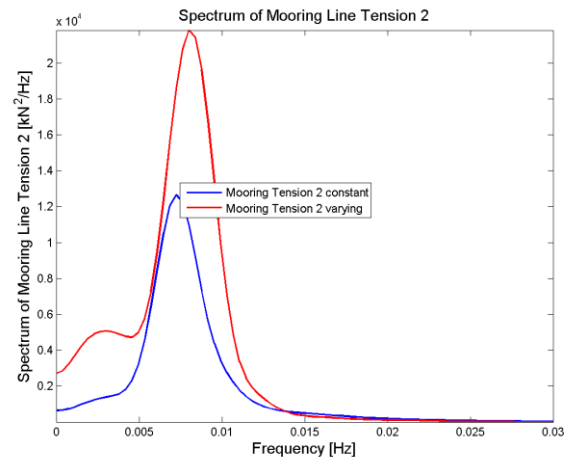
Figure 5.69 Comparison of spectra of the Mooring line tension 2

Table 5.22 Statistics for Mooring lines tension for 0.5 m/s

	Constant thickness model 0.5 m/s	FEM model 0.5 m/s (var. thickness)
Mooring line tension 1 [kN]		
Mean value	967.20	946.41
Standard deviation	4.46	12.70
Mooring line tension 2 [kN]		
Mean value	818.26	850.90
Standard deviation	7.60	10.38
Mooring line tension 3 [kN]		
Mean value	967.53	947.32
Standard deviation	6.76	11.48

The same situation as in the 0.3 m/s case is observed. The mean values of the mooring line tensions show a smaller difference between them since the mew equilibrium position is closer to the initial placement of the structure. This can also be confirmed by the mean value of the displacement in the y direction. Moreover, in both the constant thickness floe and the varying thickness floe spectra a similar peak is identified at about 0.007 Hz and corresponds closely to the platform's surge/sway motion. The effect of the speed cannot actually be seen from the mooring lines since their tension depends exclusively on the platforms motion. Meaning that, the lines stretch or loosen in the command of the displacements. Finally, the symmetry of the mooring system can be observed through the mean values of the tension.

5.4 Aerodynamic loads included

The simulations that performed for a spar structure are considered again with aerodynamic loads included. The wind speed selected to run the simulations was 12 m/s. According to the approximation mentioned in section 4.1 , the ice drifting speed can be approximated by the 2% of the wind speed. Therefore the ice drifting speed that should be used when comparing the responses due to pure wind loads, pure ice loads and combined loads should be 0.24 m/s. As a result, the most realistic environment is the combination of 12 m/s wind speed and 0.3 m/s drifting speed of ice and this is the one that is going to be examined. The effect of the aerodynamic loads is investigated both for the constant ice thickness floe and the varying one. The same responses are presented as before, namely the displacement, the force and moment and mean sea level for x and y direction, and mooring line 2 tension. In the upcoming sections, mostly focus is given in the identification of the effect of the combined aerodynamic and ice loads in comparison with the case of only pure ice loads.

5.4.1 Drifting speed 0.3 m/s and constant ice thickness

To begin with the case of 0.3 m/s drifting speed and 12 m/s wind speed. All the statistical values correspond to the steady state case. All other responses in both directions can be found in Appendix G1 (page153).
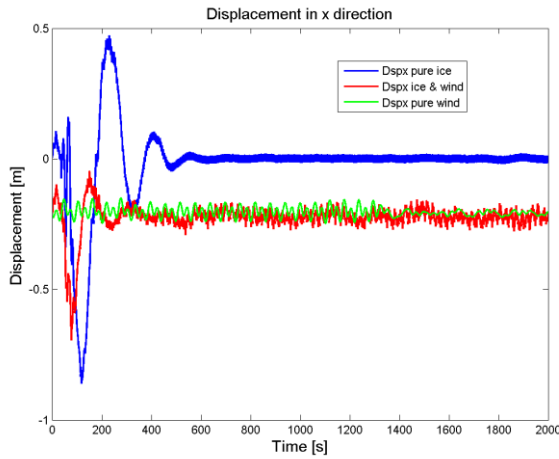
Figure 5.70 Comparison of Displacement in x direction, including aerodynamic loads (cnst thickness)
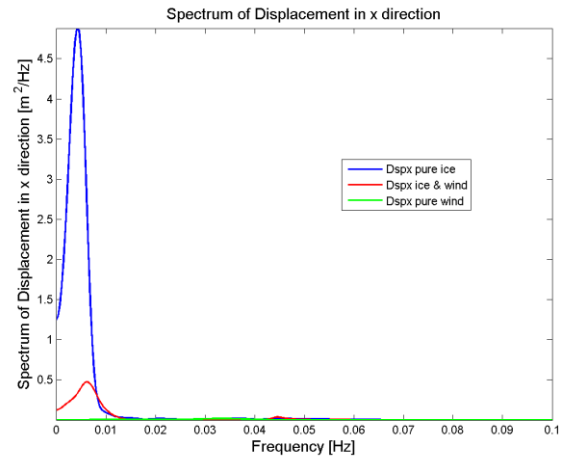
Figure 5.71 Comparison of spectra of the Displacement in x direction, including aerodynamic loads (cnst thickness)
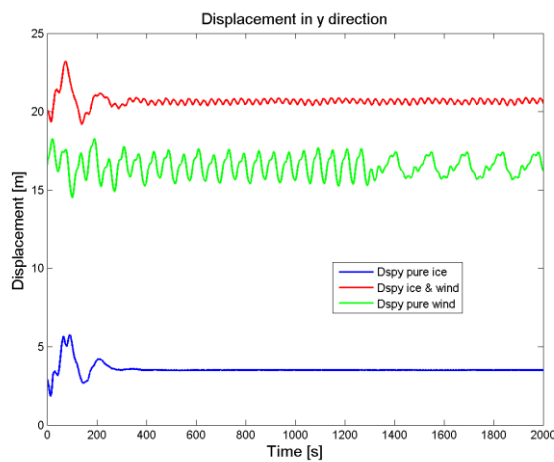
Figure 5.72 Comparison of Displacement in y direction, including aerodynamic loads (cnst thickness)
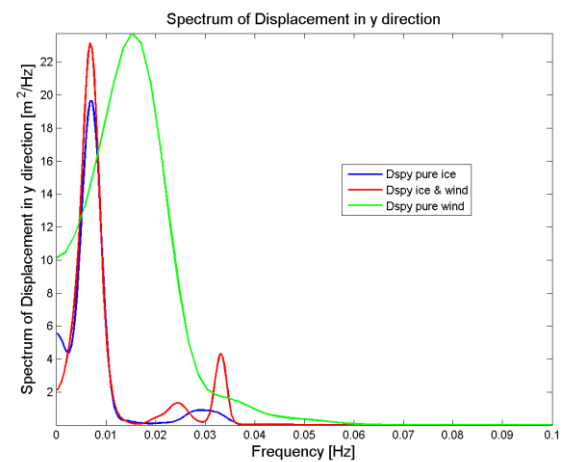
Figure 5.73 Comparison of spectra of the Displacement in y direction, including aerodynamic loads (cnst thickness)

Table 5.23 Statistics for Displacement in the x and y direction for 0.3 m/s, constant ice thickness including aerodynamic loads

	Side to side direction	Fore - Aft direction
Displacement pure ice [m]		
Mean value	-0.01	3.54
Standard deviation	0.15	0.35
Displacement ice & wind [m]		
Mean value	-0.22	20.66
Standard deviation	0.05	0.37
Displacement pure wind [m]		
Mean value	-0.20	16.5
Standard deviation	0.01	0.68

In the x direction, it is observed from the time series and the statistical values that only the ice loads have a more symmetric effect on the structure due to the mean value of the displacement that is close to zero. Regarding the spectra, the combined ice and wind loads, show a peak around 0.006 Hz, which is quite close to the platform's sway/surge motion. The energy density of the pure ice loads is quite larger than the combined loads. This can be

explained due to the fact that the combined ice loads are affected from the aerodynamic loads in such way that they are more directive towards the y direction. Regarding the y direction, where the aerodynamic load are basically acting, the effect of the combined loads is quite clear. Moreover, the energy density of the combined loads is larger than just the pure ice loads. The displacement consists of the sum of both the ice load and wind load displacement. When the combined loads spectrum is observed; the frequencies of 0.023 Hz and 0.032 Hz are pointed out. While in the pure ice loads there is a wide peak observed around 0.03 Hz and is closer to the platform's heave motion. For the combined loads, the 0.023 Hz is also identified at in the ice loading force in the x direction (see Appendix C.2.2, page 133). The peak of 0.032 Hz can be clearly corresponded with the platform's pitch/roll motion.

It is noticed that the combined loads seem to introduce a different dynamic effect by the excitation of pitch/roll motion, especially for the fore - aft direction, while he pure ice loads seem to excite the heave motion of the platform.
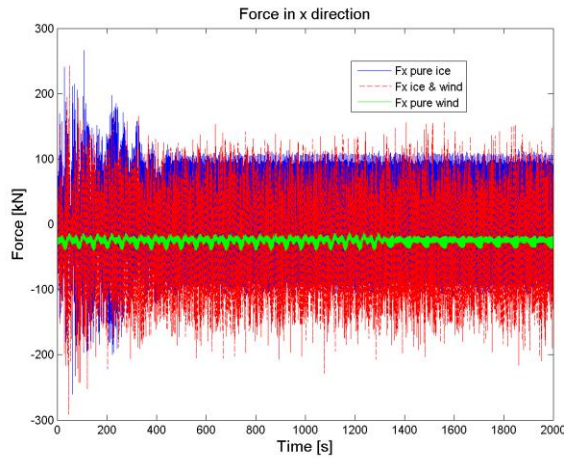
Figure 5.74 Comparison of Force in x direction, including aerodynamic loads (cnst thickness)
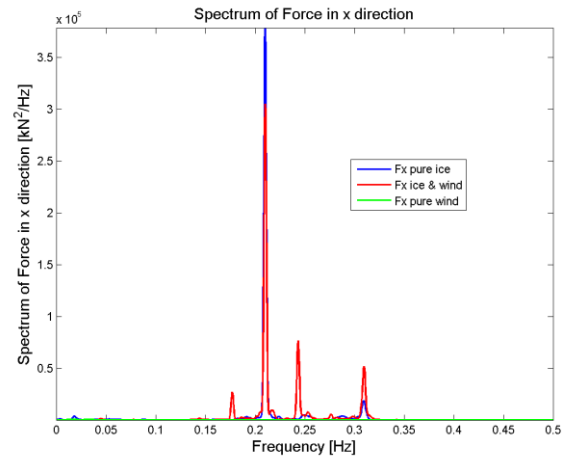
Figure 5.75 Comparison of spectra of the Force in x direction, including aerodynamic loads (cnst thickness)
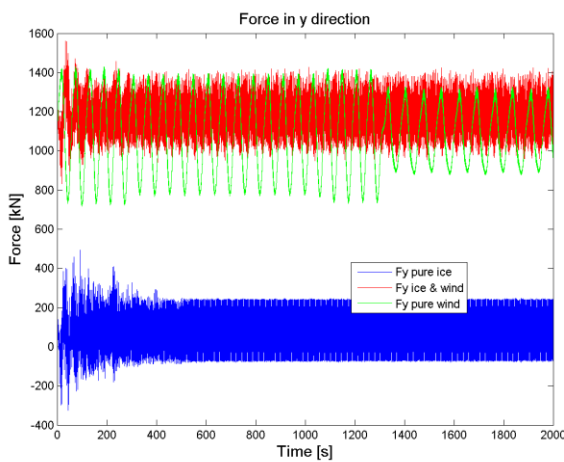
Figure 5.76 Comparison of Force in y direction, including aerodynamic loads (cnst thickness)
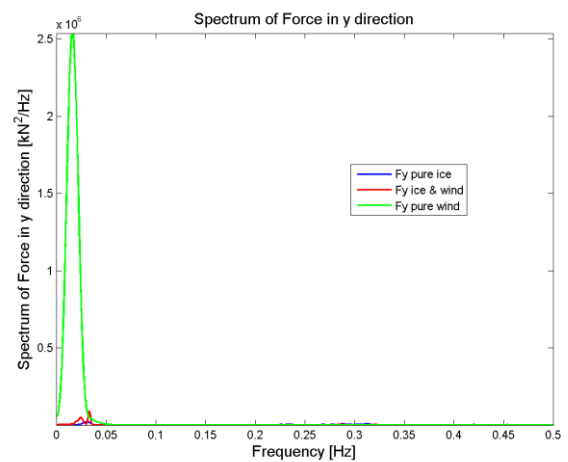
Figure 5.77 Comparison of spectra of the Force in y direction, including aerodynamic loads (cnst thickness)

Table 5.24 Statistics for Force in the x and y direction for 0.3 m/s, constant ice thickness including aerodynamic loads

	Side to side direction	Fore - Aft direction
Force pure ice [kN]		
Mean value	-0.23	44.88
Standard deviation	50.93	53.54
Force ice & wind [kN]		
Mean value	-26.03	1149.7
Standard deviation	57.14	62.38
Force pure wind [kN]		
Mean value	-25.40	1080.53
Standard deviation	4.70	190.29

The difference in the effect of the combined loads in the x direction can be observed from the spectra where two additional peak at 0.17 Hz and 0.23 Hz are identified. These two spectra are also found in the ice loading force in the x direction (see Appendix C.2.2 page 133). Moreover the same peak at about 0.21 Hz that is observed both for the constant and the varying thickness floe is similarly observed in the ice loading force in x direction. Regarding

the y direction the aerodynamic spectrum, dominates. Similarly to the displacement spectra though, two different peaks are observed in the 0.023 Hz (as in the force in the x direction) and 0.032 Hz (pitch/roll motion) while in the pure ice loads only a wide peak around 0.03 Hz (heave motion) is observed.

From a statistical point of view, the combined loads seem to be a sum of the pure wind loads and the aerodynamic loads together. Generally, it can be seen that the combined loads are introducing new frequencies of excitation on the structure especially for the side to side direction.
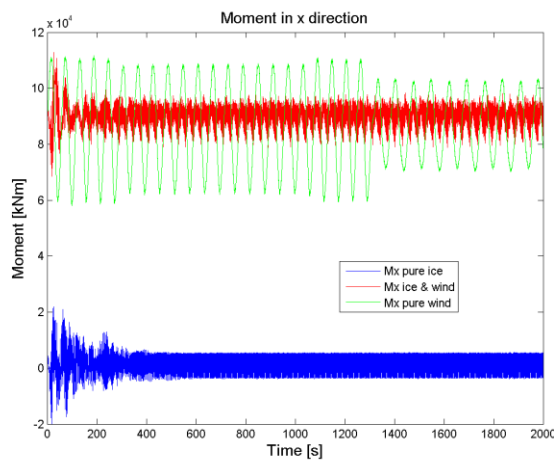
Figure 5.78 Comparison of Moment in x direction, including aerodynamic loads (cnst thickness)
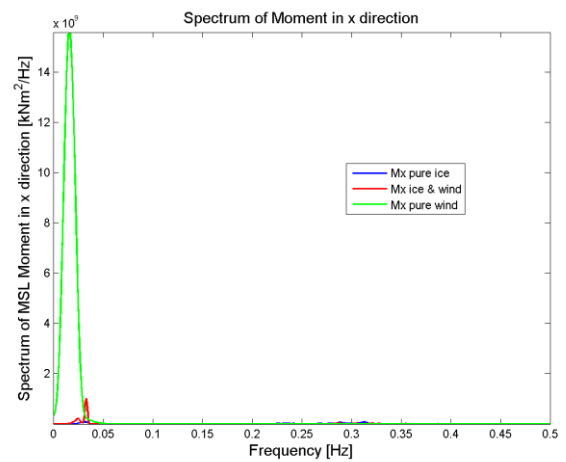
Figure 5.79 Comparison of spectra of the Moment in x direction, including aerodynamic loads (cnst thickness)
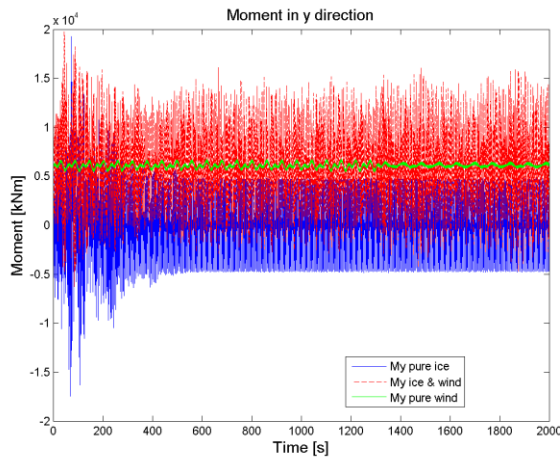
Figure 5.80 Comparison of Moment in y direction, including aerodynamic loads (cnst thickness)
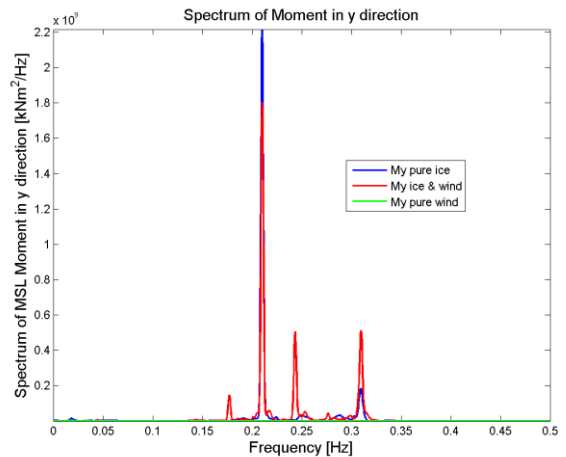
Figure 5.81 Comparison of spectra of the Moment in y direction, including aerodynamic loads (cnst thickness)

Table 5.25 Statistics for Moment in the x and y direction for 0.3 m/s, constant ice thickness including aerodynamic loads

	Side to side direction	Fore - Aft direction
Moment pure ice [kNm]		
Mean value	1331.6	14.26
Standard deviation	2967.6	3139.5
Moment ice & wind [kNm]		
Mean value	9010.9	6103.3
Standard deviation	3707.9	3626.5
Moment pure wind [kNm]		
Mean value	8661.1	6094.7
Standard deviation	1486.1	226.38

In the case of the moment responses, they seem to follow the same trend as in all other cases examined. Meaning that the force in the x direction gives its effect on the corresponding moment in the y direction and the force in the y direction gives its effect on the corresponding moment in the x direction. The same excitations occur as in the force case and similarly to both displacements and forces, the mean values of the combined loads are the sum of the pure ice loads and pure wind loads.
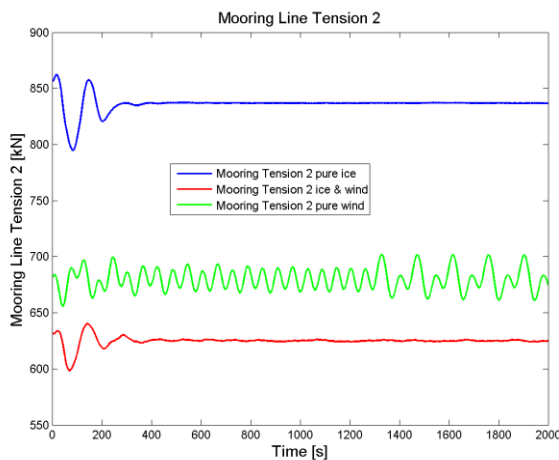
Figure 5.82 Comparison of Mooring line tension 2, including aerodynamic loads (cnst thickness)
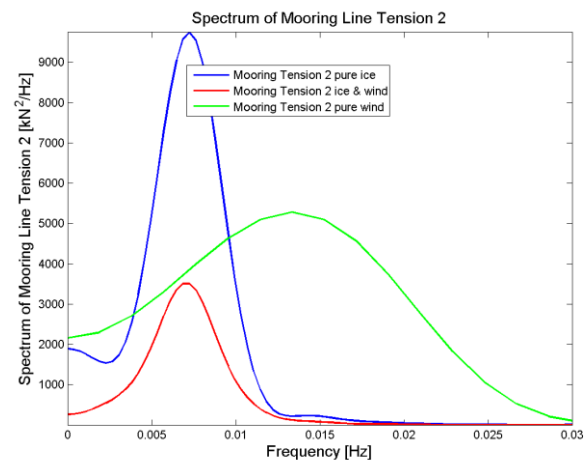
Figure 5.83 Comparison of spectra of the Mooring line tension 2, including aerodynamic loads (cnst thickness)

Table 5.26 Statistics for Mooring lines tension for 0.3 m/s, constant ice thickness including aerodynamic loads

	Pure ice [kNm]	Ice & wind [kN]	Pure wind [kN]
Mooring line tension 1			
Mean value	955.55	1155.9	1090.6
Standard deviation	5.68	5.52	10.47
Mooring line tension 2			
Mean value	836.18	624.89	679.71
Standard deviation	7.35	4.33	9.60
Mooring line tension 3			
Mean value	956.17	1152.1	1085.8
Standard deviation	6.28	8.51	10.81

The behaviour of the mooring line tension should be explained considering the displacement in the y direction. The corresponding displacement for the combined loads is approximately 20 m away from the initial position of the structure. As a result, mooring line tension 2 is the one that is more loosen compared to the other two. This can be observed by the mean values where the difference between the mooring line tensions, for the ice & wind loads is the largest one observed. The effect on the surge/sway natural frequency that is excited, has less energy density when the combined loads are considered.

5.4.2 Drifting speed 0.3 m/s and varying ice thickness

The same responses are considered also for the 0.3 m/s varying ice thickness case. All other responses for both direction can be found in Appendix G2 (page 155).
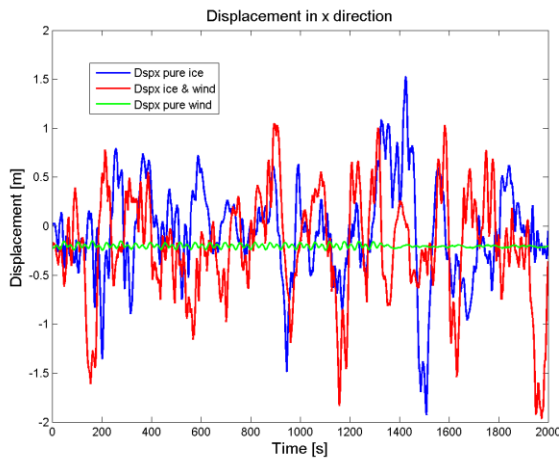
Figure 5.84 Comparison of Displacement in x direction, including aerodynamic loads (var thickness)
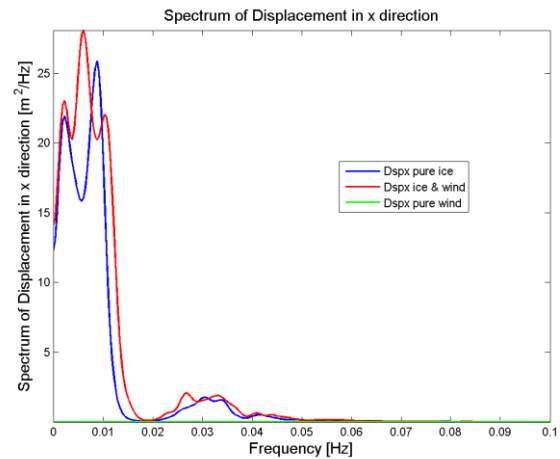
Figure 5.85 Comparison of spectra of the Displacement in x direction, including aerodynamic loads (var thickness)
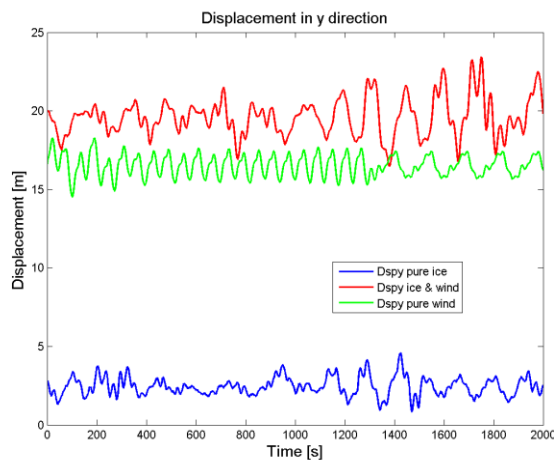
Figure 5.86 Comparison of Displacement in y direction, including aerodynamic loads (var thickness)
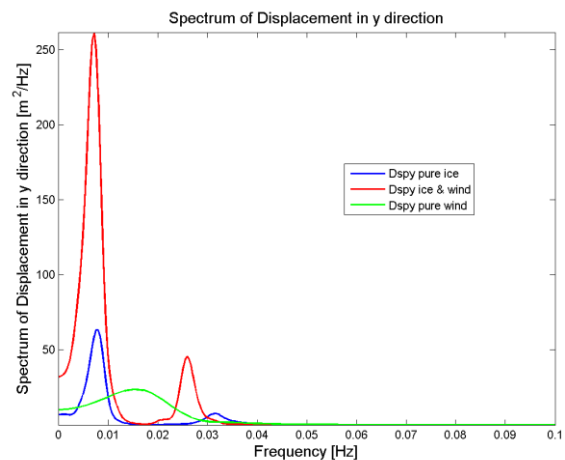
Figure 5.87 Comparison of spectra of the Displacement in y direction, including aerodynamic loads (var thickness)

Table 5.27 Statistics for Displacement in the x and y direction for 0.3 m/s, varying ice thickness including aerodynamic loads

	Side to side direction	Fore - Aft direction
Displacement pure ice [m]		
Mean value	-0.07	2.43
Standard deviation	0.49	0.58
Displacement ice & wind [m]		
Mean value	-0.22	19.57
Standard deviation	0.55	1.19
Displacement pure wind [m]		
Mean value	-0.20	16.50
Standard deviation	0.01	0.68

In the varying thickness case and the effect of the combined loads in the spectra, the main difference that can be observed is that middle high peak that occurs at 0.006 Hz and is very close to platform's sway/surge. In the y direction, the same frequency is observed but with a much higher energy density. Moreover, an additional excitation is observed at 0.024 Hz, which is also identified at the ice loading force in the x direction (see Appendix C.2.2 page 133). From a statistical point of view, as expected, the mean values of the combined loads are the sum of both the pure ice loads and wind loads.

It is noticed that the combined loads seem to introduce a different dynamic effect by the excitation of the 0.25 Hz frequency, especially for the fore - aft direction, while he pure ice loads seem to excite the heave motion of the platform.
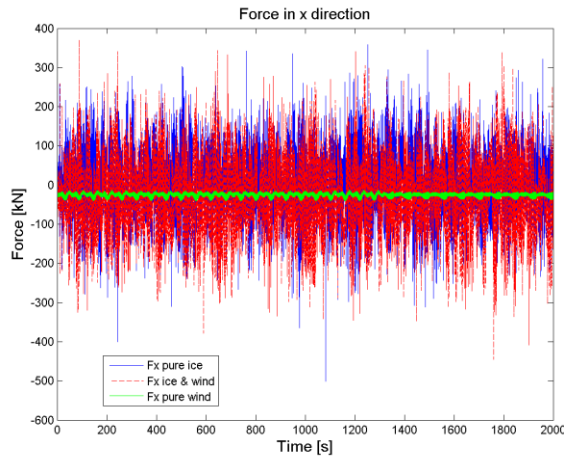
Figure 5.88 Comparison of Force in x direction, including aerodynamic loads (var thickness)
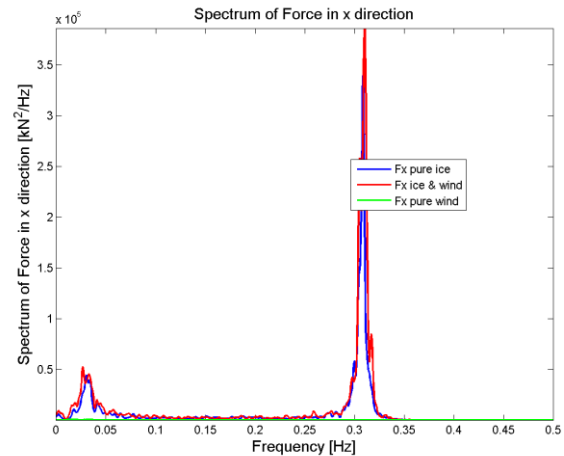
Figure 5.89 Comparison of spectra of the Force in x direction, including aerodynamic loads (var thickness)
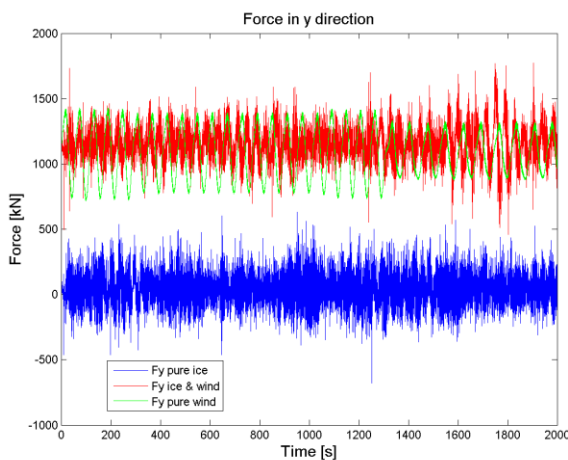
Figure 5.90 Comparison of Force in y direction, including aerodynamic loads (var thickness)
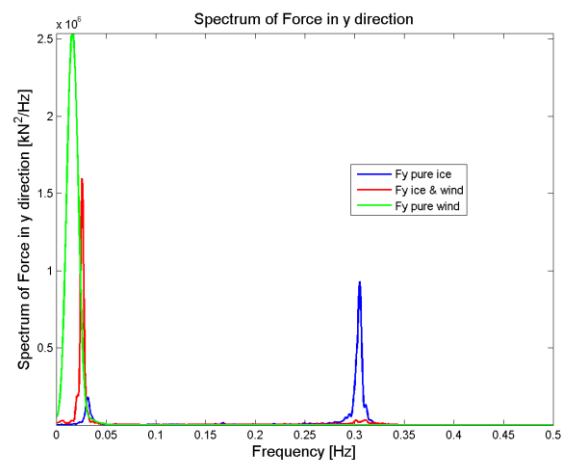
Figure 5.91 Comparison of spectra of the Force in y direction, including aerodynamic loads (var thickness)

Table 5.28 Statistics for Force in the x and y direction for 0.3 m/s, varying ice thickness including aerodynamic loads

	Side to side direction	Fore - Aft direction
Force pure ice [kN]		
Mean value	-1.27	28.01
Standard deviation	72.15	112.60
Force ice & wind [kN]		
Mean value	-25.85	1134.1
Standard deviation	83.07	108.14
Force pure wind [kN]		
Mean value	-25.40	1085.3
Standard deviation	4.70	190.29

In the x direction, the response of the combined loads seem to have no effect on the structure as can be observed from the spectra figure. Regarding the y direction though a different behaviour is observed. The platforms pitch/roll is still excited but the 0.3 Hz peak is almost vanished. The excitation about 0.031 Hz is much larger in the varying thickness floe than in the constant thickness floe. This can be explained as the aerodynamic loads are more directive

towards the y direction and in combination with the ice loads, the energy is concentrated in this low frequency band. It is noticeable that no effect in the x direction is observed when wind loads are considered, while the significant peaks of the x direction are completely changed in the y direction for the varying thickness floe.
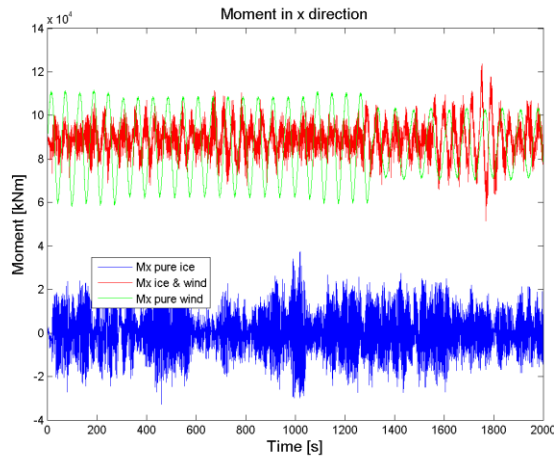
Figure 5.92 Comparison of Moment in x direction, including aerodynamic loads (var thickness)
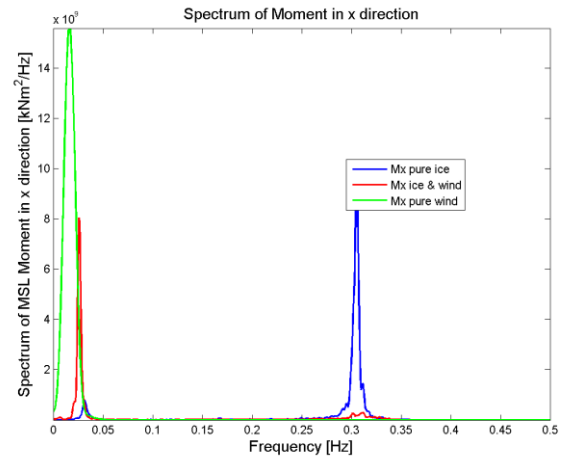
Figure 5.93 Comparison of spectra of the Moment in x direction, including aerodynamic loads (var thickness)
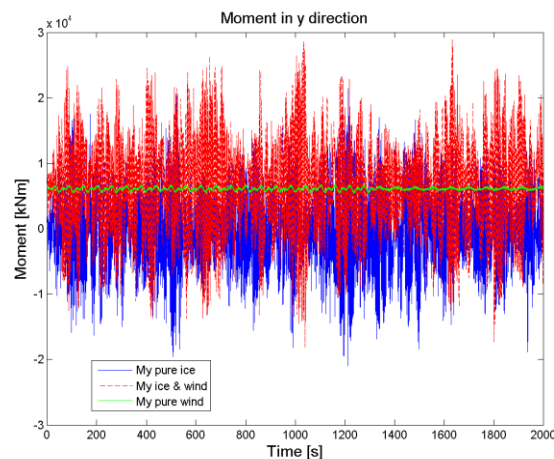
Figure 5.94 Comparison of Moment in y direction, including aerodynamic loads (var thickness)
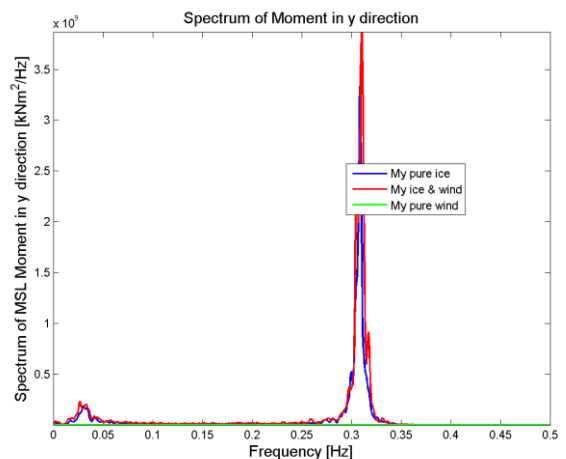
Figure 5.95 Comparison of spectra of the Moment in y direction, including aerodynamic loads (var thickness)

Table 5.29 Statistics for Moment in the x and y direction for 0.3 m/s, varying ice thickness including aerodynamic loads

	Side to side direction	Fore - Aft direction
Moment pure ice [kNm]		
Mean value	268.58	79.70
Standard deviation	9510.1	5764.9
Moment ice & wind [kNm]		
Mean value	8923.0	6099.2
Standard deviation	7352.2	6823.7
Moment pure wind [kNm]		
Mean value	8661.1	6024.7
Standard deviation	1486.1	226.38

As usually observed, the moment responses in the side to side and fore - aft direction are following the effect of the force responses in the fore - aft and side to side direction respectively. The same situation hold also for the corresponding spectra and their effect on the structure. Similarly to every observation, the mean values of the combined loads are the sum of the pure ice loads and the pure wind loads.
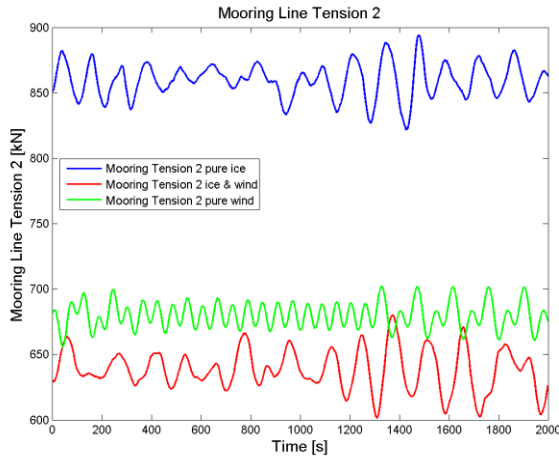
Figure 5.96 Comparison of Mooring line tension 2, including aerodynamic loads (var thickness)	Figure 5.97 Comparison of spectra of the Mooring line tension 2, including aerodynamic loads (var thickness)
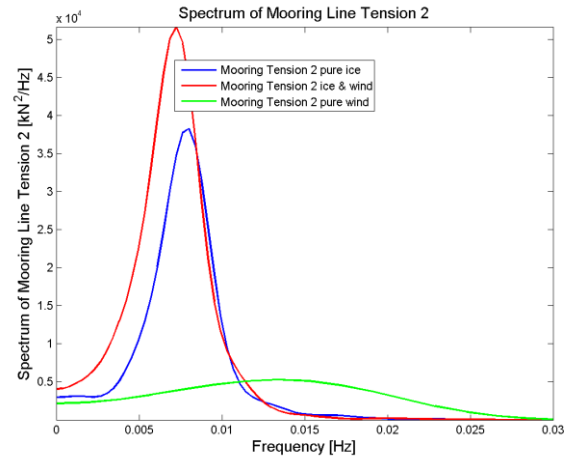
Table 5.30 Statistics for Mooring lines tension for 0.3 m/s, varying ice thickness including aerodynamic loads

	Pure ice [kNm]	Ice & wind [kN]	Pure wind [kN]
Mooring line tension 1			
Mean value	940.32	1139.2	1090.6
Standard deviation	12.45	27.70	10.47
Mooring line tension 2			
Mean value	859.39	638.31	679.71
Standard deviation	13.11	15.54	9.60
Mooring line tension 3			
Mean value	943.31	1135.3	1085.8
Standard deviation	14.92	25.87	10.81

Since the displacement is the largest for the combined loads as explained also for the constant thickness case, mooring line tension 2 is the one that is less in tension compared to the other two. This is also supported by the mean values of the tension where mooring line 2 for the combined loads shows the less tension. In both cases though (with and without wind) the effect on the structure is expressed in the same way; through the excitation of the surge/sway motion around the frequency of 0.007 Hz.

5.5 Discussion

It has been observed that when the varying thickness ice field is interacting with any structure, both monopile and spar, then the ice loads observed show a significant decrease. However, this must not trick the designers of support structures because as observed from the timeseries, some peak loads can reach very high values.

Moreover, is has also been observed that as the speed of the ice floe increases then the ice loads are accordingly increasing. This is a direct effect of the $c_f = (1.65 + 2.47v_2^{0.4})$ factor that is used to introduce the dynamic effect on the ice floe.

Regarding the responses and the 0.3 m/s drifting speed of ice. The general image shows that the varying ice thickness field introduced a more significant dynamic effect because of not only the higher energy densities that have been observed, but also because of the additional frequencies that are excited. In the case of 0.5 m/s, the situation is slightly different. For the case of the force in the x direction and the moment in the y direction, the constant thickness floe shows a higher energy density in the corresponding frequencies. Moreover, the pitch/roll/heave motion of the platform is excited by the constant thickness floe with a higher energy density. Again the effect of the higher drifting speed is also observed in the responses through the higher mean values that occur.

When the aerodynamic loads are included, and a constant ice thickness floe is considered, then the combined loads introduce more dynamic effects, as for example in the case of the force in x direction. However, there are also cases like the displacement and mooring line tension where only the pure ice loads have a more important role for design. The combination of a varying ice thickness field together with wind loads, in general shows higher energy densities at the correspondingly excited frequencies. What is also remarkable to discuss is that for the case of force in fore - aft direction and the moment in side to side direction, the excitations are completely different, like there is a transfer in the energy towards the lower frequencies as soon as the aerodynamic loads are included. On the other hand, for the force in the side to side direction and the moment in the fore - aft direction, the effect of the combined loads on the structure is the same as the effect of only ice loads.

6 Proposals for further analysis

To begin with the method proposed in section 2.5 . This method that is used to generate a random timeseries based on the spectrum of a data set seems to work quite accurate. However, this model is based on data manipulation and generally is not been used for generation of length series. Usually the direct sum equation is used in generation of a wind timeseries from a Kaimal spectrum for example. Therefore, one could wonder about the validity of its use for length series generation. A deeper investigation could be conducted and conclude regarding the use of direct sum in such way.

Assume that the model proposed for generation of length series is valid. However, problems might occur when the mean ice thickness of the ice floe is close to 0, meaning 0.1 m or 0.15 m. When the random series is generated, a random phase φ is used. This phase may cause some particular values of the thickness to be above the mean sea level, which is unrealistic. This problem could be solved by demanding all the values generated to be below mean sea level. On the other hand, this solution may cause large differences from the initial spectrum which is the input for the generated values. However, it is conjectured that these differences might not be that severe. In any case, every small mean ice thickness dataset should be investigated thoroughly when used as input for the generation of random ice thickness fields.

Moreover, in section 4.4 , it is explained that in order to cover the needs of the long simulation time, a large ice floe should be generated. The initial measurements dataset was approximately 300 m long and it was repeated until it becomes 1500 m long. Afterwards, a new 1500 m ice thickness profile is generated. When the initial dataset is repeated, the spectrum remains unchanged. If a dataset was obtained that its length was initially 1500 m, its spectrum would be totally different from the spectrum of its first 300 m. As a result, even if the length series depicted in Figure 4.7 seem to give a very good approximation of a varying ice thickness level ice profile, they are based on a 300 m spectrum. This approximation should be made in the frames of study in order to obtain a large ice - floe. In any case, for more correspondence to reality, it is proposed that the length of generated ice field should match the length of the measurements.

In all simulations both for the semi - empirical model and the varying thickness model, the flexural strength of ice was kept constant and equal to 0.58 MPa. It is shown in literature by the ISO 19906 and (Timco and Weeks 2010) that flexural strength is a function of the brine volume (section 2.4.2). In a varying thickness field, it is quite logical for the brine volume to

change continuously. Moreover, taking into account the randomness at which level ice is formed, it is quite possible the brine volume to be different in a uniform ice thickness field as well. Therefore, the assumption that the flexural strength of ice is constant does not exactly represents reality. Brine volume depends on salinity and temperature and it is extremely complicated to follow the exact procedure of the formulation of level ice and predict its percentage within the floe at specific locations. This might be a subject for study that contains a very high level of knowledge on ice properties and behaviour, in situ measurements, experiments, and years of work.

Also, when simulating such complex models, the computational cost needs to be taken into account and efficiency becomes important. It is observed that a 3000 s simulation of constant ice thickness can take up to 80 hours to finish. After updating the constant ice thickness model to account for variations in thickness the same 3000 s simulation ran for about 150 hours. As a result, since the actual time is almost double, the computational cost is double and the computational resources are occupied for double time. Moreover, 150 hours correspond to a week of simulations meaning that if there is need of fast results, it is not quite possible. Therefore, it is recommended for the sake of efficiency, the optimisation of the programme. It is believed that an efficient implementation of the numerical procedure could reduce the simulation time significantly.

Moreover, it has been observed that in low drifting speeds, the HAWC2 in combination with the DLL file results some convergence issues. In communication with the developer of HAWC2 with Dr. Wei Shi, it has been underlined that the continuous exchange of data, could cause such issues to the programme. Taking also into account the fact that HAWC2 is still under development, the most efficient way to cancel any kind of communication and convergence issues, is to implement the ice load code into HAWC2 code. This is rather difficult and time consuming but on the other hand, it is believed that could assure that any problems will be eliminated.

Last but not least, in the simulations run, only one case of ice thickness is considered. It would useful to research, more level ice measurements to be used in order for varying ice fields to be generated and tested against a spar structure or a monopile. In such way, not only the effect of the varying thickness could be examined, but also the effect of the average thickness as a whole.

References

Barker, Anne, Garry Timco, Helge Gravessen, and Per Volund. 2005. "Ice loading on Danish wind turbines Part 1: Dynamic model tests." *Cold Regions Science and Technology*, January.

Biswajt, Baju, and Van-Nguyen Dinh. 2013. *On the Modeling of Spar-type Floating Offshore Wind Turbines.*

Bjerkås, Morten, Arne Albrektsen, and Arne Gürtner. 2010. "Static and Dynamic Ice Actions in the Light of New Design Codes." *29th International Conference on Offshore Mechanics and Arctic Engineering.*

Bredmose, Henrik. 2014. "Offshore Wind Energy, Lecture notes." Copenhagen: DTU.

Cole, David. 2010. "The microstructure of ice and its influence on mechanical properties." *Engineering fracture mechanics.*

DNV-GL. 2014. "Ice load project final technical report." U.S. Department of energy.

DTU Wind Energy. 2015. *hawc2.* Accessed December 2015. http://www.hawc2.dk/HAWC2-info.

Ecofys. 2014. "Subsidies and costs of EU energy."

Enkvist, Ernst. 1972. "On the ice resistance encountered by ships operating in the continuous mode of icebreaking ." *The Swedish Academy of Engineering Science in Finland.*

European Commission. 2014. "A policy framework for climate and energy in the period from 2020 to 2030." Brussels. https://ec.europa.eu/energy/en/topics/renewable-energy.

European Wind Energy Association. 2015. "Wind energy scenarios 2030."

Faltinsen, O. M. 1990. "Sea Loads on ships and offshore structures." Cambridge: Cambridge University Press.

Fox, Colin. 2001. "A Scaling Law for the Flexural Motion of Floating Ice." *Soil Mechanics and its Applications.*

Frederking, R., and J. Schwarz. 1982. "Model tests of ice forces on fixed and oscillating cones." *Cold regions, science and technology.*

Gao, Zhen, and Erin Bachinsky. 2014. "Integrated dynamic analysis of wind turbines - Lecture Notes." Trondheim: NTNU.

Global Wind Energy Council. 2014. "Global Wind Report, Annual Market update."

Hansen, Martin O.L. 2008. *Aerodynamics of wind turbines, second edition.* London: Earthscan.

Hoving, Jeroen. 2015. "OE4680 - Arctitc Engineering." Delft: TU Delft.

IEC 61400-3. 2009. "Recommendations for design of offshore structures with respect to ice loads."

Islam, M. R., S. Mekhilef, R. Saidur, and . 2013. "Progress and recent trends of wind energy technology." *Renewable and sustainable energy reviews.*

ISO19906. 2010. "Petroleum and natural gas industries - Arctic offshore structures."

Janco, Roland. 2010. "Solution Methods for Beam and Frames on Elastic Foundation Using the Finite Element Method." *International Scientific Conference MSFE*, 13 September.

Jeon, S.H., Y.U. Cho, M.W. Seo, J.R. Cho, and W.B. Jeong. 2013. "Dynamic response of floating substructure of spar-type offshore wind turbine with catenary mooring cables." *Ocean Engineering*, August.

Jonkman, J. 2010. "Definition of the Floating System for Phase IV of OC3."

Jonkman, J., S. Butterfield, W. Musial, and G. Scott. 2009. "Definition of a 5-MW Reference Wind Turbine for Offshore System Development."

Kerr, Arnold D. 1975. "The Bearing Capacity of Floating Ice Plates Subjected to Static or Quasi- Static Loads-A Critical Survey." *Cold Regions Research and Engineering Laboratory.*

Kujala, Pentti. 1996. "Semi-empirical Evaluation of Long Term Ice Loads on a Ship Hull." *Marine Structures.*

—. 1994. "On the Statistics of Ice loads on Ship Hull in the Baltic." *Mechanical Engineering series No.116, Ship Laboratory.*

Langen, Ivan, and Ragnar Sigbjornsson. 1977. *Dynamisk analyse av konstruksjoner. 1977.*

Lewis, Alum, Oistein Johansen, Ivar Singsaas, and Lauri Solsberg. 2008. *Ice regimes for Oil Spill Response Planning.* Report, Trondheim: SINTEF Materials and Chemistry.

Mathisen, Kjell Magne. 2015. "TMR 4190 - Finite Element Method in Structural Analysis Lecture Notes." Trondheim: NTNU.

McPhee, Miles. 2008. *Air-Ice-Ocean Interaction: Turbulent Ocean Boundary Layer Exchange Processes.* Naches, WA, USA: Springer Science + Business Media B.V.

Melling, H., D.A. Reidel, Z. Gedalof, and . 2005. "Trends in thickness and extent of seasonal pack ice, Canadian Beaufort sea." *Geophysical research letters.*

Metrikine, Andrei. 2015. "OE4680 - Arctitc Engineering, Lecture notes." Delft: TU Delft.

Milano, V. R. 1973. "Ship Resistance to Continuous Motion in Ice." *Transactions of Society of Naval Architects and Marine Engineers (SNAME).*

Mroz, Arkadiusz, Jan Holnicki-Szulc, and Tuomo Karna. 2008. "Mitigation of ice loading on off-shore wind turbines: Feasibility study of a semi-active solution." *Computers & structures.*

Naess, Arvid, and Torgeir Moan. 2013. *Stochastic Dynamics of Marine Structures.* Cambridge University press.

Pfaffling, Andreas, Christian Haas, and James E. Reid. 2007. "Direct helicopter EM - Sea-ice thickness inversion." *GEOPHYSICS,VOL. 72*, August.

Riska, Kaj. 1995. "Models of ice-structure contact for engineering applications." *Mechanics of Geomaterial Interfaces.*

Saccoman, Marine. 2015. "Coupled Analysis of a Spar Floating Wind Turbine considering both Ice and Aerodynamic Loads." *TMR 4930 - Marine Technology, Master's Thesis.*

Shi, Wei, Xiang Tan, Zhen Gao, and Torgeir Moan. 2014. "Study on the effect of ice-structure interaction on the dynamic response of a monopile offshore wind turbine." *1st International Conference on Renewable Energies Offshore, RENEW 2014.*

—. 2016. "Numerical study of ice-induced loads and responses of a monopile type offshore wind turbine in parked and operating conditions." *Cold Regions Science and Technology*, December: 123, 121-139.

Singh, S.K., G.W. Timco, R.M.W Frederking, and L.J Jordam. 1990. "Test of ice crushing on a flexible structure." *9th int conference on offshore mechanics and arctic engineering.*

Statoil. 2014. *www.statoil.com.* http://www.statoil.com/en/TechnologyInnovation/NewEnergy/RenewablePowerProduction/Offshore/HywindScotland/Pages/default.aspx?redirectShortUrl=http%3a%2f%2fwww.statoil.com%2fHywindScotland.

Su, Biao, Kaj Riska, and Torgeir Moan. 2010. "A numerical method for the prediction of ship performance in level ice." *Cold Region Science and Technology.*

—. 2010. "Numerical simulation of ice loads in uniform and randomly varying ice conditions." *Cold Regions Science and Technology.*

Tan, Xiang, Kaj Riska, and Torgeir Moan. 2013. "A six-degrees-of-freedom numerical model for level ice-ship interaction." *Cold Regions Science and Technology.*

—. 2014. "Effect of dynamic bending of level ice on ship's continuous-mode icebreaking." *Cold Regions Science and Technology*, June.

Tikanmaki, Maria, Jaakko Heinonen, and Lasse Makkonen. 2012. "Estimation of local ice conditions in the baltic sea for offshore wind turbine design." *21st IAHR International Symposium on Ice.*

Timco, G.W., and S. O'Brien. 1994. "Flexural strength equation for sea ice." *Flexural strength equation for sea ice.*

Timco, G.W., and W.F. Weeks. 2010. "A review of the engineering properties of sea ice." *Cold Regions Science and Technology.*

UNESCO . 1983. "Algorithms for fundamental properties of seawater."

Varsta, Petri. 1983. *On the mechanics of ice load on ships in level ice in the Baltic Sea.* Espoo, Finland: Helsinki University of Technology.

Wang, Shuqin. 2001. *A dynamic model for breaking pattern of level ice by conical structures.* Espoo, Finland: Helsinki University of Technology.

Wang, Yihe, Xiaofei Hu, Zigi Zhao, Qianjin Yue, and Ning Xu. 2014. "Failure mode of the ice sheet loading at the junction of the upward and downward breaking cones." *Ocean Engineering.*

Xu, Ning, and Qianjin Yue. 2014. "Dynamic ice force analysis on a conical structure based on direct observation and measurement." *Journal of Offshore Mechanics and Arctic Engineering.*

Xu, Ning, Qianjin Yue, Fengwei Guo, and Yan Qu. 2011. "Mitigation of ice induced vibrations by adding cones." *International Journal of Offshore and Polar Engineering.*

Appendices

A. Curve fitting attempt

Characteristic length

Failure load
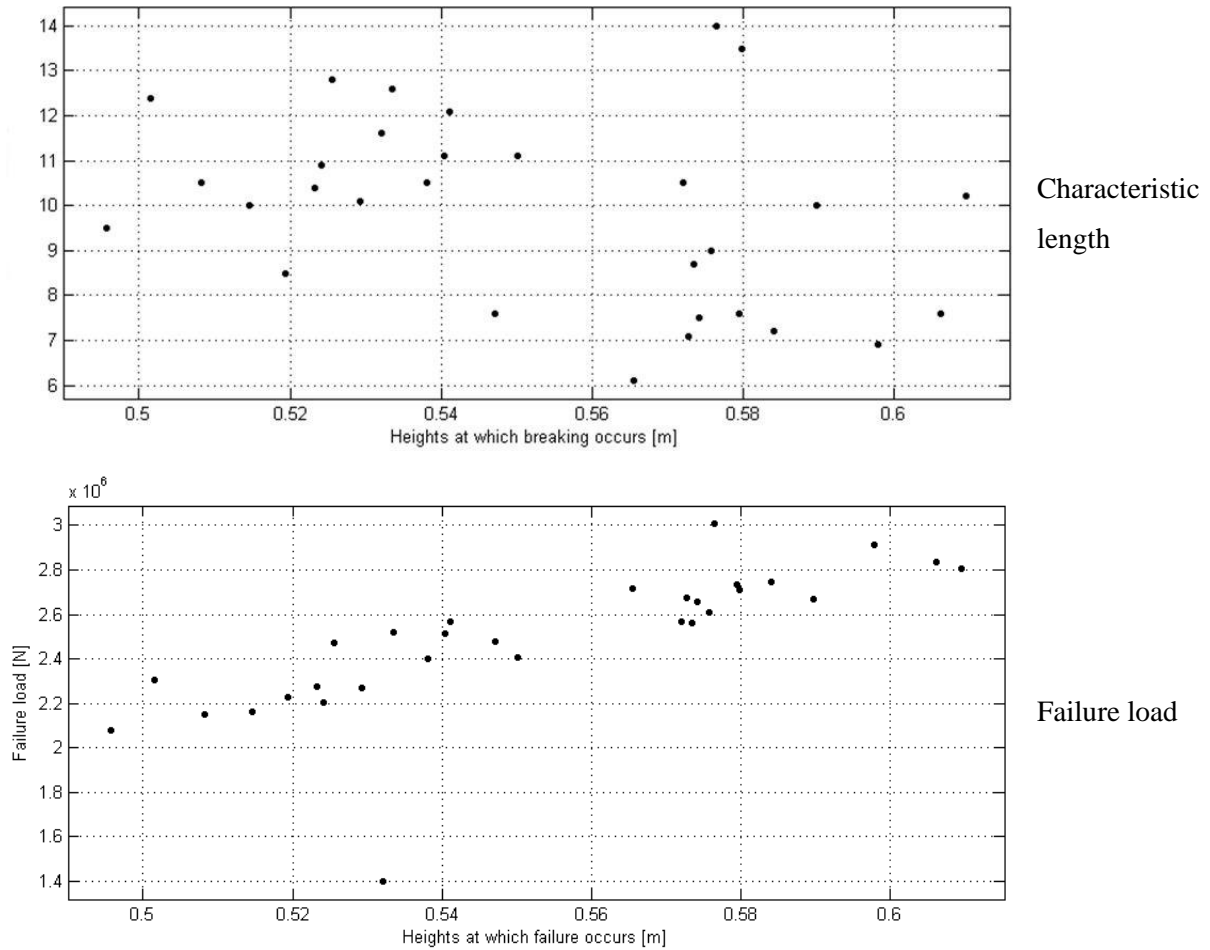
B. Simulations in order to find the proper length interval
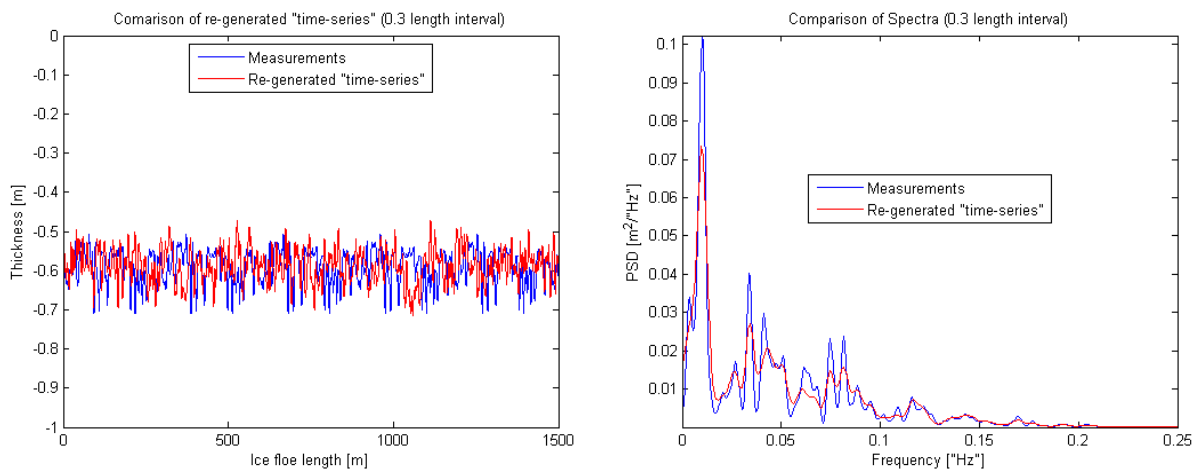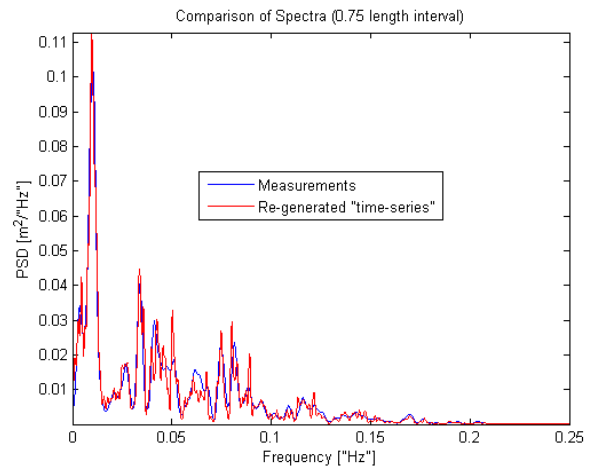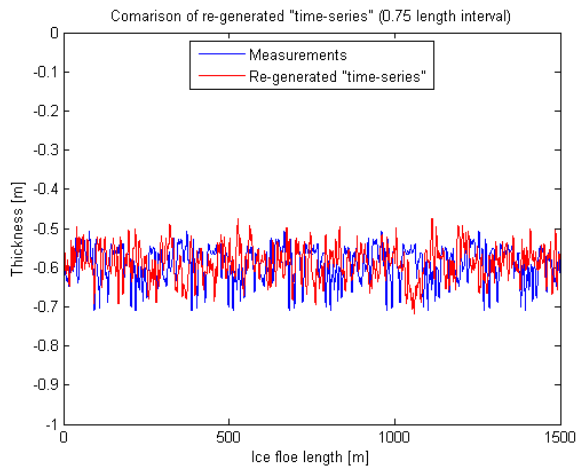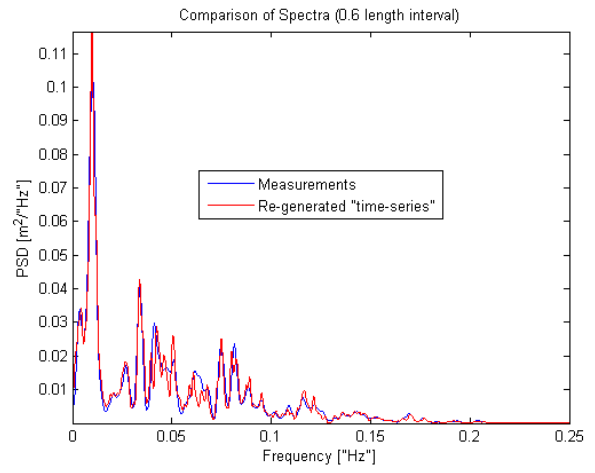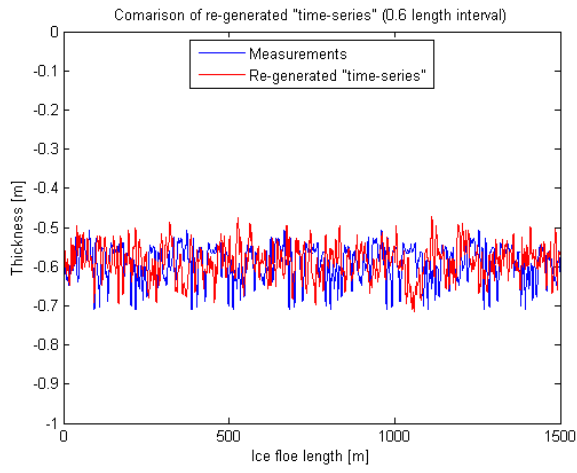
C1. Validation considering Monopile

C.1.1 - Case of 0.1 m/s drifting speed
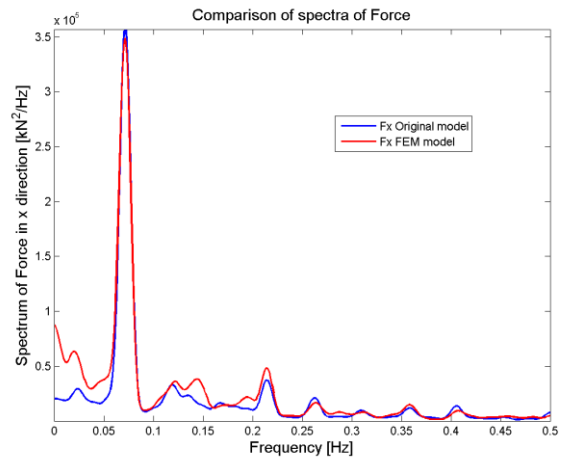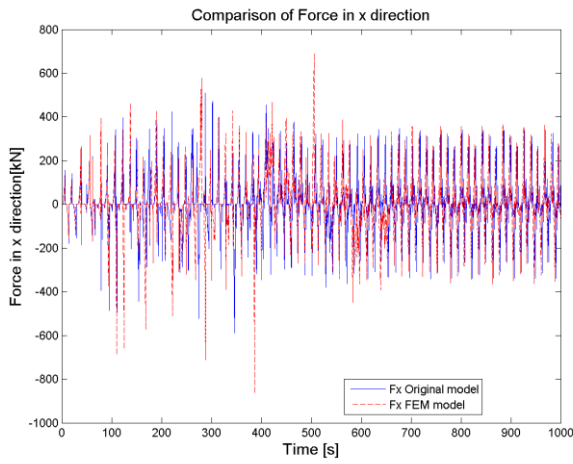
Comparison of Force in x direction at 0.1 m/s

Force Spectra in x direction at 0.1 m/s
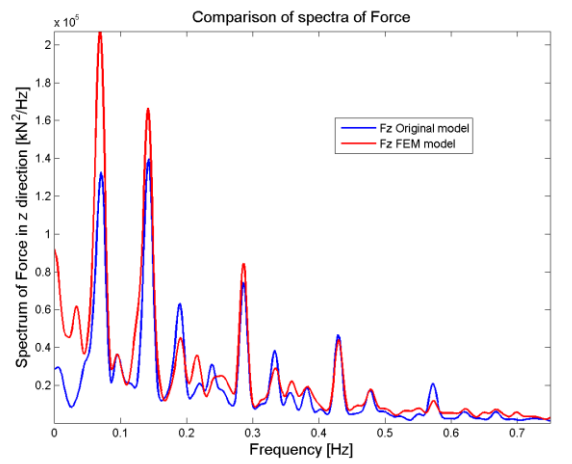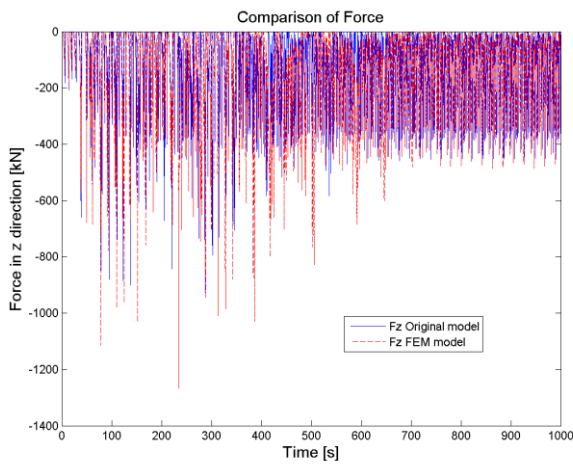
Comparison of Force in z direction at 0.1 m/s
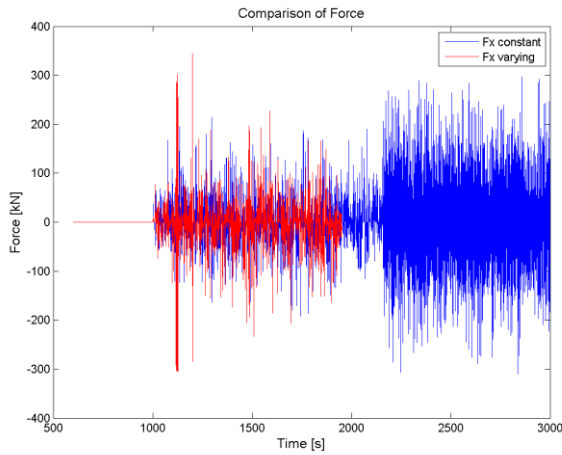

Force Spectra in z direction at 0.1 m/s
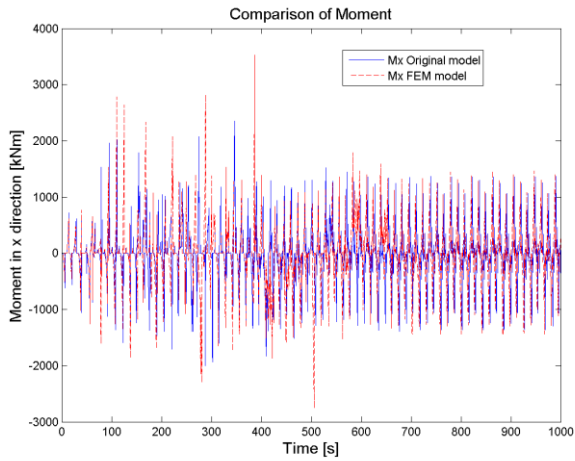
Comparison of Moment in x direction at 0.1 m/s
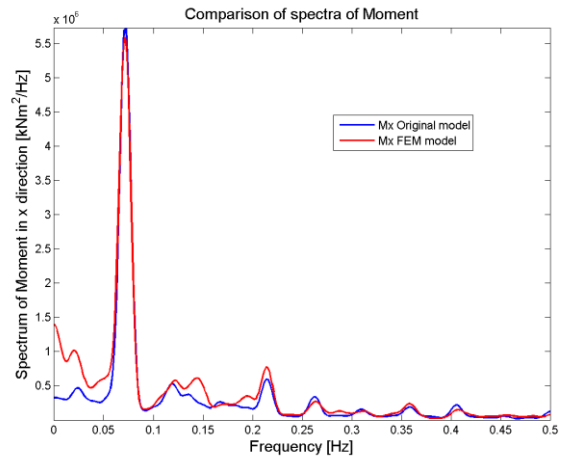
Moment Spectra in x direction at 0.1 m/s
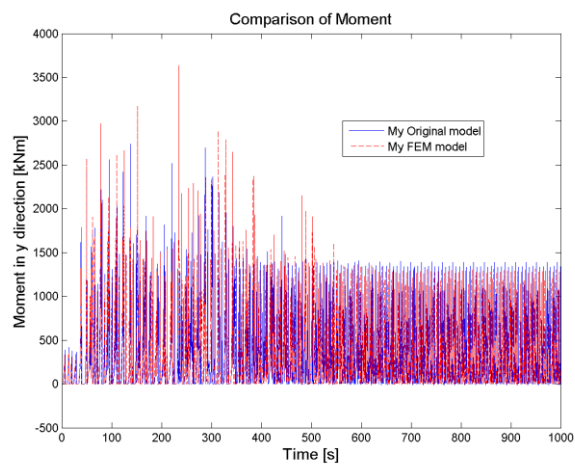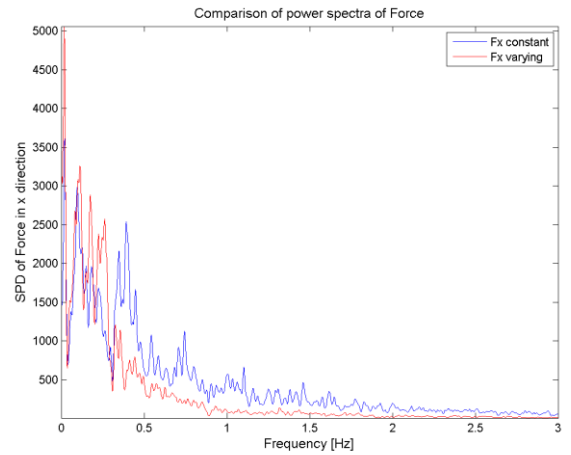

Comparison of Moment in y direction at 0.1 m/s
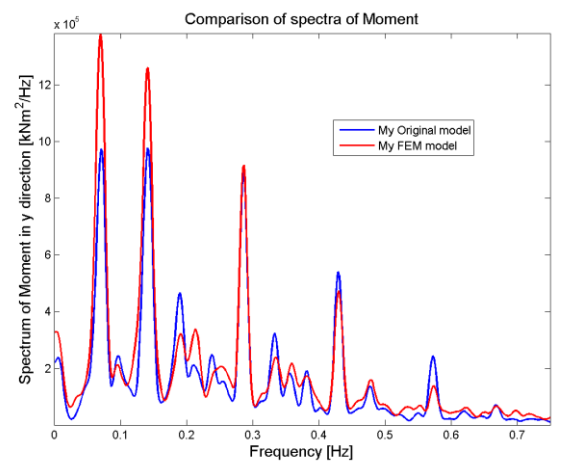
Moment Spectra in y direction at 0.1 m/s
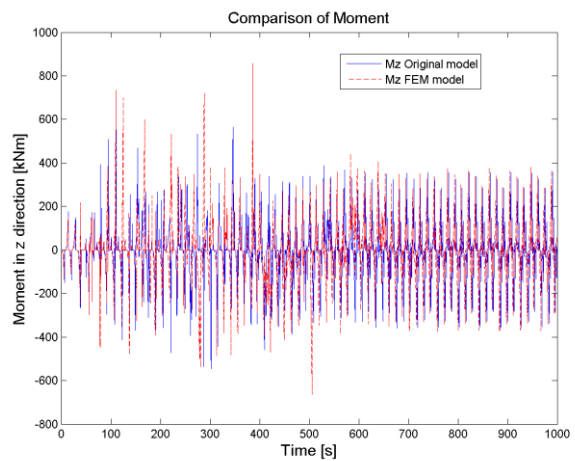
Comparison of Moment in z direction at 0.1 m/s
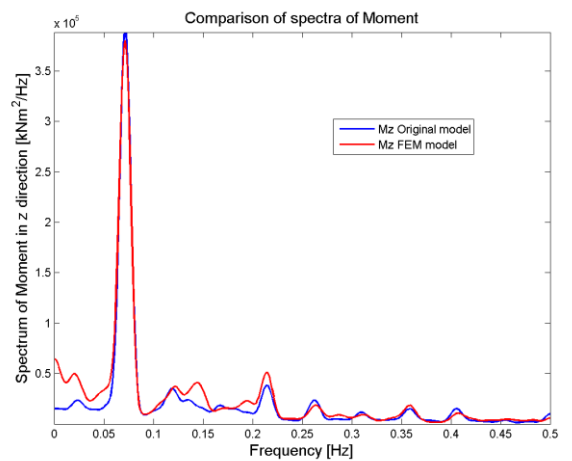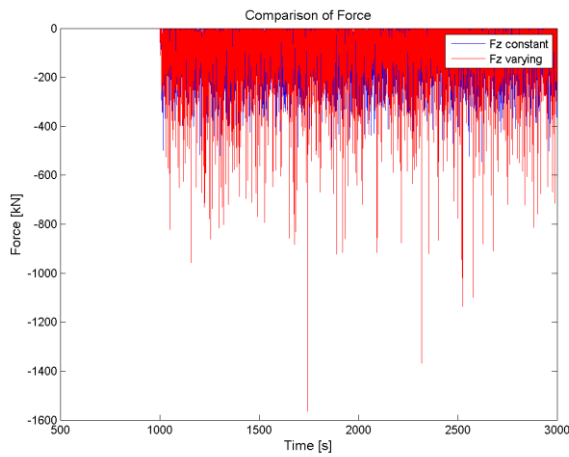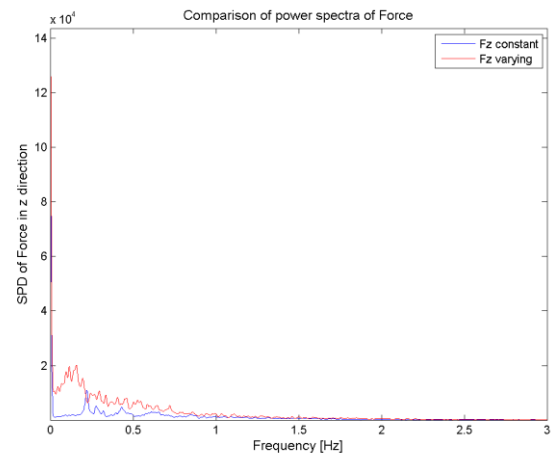

Moment Spectra in z direction at 0.1 m/s

C.1.2 - Case of 0.3 m/s drifting speed
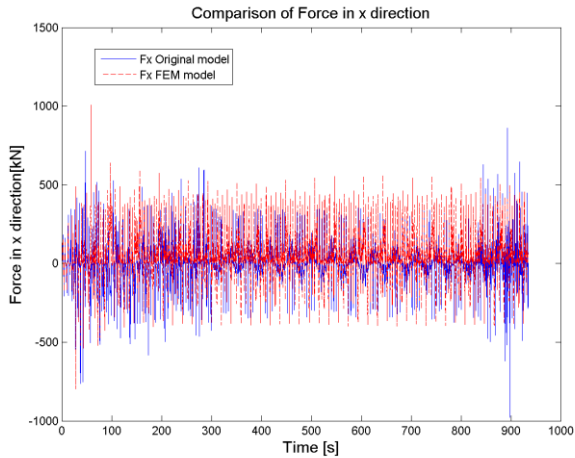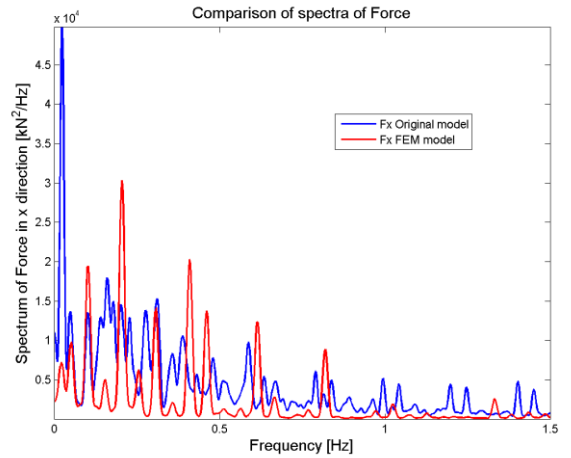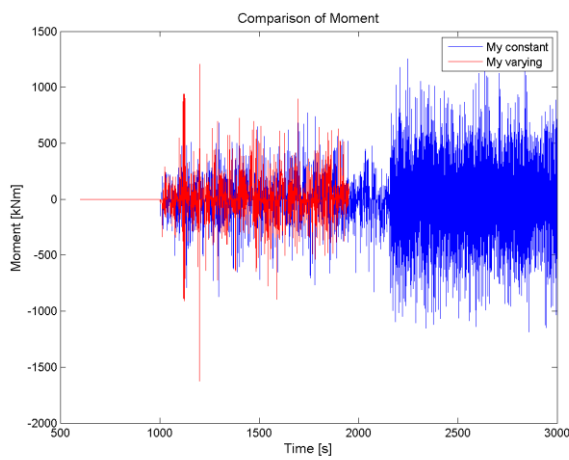

Comparison of Force in x direction at 0.3 m/s

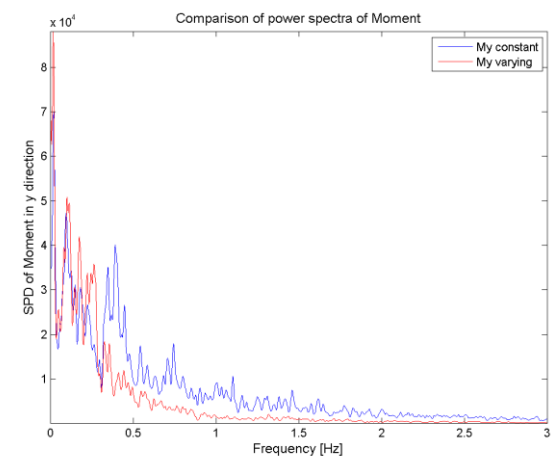Force Spectra in x direction at 0.3 m/s
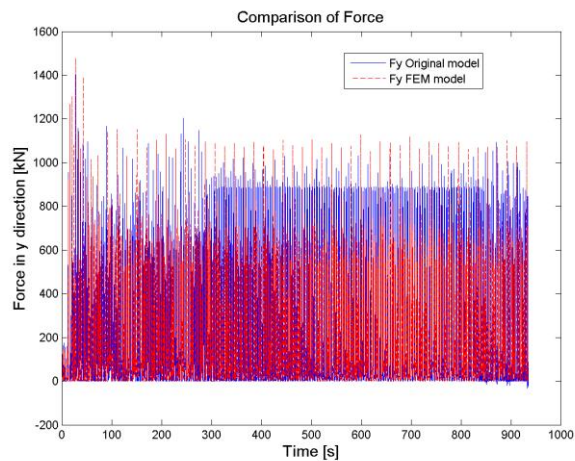
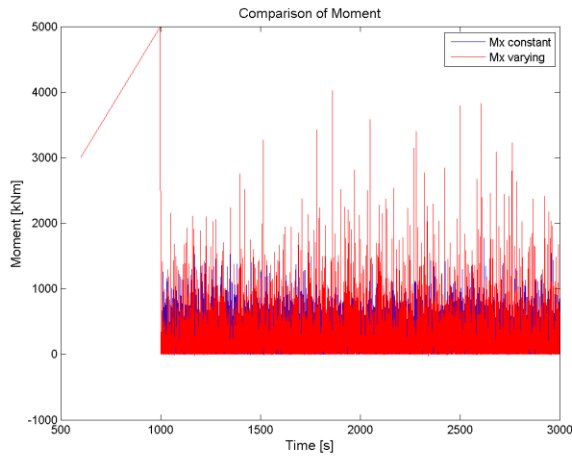Comparison of Force in y direction at 0.3 m/s
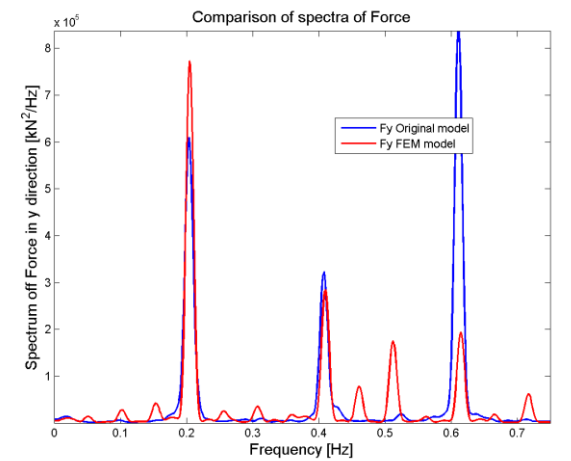
Force Spectra in y direction at 0.3 m/s
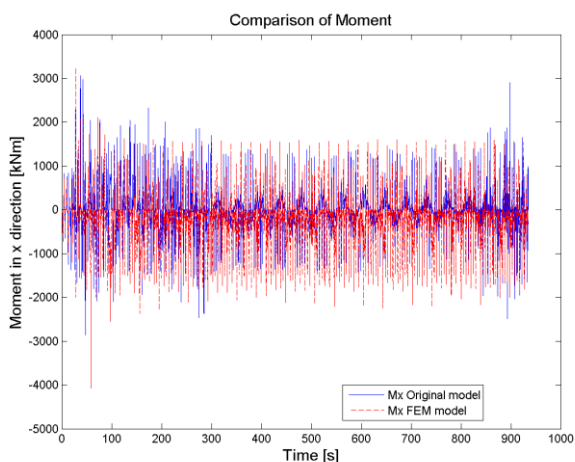
Comparison of Moment in x direction at 0.3 m/s
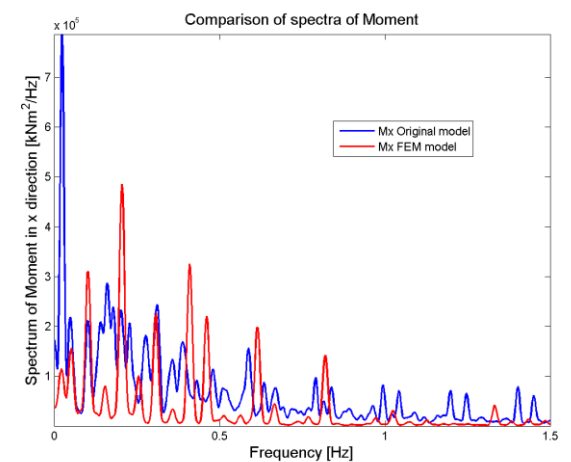
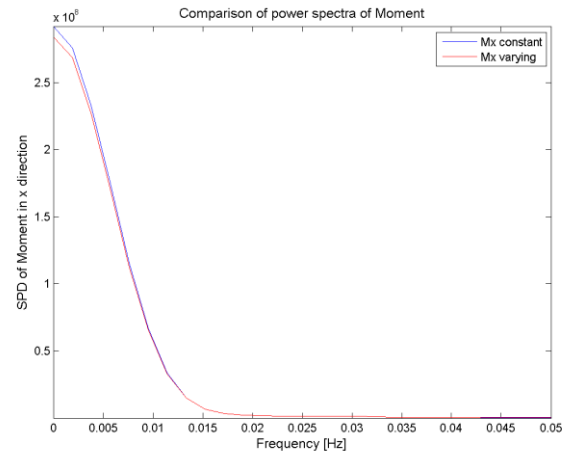Moment Spectra in x direction at 0.3 m/s
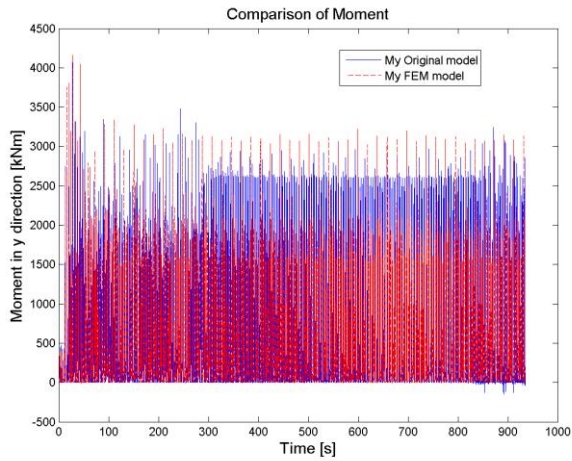
Comparison of Moment in y direction at 0.3 m/s
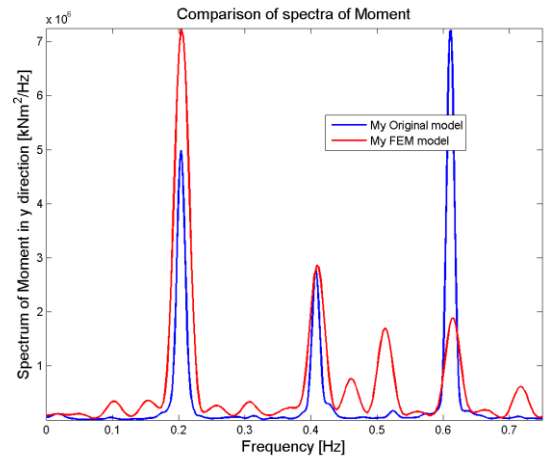
Moment Spectra in y direction at 0.3 m/s
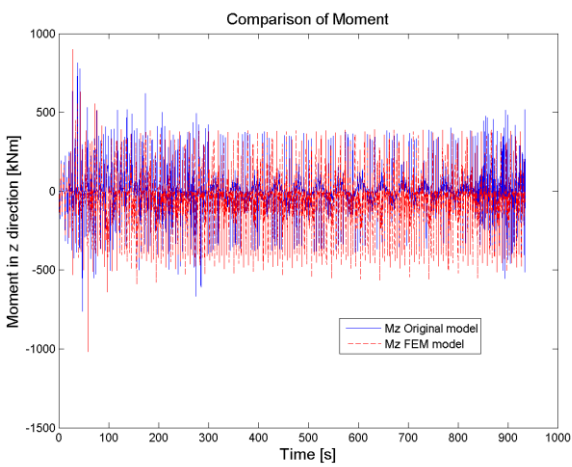
Comparison of Moment in z direction at 0.3 m/s
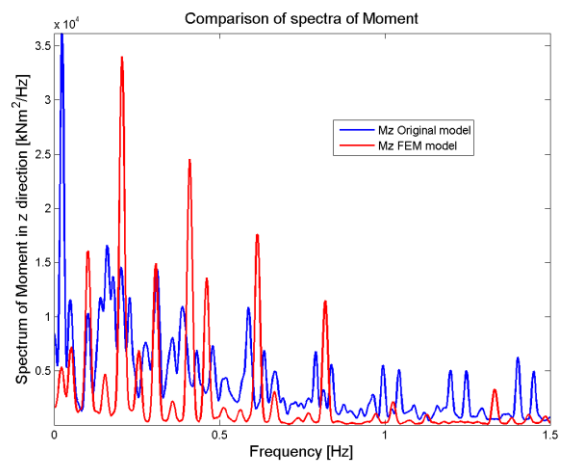
Moment Spectra in z direction at 0.3 m/s

C.1.3 - Case of 0.5 m/s drifting speed
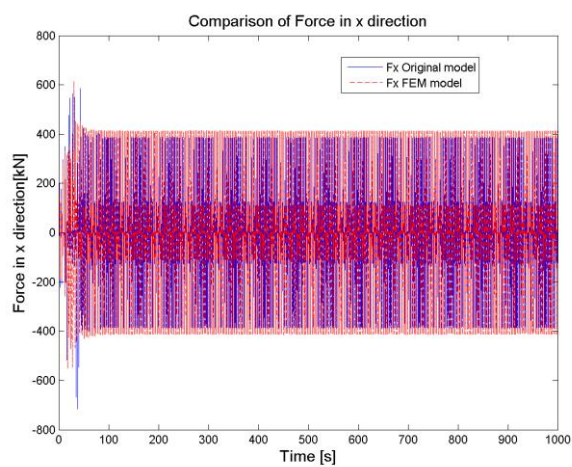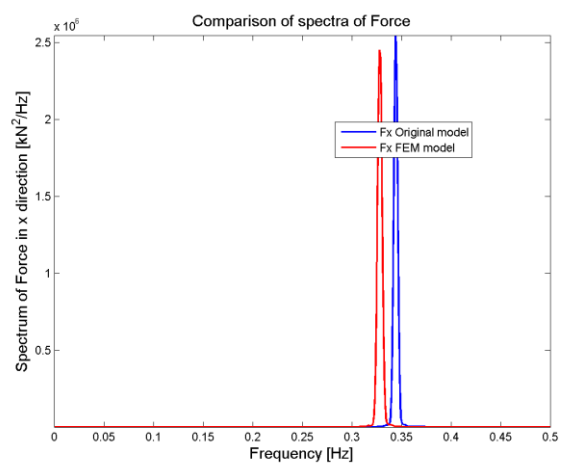
Comparison of Force in x direction at 0.5 m/s

Force Spectra in x direction at 0.5 m/s
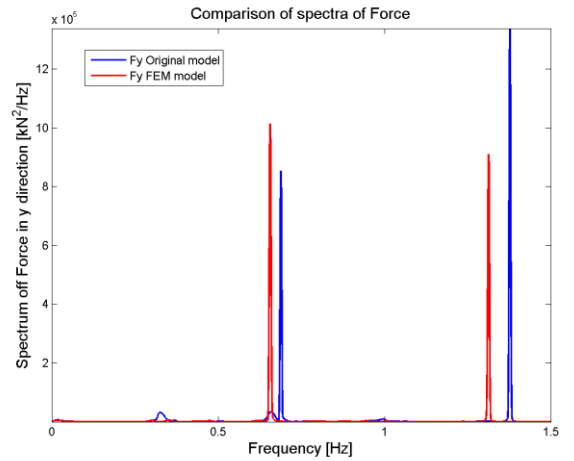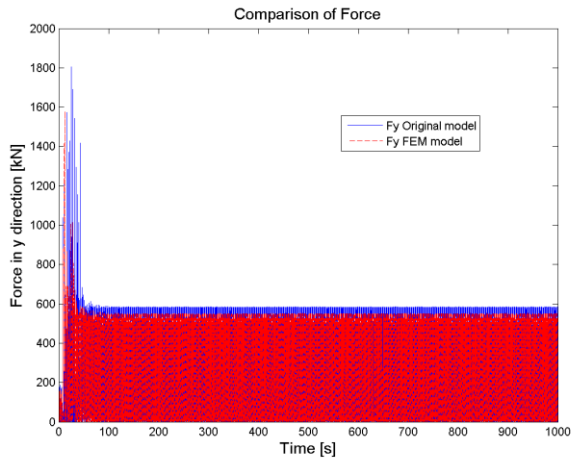
Comparison of Force in y direction at 0.5 m/s

Force Spectra in y direction at 0.5 m/s
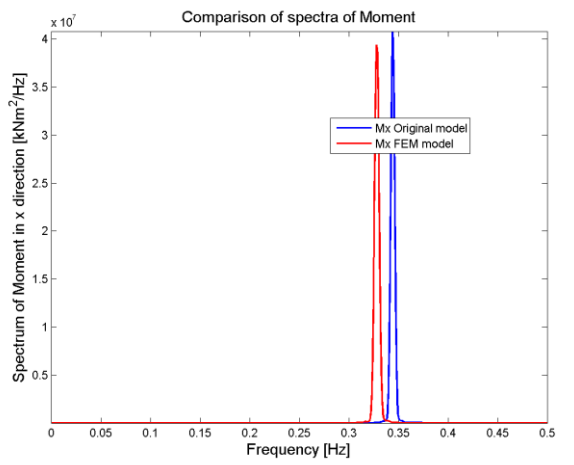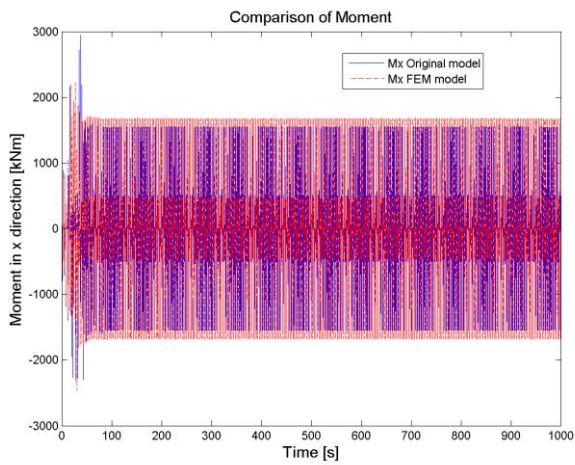
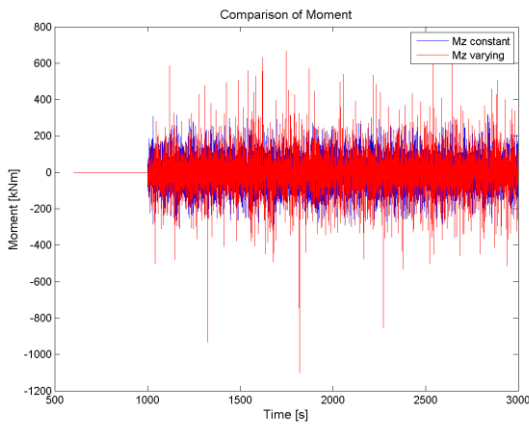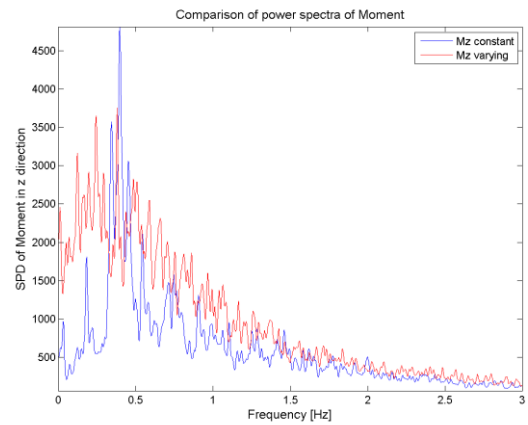

Comparison of Moment in x direction at 0.5 m/s

Moment Spectra in x direction at 0.5 m/s
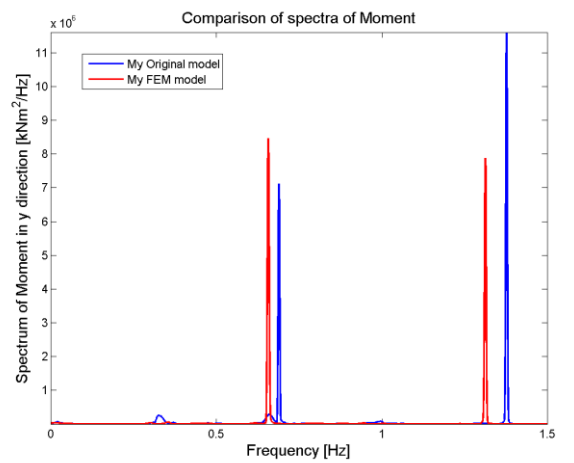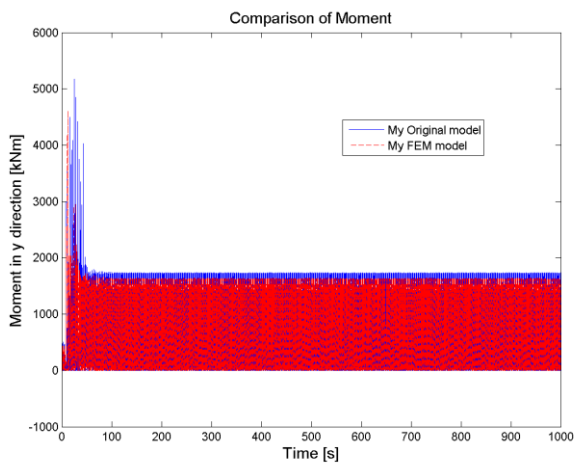
Comparison of Moment in y direction at 0.5 m/s

Moment Spectra in y direction at 0.5 m/s
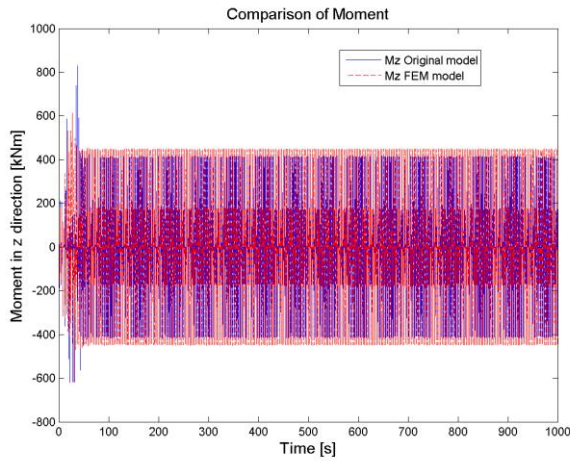
Comparison of Moment in z direction at 0.5 m/s
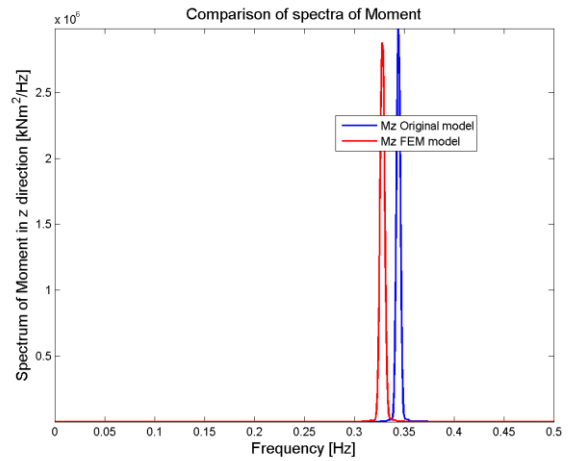
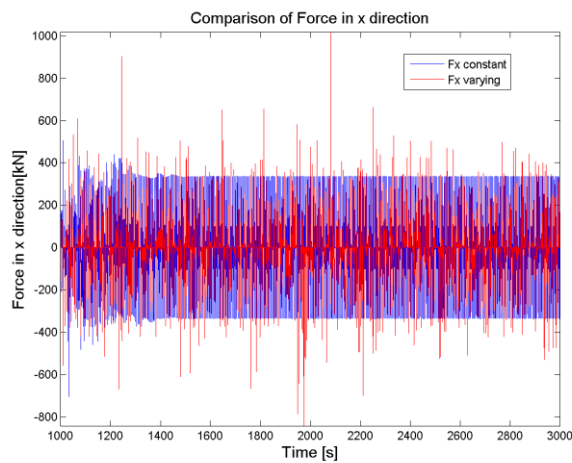Moment Spectra in z direction at 0.5 m/s

C2. Validation considering Spar

C.2.1 - Case of 0.3 m/s drifting speed
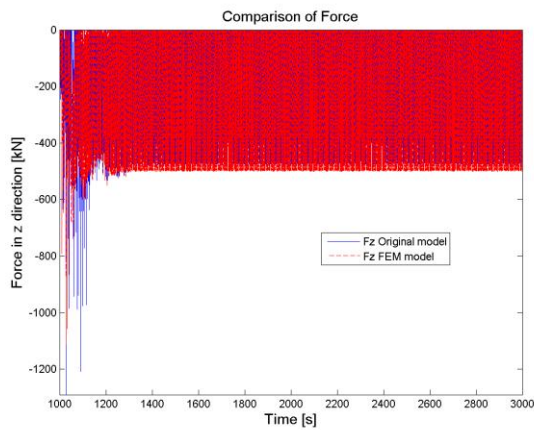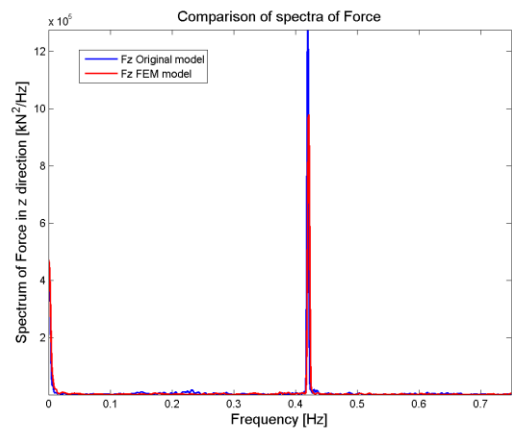
Comparison of Force in z direction at 0.3 m/s

Force Spectra in z direction at 0.3 m/s
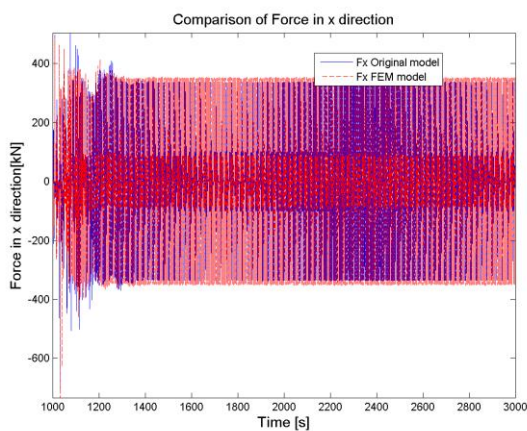
Comparison of Force in x direction at 0.3 m/s
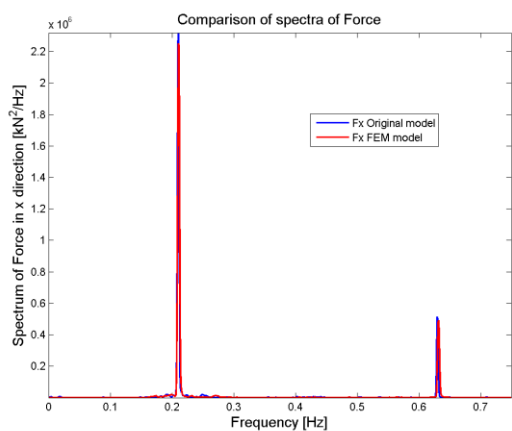
Force Spectra in x direction at 0.3 m/s
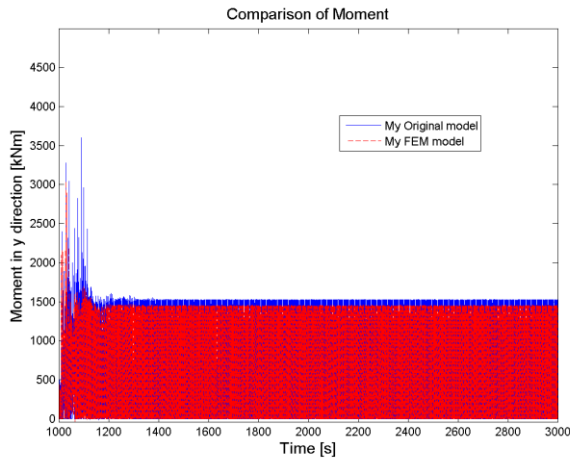
Comparison of Moment in y direction at 0.3 m/s
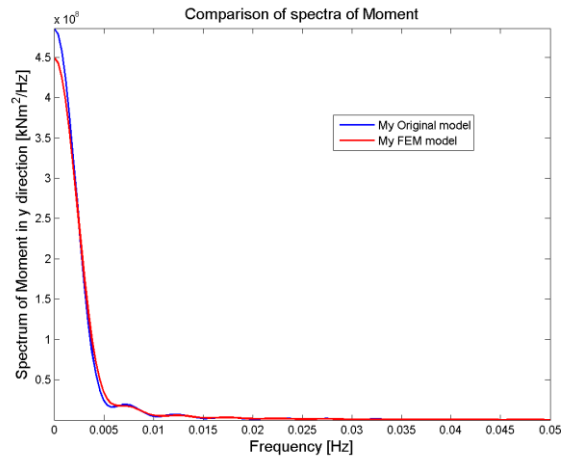
Moment Spectra in y direction at 0.3 m/s
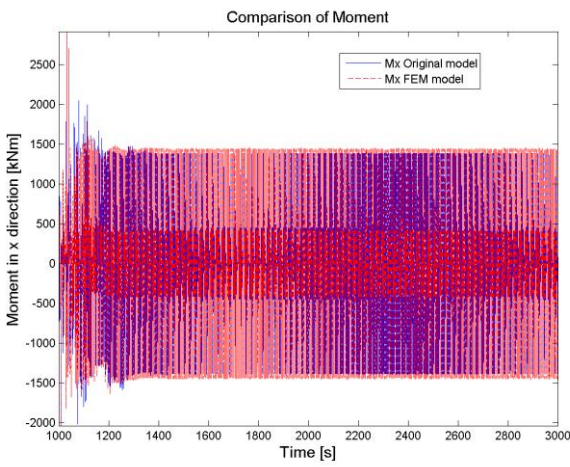
Comparison of Moment in x direction at 0.3 m/s
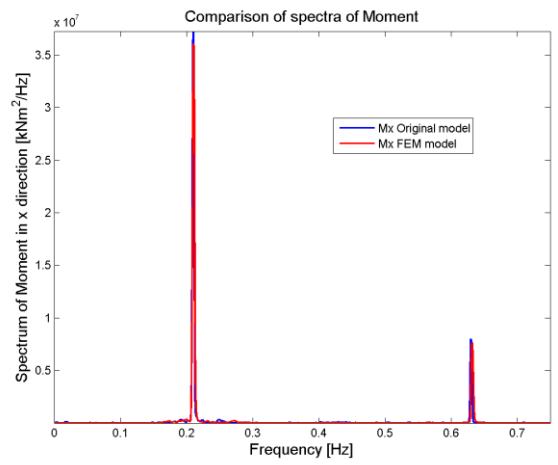
Moment Spectra in x direction at 0.3 m/s
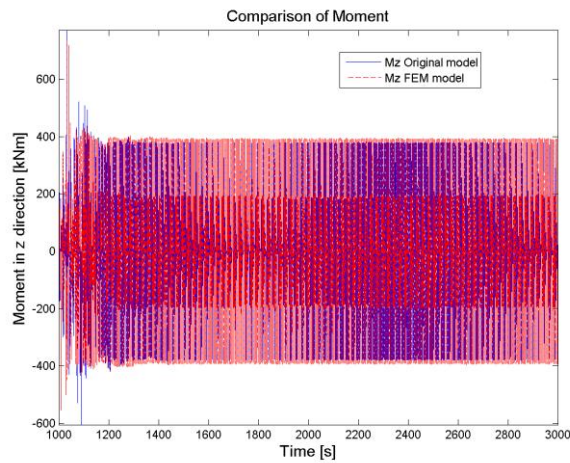
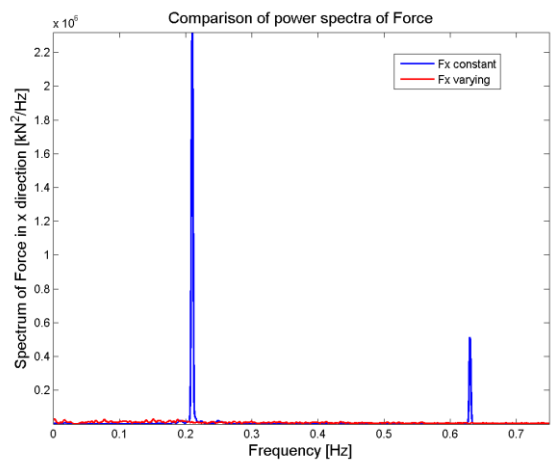Comparison of Moment in z direction at 0.3 m/s
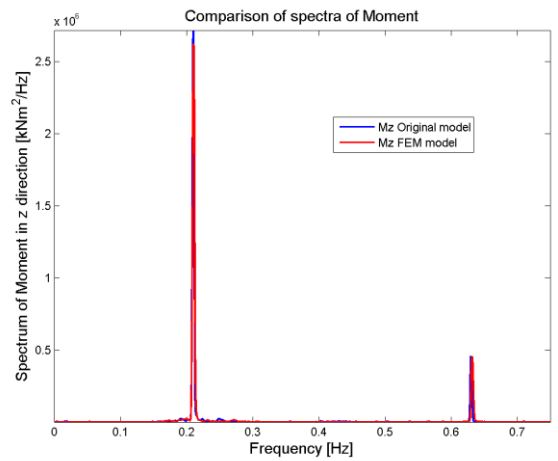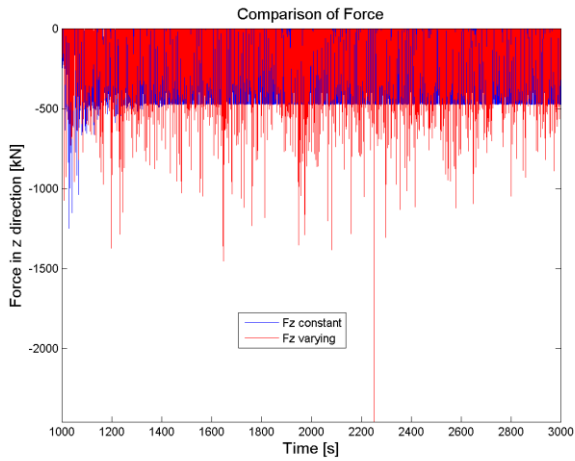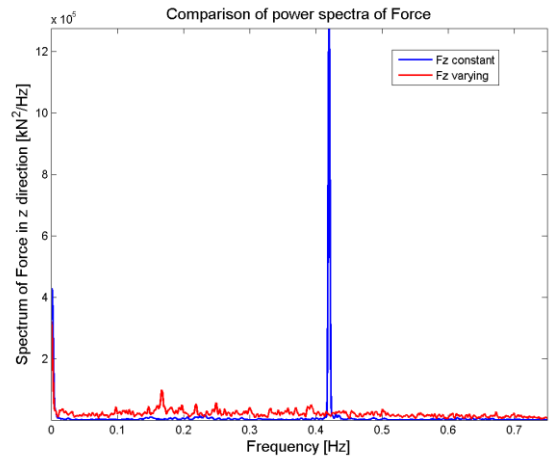

Moment Spectra in z direction at 0.3 m/s

C.2.2 - Case of 0.3 m/s drifting speed with constant wind speed of 12 m/s
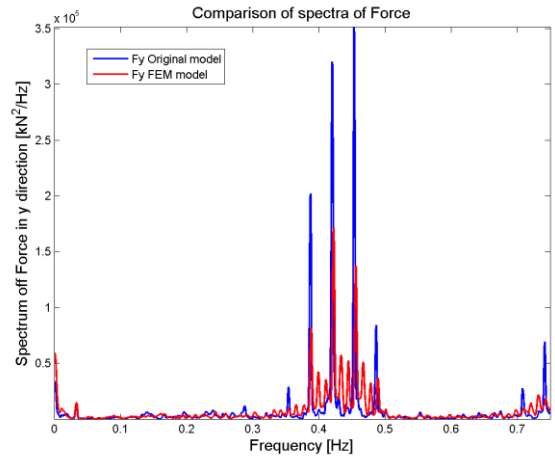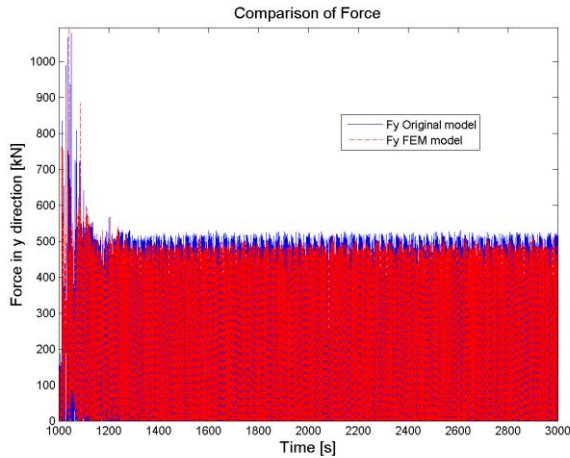
Comparison of Force in y direction at 0.3 m/s with wind

Force Spectra in y direction at 0.3 m/s with wind
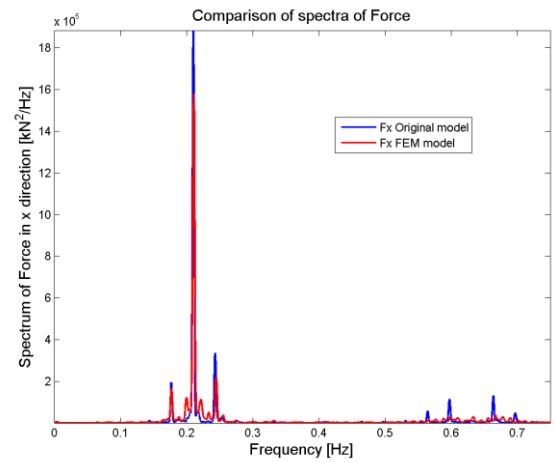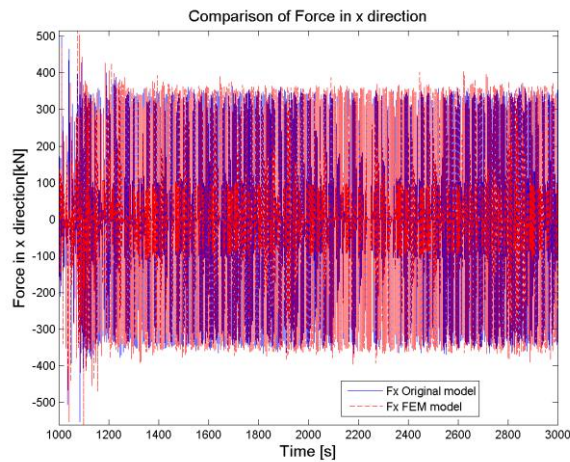
Comparison of Force in z direction at 0.3 m/s with wind

Force Spectra in z direction at 0.3 m/s with wind
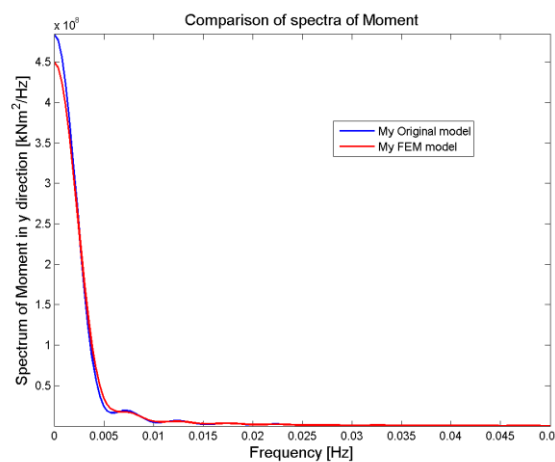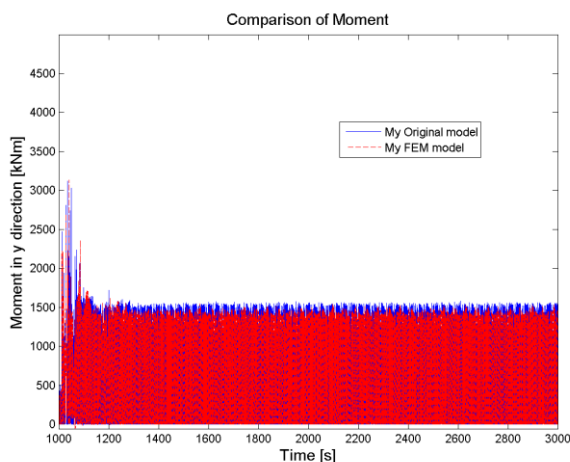
Comparison of Moment in y direction at 0.3 m/s with wind

Moment Spectra in y direction at 0.3 m/s with wind
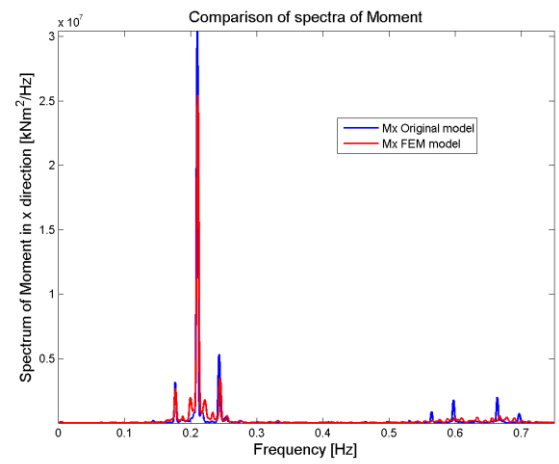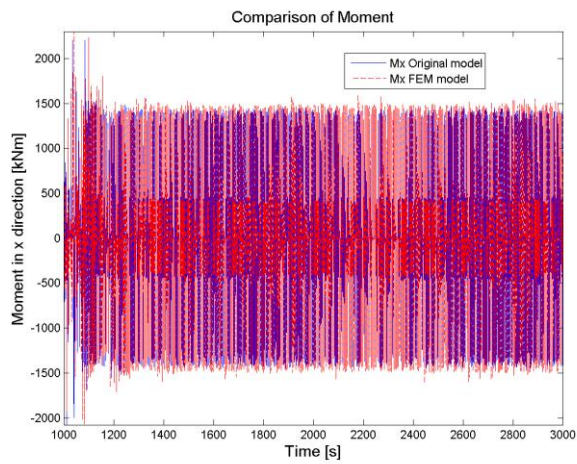
Comparison of Moment in x direction at 0.3 m/s with wind

Moment Spectra in x direction at 0.3 m/s with wind
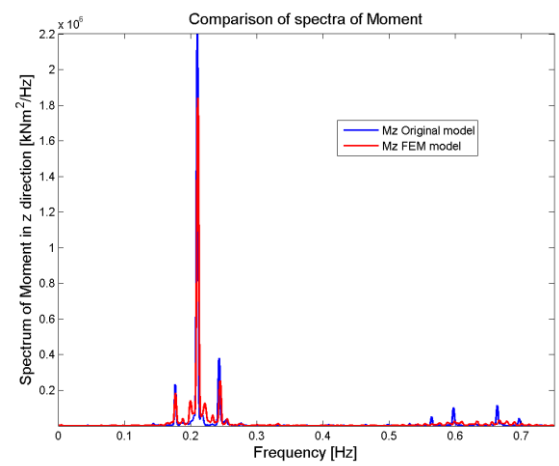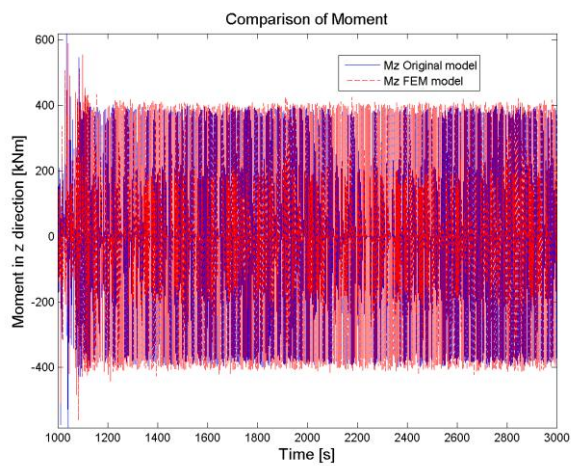
Comparison of Moment in z direction at 0.3 m/s with wind

Moment Spectra in z direction at 0.3 m/s with wind

C.2.3 - Case of 0.5 m/s drifting speed
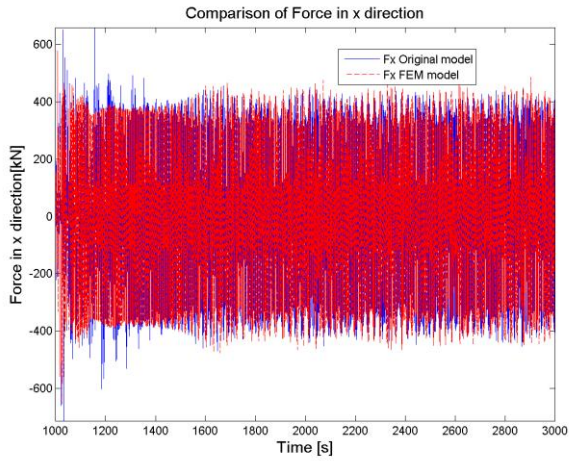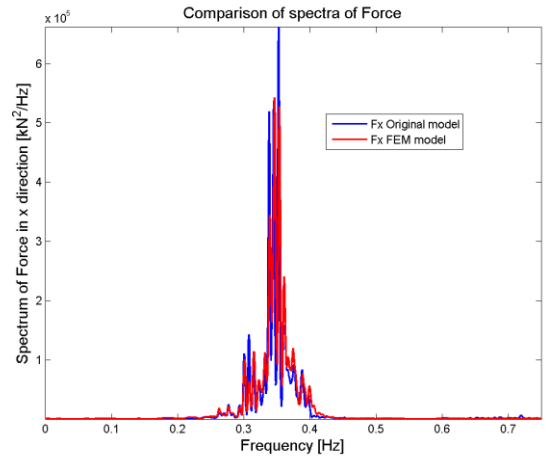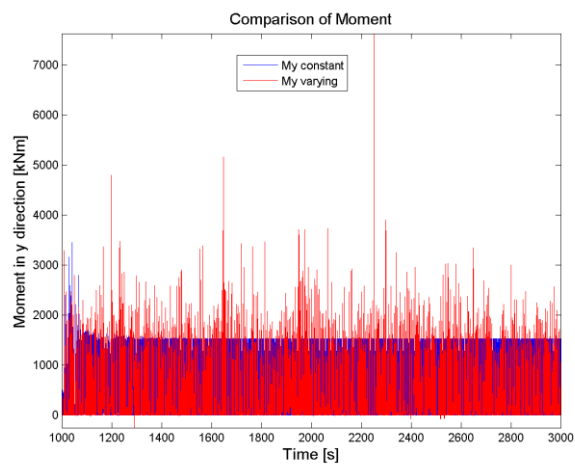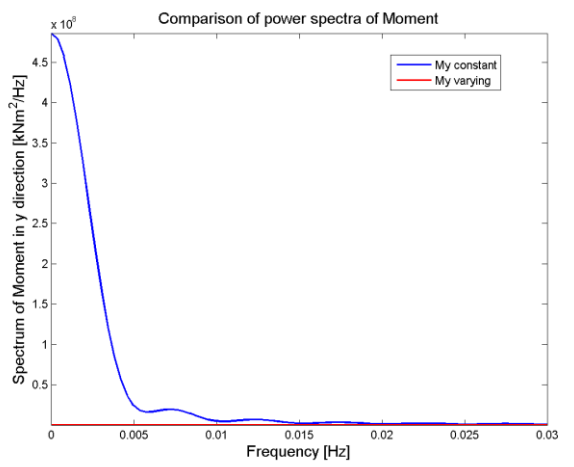

Comparison of Force in x direction at 0.5 m/s

Force Spectra in x direction at 0.5 m/s
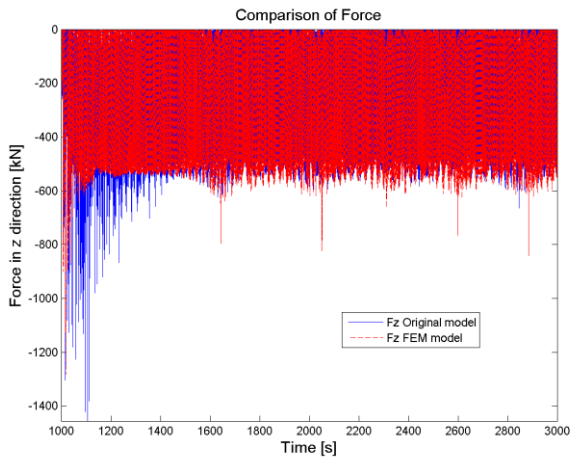
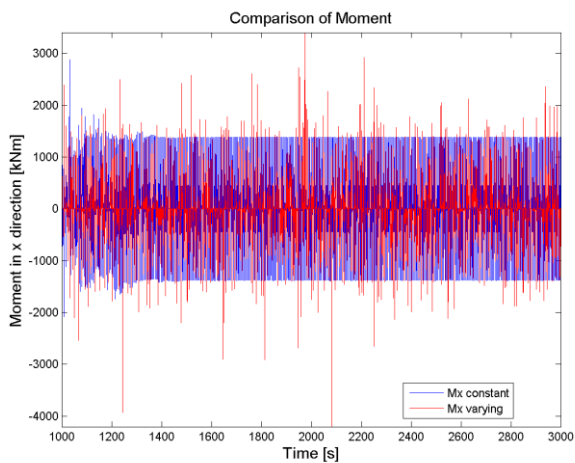Comparison of Force in z direction at 0.5 m/s
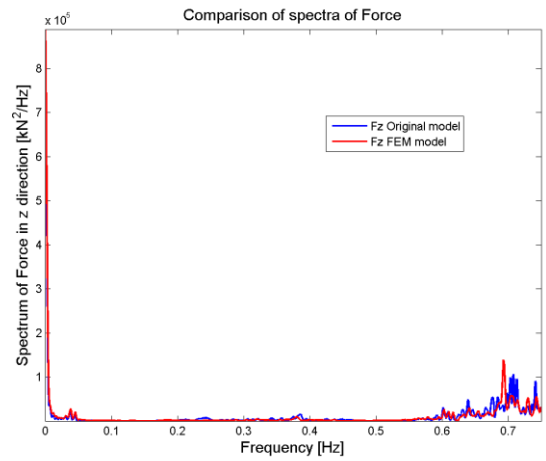
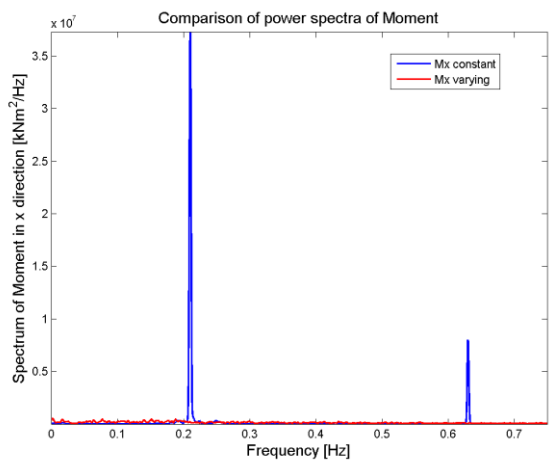
Force Spectra in z direction at 0.5 m/s
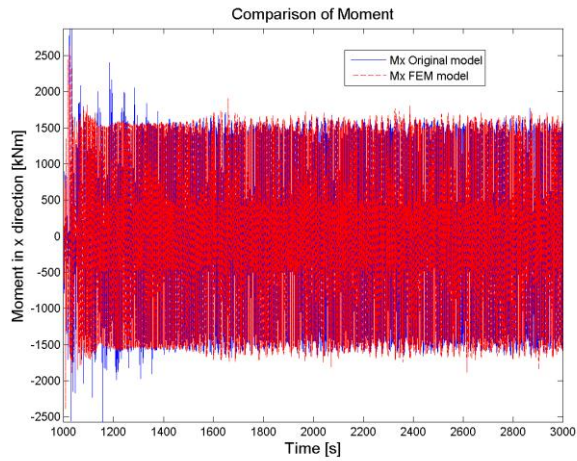
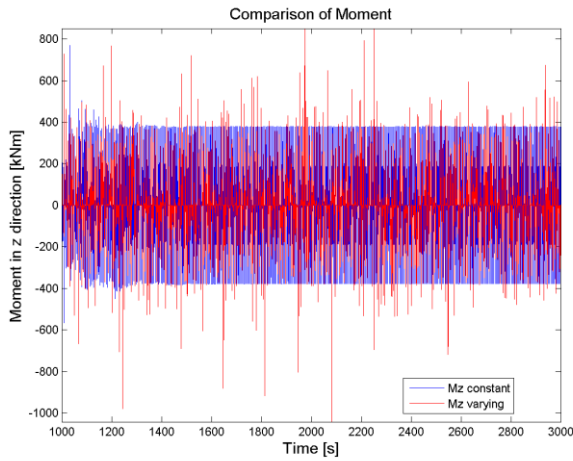Comparison of Moment in x direction at 0.5 m/s
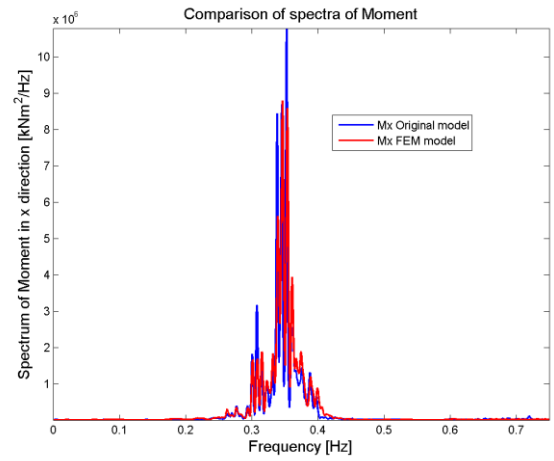
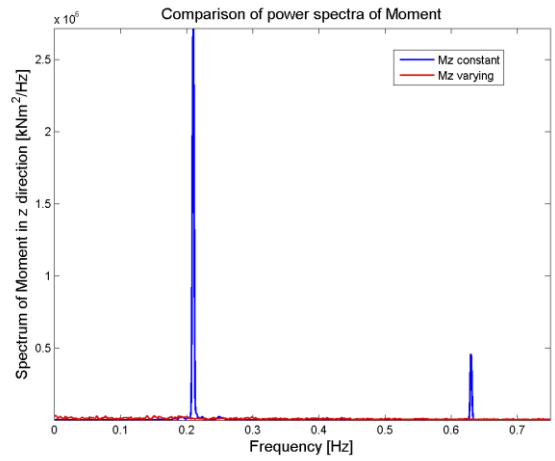Moment Spectra in x direction at 0.5 m/s
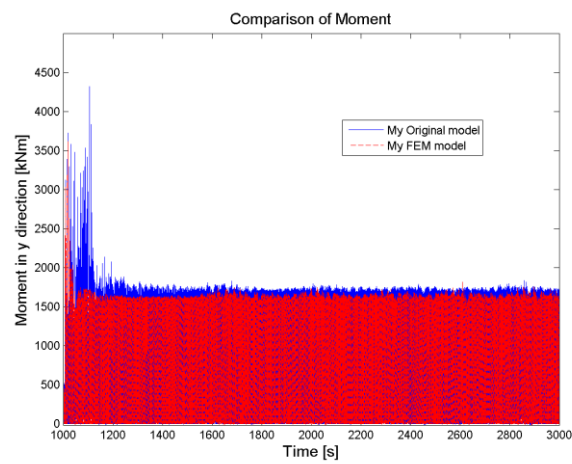
Comparison of Moment in y direction at 0.5 m/s
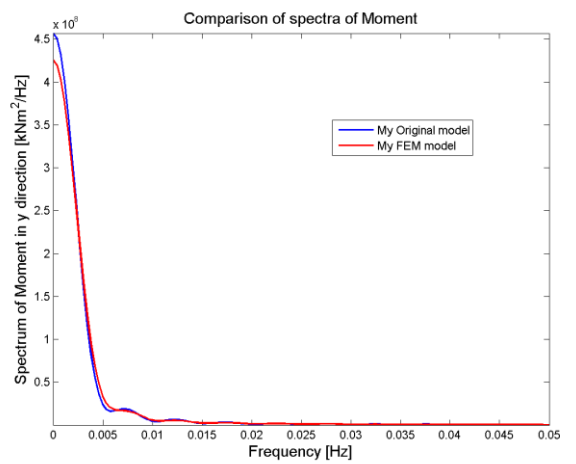
Moment Spectra in y direction at 0.5 m/s
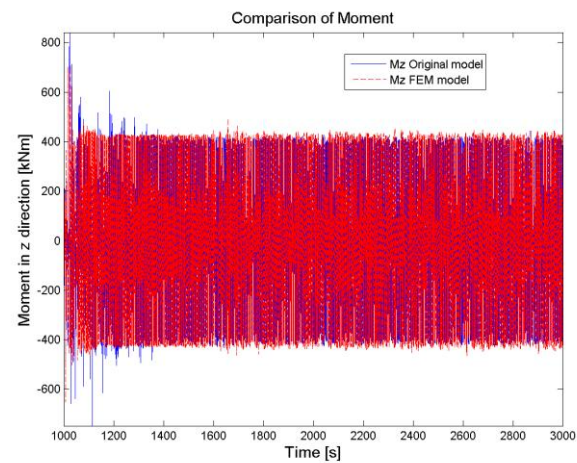
Comparison of Moment in z direction at 0.5 m/s
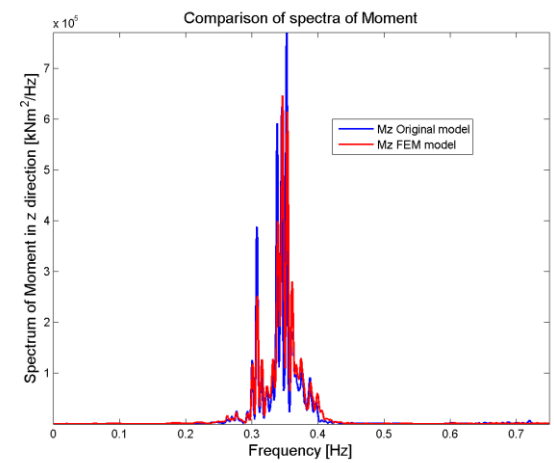
Moment Spectra in z direction at 0.5 m/s

D1. Ice actions constant vs varying thickness, monopile 0.1 m/s drifting speed
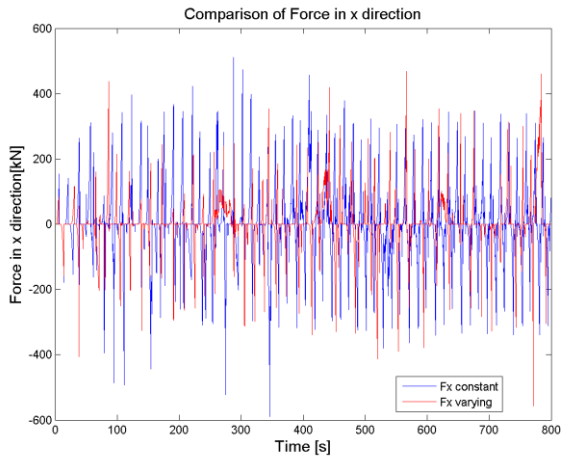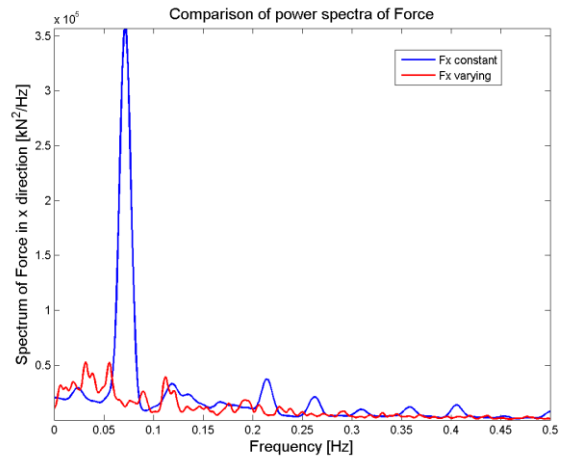
Comparison of Force in x direction at 0.1 m/s

Force Spectra in x direction at 0.1 m/s
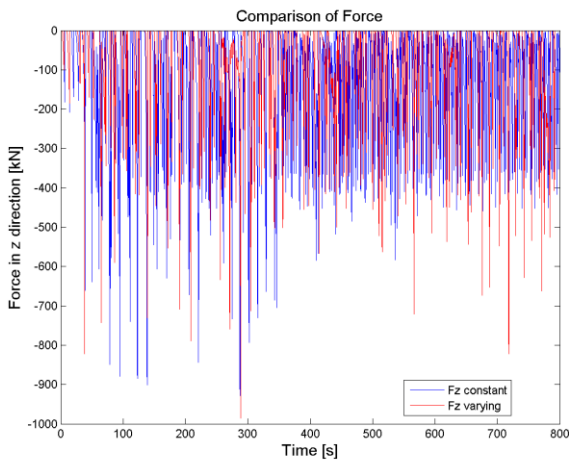
Comparison of Force in z direction at 0.1 m/s
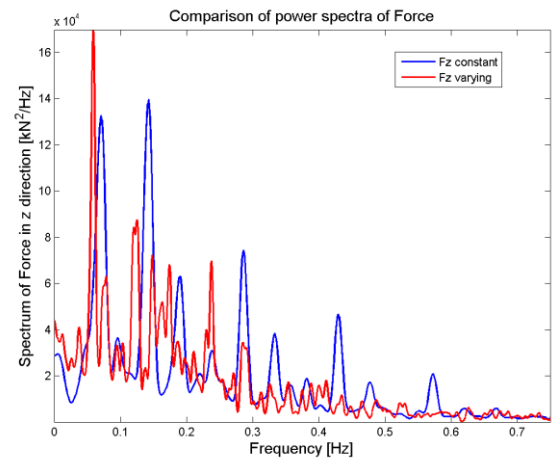
Force Spectra in z direction at 0.1 m/s
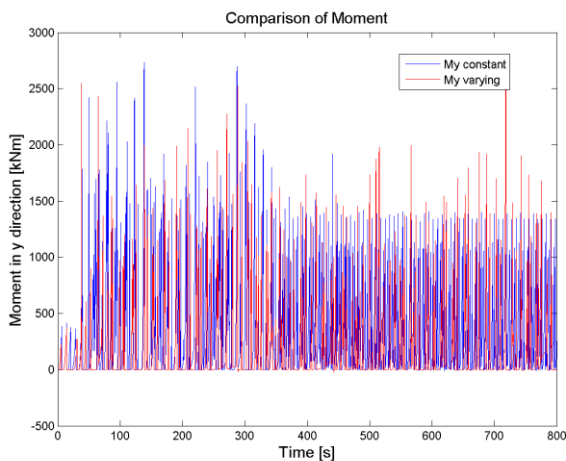
Comparison of Moment in x direction at 0.1 m/s
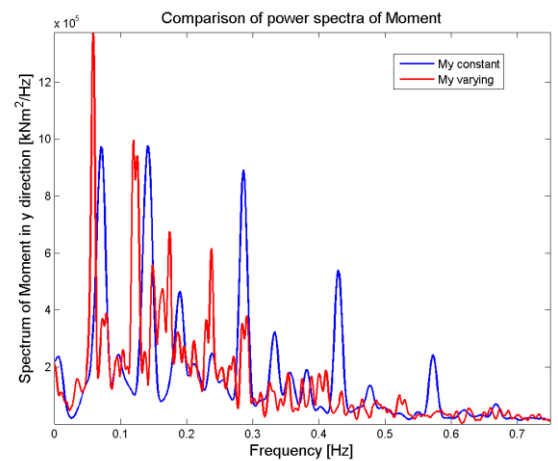
Moment Spectra in x direction at 0.1 m/s
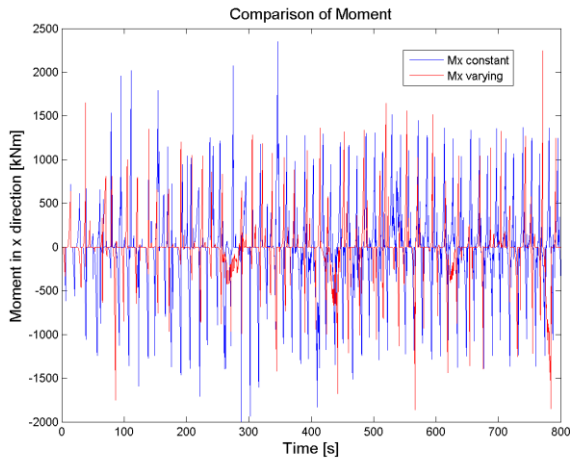
Comparison of Moment in y direction at 0.1 m/s
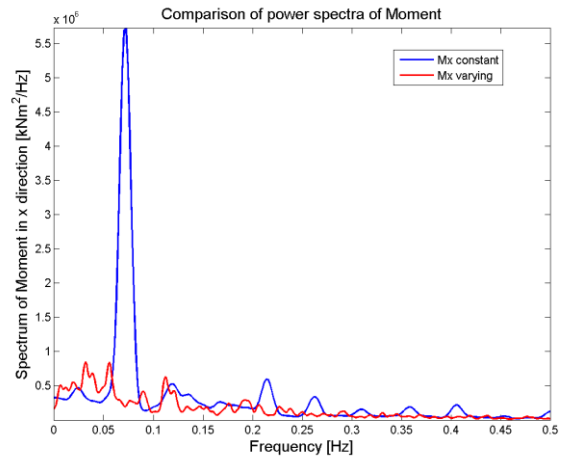
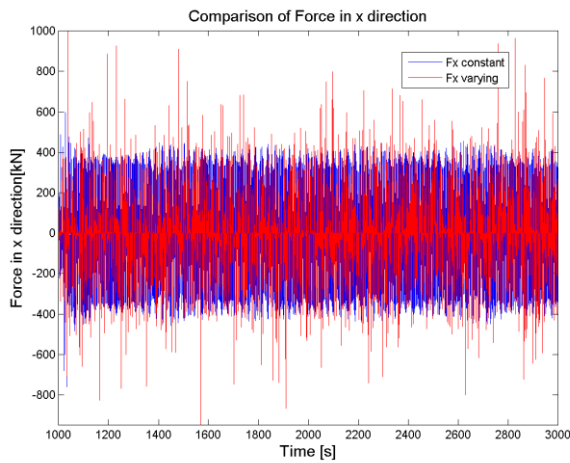Moment Spectra in y direction at 0.1 m/s
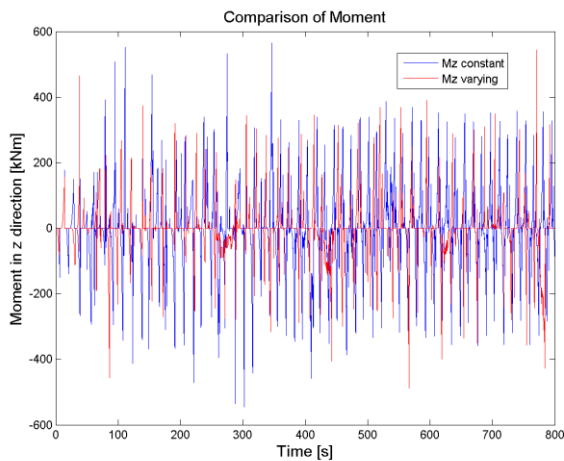
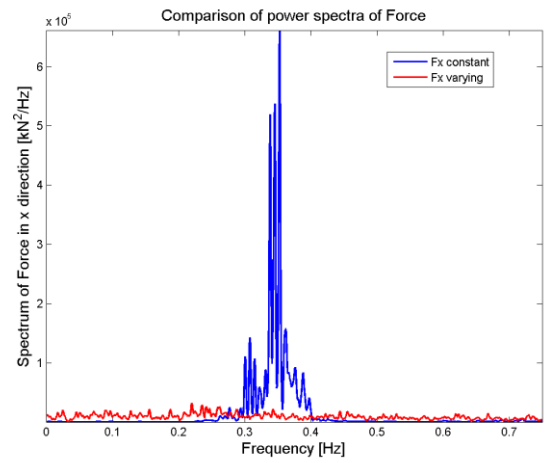Comparison of Moment in z direction at 0.1 m/s
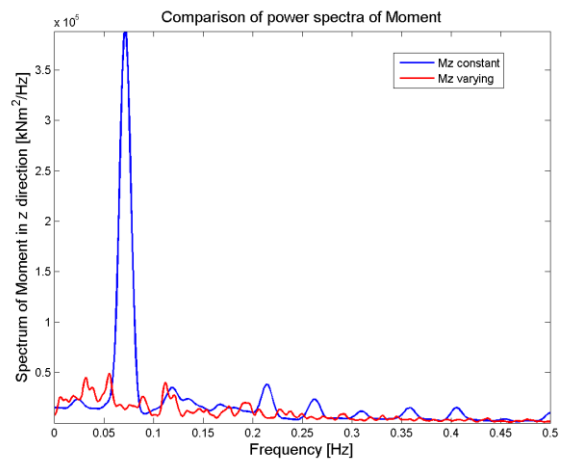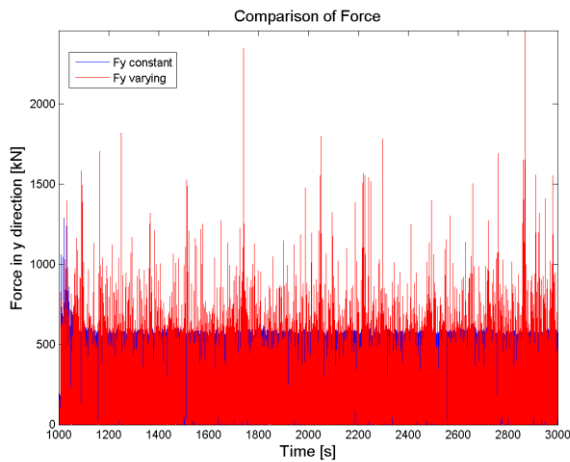

Moment Spectra in z direction at 0.1 m/s

D2. Ice actions constant vs varying thickness, monopile 0.3 m/s drifting speed
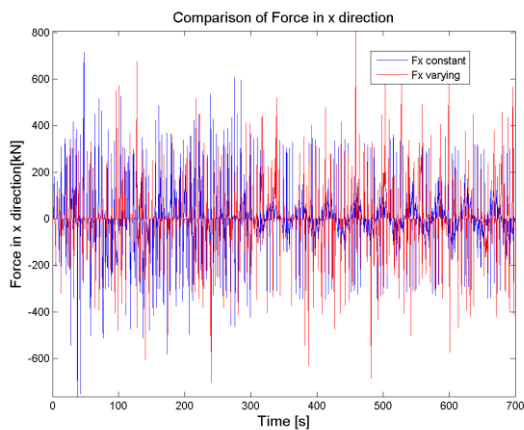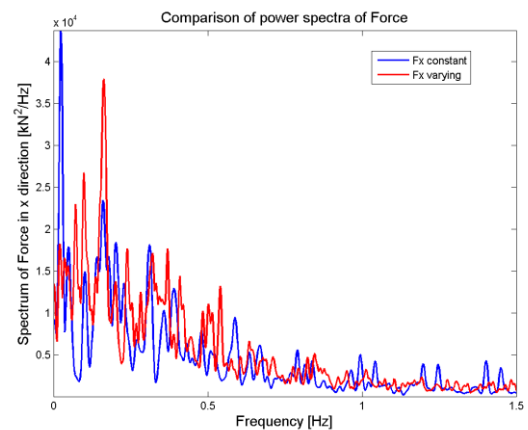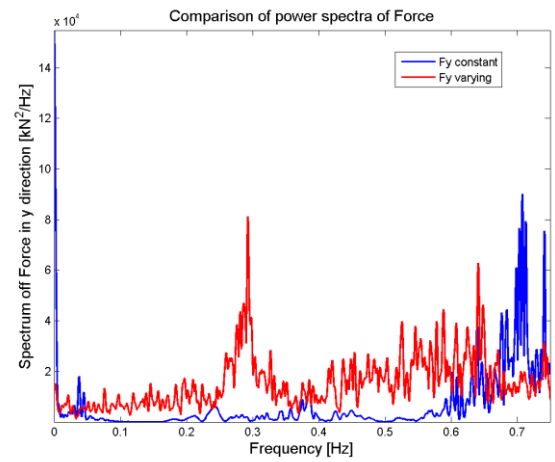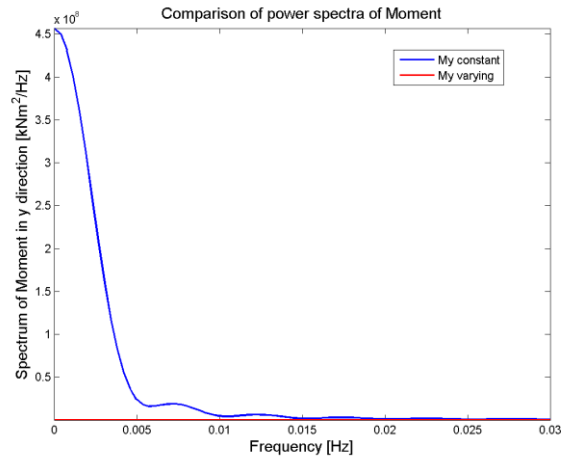

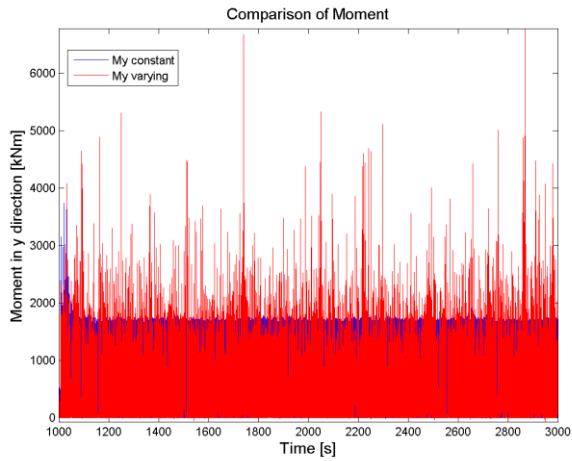Comparison of Force in x direction at 0.3 m/s

Force Spectra in x direction at 0.3 m/s
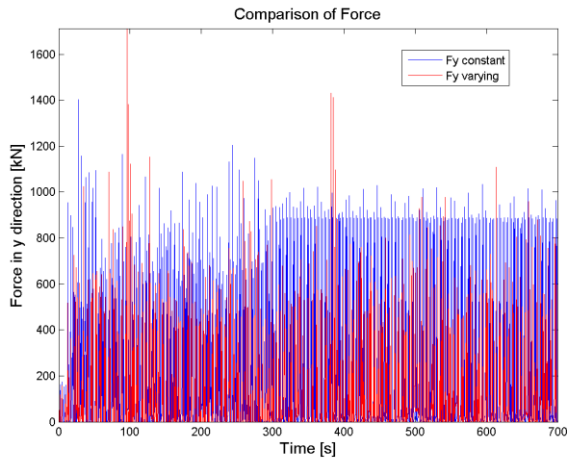
Comparison of Force in y direction at 0.3 m/s
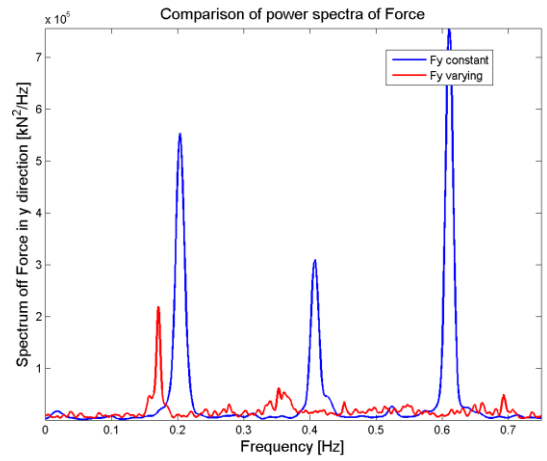
Force Spectra in y direction at 0.3 m/s
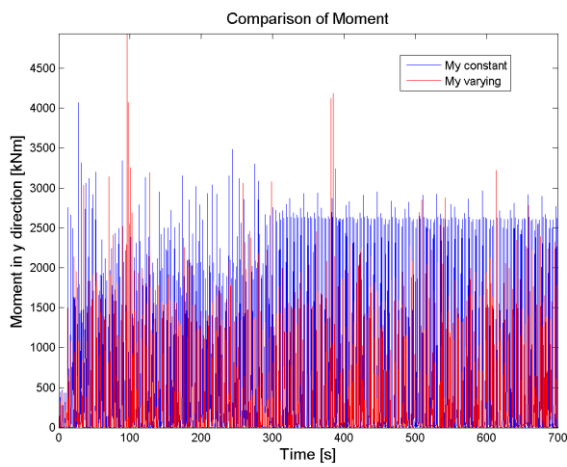
Comparison of Moment in x direction at 0.3 m/s
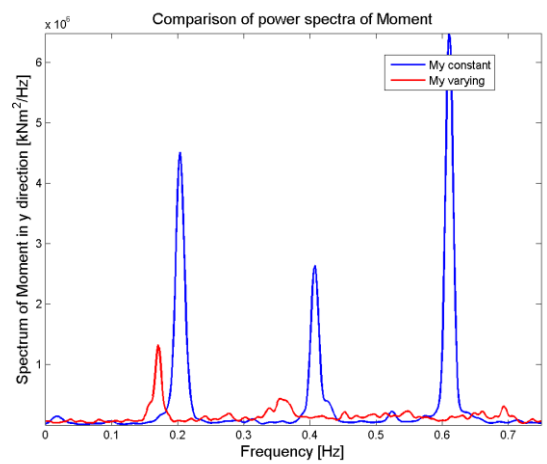
Moment Spectra in x direction at 0.3 m/s
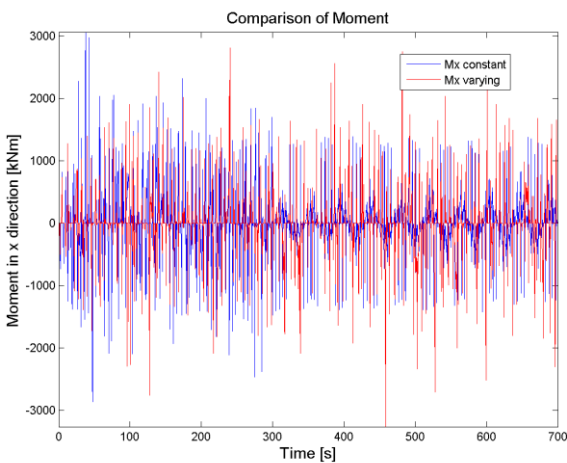
Comparison of Moment in y direction at 0.3 m/s
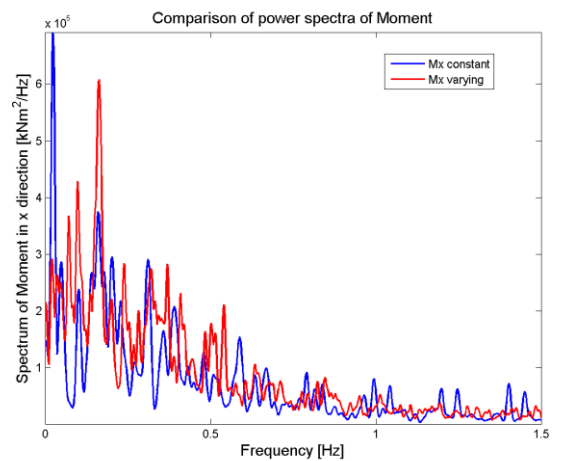
Moment Spectra in y direction at 0.3 m/s
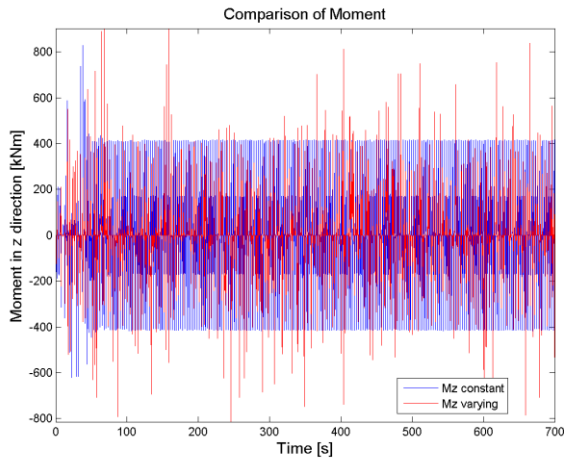
Comparison of Moment in z direction at 0.3 m/s
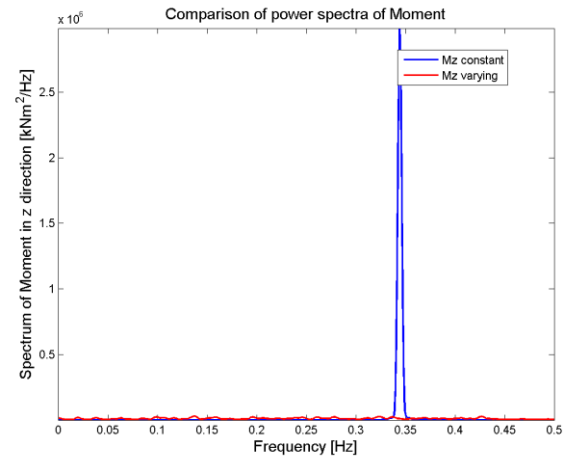
Moment Spectra in z direction at 0.3 m/s

D3. Ice actions constant vs varying thickness, monopile 0.5 m/s drifting speed
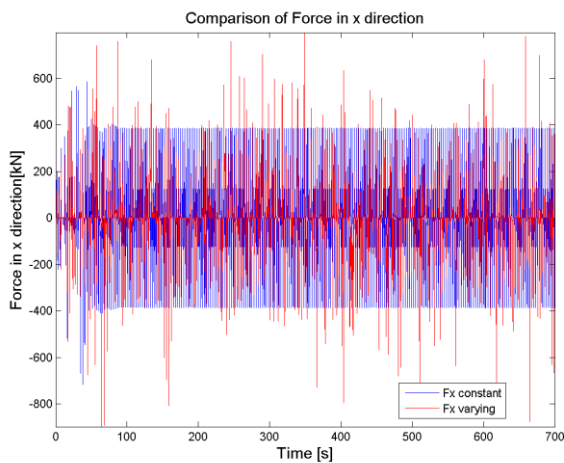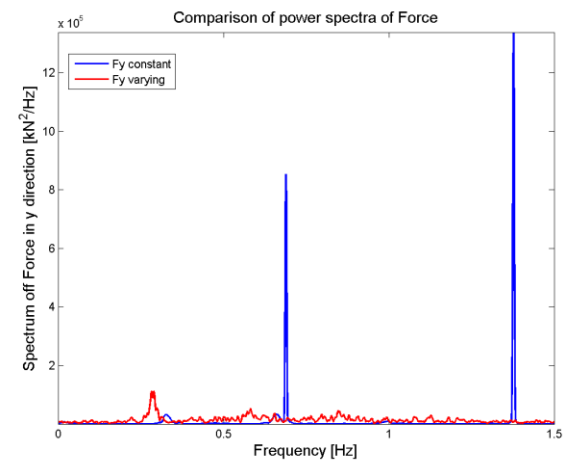
Comparison of Force in x direction at 0.5 m/s

Force Spectra in x direction at 0.5 m/s
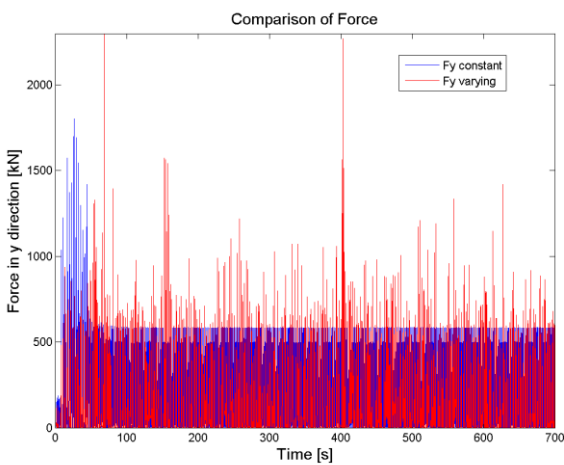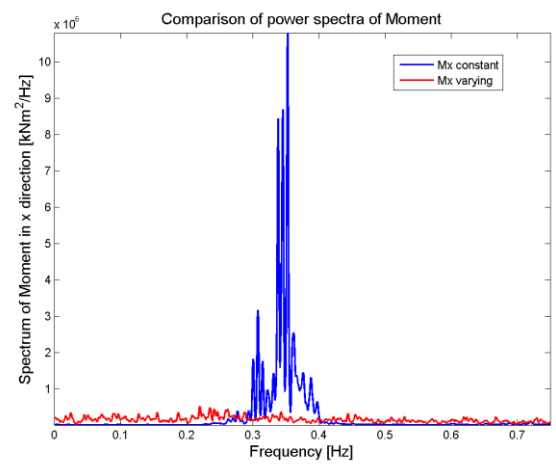

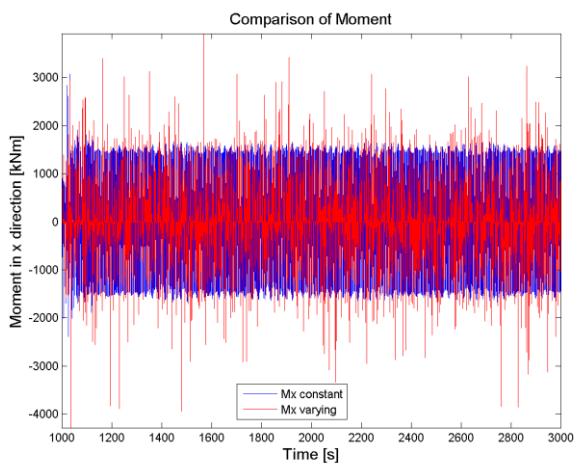Comparison of Force in y direction at 0.5 m/s
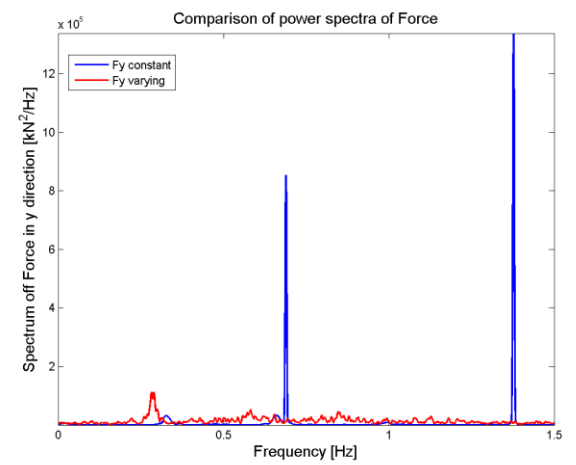
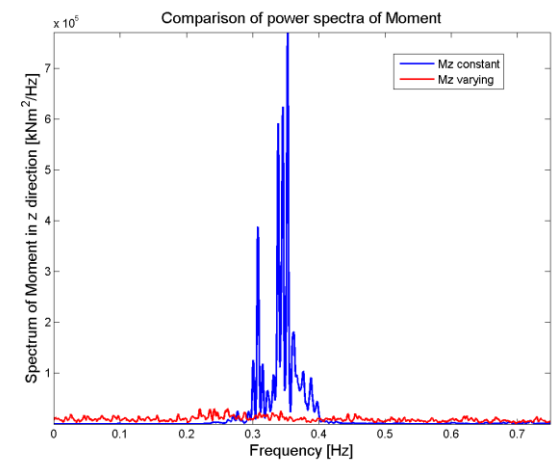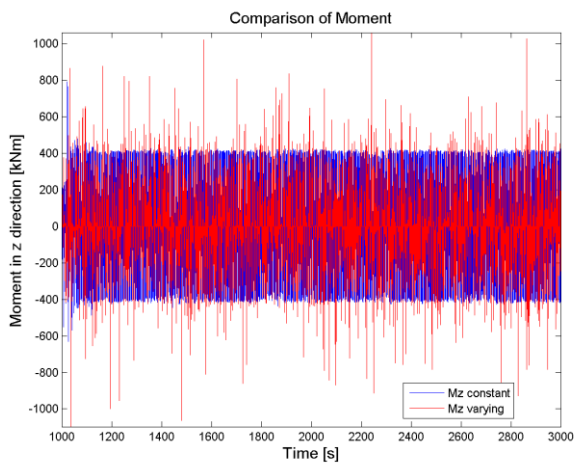Force Spectra in y direction at 0.5 m/s
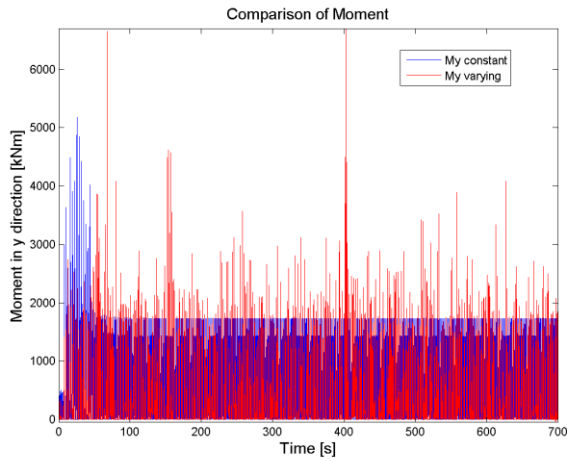
Comparison of Moment in x direction at 0.5 m/s
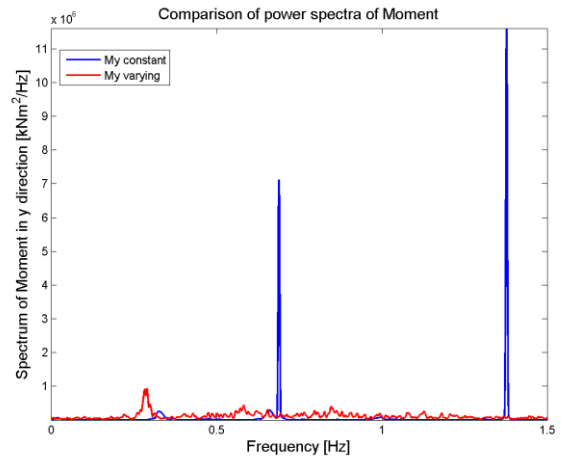
Moment Spectra in x direction at 0.5 m/s
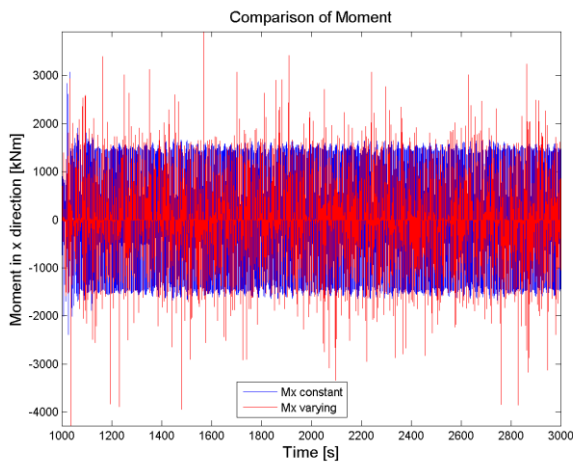
Comparison of Moment in y direction at 0.5 m/s
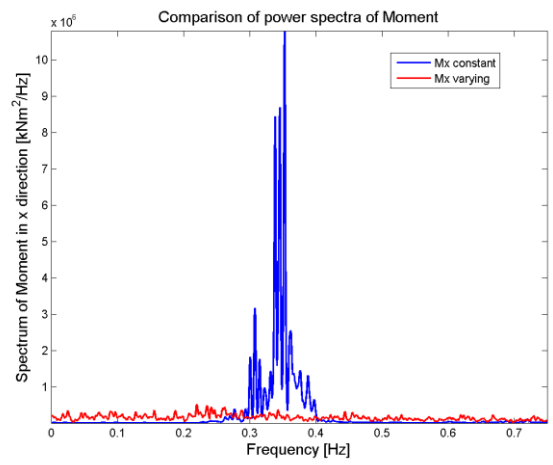
Moment Spectra in y direction at 0.5 m/s
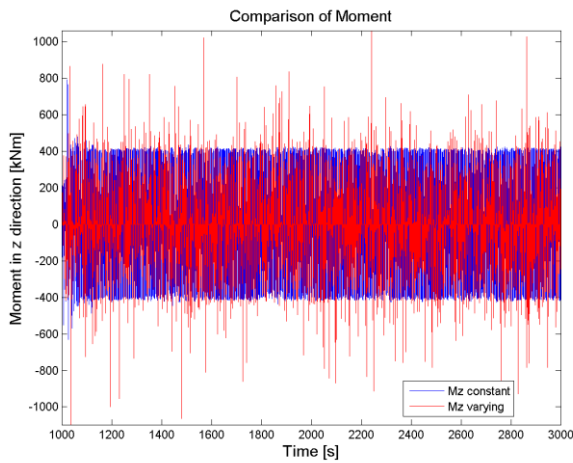
Comparison of Moment in z direction at 0.5 m/s
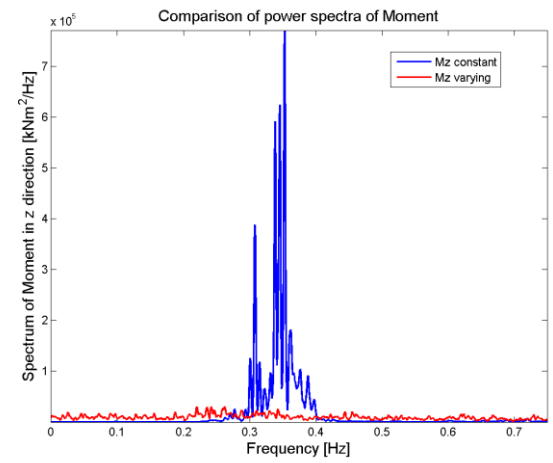
Moment Spectra in z direction at 0.5 m/s

E1. Ice actions initial constant thickness model results (project assignment)

Comparison of Force in x direction at 0.1 m/s

Force Spectra in x direction at 0.1 m/s

Comparison of Force in z direction at 0.3 m/s

Force Spectra in z direction at 0.3 m/s

Comparison of Moment in y direction at 0.1 m/s

Moment Spectra in y direction at 0.1 m/s

Comparison of Moment in x direction at 0.3 m/s

Moment Spectra in x direction at 0.3 m/s

Comparison of Moment in z direction at 0.5 m/s
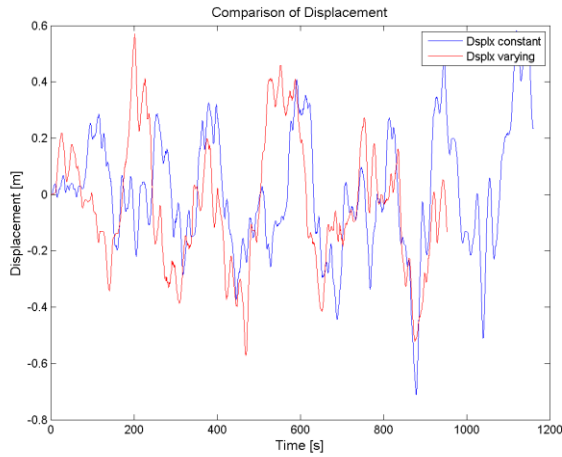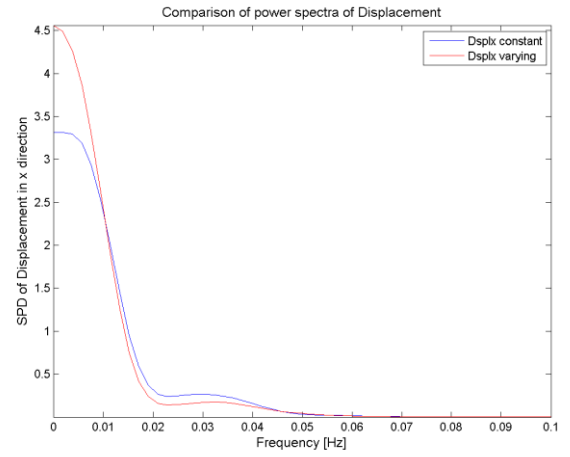

Moment Spectra in z direction at 0.5 m/s

E2. Ice actions constant vs varying ice thickness, spar 0.3 m/s drifting speed

Comparison of Force in x direction at 0.3 m/s

Force Spectra in x direction at 0.3 m/s

Comparison of Force in z direction at 0.3 m/s

Force Spectra in z direction at 0.3 m/s
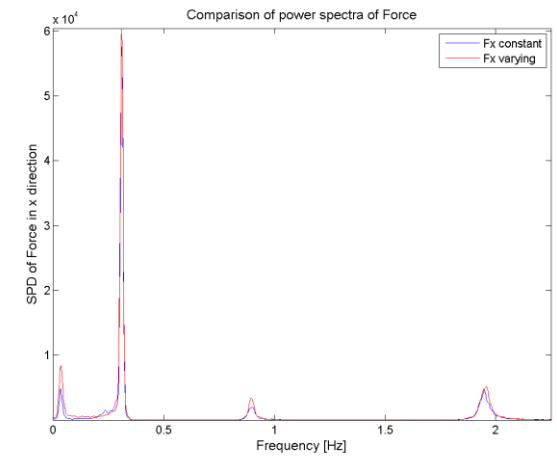

Comparison of Moment in x direction at 0.3 m/s

Moment Spectra in x direction at 0.3 m/s

Comparison of Moment in y direction at 0.3 m/s

Moment Spectra in y direction at 0.3 m/s

Comparison of Moment in z direction at 0.3 m/s

Moment Spectra in z direction at 0.3 m/s

E3. Ice actions constant vs varying ice thickness, spar 0.5 m/s drifting speed

Comparison of Force in x direction at 0.5 m/s

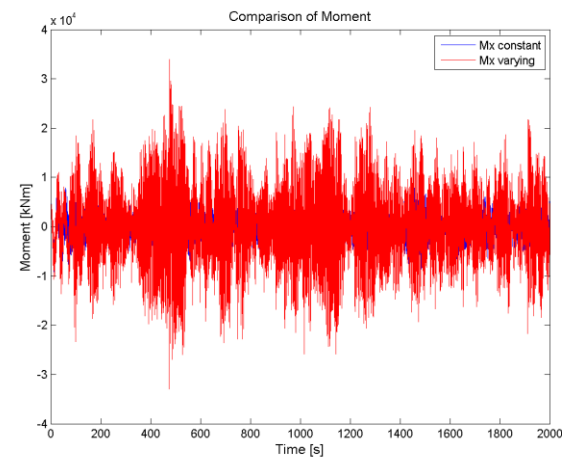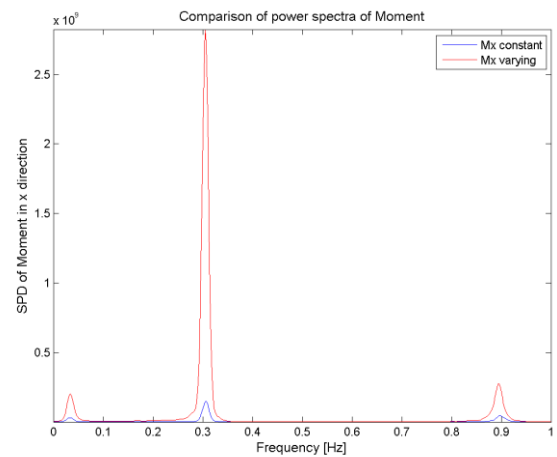Force Spectra in x direction at 0.5 m/s

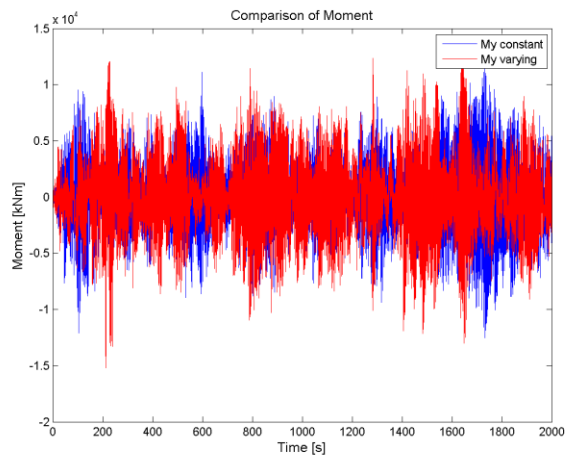Comparison of Force in y direction at 0.5 m/s

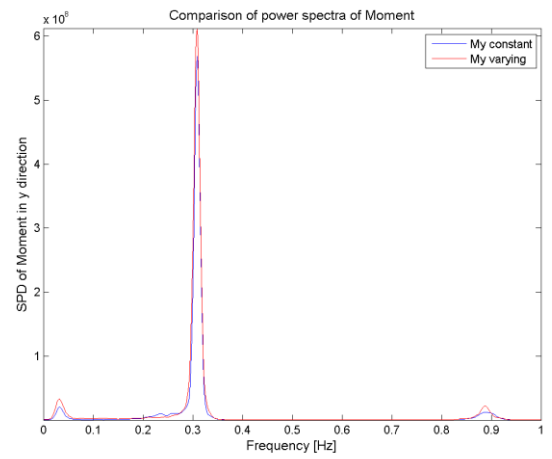Force Spectra in y direction at 0.5 m/s

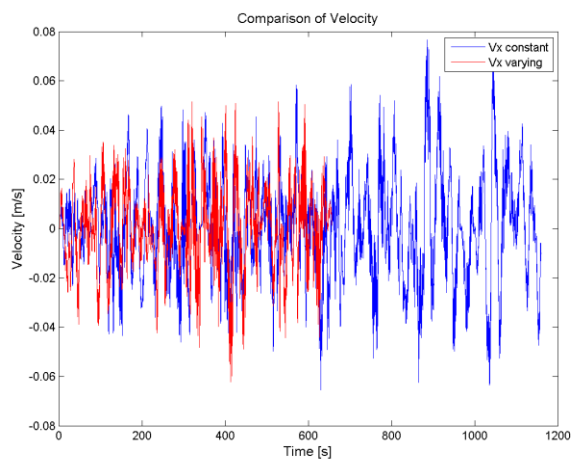Comparison of Moment in x direction at 0.5 m/s

Moment Spectra in x direction at 0.5 m/s

Comparison of Moment in y direction at 0.5 m/s

Moment Spectra in y direction at 0.5 m/s

Comparison of Moment in z direction at 0.5 m/s

Moment Spectra in z direction at 0.5 m/s

F1. Responses initial constant ice thickness model results (project assignment)

Every simulation with 0.1 m/s drifting speed after a point did not converge.

Comparison of Displacement in x direction at 0.1 m/s

Displacement Spectra in x direction at 0.1 m/s
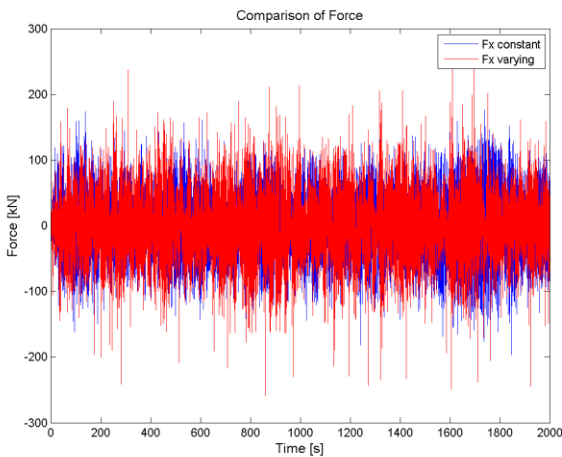
Comparison of Force in x direction at 0.3 m/s

Force Spectra in x direction at 0.3 m/s

Comparison of Moment in x direction at 0.5 m/s

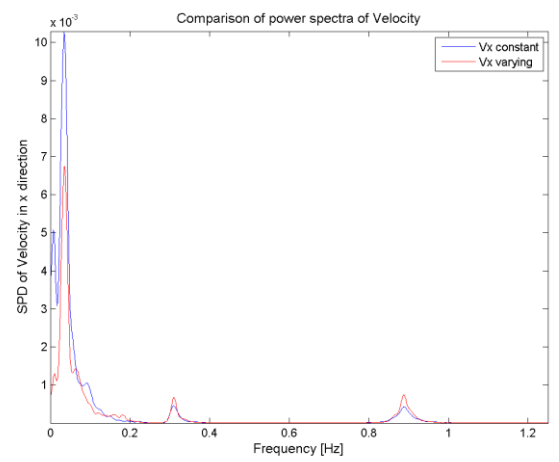Moment Spectra in x direction at 0.5 m/s

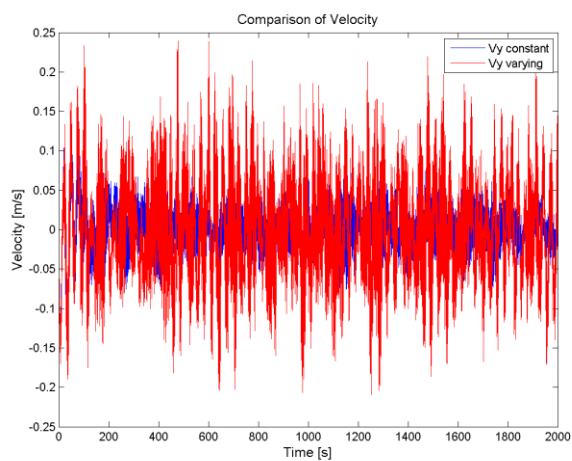Comparison of Moment in y direction at 0.3 m/s

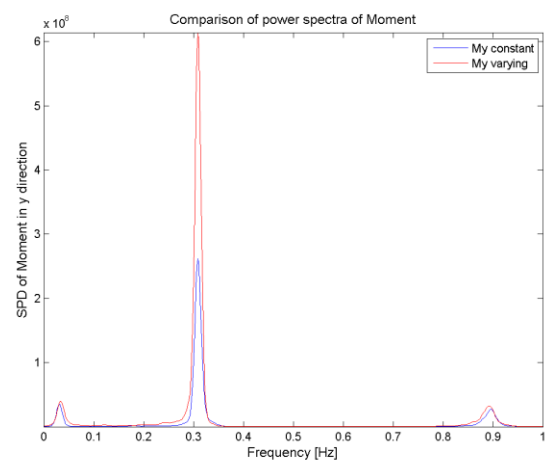Moment Spectra in y direction at 0.3 m/s

Comparison of Velocity in x direction at 0.1 m/s
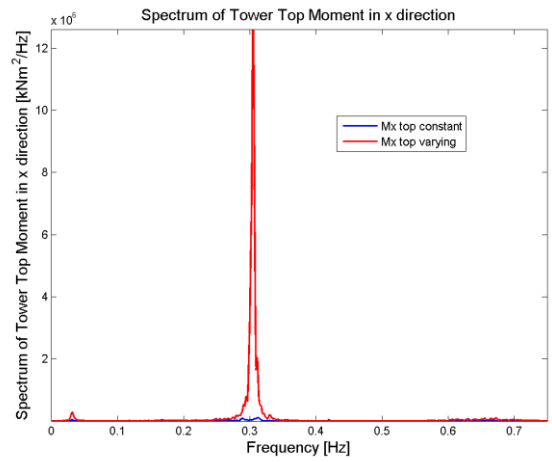

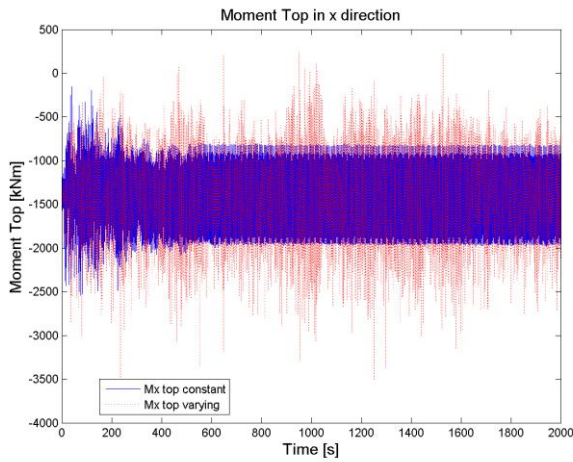Velocity Spectra in x direction at 0.1 m/s
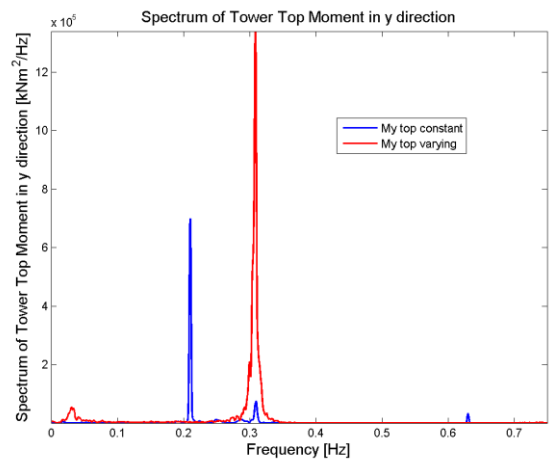

Comparison of Velocity in y direction at 0.5 m/s

Velocity Spectra in y direction at 0.5 m/s

F2. Responses constant vs varying ice thickness, spar 0.3 m/s drifting speed

Comparison of Moment Top in x direction at 0.3 m/s

Moment Top Spectra in x direction at 0.3 m/s

Comparison of Moment Top in y direction at 0.3 m/s

Moment Top Spectra in y direction at 0.3 m/s

Comparison of Velocity in x direction at 0.3 m/s

Moment Velocity in x direction at 0.3 m/s
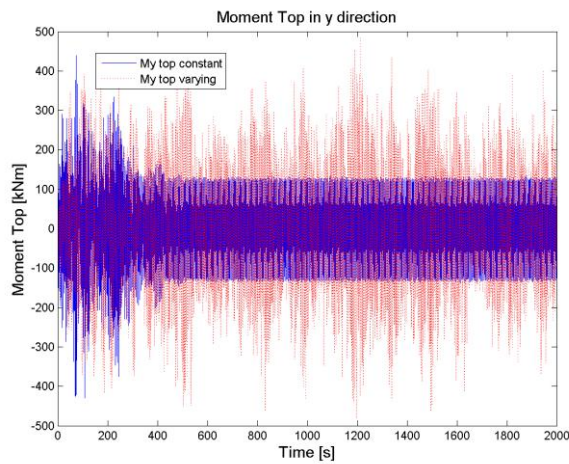
Comparison of Velocity in y direction at 0.3 m/s

Velocity Spectra in y direction at 0.3 m/s

Comparison of Mooring line tension 1 at 0.3 m/s

Mooring line tension 1 Spectra at 0.3 m/s

Comparison of Mooring line tension 3 at 0.3 m/s

Mooring line tension 3 Spectra at 0.3 m/s

F3. Responses constant vs varying ice thickness, spar 0.5 m/s drifting speed
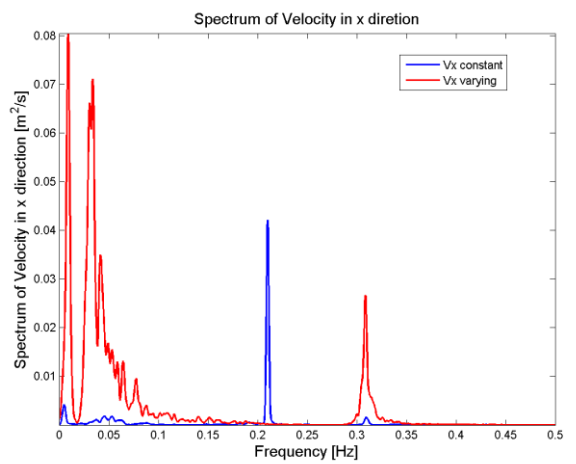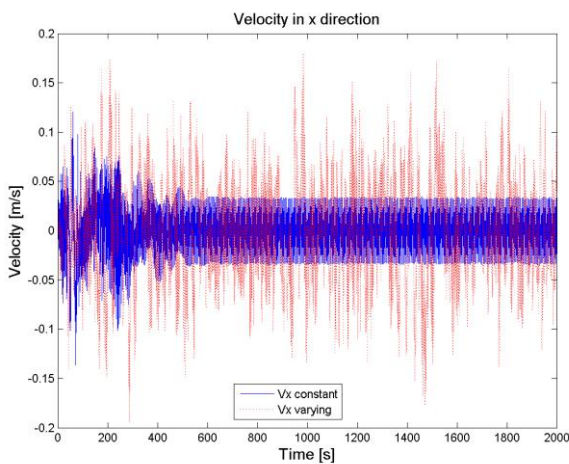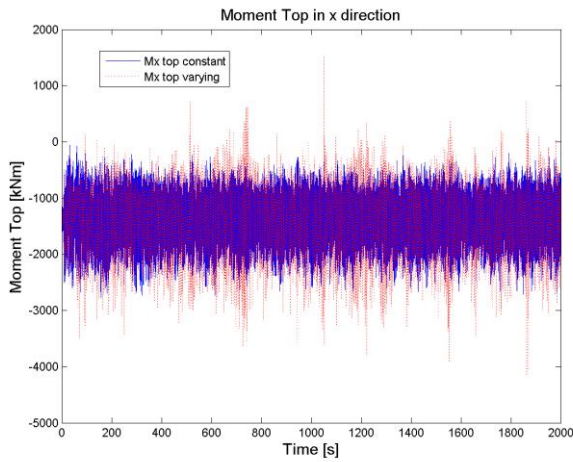

Comparison of Moment Top in x direction at 0.5 m/s

Moment Top Spectra in x direction at 0.5 m/s
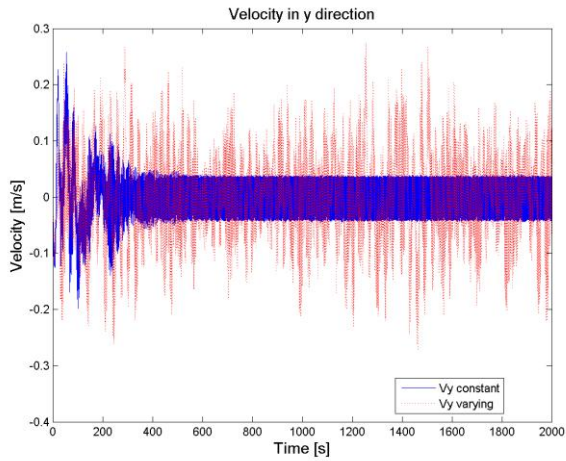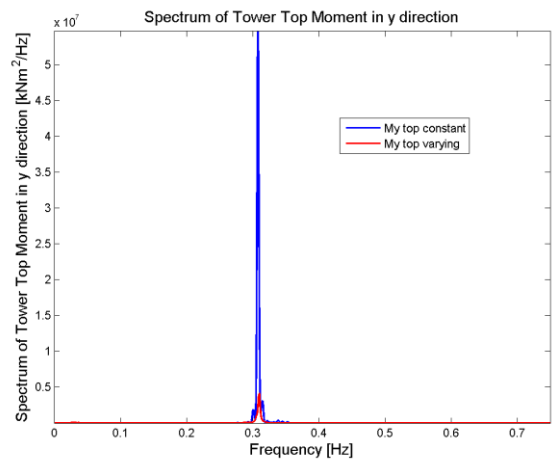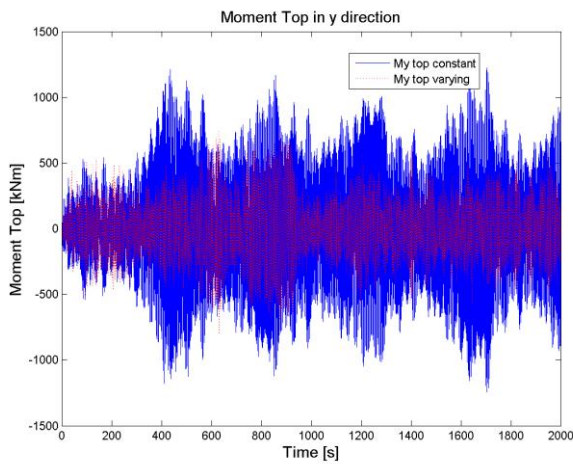

Comparison of Moment Top in y direction at 0.5 m/s

Moment Top Spectra in y direction at 0.5 m/s
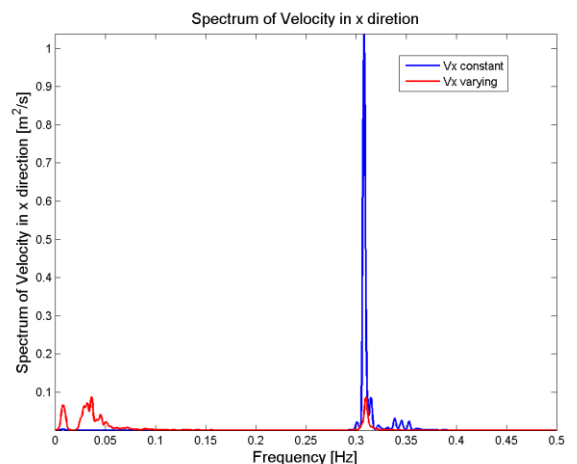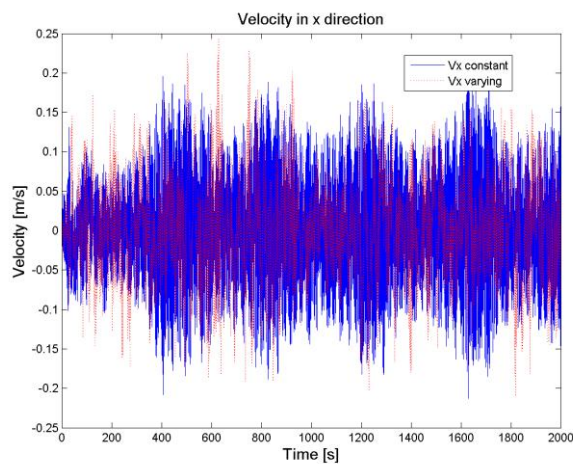
Comparison of Velocity in x direction at 0.5 m/s

Moment Velocity in x direction at 0.5 m/s
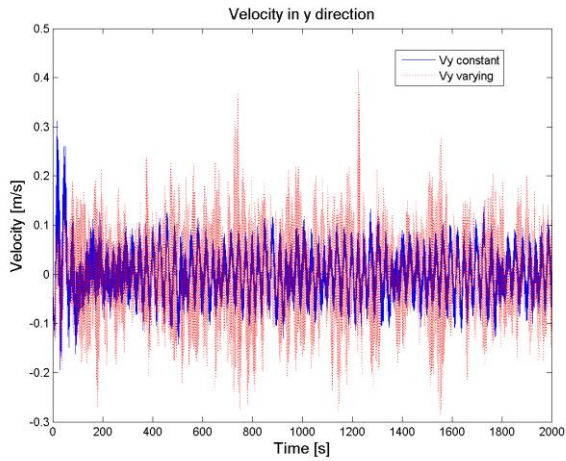
Comparison of Velocity in y direction at 0.5 m/s

Velocity Spectra in y direction at 0.5 m/s

Comparison of Mooring line tension 1 at 0.5 m/s

Mooring line tension 1 Spectra at 0.5 m/s

Comparison of Mooring line tension 3 at 0.5 m/s

Mooring line tension 3 Spectra at 0.5 m/s

G1. Responses aerodynamic loads included, constant ice thickness, 0.3 m/s drifting speed
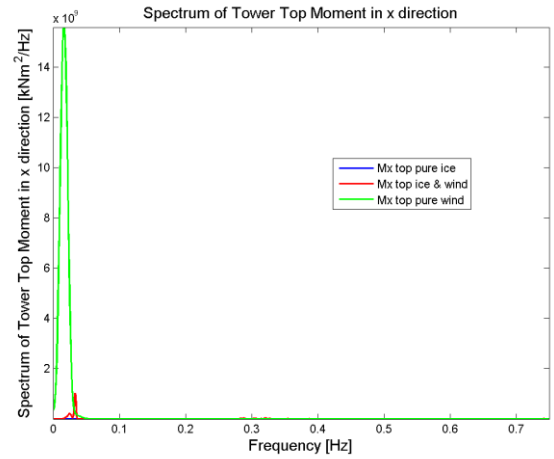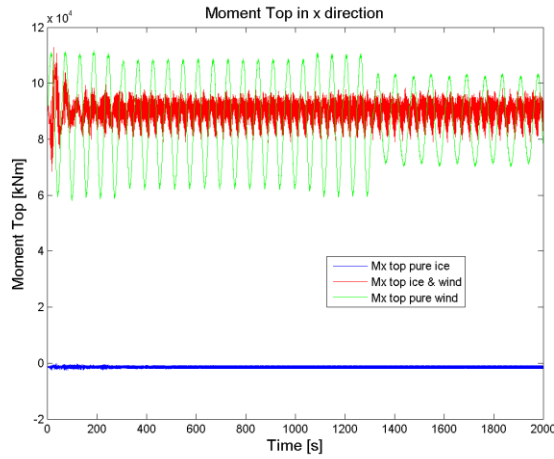
Comparison of Moment Top in x direction at 0.3 m/s

Moment Top Spectra in x direction at 0.3 m/s

Comparison of Moment Top in y direction at 0.3 m/s
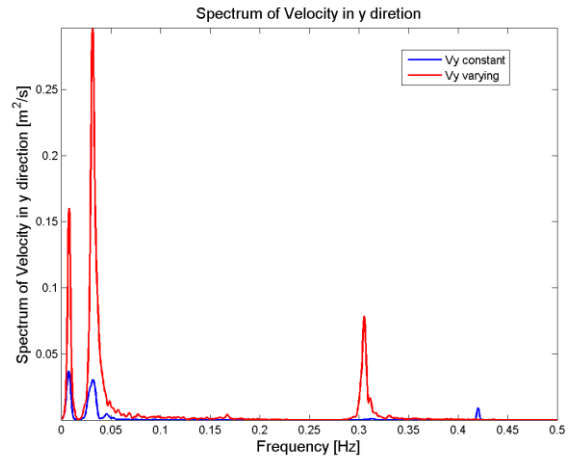

Moment Top Spectra in y direction at 0.3 m/s
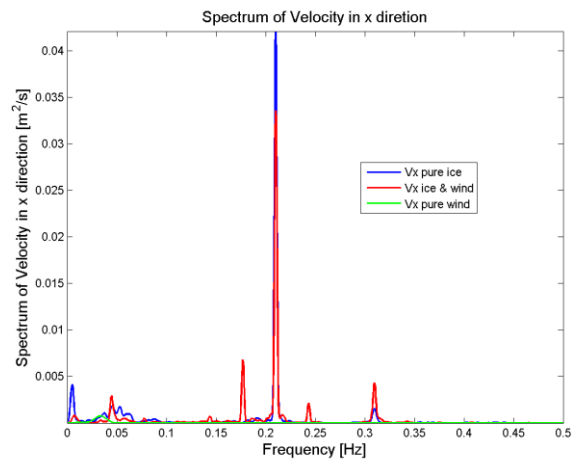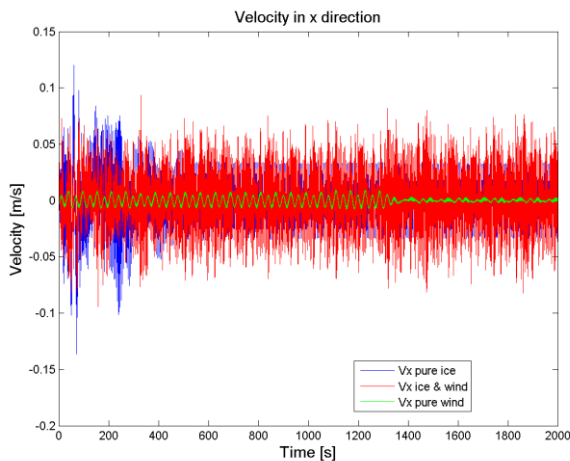
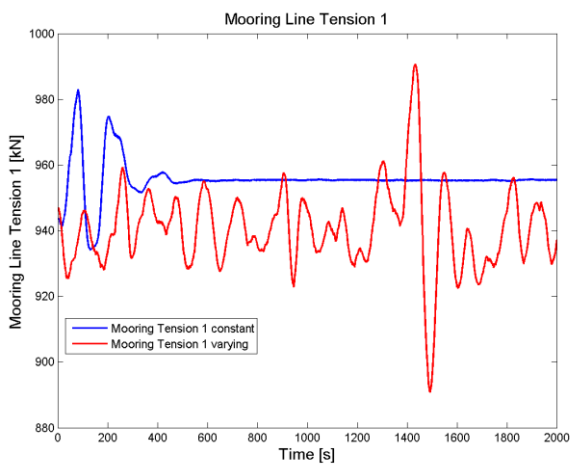Comparison of Velocity in x direction at 0.3 m/s

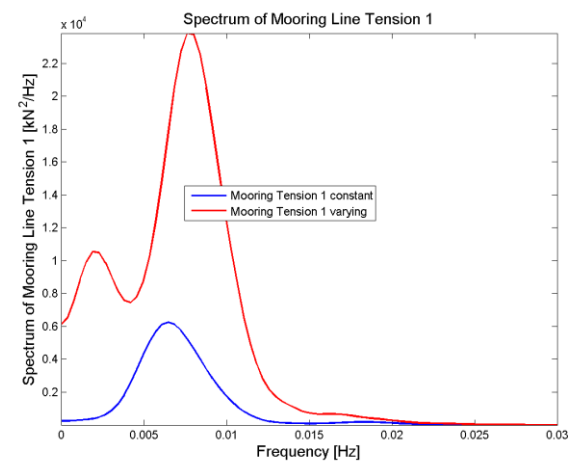Moment Velocity in x direction at 0.3 m/s
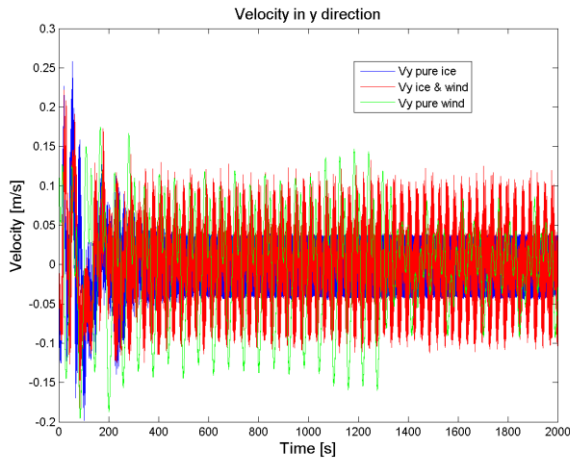
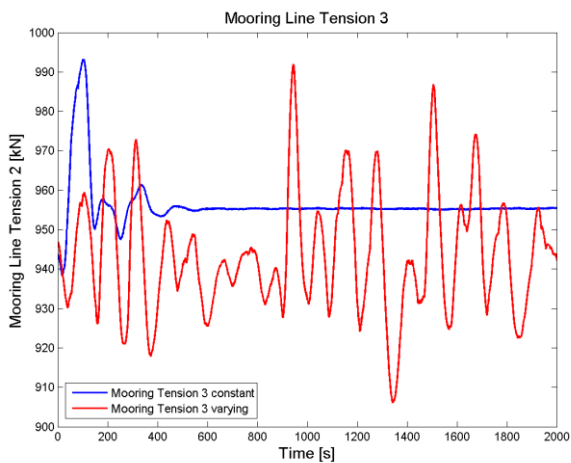Comparison of Velocity in y direction at 0.3 m/s
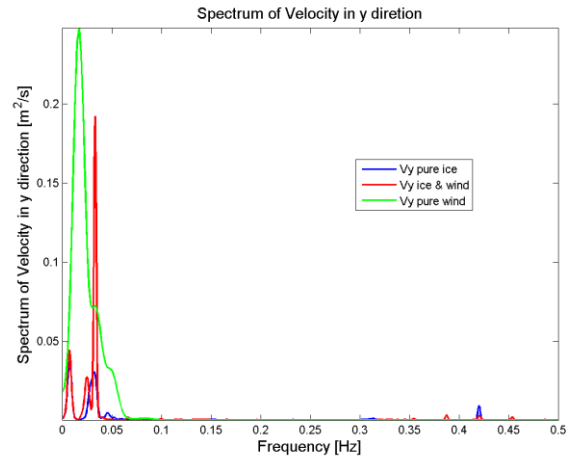
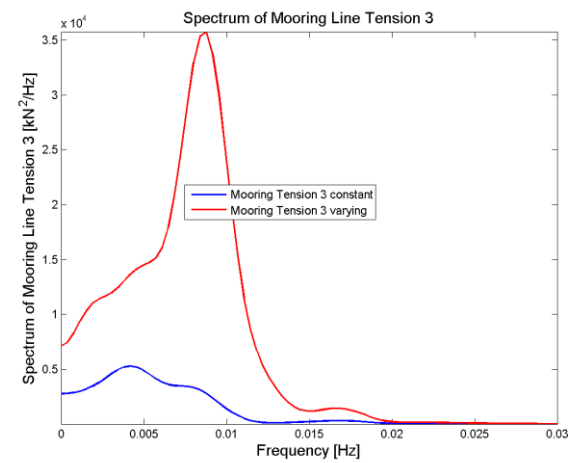
Velocity Spectra in y direction at 0.3 m/s

Comparison of Mooring line tension 1 at 0.3 m/s
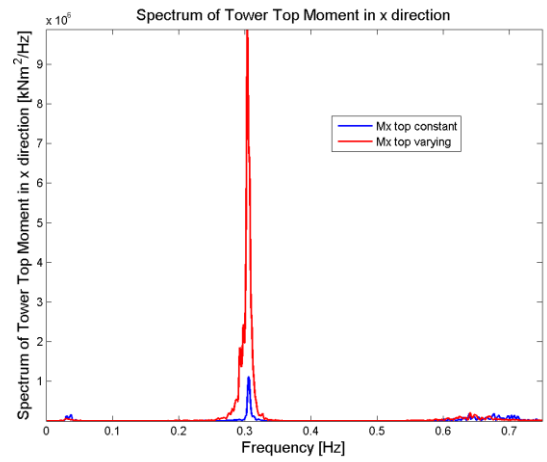

Mooring line tension 1 Spectra at 0.3 m/s
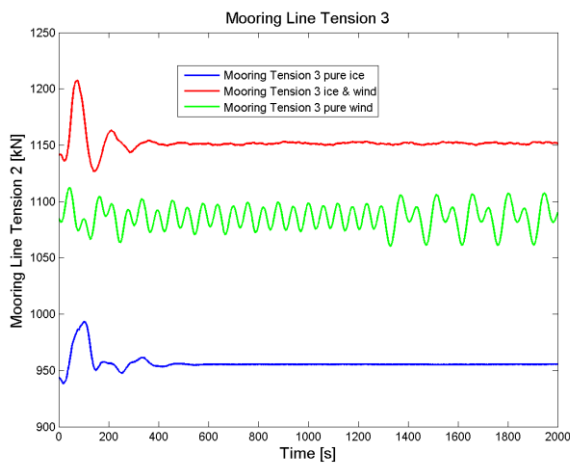
Comparison of Mooring line tension 3 at 0.3 m/s
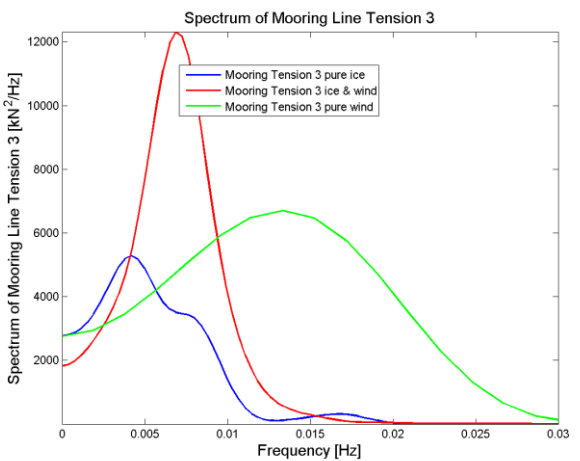
Mooring line tension 3 Spectra at 0.3 m/s

G2. Responses aerodynamic loads included, varying ice thickness, 0.3 m/s drifting speed
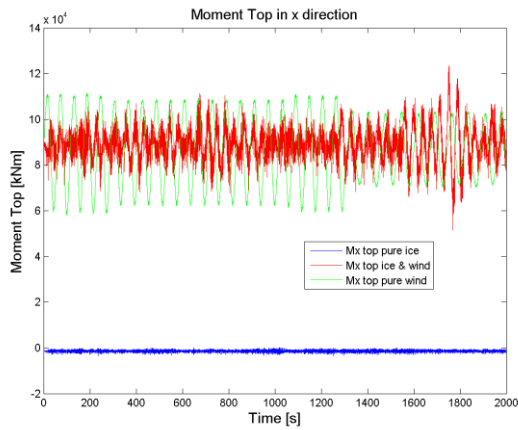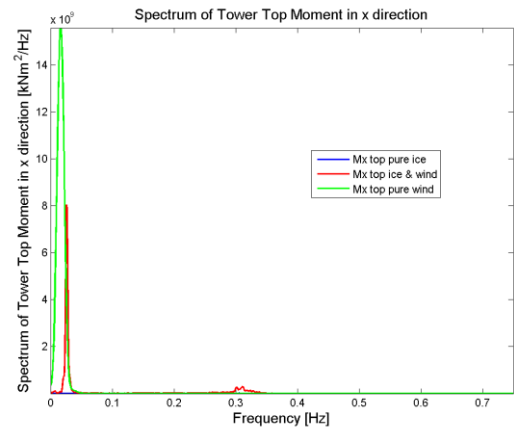
Comparison of Moment Top in x direction at 0.3 m/s

Moment Top Spectra in x direction at 0.3 m/s

Comparison of Moment Top in y direction at 0.3 m/s

Moment Top Spectra in y direction at 0.3 m/s
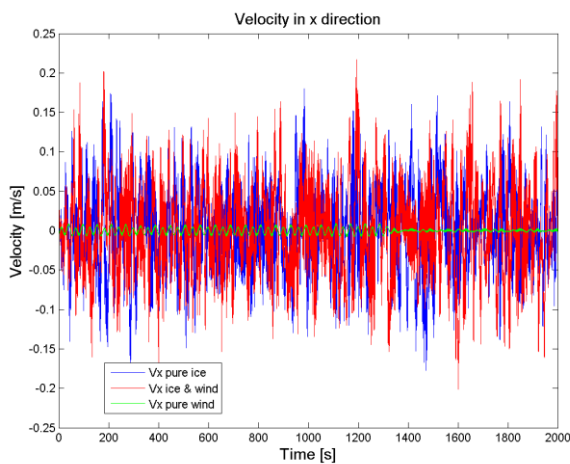
Comparison of Velocity in x direction at 0.3 m/s
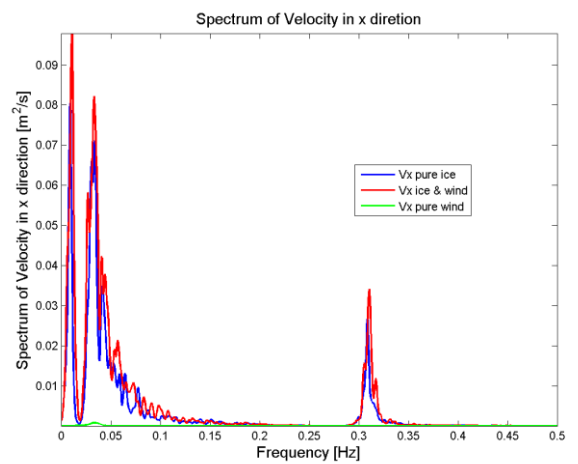
Moment Velocity in x direction at 0.3 m/s
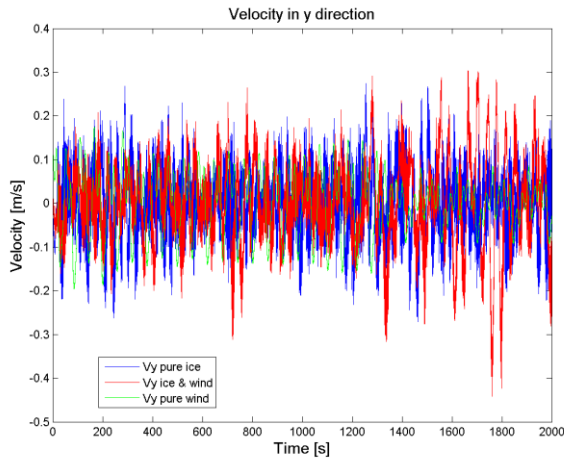
Comparison of Velocity in y direction at 0.3 m/s
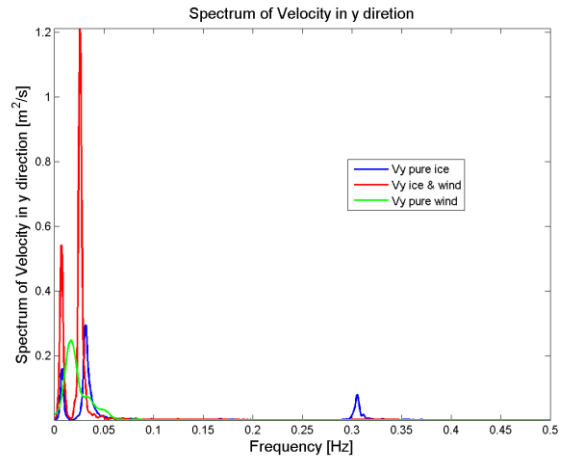
Velocity Spectra in y direction at 0.3 m/s

Comparison of Mooring line tension 1 at 0.3 m/s

Mooring line tension 1 Spectra at 0.3 m/s
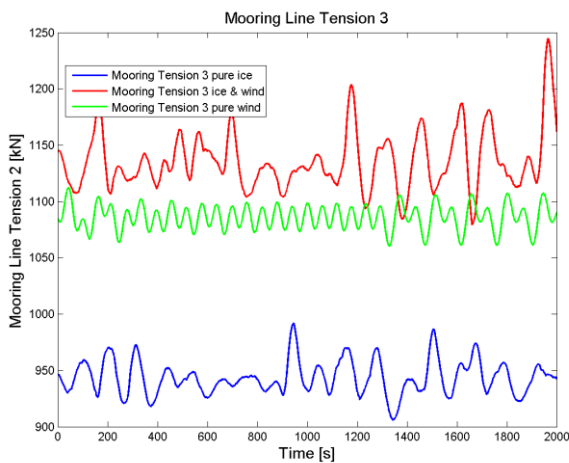
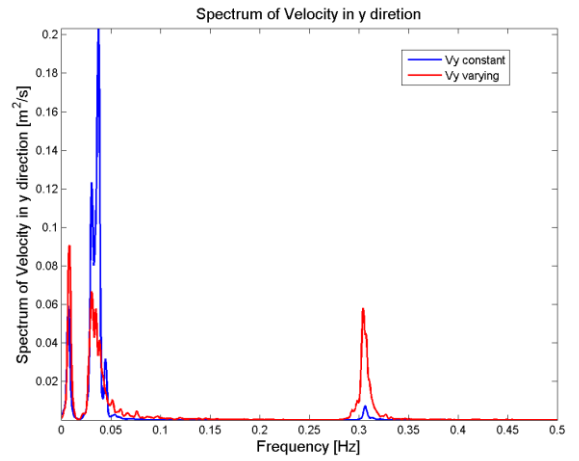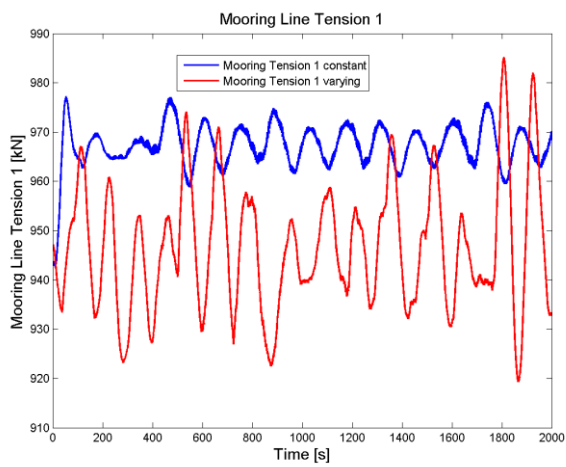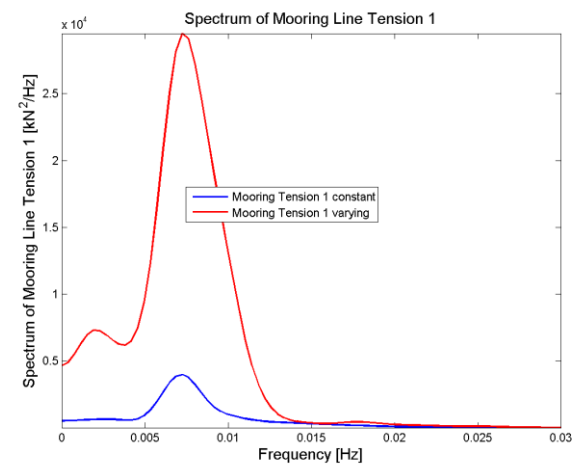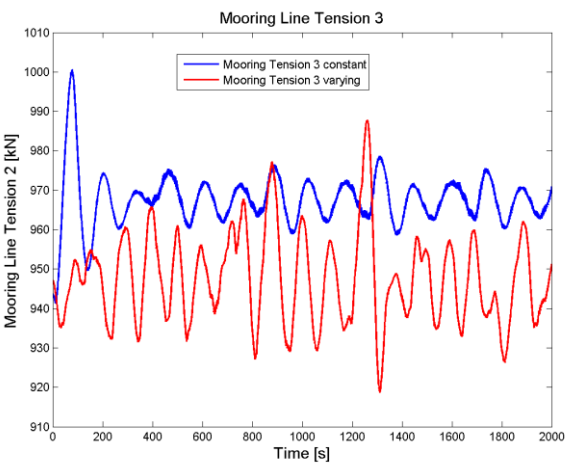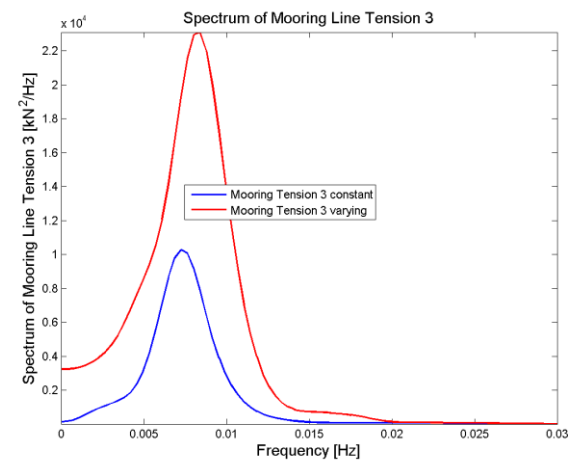Comparison of Mooring line tension 3 at 0.3 m/s

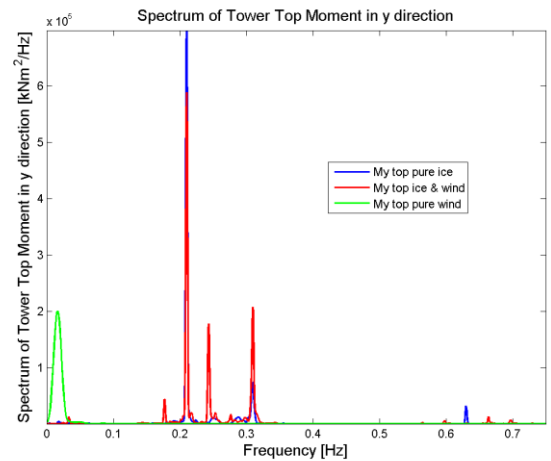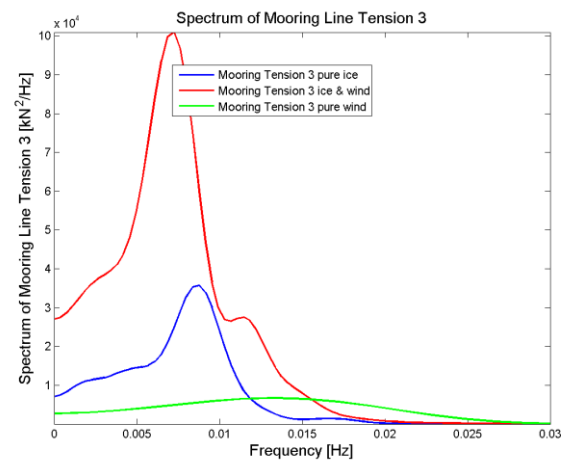
Mooring line tension 3 Spectra at 0.3 m/s

H. FEM Fortran code

The implementation of the FEM model into a DLL file consists of two subroutines that are connected to the initial DLL.

Code for Characteristic length

```fortran
Function Charlength(index, lc)
implicit none
INCLUDE 'LAPACK_INCLUDE.F90'
double precision, parameter :: pwater = 1013d0, g = 9.81d0, sf = 0.58000d06, b = 1d0, pi=
3.14159265358979d0
double precision, parameter :: ym = 5.40d9, L = 0.10d0
integer:: j, numnode, numelem, numelem2, i, ie, icounter, index, ni, INFO, kk, jj,index2,meion,
arithmos1,arithmos2
integer, parameter:: Fvar = -1
double precision :: theta, Kapa, slratio, lc, s, Fminimum3, sfcheck, T
double precision, allocatable :: Kb(:,:), Kf(:,:), Ktotal(:,:), F(:), U(:), EI(:), x(:), v(:),
Moment(:), act(:), stress(:), Ktotal2(:,:)
double precision, allocatable :: Nodes(:), Elements_Arxi(:), Elements_Telos(:), Heights(:),
moi(:), F2(:),U2(:)
INTEGER, allocatable :: ipiv(:)
double precision:: DOFs(4), Help1(4,4), Help2(4,4), N(4), Bmatrix(4)

Allocate(Nodes(index),  Elements_Arxi(index-1),  Elements_Telos(index-1),  Heights(index-1),
moi(index-1))

open(1, FILE='Nodes_ALL.txt')
  read(1,*), Nodes
close(1)
open(2, FILE='Elements_Arxi_ALL.txt')
  read(2,*), Elements_Arxi
close(2)
open(3, FILE='Elements_Telos_ALL.txt')
  read(3,*), Elements_Telos
close(3)
open(4, FILE='Heights_ALL.txt')
 read(4,*), Heights
close(4)
open(5, FILE='moi_ALL.txt')
 read(5,*), moi
close(5)

Kapa = pwater*g
numnode  = size(Nodes)-1
numelem  = size(Elements_Arxi)-1
numelem2 = Elements_Telos(index-1)-1

Allocate(Kb(2*numnode,2*numnode), Kf(2*numnode,2*numnode), Ktotal(2*numnode,2*numnode))
Allocate(F(2*numnode), U(2*numnode), EI(numelem))
Allocate(x(numnode), v(numnode), Moment(numnode))
Allocate(act(3:2*numelem2), stress(numnode))

do i = 3,2*numelem2
      act(i) = i
enddo
do i = 1,2*numnode
      do j = 1,2*numnode
            Kf(i,j) = 0.0d0
            Kb(i,j) = 0.0d0
            Ktotal(i,j) = 0.0d0
      enddo
enddo
do i = 1,2*numnode
      F(i) = 0.0d0
      U(i) = 0.0d0
enddo
do i = 1,numnode
```

```
        x(i) = 0.0d0
        v(i) = 0.0d0
        Moment(i) = 0.0d0
        stress(i) = 0.0d0
enddo

Help1(1,1) = 13d0*L*Kapa/35d0
Help1(1,2) = 11d0*(L**2d0)*Kapa/210d0
Help1(1,3) = 9d0*L*Kapa/70d0
Help1(1,4) = -13d0*(L**2d0)*Kapa/420d0
Help1(2,1) = 11d0*(L**2d0)*Kapa/210d0
Help1(2,2) = (L**3d0)*Kapa/105d0
Help1(2,3) = 13d0*(L**2d0)*Kapa/420d0
Help1(2,4) = -(L**3d0)*Kapa/140d0
Help1(3,1) = 9d0*L*Kapa/70d0
Help1(3,2) = 13d0*(L**2d0)*Kapa/420d0
Help1(3,3) = 13d0*L*Kapa/35d0
Help1(3,4) = -11d0*(L**2d0)*Kapa/210d0
Help1(4,1) = -13d0*(L**2d0)*Kapa/420d0
Help1(4,2) = -(L**3d0)*Kapa/140d0
Help1(4,3) = -11d0*(L**2d0)*Kapa/210d0
Help1(4,4) = (L**3d0)*Kapa/105d0
Help2(1,1) = 12d0
Help2(1,2) = 6d0*L
Help2(1,3) = -12d0
Help2(1,4) = 6d0*L
Help2(2,1) = 6d0*L
Help2(2,2) = 4d0*(L**2d0)
Help2(2,3) = -6d0*L
Help2(2,4) = 2d0*(L**2d0)
Help2(3,1) = -12d0
Help2(3,2) = -6d0*L
Help2(3,3) = 12d0
Help2(3,4) = -6d0*L
Help2(4,1) = 6d0*L
Help2(4,2) = 2d0*(L**2d0)
Help2(4,3) = -6d0*L
Help2(4,4) = 4d0*(L**2d0)
do ie = 1,numelem
        DOFs(1) = 2d0*Elements_Arxi(ie)-1d0
        DOFs(2) = 2d0*Elements_Arxi(ie)
        DOFs(3) = 2d0*Elements_Telos(ie)-1d0
        DOFs(4) = 2d0*Elements_Telos(ie)
        EI(ie)  = ym*moi(ie)*b
        Kf(DOFs,DOFs) = Kf(DOFs,DOFs) + b*Help1
        Kb(DOFs,DOFs) = Kb(DOFs,DOFs) + (EI(ie)/(L**3d0))*Help2
enddo
Ktotal = (Kf+Kb)
Allocate(Ktotal2(2*numnode-2,2*numnode-2), F2(2*numnode-2), U2(2*numnode-2))
F(size(act)+1) = Fvar*b
kk = 0
do i = 3,2*numnode
        kk = kk+1
        F2(kk) = F(i)
enddo
ni = size(F2)
kk = 0
do i = 3,2*numnode
        kk = kk+1
        jj = 0
        do j = 3,2*numnode
                jj = jj+1
                Ktotal2(kk,jj) = Ktotal(i,j)
        enddo
enddo
Allocate(ipiv(ni))
CALL DGESV( ni, 1, Ktotal2, ni, IPIV, F2, ni, INFO )
U2 = F2
jj = 2
do i = 1,2*numnode-2
        jj = jj+1
        U(jj) = U2(i)
```

```
enddo

icounter = 0
do ie = 1,numelem
        DOFs(1) = 2d0*Elements_Arxi(ie)-1
        DOFs(2) = 2d0*Elements_Arxi(ie)
        DOFs(3) = 2d0*Elements_Telos(ie)-1
        DOFs(4) = 2d0*Elements_Telos(ie)
        if (ie==1) then
                s = 0d0
                icounter = icounter+1
                slratio = s/L
                N(1) = 1d0-3d0*(slratio**2d0)+2d0*(slratio**3d0)
                N(2) = L*(slratio-2d0*(slratio**2d0)+(slratio**3d0))
                N(3) = 3d0*(slratio**2d0)-2*(slratio**3d0)
                N(4) = L*(-(slratio**2d0)+(slratio**3d0))
                x(icounter) = s + Nodes(Elements_Arxi(ie))
                v(icounter) = 0.0d0
                do i = 1,4
                        v(icounter) = v(icounter) + N(i)*U(DOFs(i))
                enddo
                Bmatrix(1) = -6d0+12d0*slratio
                Bmatrix(2) = L*(-4d0+6d0*slratio)
                Bmatrix(3) = 6d0-12d0*slratio
                Bmatrix(4) = L*(-2d0+6d0*slratio)
                Moment(icounter) = 0.0d0
                do i = 1,4
                        Moment(icounter)=Moment(icounter)-(EI(ie)*Bmatrix(i)*U(DOFs(i)))/(L**2d0)
                enddo
                s = L
                icounter = icounter  + 1
                slratio = s/L
                N(1) = 1d0-3d0*(slratio**2d0)+2d0*(slratio**3d0)
                N(2) = L*(slratio-2d0*(slratio**2d0)+(slratio**3d0))
                N(3) = 3d0*(slratio**2d0)-2d0*(slratio**3d0)
                N(4) = L*(-(slratio**2d0)+(slratio**3d0))
                x(icounter) = s + Nodes(Elements_Arxi(ie))
                v(icounter) = 0.0d0
                do i = 1,4
                        v(icounter) = v(icounter) + N(i)*U(DOFs(i))
                enddo
                Bmatrix(1) = -6d0+12d0*slratio
                Bmatrix(2) = L*(-4d0+6d0*slratio)
                Bmatrix(3) = 6d0-12d0*slratio
                Bmatrix(4) = L*(-2d0+6d0*slratio)
                Moment(icounter) = 0.0d0
                do i = 1,4
                        Moment(icounter)=Moment(icounter)-(EI(ie)*Bmatrix(i)*U(DOFs(i)))/(L**2d0)
                enddo
        else
                s = L
                icounter = icounter+1
                slratio = s/L
                N(1) = 1d0-3d0*slratio**2d0+2d0*(slratio**3d0)
                N(2) = L*(slratio-2d0*(slratio**2d0)+(slratio**3d0))
                N(3) = 3d0*(slratio**2d0)-2d0*(slratio**3d0)
                N(4) = L*(-(slratio**2d0)+(slratio**3d0))
                x(icounter) = s + Nodes(Elements_Arxi(ie))
                v(icounter) = 0.0d0
                do i = 1,4
                        v(icounter) = v(icounter) + N(i)*U(DOFs(i))
                enddo
                Bmatrix(1) = -6d0+12d0*slratio
                Bmatrix(2) = L*(-4d0+6d0*slratio)
                Bmatrix(3) = 6d0-12d0*slratio
                Bmatrix(4) = L*(-2d0+6d0*slratio)
                Moment(icounter) = 0.0d0
                do i = 1,4
                        Moment(icounter)=Moment(icounter)-(EI(ie)*Bmatrix(i)*U(DOFs(i)))/(L**2d0)
                enddo
        endif
enddo
```

```
do i = 1,icounter
        stress(i) = (Moment(i)*(Heights(i)/2d0))/(moi(i)*b)
enddo
sfcheck = sf
Fminimum3 = ((sfcheck/maxval(stress))*F(size(act)+1))
F(size(act)+1) = Fminimum3
kk = 0
do i = 3,2*numnode
        kk = kk+1
        F2(kk) = F(i)
enddo
ni = size(F2)
kk = 0
do i = 3,2*numnode
        kk = kk+1
        jj = 0
        do j = 3,2*numnode
                jj = jj+1
                Ktotal2(kk,jj) = Ktotal(i,j)
        enddo
enddo
CALL DGESV( ni, 1, Ktotal2, ni, IPIV, F2, ni, INFO )
U2 = F2
jj = 2
do i = 1,2*numnode-2
        jj = jj+1
        U(jj) = U2(i)
enddo
icounter = 0
do ie = 1,numelem
        DOFs(1) = 2d0*Elements_Arxi(ie)-1
        DOFs(2) = 2d0*Elements_Arxi(ie)
        DOFs(3) = 2d0*Elements_Telos(ie)-1
        DOFs(4) = 2d0*Elements_Telos(ie)
        if (ie==1) then
                s = 0d0
                icounter = icounter+1
                slratio = s/L
                N(1) = 1d0-3d0*(slratio**2d0)+2d0*(slratio**3d0)
                N(2) = L*(slratio-2d0*(slratio**2d0)+(slratio**3d0))
                N(3) = 3d0*(slratio**2d0)-2*(slratio**3d0)
                N(4) = L*(-(slratio**2d0)+(slratio**3d0))
                x(icounter) = s + Nodes(Elements_Arxi(ie))
                v(icounter) = 0.0d0
                do i = 1,4
                        v(icounter) = v(icounter) + N(i)*U(DOFs(i))
                enddo
                Bmatrix(1) = -6d0+12d0*slratio
                Bmatrix(2) = L*(-4d0+6d0*slratio)
                Bmatrix(3) = 6d0-12d0*slratio
                Bmatrix(4) = L*(-2d0+6d0*slratio)
                Moment(icounter) = 0.0d0
                do i = 1,4
                        Moment(icounter)=Moment(icounter)-(EI(ie)*Bmatrix(i)*U(DOFs(i)))/(L**2d0)
                enddo
                s = L
                icounter = icounter  + 1;
                slratio = s/L
                N(1) = 1d0-3d0*(slratio**2d0)+2d0*(slratio**3d0)
                N(2) = L*(slratio-2d0*(slratio**2d0)+(slratio**3d0))
                N(3) = 3d0*(slratio**2d0)-2d0*(slratio**3d0)
                N(4) = L*(-(slratio**2d0)+(slratio**3d0))
                x(icounter) = s + Nodes(Elements_Arxi(ie))
                v(icounter) = 0.0d0
                do i = 1,4
                        v(icounter) = v(icounter) + N(i)*U(DOFs(i))
                enddo
                Bmatrix(1) = -6d0+12d0*slratio
                Bmatrix(2) = L*(-4d0+6d0*slratio)
                Bmatrix(3) = 6d0-12d0*slratio
                Bmatrix(4) = L*(-2d0+6d0*slratio)
                Moment(icounter) = 0.0d0
```

```
                do i = 1,4
                        Moment(icounter)=Moment(icounter)-(EI(ie)*Bmatrix(i)*U(DOFs(i)))/(L**2d0)
                enddo
        else
                s = L
                icounter = icounter+1
                slratio = s/L
                N(1) = 1d0-3d0*slratio**2d0+2d0*(slratio**3d0)
                N(2) = L*(slratio-2d0*(slratio**2d0)+(slratio**3d0))
                N(3) = 3d0*(slratio**2d0)-2d0*(slratio**3d0)
                N(4) = L*(-(slratio**2d0)+(slratio**3d0))
                x(icounter) = s + Nodes(Elements_Arxi(ie))
                v(icounter) = 0.0d0
                do i = 1,4
                        v(icounter) = v(icounter) + N(i)*U(DOFs(i))
                enddo
                Bmatrix(1) = -6d0+12d0*slratio
                Bmatrix(2) = L*(-4d0+6d0*slratio)
                Bmatrix(3) = 6d0-12d0*slratio
                Bmatrix(4) = L*(-2d0+6d0*slratio)

                Moment(icounter) = 0.0d0
                do i = 1,4
                        Moment(icounter)=Moment(icounter)-(EI(ie)*Bmatrix(i)*U(DOFs(i)))/(L**2d0)
                enddo
        endif
enddo
do i = 1,icounter
        stress(i) = (Moment(i)*(Heights(i)/2d0))/(moi(i))
        if (stress(i).GT.sf) then
                index2 = i
        endif
enddo

lc = (size(Nodes)-(index2))/10d0
index = index2

Deallocate(Kb, Kf, Ktotal, Ktotal2, F, U, EI, x, v, Moment, act, stress)
Deallocate(Nodes, Elements_Arxi, Elements_Telos, Heights, moi, F2, ipiv, U2)
return
end
```

Code for Failure load

```
Function Fminimum2(theta, index)
implicit none
INCLUDE 'LAPACK_INCLUDE.F90'
double precision, parameter :: pwater = 1013d0, g = 9.81d0, sf = 0.58000d06, b = 1d0, pi=
3.14159265358979d0
double precision, parameter :: ym = 5.40d9, L = 0.10d0
integer:: j, numnode, numelem, numelem2, i, ie, icounter, index, ni, INFO, kk, jj,index2,meion,
arithmos1,arithmos2
integer, parameter:: Fvar = -1
double precision :: theta, Kapa, slratio, lc, s, Fminimum3, sfcheck, T
double precision, allocatable :: Kb(:,:), Kf(:,:), Ktotal(:,:), F(:), U(:), EI(:), x(:), v(:),
Moment(:), act(:), stress(:), Ktotal2(:,:)
double precision, allocatable :: Nodes(:), Elements_Arxi(:), Elements_Telos(:), Heights(:),
moi(:), F2(:),U2(:)
INTEGER, allocatable :: ipiv(:)
double precision:: DOFs(4), Help1(4,4), Help2(4,4), N(4), Bmatrix(4)

Allocate(Nodes(index),  Elements_Arxi(index-1),  Elements_Telos(index-1),  Heights(index-1),
moi(index-1))

open(1, FILE='Nodes_ALL.txt')
  read(1,*), Nodes
close(1)
open(2, FILE='Elements_Arxi_ALL.txt')
  read(2,*), Elements_Arxi
close(2)
open(3, FILE='Elements_Telos_ALL.txt')
  read(3,*), Elements_Telos
close(3)
open(4, FILE='Heights_ALL.txt')
 read(4,*), Heights
close(4)
open(5, FILE='moi_ALL.txt')
 read(5,*), moi
close(5)

Kapa = pwater*g
numnode  = size(Nodes)-1
numelem  = size(Elements_Arxi)-1
numelem2 = Elements_Telos(index-1)-1
Allocate(Kb(2*numnode,2*numnode), Kf(2*numnode,2*numnode), Ktotal(2*numnode,2*numnode))
Allocate(F(2*numnode), U(2*numnode), EI(numelem))
Allocate(x(numnode), v(numnode), Moment(numnode))
Allocate(act(3:2*numelem2),b(numelem+1), stress(numnode))
do i = 3,2*numelem2
       act(i) = i
enddo
do i = 1,2*numnode
       do j = 1,2*numnode
               Kf(i,j) = 0.0d0
               Kb(i,j) = 0.0d0
               Ktotal(i,j) = 0.0d0
       enddo
enddo
do i = 1,2*numnode
       F(i) = 0.0d0
       U(i) = 0.0d0
enddo
do i = 1,numnode
       x(i) = 0.0d0
       v(i) = 0.0d0
       Moment(i) = 0.0d0
       stress(i) = 0.0d0
enddo

Help1(1,1) = 13d0*L*Kapa/35d0
Help1(1,2) = 11d0*(L**2d0)*Kapa/210d0
Help1(1,3) = 9d0*L*Kapa/70d0
Help1(1,4) = -13d0*(L**2d0)*Kapa/420d0
```

```fortran
Help1(2,1) = 11d0*(L**2d0)*Kapa/210d0
Help1(2,2) = (L**3d0)*Kapa/105d0
Help1(2,3) = 13d0*(L**2d0)*Kapa/420d0
Help1(2,4) = -(L**3d0)*Kapa/140d0
Help1(3,1) = 9d0*L*Kapa/70d0
Help1(3,2) = 13d0*(L**2d0)*Kapa/420d0
Help1(3,3) = 13d0*L*Kapa/35d0
Help1(3,4) = -11d0*(L**2d0)*Kapa/210d0
Help1(4,1) = -13d0*(L**2d0)*Kapa/420d0
Help1(4,2) = -(L**3d0)*Kapa/140d0
Help1(4,3) = -11d0*(L**2d0)*Kapa/210d0
Help1(4,4) = (L**3d0)*Kapa/105d0
Help2(1,1) = 12d0
Help2(1,2) = 6d0*L
Help2(1,3) = -12d0
Help2(1,4) = 6d0*L
Help2(2,1) = 6d0*L
Help2(2,2) = 4d0*(L**2d0)
Help2(2,3) = -6d0*L
Help2(2,4) = 2d0*(L**2d0)
Help2(3,1) = -12d0
Help2(3,2) = -6d0*L
Help2(3,3) = 12d0
Help2(3,4) = -6d0*L
Help2(4,1) = 6d0*L
Help2(4,2) = 2d0*(L**2d0)
Help2(4,3) = -6d0*L
Help2(4,4) = 4d0*(L**2d0)
do ie = 1,numelem
        DOFs(1) = 2d0*Elements_Arxi(ie)-1d0
        DOFs(2) = 2d0*Elements_Arxi(ie)
        DOFs(3) = 2d0*Elements_Telos(ie)-1d0
        DOFs(4) = 2d0*Elements_Telos(ie)
        b(ie) = 2*abs(tan(theta/2)*L*((numelem+2)-ie))
        EI(ie)  = ym*moi(ie)*b(ie)
        Kf(DOFs,DOFs) = Kf(DOFs,DOFs) + b(ie)*Help1
        Kb(DOFs,DOFs) = Kb(DOFs,DOFs) + (EI(ie)/(L**3d0))*Help2
enddo
Ktotal = (Kf+Kb)
Allocate(Ktotal2(2*numnode-2,2*numnode-2), F2(2*numnode-2), U2(2*numnode-2))
F(size(act)+1) = Fvar
kk = 0
do i = 3,2*numnode
        kk = kk+1
        F2(kk) = F(i)
enddo
ni = size(F2)
kk = 0
do i = 3,2*numnode
        kk = kk+1
        jj = 0
        do j = 3,2*numnode
                jj = jj+1
                Ktotal2(kk,jj) = Ktotal(i,j)
        enddo
enddo
Allocate(ipiv(ni))
CALL DGESV( ni, 1, Ktotal2, ni, IPIV, F2, ni, INFO )
U2 = F2
jj = 2
do i = 1,2*numnode-2
        jj = jj+1
        U(jj) = U2(i)
enddo
icounter = 0
do ie = 1,numelem
        DOFs(1) = 2d0*Elements_Arxi(ie)-1
        DOFs(2) = 2d0*Elements_Arxi(ie)
        DOFs(3) = 2d0*Elements_Telos(ie)-1
        DOFs(4) = 2d0*Elements_Telos(ie)
        if (ie==1) then
                s = 0d0
```

```
                        icounter = icounter+1
                        slratio = s/L
                        N(1) = 1d0-3d0*(slratio**2d0)+2d0*(slratio**3d0)
                        N(2) = L*(slratio-2d0*(slratio**2d0)+(slratio**3d0))
                        N(3) = 3d0*(slratio**2d0)-2*(slratio**3d0)
                        N(4) = L*(-(slratio**2d0)+(slratio**3d0))
                        x(icounter) = s + Nodes(Elements_Arxi(ie))
                        v(icounter) = 0.0d0
                        do i = 1,4
                                v(icounter) = v(icounter) + N(i)*U(DOFs(i))
                        enddo
                        Bmatrix(1) = -6d0+12d0*slratio
                        Bmatrix(2) = L*(-4d0+6d0*slratio)
                        Bmatrix(3) = 6d0-12d0*slratio
                        Bmatrix(4) = L*(-2d0+6d0*slratio)
                        Moment(icounter) = 0.0d0
                        do i = 1,4
                                Moment(icounter)=Moment(icounter)-(EI(ie)*Bmatrix(i)*U(DOFs(i)))/(L**2d0)
                        enddo
                        s = L
                        icounter = icounter  + 1;
                        slratio = s/L
                        N(1) = 1d0-3d0*(slratio**2d0)+2d0*(slratio**3d0)
                        N(2) = L*(slratio-2d0*(slratio**2d0)+(slratio**3d0))
                        N(3) = 3d0*(slratio**2d0)-2d0*(slratio**3d0)
                        N(4) = L*(-(slratio**2d0)+(slratio**3d0))
                        x(icounter) = s + Nodes(Elements_Arxi(ie))
                        v(icounter) = 0.0d0
                        do i = 1,4
                                v(icounter) = v(icounter) + N(i)*U(DOFs(i))
                        enddo
                        Bmatrix(1) = -6d0+12d0*slratio
                        Bmatrix(2) = L*(-4d0+6d0*slratio)
                        Bmatrix(3) = 6d0-12d0*slratio
                        Bmatrix(4) = L*(-2d0+6d0*slratio)
                        Moment(icounter) = 0.0d0
                        do i = 1,4
                                Moment(icounter)=Moment(icounter)-(EI(ie)*Bmatrix(i)*U(DOFs(i)))/(L**2d0)
                        enddo
                else
                        s = L
                        icounter = icounter+1
                        slratio = s/L
                        N(1) = 1d0-3d0*slratio**2d0+2d0*(slratio**3d0)
                        N(2) = L*(slratio-2d0*(slratio**2d0)+(slratio**3d0))
                        N(3) = 3d0*(slratio**2d0)-2d0*(slratio**3d0)
                        N(4) = L*(-(slratio**2d0)+(slratio**3d0))
                        x(icounter) = s + Nodes(Elements_Arxi(ie))
                        v(icounter) = 0.0d0
                        do i = 1,4
                                v(icounter) = v(icounter) + N(i)*U(DOFs(i))
                        enddo
                        Bmatrix(1) = -6d0+12d0*slratio
                        Bmatrix(2) = L*(-4d0+6d0*slratio)
                        Bmatrix(3) = 6d0-12d0*slratio
                        Bmatrix(4) = L*(-2d0+6d0*slratio)
                        Moment(icounter) = 0.0d0
                        do i = 1,4
                                Moment(icounter)=Moment(icounter)-(EI(ie)*Bmatrix(i)*U(DOFs(i)))/(L**2d0)
                        enddo
                endif
        enddo
enddo

do i = 1,icounter
        stress(i) = (Moment(i)*(Heights(i)/2d0))/(moi(i)*b(i))
enddo
sfcheck = sf
Fminimum2 = ((sfcheck/maxval(stress))*F(size(act)+1))
Deallocate(Kb, Kf, Ktotal, Ktotal2, F, U, EI, x, v, Moment, act, stress)
Deallocate(Nodes, Elements_Arxi, Elements_Telos, Heights, moi, F2, ipiv, U2)
return
end
```